TU Delft

Delft University of Technology

Energy Balance and Heat Storage of Small Shallow Water Bodies in Semi-arid Areas

Abbasi, Ali

DOI
10.4233/uuid:9b177744-faba-43d9-8e08-464454a91b4e

Publication date
2016

Document Version
Final published version

Citation (APA)
Abbasi, A. (2016). *Energy Balance and Heat Storage of Small Shallow Water Bodies in Semi-arid Areas*. [Dissertation (TU Delft), Delft University of Technology]. https://doi.org/10.4233/uuid:9b177744-faba-43d9-8e08-464454a91b4e

Important note
To cite this publication, please use the final published version (if applicable).
Please check the document version above.

Copyright
Other than for strictly personal use, it is not permitted to download, forward or distribute the text or part of it, without the consent of the author(s) and/or copyright holder(s), unless the work is under an open content license such as Creative Commons.

Takedown policy
Please contact us and provide details if you believe this document breaches copyrights.
We will remove access to the work immediately and investigate your claim.

This work is downloaded from Delft University of Technology.
For technical reasons the number of authors shown on this cover page is limited to a maximum of 10.

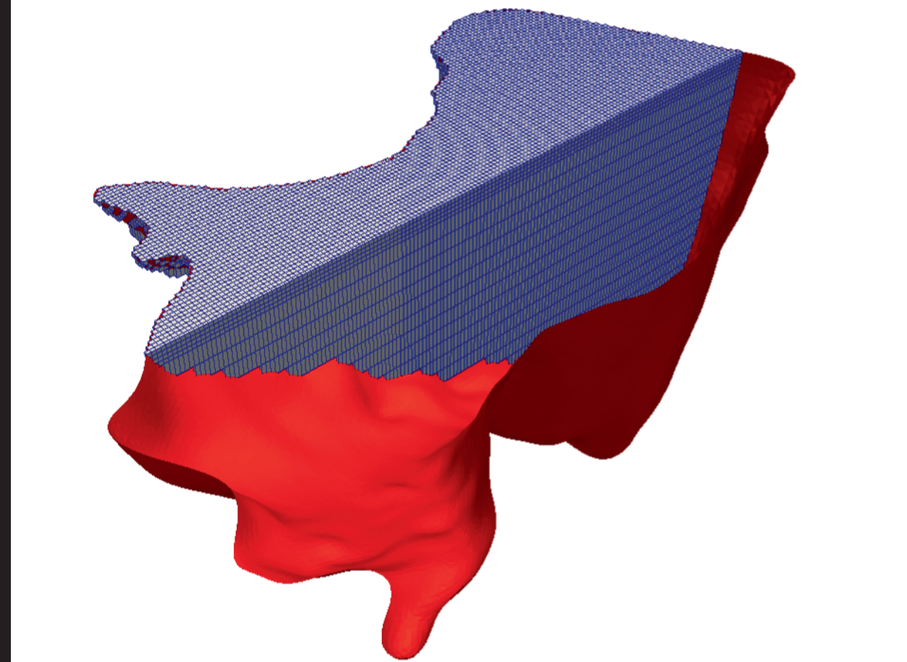
Small reservoirs in arid and semi-arid regions, especially in developing countries, provide water to improve the food security, stimulate the agricultural economy and income diversification. All the economic activities enabled by the direct uses of the small reservoir contribute to development of indirect economic activities and therefore, help significantly slowdown rural migration.

Considering significant impacts of small shallow lakes in developing countries, a comprehensive study of heat and flow dynamics is critically important. Heat exchange as well as air-water interaction, as driving forces, affects evaporative losses from these water sources and consequently, their storage efficiency. However, evaporation is perhaps the most difficult component of all hydrological cycle components to estimate, especially for small reservoirs.



Ali Abbasi Energy Balance and Heat Storage of Small Shallow Water Bodies in Semi-arid Areas

Energy Balance and Heat Storage of Small Shallow Water Bodies in Semi-arid Areas



Ali Abbasi

INVITATION TO PUBLIC PhD DEFENSE CEREMONY

ENERGY BALANCE AND HEAT STORAGE OF SMALL SHALLOW WATER BODIES IN SEMI-ARID AREAS

ALI ABBASI

MONDAY, 28th OF NOVEMBER 2016
AT 12:30
A BRIEF PRESENTATION ON THE TOPIC STARTS AT 12:00

SENAATSZALL, AULA
DELFT UNIVERSITY OF TECHNOLOGY
MEKELWEG 5,
2628 CC, DELFT

506469-sub01-os-Abbasi.indd 1,6 09-11-16 13:19

506469-L-sub01-os-Abbasi Processed on: 9-11-2016

Propositions

accompanying the dissertation

ENERGY BALANCE AND HEAT STORAGE OF SMALL SHALLOW WATER BODIES
IN SEMI-ARID AREAS

by

Ali ABBASI

1. Using Computational Fluid Dynamics (CFD) for environmental problems needs deep knowledge of the mathematical and physical issues of the problem.
2. In small shallow water bodies, the time-scale of the study is an important parameter which impacts model results as well as validation.
3. To investigate the interactions of the inland water surfaces and the Atmospheric Boundary Layer (ABL), gathering long-term measurements over the water surface as well as the surrounding lands are required.
4. A simple simulation is very useful in setting-up the measurement methodology.
5. To reach the ultimate goal of simulation, which is prediction, understanding the different parts of the problem as well as their interactions is necessary.
6. Setting-up a model is similar to raising a baby. Giving additional and correct information to a model is the same as the education for the child. In both cases, giving correct information, or education, will give us better solutions or behaviour. However, both of them will have errors.
7. Cloud-based and high-performance computing as well as data assimilation are the two hottest skills required in the job market.
8. Before starting to solve the problems, there are no difficulties. When you try to find the solution, everything seems difficult.
9. Converting a theory to a practical approach is the most difficult part in modelling.
10. Comprehensive models without suitable inputs cannot guarantee good results.

These propositions are regarded as opposable and defendable, and have been approved as such by the supervisor prof. dr. ir. N.C van de Giesen.

506469-L-sub02-st-Abbasi
Processed on: 9-11-2016

IPSKAMP printing
books and more

ENERGY BALANCE AND HEAT STORAGE OF SMALL SHALLOW WATER BODIES IN SEMI-ARID AREAS

506469-L-sub01-bw-Abbasi
Processed on: 9-11-2016

506469-L-sub01-bw-Abbasi
Processed on: 9-11-2016

ENERGY BALANCE AND HEAT STORAGE OF SMALL SHALLOW WATER BODIES IN SEMI-ARID AREAS

Proefschrift

ter verkrijging van de graad van doctor
aan de Technische Universiteit Delft,
op gezag van de Rector Magnificus prof. ir. K.C.A.M. Luyben,
voorzitter van het College voor Promoties,
in het openbaar te verdedigen op maandag 28 november 2016 om 12:30 uur

door

Ali ABBASI

Master of Science in Civil Engineering
Khajeh Nasir Toosi University of Technology
geboren te Birjand, Iran.

506469-L-sub01-bw-Abbasi
Processed on: 9-11-2016

Dit proefschrift is goedgekeurd door de

promotor: Prof. Dr. Ir. N.C van de Giesen

Samenstelling promotiecommissie:

Rector Magnificus,	voorzitter
Prof. Dr. Ir. N.C. van de Giesen,	Technische Universiteit Delft
Onafhankelijke leden:	
Prof. Dr. -Ing. R. Hinkelmann	Technische Universiteit Berlin
Prof. Dr. Ir. P. van der Zaag	UNESCO-IHE / Technische Universiteit Delft
Prof. Dr. Ir. B. Schultz	UNESCO-IHE / Wageningen University
Prof. Dr. Ir. W.S.J. Uijttewaal	Technische Universiteit Delft
Prof. Dr. Ir. H.H.G. Savenije	Technische Universiteit Delft
Dr. Ir. M. Zijlema	Technische Universiteit Delft
Prof. Dr. Ir. J.B. van Lier	Technische Universiteit Delft, reservelid

Keywords:	Small Shallow Lakes, Computational Fluid Dynamics (CFD), Atmospheric Boundary Layer (ABL), Evaporation, Turbulence, Arid and Semi-arid Regions
Printed by:	Ipskamp Drukkers
Front & Back:	Designed by Ali Abbasi.

Copyright © 2016 by author Ali Abbasi
This thesis was accomplished with financial support from Ministry of Science, Research and Technology (MSRT), I.R. IRAN.

ISBN 978-94-028-0444-7

An electronic version of this dissertation is available at
http://repository.tudelft.nl/.
The codes developed in this dissertation are available at GitHUB
https://github.com/aabbasi59.

506469-L-sub01-bw-Abbasi
Processed on: 9-11-2016

PREFACE

This PhD thesis contains the result of research undertaken at the Department of Water Management of Delft University of Technology. Doing my PhD has been a challenging trip, with both ups and downs. Certainly, I would have never reached the point of finishing my dissertation without the help and support of others. My most important coach throughout all these years was Professor Nick van de Giesen: "You are full of knowledge and ideas and you are eager to share them. Thank you so much for always being there for me, in times of when the research was going to plan, but also in stressful periods, for your understanding and emotional support during my PhD dips". I would like to truly thank you that have given me the opportunity and freedom to determine the direction of my research, along the lines that I thought was best. Furthermore, I would like to thank Frank Ohene Annor for his comments and suggestions on my work and his continuous support.

Ali Abbasi
Delft, November 2016

506469-L-sub01-bw-Abbasi
Processed on: 9-11-2016

506469-L-sub01-bw-Abbasi
Processed on: 9-11-2016

CONTENTS

1 Introduction **1**
- 1.1 Small Reservoirs . . . 1
- 1.2 Region of Study . . . 2
- 1.3 Estimating Evaporation from Water Surface . . . 3
- 1.4 CFD Approach to Water Surface Evaporation Estimation . . . 5
- 1.5 Small Water Body Model . . . 6
- 1.6 Atmospheric Boundary Layer Model . . . 7
- 1.7 Aims and Goals . . . 8

2 Effects of Atmospheric Stability Conditions on Heat Fluxes **11**
- 2.1 Introduction . . . 11
- 2.2 Atmospheric Stability Condition . . . 13
- 2.3 Description of Study Site and Data Collection . . . 15
- 2.4 Bulk Aerodynamic Method . . . 17
- 2.5 Neutral Transfer Coefficients . . . 19
- 2.6 Modifying Transfer Coefficients for Atmospheric Stability Conditions . . . 21
- 2.7 Water Surface Temperature . . . 22
- 2.8 Model Algorithm . . . 23
- 2.9 Model Verification and Validation . . . 23
- 2.10 Results of the Model and Discussion . . . 26
- 2.11 Conclusion . . . 33

3 A CFD-based Approach for Estimating Water Surface Evaporation **35**
- 3.1 Introduction . . . 35
- 3.2 Description of Study Site and Data Collection . . . 37
- 3.3 Heat and Mass Transfer in Atmospheric Boundary Layer . . . 39
- 3.4 Heat and Mass Transfer Analogy . . . 42
- 3.5 Application of Computational Fluid Dynamics . . . 43
- 3.6 Numerical Results and Discussion . . . 48
- 3.7 Conclusion . . . 56

4 A Framework to Simulate Small and Shallow Reservoirs **57**
- 4.1 Introduction . . . 57
- 4.2 Pre-Processing Phase . . . 61
- 4.3 Simulation Phase . . . 67
- 4.4 Numerical Simulation . . . 79
- 4.5 Post-processing and Model Validation Phase . . . 80
- 4.6 Model Application for Lake Binaba . . . 84
- 4.7 Conclusion . . . 89

506469-L-sub01-bw-Abbasi
Processed on: 9-11-2016

5 Investigation of Temperature Dynamics in Lake Binaba **91**
5.1 Introduction . . . 91
5.2 Water Bodies Modelling . . . 92
5.3 Description of Study Site and Data Collection . . . 93
5.4 Mathematical Model . . . 95
5.5 Numerical Simulation . . . 100
5.6 Boundary Conditions . . . 101
5.7 Numerical Results and Discussion . . . 105
5.8 Conclusion . . . 116

6 Small Water Surfaces and Atmospheric Boundary Layer Interactions **117**
6.1 Introduction . . . 117
6.2 Model Structure . . . 120
6.3 Atmospheric Stability Condition . . . 124
6.4 Computational Domain . . . 127
6.5 Initial and Boundary Conditions . . . 130
6.6 Validation of the Model . . . 133
6.7 Description of Study Site and Data Collection . . . 135
6.8 Results and Discussion . . . 139
6.9 Conclusion . . . 144

7 Conclusion and Recommendations **149**
7.1 Evaporation from Small Reservoirs . . . 149
7.2 CFD-based Approach to Estimate Evaporation (CF- DEvap) . . . 149
7.3 Small Shallow Lake Framework (SSLF) . . . 150
7.4 Applying SSLF for a Case Study . . . 151
7.5 ABL-SSL Interaction Simulation . . . 151
7.6 Recommendations . . . 152

Summary **155**

Acknowledgment **157**

About the author **159**

List of publications **161**

References **163**

506469-L-sub01-bw-Abbasi
Processed on: 9-11-2016

1

INTRODUCTION

1.1. SMALL RESERVOIRS

Small reservoirs or lakes in arid and semi-arid regions, especially in developing countries, constitute a substantial fraction of the regionally available water resources. These reservoirs provide water to improve the food security, stimulate the agricultural economy and income diversification through irrigating farms and making possible livestock farming, particularly in rural areas where most of their inhabitants rely on rainfed agriculture. All the economic activities enabled by the direct uses of the small reservoir (e.g. the use and maintenance of agricultural equipment, the supply of agricultural inputs for irrigated crops and of livestock feed, agricultural and fish processing, stock watering, brick making, etc.) contribute to local development and also to the development of indirect economic activities and therefore, help significantly to slow down rural migration (Poussin et al., 2015). As small reservoirs have a significant impact on rural communities, they are a priority for national governments and local authorities (Poussin et al., 2015). While there are many benefits associated with small reservoirs, there are some possible threats to the sustainability of these systems (e.g. siltation, the spread of water borne diseases, deterioration of water quality, etc.).

The key characteristics of small reservoirs, such as, their modest size, their wide distribution, the requirement for few parties to come together to operate them (local community management), and closeness to the point of use, among others, make these water resources operationally efficient with high flexibility in (semi-)arid regions with scattered rural population. In addition, in the regions, such as the one of interest here, small reservoirs are the only permanent open water bodies. While the wide distribution of these water systems in this region reinforces the positive impacts of small reservoirs in rural areas, this dispersion can be considered as an obstacle to access markets and ensuring farmers' position in value chains (Poussin et al., 2015).

Due to the small sizes, small inland water bodies (reservoirs and lakes) are usually neglected in hydrological and water resources management plans, especially in developing countries. Although the hydrological impact of an individual small reservoir is relatively

506469-L-sub01-bw-Abbasi
Processed on: 9-11-2016

1

small because it can capture only a small part of the total runoff, the existence of several hundreds of such structures may have a notable impact on a regional scale (Liebe et al., 2007a). These small shallow lakes are scattered in large numbers, and hence monitoring them could be difficult and costly on a regional scale. Often, there is limited information on small reservoirs due to the inadequate in-situ measurements which can lift our insight from qualitative to quantitative.

However, many decision makers feel that small reservoirs are unsuitable for rural water supply due to extremely high evaporation losses. A detailed investigation in the study area (as described in Section(1.2)) showed that evaporation losses are moderate (Liebe et al., 2007b; Abbasi et al., 2015b, 2016a). In addition, in this region, water is not considered to be a constraint, specially for irrigated agriculture, because the capacity of the reservoirs provide enough water for the irrigation schemes (Faulkner et al., 2008; Poussin et al., 2015). However, due to lack of maintenance of these systems and irrigation schemes, sub-optimal crop management, and poor product marketing the agronomic and economic performance of small reservoirs are far from perfect (Poussin et al., 2015).

1.2. REGION OF STUDY

The Upper East Region of Ghana (UER) is one of the poorest regions in the country with high population density. Annual rainfall is about 1100 mm, falling mainly in a single rainy season from late May to Mid-October. Annual reference evaporation can reach 2000 mm (Faulkner et al., 2008). Limited access to perennial rivers in this semi-arid region led to the construction of more than 160 small and shallow reservoirs which have surface areas ranging from 1 to 100 hectares. These reservoirs were constructed by the Ghanaian government and development partners in the late 1960s to early 1980s to improve the local farmers' livelihoods and enhance food security. They were constructed as multi-purpose water sources to promote dry season farming (crop and livestock), fishing and domestic water uses. However with recent changes in weather patterns, theses reservoirs which were to increase the resilience of the communities risk high evaporation losses.

In this research, Binaba dam, a small and shallow reservoir located in this region was chosen as a pilot for studying and developing the Small and Shallow Lake Framework (SSLF) (Figure 1.1). Lake Binaba provides water for fishing, domestic use and small-scale irrigation in the vicinity of a small town called Binaba (Figure 1.2). The lake surface area is 31 ha with an average and maximum depth of 1.1 m and 4.0 m, respectively, at full storage conditions. To monitor the meteorological parameters, a floating measurement station was installed over the water surface in Lake Binaba and utilized in validating the model developed. Measurements taken included atmospheric parameters namely wind speed at 2 m above the water surface (U_2), relative humidity (RH), air temperature (T_a), wind direction (WD), incoming short-wave radiation (R_s), water temperature profile (T_w), and sensible heat flux (H_s) using a 3-D sonic anemometer. The installed 3-D sonic anemometer recorded sensible heat flux over the water surface and accumulated over 30-minutes intervals at 10 Hz. The air temperature fluctuated from 18.0 to 40.0$^\circ C$ with an average of 28.7$^\circ C$, while the water surface temperature varied between 24.0$^\circ C$ and 32.5$^\circ C$, with an average of 27.5$^\circ C$ during the measurement period. Measurements were taken from November 23, 2012, to December 22, 2012. The wind speeds

during the study period were low to moderate with the South-Western direction as the most dominant direction with a maximum speed of 4.5 ms^{-1}. Since the wind speed values have been averaged on 30-minutes intervals, instantaneous wind speed may be larger.

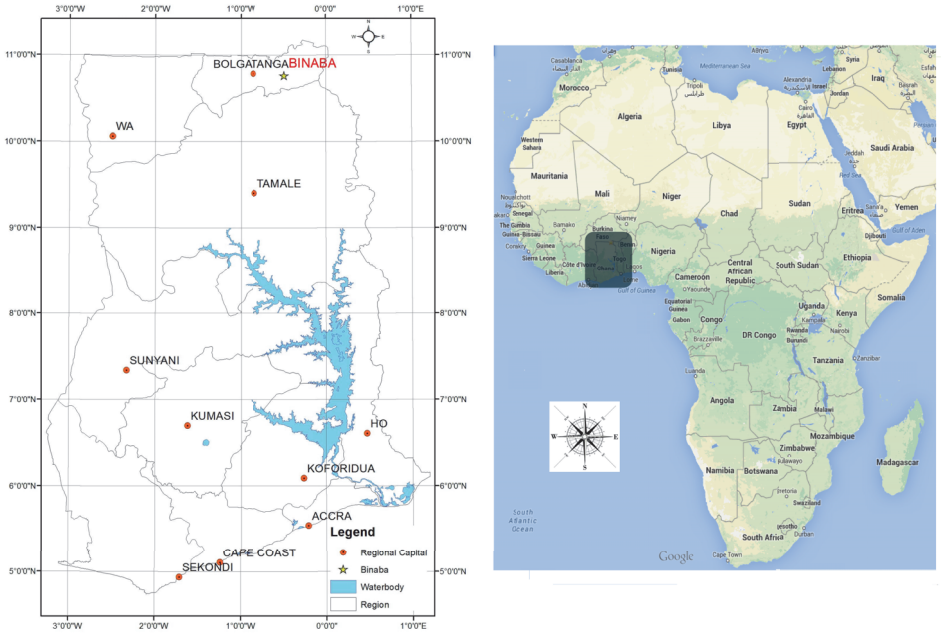


Figure 1.1: Location of Lake Binaba in Upper East Region of Ghana, West Africa.

1.3. ESTIMATING EVAPORATION FROM WATER SURFACE

Annual evaporation losses from lakes and reservoirs in arid and semi-arid regions could reduce up to 50% of the accumulated stored water (Fowe et al., 2015), and hence, it should be considered as the primary source of water loss which significantly affects the storage efficiency of these aquatic bodies. In order to assess the important role that these water resources can play at regional scale and to manage them efficiently, accurate estimation of evaporation is critically important. However, evaporation is perhaps the most difficult component of all hydrological cycle components to estimate, especially for small reservoirs.

Evaporation in small lakes is a function of Atmospheric Boundary Layer (ABL, wind speed, solar and atmosphere radiation, air temperature, water surface temperate, vapor pressure deficit, atmosphere stability conditions, lake surrounding environment, etc.) and the water body temperature dynamics. Contrary to large and deep lakes, small shallow reservoirs usually experience high fluctuation in ABL conditions because of the fast heating and cooling of these water bodies by the surrounding lands, as well as the usually low wind speeds over the water surface of small lakes. Due to these complex inter-

1

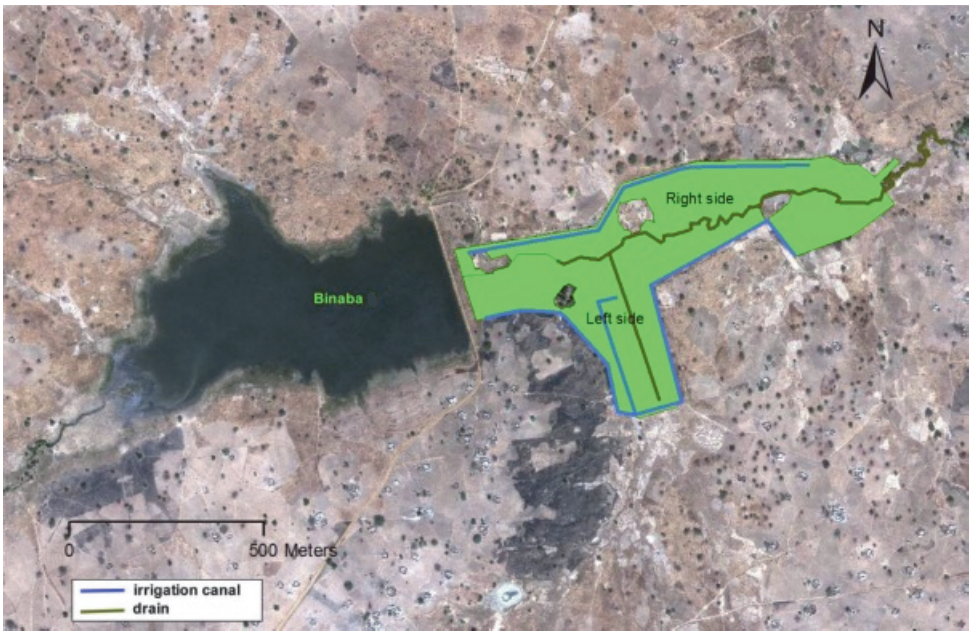


Figure 1.2: Lake Binaba and its irrigation scheme [adopted from Poussin et al. (2015)].

actions between the water surface and the above atmosphere, small inland water bodies are significantly influenced by the atmospheric boundary layer stability conditions. The unstable atmosphere over the water surface which could last for a long time, enhances the sensible and latent heat fluxes. A stable atmosphere reduces the heat fluxes from the water surface.

Since there is a complex interaction in water-atmosphere system and evaporation in small shallow lakes depends on many parameters, using the conventional methods for estimating evaporation leads to significant errors. Most of proposed methods to estimate evaporation from water surface were developed for large and deep lakes and in specific climatic conditions. Therefore, it is vital to develop a model for estimating evaporation from these small water surfaces considering their climatic and geometric conditions.

A wide range of approaches have been proposed for estimation of evaporation of open water surfaces with various complexity levels. These methods can be put into five general categories which include: (1) water budget (balance) method, (2) measurements, such as, evaporation pan and Eddy Covariance (EC) system, (3) energy balance and combination methods, (4) aerodynamic or mass transfer method, and (5) radiation and temperature-based methods. Investigating the applicability of these methods for small shallow water bodies, especially in arid and semi-arid regions, could help us choose the proper method for estimating evaporation. Generally, the water balance method is simple in theory but difficult in practice due to the required water budget components. In this method, evaporation is computed as the change in volume of water

stored and the difference between the inflows and outflows of the lake. The relative importance of the terms depend on the hydrological and physiographical settings. Direct measurement of evaporation at the air-water interface is often very expensive and has to be designed carefully to obtain reliable data. The energy balance and combination methods have been proven to be reliable in providing precise estimation of evaporation but these methods need a wide range of data sets as input parameters, such as, net radiation, conduction heat flux and the heat stored in the reservoir to estimate evaporation. So far, profiles taken by the temperature loggers have been used to calculate heat storage of water bodies. The aim of this study is to develop a computational method to provide the 3D temperature profiles during the study period.

In most of these methods, the models' parameters used are specific for the given water body, under the prevailing surrounding environment and climate. But these are valid only for the specific ranges of parameters (reservoir size, air and water surface temperature difference, humidity, atmosphere conditions, etc.) that are used in the designed experiment. This means that these coefficients may not provide satisfactory estimation for other regions. The parameters that affect evaporation rate from water surface can be grouped into two categories: (1) climatological and meteorological factors such as wind speed, temperature, relative humidity, etc. (2) geology and physiography of water bodies such as shape, depth, water quality, size, circulation in water body, advective and storage energy sources and sinks, and even the location. Water surface (the lake surface area) determines the effect of advective energy from the surrounding environment. The water depth is critical for heat storage and release. It means that to estimate evaporation accurately for (small) water surfaces all of these parameters should be considered. However, most available methods ignore the water bodies' various characteristics in evaporation estimation.

In order to accurately measure evaporation for the described water bodies, utilizing the available data, a mass-transfer based method is developed in this research. Developing the present model is done in two steps. In the first step, a mass-transfer (aerodynamic) based method is developed to consider the effects of atmospheric stability conditions on evaporation. In the second step, taking into account the properties of the water body and its surroundings as well as the atmospheric conditions, a generalizable approach is developed to obtain the wind function or transfer coefficients which are used in mass-transfer methods. It is expected that the mass and heat transfer coefficients obtained from this approach provide a dramatic increase in the accuracy of evaporation estimation for small reservoirs.

1.4. CFD APPROACH TO WATER SURFACE EVAPORATION ESTIMATION

The mass-transfer approach which needs moderate data as input, correlates evaporation to the vapour pressure deficit between the water surface and its atmosphere above, through a mass-transfer coefficient, usually considered as a linear function of wind speed referred to as the "wind function". A wide range of empirical mass-transfer formulae have been applied by researchers. Some of them attempted to propose generalizable wind functions by correlating the mass transfer coefficient to the surface area of the wa-

506469-L-sub01-bw-Abbasi
Processed on: 9-11-2016

1

ter body, but these proposed formulae usually are applicable only to the conditions similar to the places where the formulae or functions were parameterized. Considering this limitation and due to existence of the urgent need to estimate evaporation from small water surfaces it was deemed helpful to establish a cost effective and generalisable approach to determine reliable wind functions.

Computational Fluid Dynamics (CFD) is a very powerful computational tool and it is utilized in this research to obtain the heat and mass transfer coefficients between the atmospheric boundary layer (ABL) and the water surface (WS). Results from the proposed CFD model could be used to analyse the spatial and temporal variations of the convective and evaporative heat fluxes over the water surface and determine the effects of advection on heat fluxes from water surfaces, under arid and semi-arid conditions. The analysis is not possible by using traditional methods because most of them are "one dimensional" models with areal homogeneity assumption.

The current study presents a new applicable computational method based on CFD for calculating convective heat flux and mass transfer coefficients and consequently estimating evaporation rate from water surface using the estimated mass-transfer coefficient. Using the results of the proposed CFD method and a wind function which includes the water body specifications, environmental and meteorological conditions are extracted.

1.5. SMALL WATER BODY MODEL

Knowledge of the updated (real-time) information on various characteristics and temperature profiles of a lake are important for its operation and management. The ability of these water bodies to function depends on the quality of the water which can be influenced by the flow conditions, the temperature distribution and distribution of other compositions such as salinity. The thermal structure of water bodies, temperature stratification dynamics and changes in temperature values have a direct impact on the heat storage of lakes and their water quality. Estimating the heat stored in lakes and reservoirs is crucial to estimate evaporation in energy budget methods which are widely used. Moreover, the incorporation of turbulent transport phenomena in energy transfer in water bodies makes it important to understand the temperature distribution within the water body.

Understanding the conditions that exist within shallow water bodies calls for details of the flow through the water body, obtained either by measuring the flow parameters and temperature distribution or simulating the processes of stratification and circulation in the water body. Experimental temperature profiles in lakes are available, but the vertical and horizontal resolutions are often not sufficient for assessing small-scale turbulence effects or investigating variations of water temperature induced by radiative forcing, air temperature as well as wind velocity in shallow waters. As small shallow lakes and reservoirs respond to atmospheric conditions very fast, precise estimation of the heat transfer between the atmosphere and their surface is extremely important to model the temperature dynamics and stratification in these water bodies.

In this research, a fully three-dimensional and unsteady hydrothermal model is developed which is capable of simulating the effects of wind and atmospheric conditions over a complex bathymetry to predict the circulation patterns as well as the tempera-

506469-L-sub01-bw-Abbasi
Processed on: 9-11-2016

ture distribution in the water body. This framework is completely based on open-source software and covers all steps needed in the simulation, from generating applicable geometry to visualizing the results. All software used here are open-source and allow continuous community-based improvement of the model without any requirement for software licenses. The main toolkit used is OpenFOAM, a powerful CFD simulation toolkit, which uses the finite volume numerical schemes to solve the governing equations. The proposed CFD simulation requires an additional degree of complexity beyond a typical industrial CFD simulation due to the complexity of the natural processes that drive the system. Most of the driving forces in a shallow water body simulation such as solar radiation, wind speed, precipitation, cloud cover, air temperature and water surface temperature, variation in water composition (such as salinity and density) and the possibility of a stratified flow, vary in time and make it difficult to include their effects in the simulation.

1.6. ATMOSPHERIC BOUNDARY LAYER MODEL

In studying the small reservoirs, understanding the interaction of the atmospheric boundary layer with its underlying water surface is crucial. However, in most of the current mesoscale and global atmosphere models, the influences of small inland water bodies in the surface parametrization are neglected. Compared to the land surface, inland water surfaces such as small lakes and reservoirs have different interactions with the atmospheric boundary layer, considering the evaporation, wind speed and heat exchanges over water surfaces.

Due to the logistical difficulties and economical issues in operating measurements over water surfaces especially for small reservoirs, water-atmosphere interaction has generally received less attention than land-atmosphere interaction. Since measurements over the water surfaces are rarely available or are usually confined to a single point, developing a model to simulate the air-water surface system would be promising in order to obtain spatial information of air flow passing over different surfaces. In addition, this model could be used to estimate meteorological parameters over the small water surfaces where carrying out measurements is difficult and expensive and there is a need for a high level of expertise to obtain reliable measurements by using ground-based measurements.

However, implementing the small water surfaces in the Atmospheric Boundary Layer (ABL) models introduces extra complexities, which should be considered in the study region with a huge numbers of small water surfaces. One complexity which emerges from involving the water-atmosphere interaction in regional climate model comes from the fact that the presence of lakes has significant effects on the atmosphere dynamics due to the change of roughness length, moisture contents and temperature of water versus the land. The distribution of the sensible and latent heat fluxes can affect the flow on small, regional and global scales, where the exchanges of water, heat and momentum over grid cells should be improved for water surface.

A big challenge in simulations of atmospheric boundary layer over the heterogeneous surfaces (for instance land-water surface) is that there are sharp changes of the surfaces' properties from land to water surface and vice versa. In addition, small inland water bodies usually have a limited fetch and depending on the fetch values, the airflow

506469-L-sub01-bw-Abbasi
Processed on: 9-11-2016

over the lakes may or may not have time to adjust to its underlying water surface. In these cases, the horizontal inhomogeneity can be very important and the effect of this limited fetch still needs to be assessed. Such strong spatial differences in surface characteristics (temperature, wetness and roughness) affect the airflow and transfer processes of heat and water vapor, specifically the evaporation rates.

The model developed in this research, which is based on Computational Fluid Dynamics (CFD), aids in understanding the effect of inland water bodies on the surrounding atmosphere and vice versa. Using this model provides useful information on all flow parameters in the computational domain, which is difficult to achieve using experimental measurements. In addition, the state of the atmosphere and water surface as air passes from a dry surface to a wet surface (and vice versa) is taken into consideration. The effect of a surface transition and sharp changes in surfaces' properties on the flow which strongly depend on upwind and possibly downwind surface features, is investigated and the change in heat flux patterns over the water surface is assessed. Furthermore, the atmospheric stability conditions are included in the simulation to find how the stability conditions influence the airflow over a non-homogeneous surface.

Even though on-site measurements are preferred, the proposed computational model could be considered as a great supplement to field experiments, especially for regions where sufficient parameters are rarely available. In addition, effects of different parameters on the flow variables can be easily investigated using this model.

1.7. AIMS AND GOALS

In summary, the present thesis deals with a atmosphere-water system which consists of different parts. Regarding these components, the primary aims and objectives of this research can be summarized as following:

1. provide an accurate estimation of evaporation from small shallow water surfaces in arid and semi-arid regions by improving the mass transfer method and including the effects of atmospheric stability conditions (Chapter 2);

2. develop a cost-effective and generalizable approach (CFDEvap) for determining the heat and mass transfer coefficients (or wind function), which are used widely in mass transfer (aerodynamic) method for estimating evaporation from water surfaces (Chapter 3);

3. develop a three-dimensional CFD framework based on open-source tools and software for shallow small water bodies with arbitrary topography (bathymetry) to investigate the temperature and flow dynamics in water, in order to compute heat storage (heat budget) of lakes which could be utilized in energy balance methods for estimating evaporation from open water surfaces (Chapter 4);

4. applying and evaluating the performance of the model which is developed for small lakes in this research to simulate and analyse the temperature structure of Lake Binaba, a shallow small lake in Upper East Region of Ghana (Chapter 5);

5. develop an Atmospheric Boundary Layer (ABL) model which includes the stratification and atmospheric stability conditions to investigate the effects of surface

506469-L-sub01-bw-Abbasi
Processed on: 9-11-2016

heterogeneity (complexity) on airflow from land surface to water surface and vice versa. The results of this simulation would be used in prediction of over water meteorological parameters using ground based measured values (Chapter 6);

Regarding the computational issues, the major products of the present research are methods, codes, solvers, boundary conditions, various turbulence models, etc. developed to be used in Computational Fluid Dynamics simulations for both water bodies and Atmospheric Boundary Layer. All of these codes and tools are open-source and available free of charge to use and develop without any need for commercial license.

In Figure 1.3 structure and different components of this research are presented. The details of included components are presented in next chapters. The expected results of the integration of the parts which are discussed and elaborated in this research provide a promising increase in the accuracy of small water surfaces studies, through a generalizable and cost-effective methodology.

506469-L-sub01-bw-Abbasi
Processed on: 9-11-2016

1

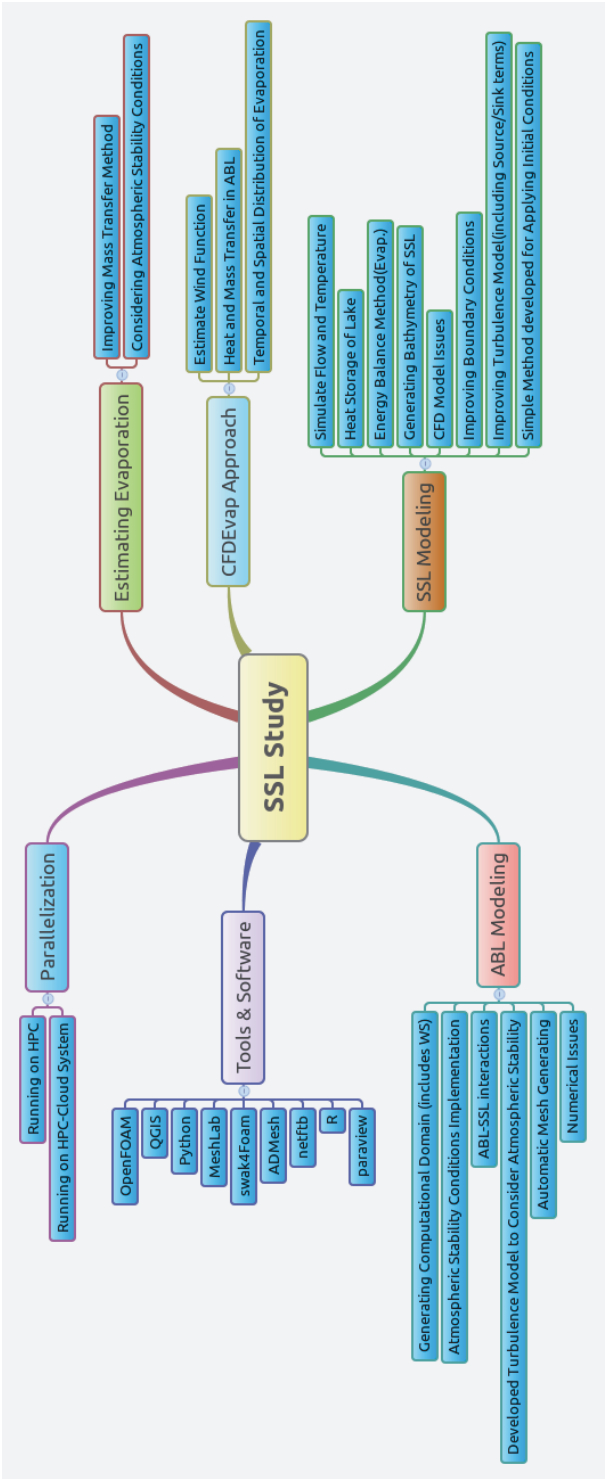


Figure 1.3: Structure and different components of current research (**ABL**: Atmospheric Boundary Layer; **SSLF**: Small Shallow Lake Framework; **CFDEvap**: CFD Evaporation Model; **WS**: Water Surface; **SSL**: Small Shallow Lake)

506469-L-sub01-bw-Abbasi
Processed on: 9-11-2016

2

EFFECTS OF ATMOSPHERIC STABILITY CONDITIONS ON HEAT FLUXES

2.1. INTRODUCTION

Small reservoirs, or lakes, in (semi-) arid regions provide a means to improve food security through irrigated agriculture and livestock farming. The storage efficiency of these small reservoirs is affected significantly by the primary source of water loss, evaporation (Liebe, 2009). In arid and semi-arid areas, annual evaporation losses from lakes and reservoirs could rise up to 50% of the accumulated stored water (Fowe et al., 2015; Gallego-Elvira et al., 2012; Martínez-Granados et al., 2011; Gokbulak and Ozhan, 2006; Mugabe et al., 2003). Accurate estimation of evaporation is critically important to assess the reliability of using small reservoirs to enhance water security for food production, especially in arid regions where they may constitute a substantial fraction of the regionally available water resources (Liebe et al., 2009). In spite of the importance of accurate estimations in water resources management, evaporation is perhaps the most difficult component of all hydrological cycle components to estimate because of the existence of complex interactions between the water surface-atmosphere system (Singh and Xu, 1997a). Small inland water bodies are influenced significantly by the atmospheric boundary layer stability conditions. The unstable atmosphere over the water surface enhances the sensible and latent heat fluxes and a stable atmosphere reduces the heat fluxes from the water surface (Brutsaert, 1982). In case of small inland water bodies, unstable atmospheric conditions could last for a long time (Rouse et al., 2003). Shallow and small lakes, usually experience high variabilities in atmospheric boundary layer stability conditions because of the fast heating and cooling of these water bodies

This chapter is based on Abbasi et al. (2016a): Abbasi, A.; Annor, F.O.; van de Giesen, N.: Effects of Atmosphere Stability Conditions on Heat Fluxes from Small Water Surfaces in (Semi-) Arid Regions. Hydrological Sciences Journal (Manuscript accepted for publication), 2016.

506469-L-sub01-bw-Abbasi
Processed on: 9-11-2016

by the surrounding lands, as well as the usually low wind speeds over the water surface of small lakes (Verburg and Antenucci, 2010).

The available methods for estimating evaporation from the water surface can be put into five categories which include: 1) water budget (balance) method; 2) measurements, like evaporation pan (Fu et al., 2009, 2004) and Eddy Covariance (EC) (Assouline et al., 2008; Blanken et al., 2000; McGloin et al., 2014; Stannard and Rosenberry, 1991); 3) energy balance and combination methods (Gianniou and Antonopoulos, 2007; Rosenberry et al., 2007); 4) aerodynamic or mass transfer method (Singh and Xu, 1997a); and 5) radiation- and temperature-based methods (Xu and Singh, 2001, 2000). The water balance method is simple in theory but difficult in practice (Finch and Calver, 2008). In this method, evaporation is computed as the change in volume of water stored and the difference between the inflows and outflows of the lake. The relative importance of the terms depend on the hydrological and physiographical settings (Finch and Calver, 2008). Direct measurement of evaporation at the air-water interface is often very expensive and has to be designed carefully to obtain reliable data. The energy balance and combination methods have been seen to be reliable in providing precise estimation of evaporation (Delclaux et al., 2007; Ali et al., 2008; Rosenberry et al., 2007) but these methods need a wide range of data sets as input parameters such as net radiation, conduction heat flux and heat storage of the water body (Gallego-Elvira et al., 2012; Vidal-López et al., 2012) to estimate evaporation. In most of these methods, the models' parameters used are specific for the given water body under the prevailing surrounding environment and climate, which are valid only for the specific ranges of parameters (reservoir size, air and water surface temperature difference, humidity, atmosphere conditions, etc.) that are used in the designed experiment (Vinnichenko et al., 2011). This means that, these coefficients may not provide satisfactory estimation for other regions (Sartori, 2000).

In this study, evaporation from small water bodies is estimated using an improved mass-transfer method considering the effects of atmospheric stability conditions. This method needs moderate input data and correlates evaporation to the vapour pressure deficit between the surrounding air and the water surface. Although, a wide range of empirical mass-transfer approaches have been applied by researcher, in most of these methods a linear function of wind speed referred as "wind function" with constant coefficients were applied to estimate evaporative heat fluxes from the water surface. Applying some of the common mass-transfer methods to estimate evaporation from the study lake (Lake Binaba) revealed that the differences between the estimated values from different methods were very high choosing a suitable method was therefore difficult. In addition, developing a method which includes time varying effects of atmospheric conditions on the transfer coefficient (or wind function which correlate the evaporation to the vapour pressure deficit between the water surface and the atmosphere) would be very promising especially for small lakes in data (measurements) scarcity conditions.

As in most small lakes (e.g. in the study region), the micrometeorological parameters measured over the water surface are rarely available, developing a method to estimate heat fluxes from water surface using only on land-based stations would be practical. Investigation the correlation matrix of (measured) water surface temperature values shows that water surface temperature could be estimated from the standard micrometeorological parameters measured over the surrounding lands. Using the estimated water sur-

face temperature as well as the measured ones, the heat fluxes from water surface were calculated and validated with processed sensible heat fluxes (considering the footprint filtering) measured over the water surface.

The developed approaches (for both water surface calculation from land-based measurements and the heat flux estimation from small water surfaces) were used to estimate heat fluxes from a small water body in Northern Ghana and Southern Burkina Faso. As the method developed in this study uses only land-based measurements, it could be easily applied to estimate heat fluxes from small water surfaces using the available measurements and the small reservoirs' conditions in this area. In addition, this approach with some minor modification (for instance in the equation used to calculate the water surface temperature) is generalizable and cost-effective and can be used for other similar inland water bodies.

To determine the effects of atmospheric stability on estimated heat fluxes, sensible and latent heat fluxes were estimated during the study period (November 23, 2012 to December 22, 2012) using the proposed improved mass-transfer (bulk aerodynamic) method for a shallow and small lake in Binaba (Ghana). Using the proposed (aerodynamic) method and standard micrometeorological variables measured over the lake surroundings (air temperature, wind speed, relative humidity and air pressure) the sensible and latent heat fluxes were calculated taking into account the stability conditions of the atmospheric boundary layer over the water surface. To determine the influence of atmospheric stability conditions on the estimated heat fluxes from the water surface, the components and parameters were adjusted for the study site conditions. The mass transfer coefficient was adjusted using stability functions to include the atmospheric stability conditions in estimating evaporation.

In addition, the time-dependent atmosphere's conditions and water surface characteristics were used in the model to improve the developed algorithm for estimating the evaporation.

Considering the importance of heat fluxes (e.g. evaporation) estimation from small water surfaces and the difficulties available to do that, the main aims of the current work are: 1) to develop a model for calculating the water surface temperature in small lakes using only the standard land-based measurements to close the gap in needed data for heat fluxes estimation; 2) to develop a generalizable and cost-effective method to estimate heat fluxes from inland water surfaces; 3) to consider the effects of atmospheric stability conditions on the heat fluxes; 4) to analyse heat flux data footprint and data-filtering issues of measured heat fluxes to use them in model validation. To evaluate the performance of the model against the observed values of sensible heat flux, some quantitative metrics, including root mean square error (RMSE), mean absolute error (MAE), index of agreement (d) and the bias values were applied. In addition, the performance of the model were investigated in different atmospheric stability conditions. From these metrics, the results show that the simulated sensible heat fluxes are in good agreement with the observed ones.

2.2. ATMOSPHERIC STABILITY CONDITION

Atmospheric stability over the water surface has an impact on the sensible and latent heat fluxes from the water body. When the skin (water surface) temperature (T_{ws}) is

higher than air temperature (T_a), the atmospheric boundary layer is unstable and convective. The air and water surface temperature (skin temperature) differences could be used as a measure of atmospheric stability (Derecki, 1981; Croley, 1989). In an unstable atmospheric boundary layer, commonly the water surface temperature is higher than the air temperature. However, using the differences between the absolute water surface temperate and air temperate is not strictly correct since the effects of wind speed and relative humidity play key roles in the atmospheric stability.

One of the most popular frameworks for describing the atmospheric stability conditions is the Monin-Obukhov Similarity Theory (MOST) that relates changes of vertical wind speed gradients, temperature and water vapor concentration. The Obukhov length (L in m) is the parameter used to define atmospheric stability. L is linked to a dimensional analysis of the turbulent kinetic energy (TKE) equation and the ratio of the shearing and buoyancy effects (Stull, 1988). Monin and Obukhov (1959) suggested that the vertical changes of mean flow parameters and turbulence characteristics in the atmospheric boundary layer could depend only on the surface momentum flux or measured friction velocity (u_*), sensible heat (H) and latent heat (E) fluxes and height (z):

$$L = \frac{-u_*^3 \rho_a T_{av}}{\kappa g \left[\left(\frac{H}{C_p}\right) + 0.61 \times \frac{(T_a + 273.16)E}{\lambda}\right]} \tag{2.1}$$

which could be an indicator of the ratio of the turbulent kinetic energy reduction due to wind mixing and the atmospheric stratification growth due to the heat flux (Brutsaert, 1982). In this equation, ρ_a is air density (kgm^{-3}), u_* is friction velocity (ms^{-1}), κ is the von Karman constant (≈ 0.41), T_{av} is the virtual air temperature (K), H is sensible heat flux (Wm^{-2}), E is latent heat flux (Wm^{-2}), C_p is the specific heat of air ($Jkg\,K^{-1}$), g is the gravitational acceleration ($\approx 9.81\,ms^{-2}$), T_a is air temperature ($^\circ C$) and λ is latent heat of vaporization of water ($\approx 2264.76\,Jkg^{-1}$). According to the values of L, the stability is usually classified as reported in Table 2.1. In most cases, the non-dimensional stability parameter ($\zeta = z/L$ where z is the height above the water surface in m) can be used as an indicator for atmospheric stability (as shown in Table 2.1). To consider the effect

Table 2.1: Stability classification of atmospheric boundary layer, adopted from Barthlott et al. (2007).

$L[m]$	$\zeta[-]$	Stability Class	Characteristics
$L<0$	$\zeta<0$	unstable	unstable and convective ABL, enhancing the vertical heat fluxes
$L>0$	$\zeta>0$	stable	stable boundary layer, reducing the vertical heat fluxes
$L\to\infty$	$\zeta=0$	neutral	atmospheric transfer coefficients are equal to their neutral values
$L\to-\infty$	$\zeta=0$	neutral	atmospheric transfer coefficients are equal to their neutral values

of water vapor concentration, L is calculated using the virtual temperature instead of absolute temperature to take into consideration the fact that the density of moist air is smaller than that of dry air (Monteith and Unsworth, 2008). The virtual air temperature (T_{av}) can be calculated as:

$$T_{av} = (T_a + 273.16)\left[1 + 0.61 q_z\right] \tag{2.2}$$

and similarly, the virtual temperature of saturated air at the water surface (T_{wsv}) is given by:

$$T_{wsv} = (T_{ws} + 273.16)\left[1 + 0.61 q_s\right] \tag{2.3}$$

and the virtual air-surface temperature difference is written as following

$$\Delta T_v = T_{wsv} - T_{av} \tag{2.4}$$

where T_{av} is the virtual air temperature in K , T_{wsv} is the virtual temperature of saturated air at the water surface in K , ΔT_v is the virtual air-surface temperature difference (in K), T_a and T_{ws} are air temperature and water surface temperature respectively ($^\circ C$), q_s is saturated specific humidity at water surface temperature ($kg\,kg^{-1}$) which can be calculated using Equation (2.10), and q_z is specific humidity of air ($kg\,kg^{-1}$) calculated from Equation (2.11). Although the water surface temperature is needed to compute the atmosphere stability parameter, its measurements are rarely available in case of small and shallow lakes. However, in the study lake water surface measurements are available, to close the gap in the input data especially for water surface temperature, a correlation approach was developed in this study to estimate this variable from micrometeorological parameters measured over the nearby lands (Section (2.7)).

2.3. DESCRIPTION OF STUDY SITE AND DATA COLLECTION

The Upper East Region of Ghana (UER) (shown in Figure 1.1) has more than 160 small and shallow reservoirs which have different surface areas ranging from 0.01 to 1.0 km^2 (Annor et al., 2009). These small reservoirs have the advantage of being operationally efficient with their flexibility, closeness to the point of use, and requirement for few parties for management (Keller et al., 2000). The studied lake is a small and shallow reservoir located in this region. Lake Binaba ($10°53'20''N$, $00°26'20''W$) is an artificial lake, used for water supply, irrigation, livestock watering, construction, fishing, domestic uses and recreation. A natural stream has been dammed, storing and providing water for all these uses in Binaba, a small town in the sub-humid region of Ghana (van Emmerik et al., 2013). The lake surface area is around 306000 m^2 with an average and maximum depth of 1.1 m and 4.0 m respectively. The length of lake in $x-$ and $y-$directions (as length and width) are around 900.0 m and 600.0 m respectively (Figure 2.1).

To measure the heat fluxes as well as the atmospheric stability conditions over the lake, a 3-D sonic anemometer was installed at 1.90 m height above the water surface. Measurements (and the computed variables) taken by 3-D sonic anemometer included turbulent fluctuations of vertical wind, sonic temperature, sensible heat flux, momentum flux, Obukhov length (or equivalently stability parameter), the source areas of 80% of the integrated flux (footprint), etc.. The installed 3-D sonic anemometer recorded the measurements (e.g. sensible heat flux) over the water surface at 10 Hz and accumulated over 30-minutes intervals. The raw eddy correlation data was processed by Alteddy software (version 3.90) (Elbers, 2016, 2002). As processing the raw eddy correlation data is beyond the goals of this work, the reader is referred to Annor et al. (2016) for more details and challenges on processing this data over small water surfaces. After processing the raw eddy correlation data, the footprint analysis should be executed to select only the measurements which represent the water surface (Section (2.9.1)). Finally, the filtered

and processed data (sensible heat flux) was used to validate the computed sensible heat fluxes using the proposed model.

In addition, the atmospheric parameters which are needed as input in the model should be measured. The standard climatic parameters include air temperature, relative humidity, wind speed and wind direction and were recorded on surrounding the lake (over the land) approximately at height of 2.0 m above the ground (Figure 2.1). The installed automatic weather station (AWS) on the land was provided with a solar radiation sensor (model PYR from Decagon Devices, USA; ±5%) for solar radiation flux density (in Wm^{-2}) measurement, a humidity/temperature sensor (model VP-4 from Decagon Devices, USA; ±2% and ±0.25 $^{\circ}C$ for humidity and temperature respectively) for air humidity measurement and the air temperature, and a sonic anemometer (model DS2 from Decagon Devices, USA; ±3% and ±3 degrees for wind speed and wind direction respectively) to measure wind speed and its direction. The microclimatic parameters (air temperature, relative humidity, wind speed and its direction) were averaged on 30-minutes intervals and used as input values in the proposed model.

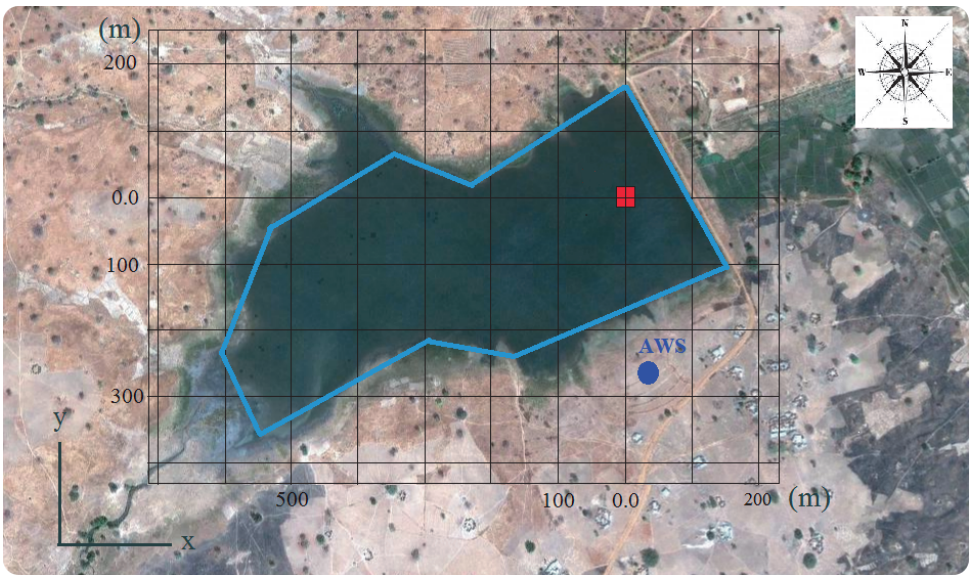


Figure 2.1: Shape of Lake Binaba and its surroundings (Google, 2015). Location of floating 3-D sonic anemometer and land-based automatic weather station (AWS) are shown with filled red square and blue circle respectively on the map. Blue region shows area over water surface which was used in footprint analysis of heat flux data as explained in Section (2.9.1). The lengths shown on map are in m.

As water surface temperature is a crucial parameter in calculating heat fluxes (especially for sensible heat), it has been measured during the study period. The water surface values were measured by HOBO tidbit v2 temperature loggers with nominal accuracy of ±0.2$^{\circ}C$ (HOBOTidbiT, 2015). The measured water surface temperature values were used in the model to estimate heat fluxes. In addition, these measured values were used to

validate the calculated water surface temperature values by using the standard meteorological parameters measured in the AWS installed over the surrounding land (Section (2.7)).

During the study period (from November 23, 2012 to December 22, 2012) the air temperature fluctuated from 18.0 to 40.0 $^{\circ}C$ with an average of 28.7 $^{\circ}C$ while the water surface temperature varied between 24.0 $^{\circ}C$ and 32.5 $^{\circ}C$ with an average of 27.5 $^{\circ}C$ during the measurement period. Figure 2.2(a) shows the diurnal changes of water surface temperature and air temperature, with daily variations of approximately 10 $^{\circ}C$. The wind speed values recorded by the land-based automatic weather station (AWS) are shown in Figure 2.2(b) with South-Western direction being the most dominant direction with a maximum speed of 3.5 ms^{-1} (the maximum wind speed measured over the water surface was 4.5 ms^{-1}). Since the wind speed values have been averaged on 30-minutes intervals, instantaneous wind speed may be larger.

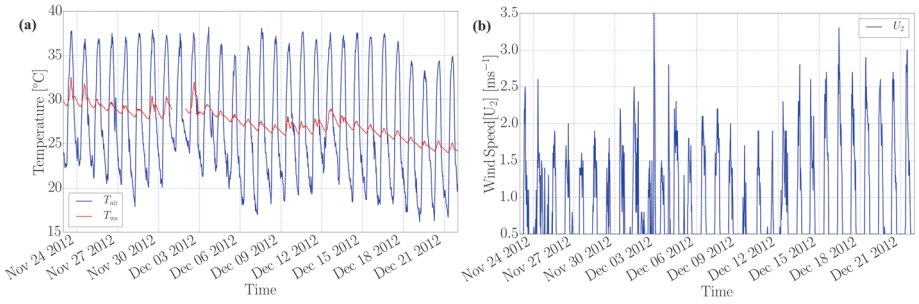


Figure 2.2: **(a)** Measured water surface and air temperature at 2.0 m above land surface; **(b)** Measured wind speed at 2.0 m above land surface during the simulation period. Wind speed values have been averaged on 30-minutes intervals.

2.4. BULK AERODYNAMIC METHOD

Field studies of sensible and latent heat fluxes from water surfaces comprise a large body of literature. One of the most suitable methods with moderate input data is the bulk-aerodynamic transfer method. The bulk-aerodynamic approach, which is based on the Dalton-type equation and Fick's first law of diffusion, can be used to estimate sensible heat and latent heat fluxes through a fixed boundary layer such as that developed over the free water surface of a reservoir (Dingman, 2015). It is based on the concept of mass transfer theory, which states that the diffusion of heat and water vapor into the atmosphere moves from where its concentration is larger to where its concentration is smaller at a rate that is proportional to the spatial gradient of that concentration. This method is straightforward because it relies on relatively routine measurements of wind speed, air temperature, relative humidity, and water surface temperature. In except for the water surface temperature, all needed input parameters are measured over the surrounding land. In addition, for water surface measurements, as they are not available in most cases, a model developed in this study can be used. Assuming that the boundary layer over a smooth water surface is similar to that over a rough water surface, the following

equations could be used to calculate sensible and latent heat fluxes (Hicks, 1975):

$$H = \rho_a C_p C_H U_z (T_{ws} - T_a) \tag{2.5}$$

$$E = \rho_a \lambda C_E U_z (q_s - q_z) \tag{2.6}$$

where T_a is air temperature ($^\circ C$), T_{ws} is water surface temperature ($^\circ C$), H is the sensible heat flux ($W\,m^{-2}$), E the latent heat flux ($W\,m^{-2}$), C_H and C_E are the (bulk) transfer coefficients for sensible heat and latent heat respectively (dimensionless), U_z is wind speed at height z above the water surface (ms^{-1}), C_p is the specific heat of air (≈ 1006.43 $Jkg^{-1}K^{-1}$), ρ_a density of air (kgm^{-3}), λ latent heat of vaporization of water (Jkg^{-1}), q_s saturated specific humidity at water-surface temperature ($kg\,kg^{-1}$) and q_z is specific humidity ($kg\,kg^{-1}$).

Density of air (ρ_a) can be calculated as follow:

$$\rho_a = 100 \times \left(\frac{P_{atm}}{R_a (T_a + 273.16)} \right) \tag{2.7}$$

where

$$R_a = 287.00 \times \left[1 + 0.608 q_z \right] \tag{2.8}$$

P_{atm} is atmospheric pressure (Pa) and R_a is gas constant for moist air ($Jkg^{-1}K^{-1}$). Latent heat of vaporization of water (λ) is a function of temperature and can be given by:

$$\lambda = 2.501 \times 10^6 - 2361 \times T_a \tag{2.9}$$

where T_a is in $^\circ C$. Specific humidity for water surface temperature and air temperature can be obtained from:

$$q_s = \frac{0.6108 e_{sat}}{P_{atm}} \tag{2.10}$$

$$q_z = \frac{0.6108 e_a}{P_{atm}} \tag{2.11}$$

where e_{sat} is saturated vapor pressure at T_{ws} in kPa, e_a actual vapor pressure (kPa) and e_s saturated vapor pressure at T_a in kPa:

$$e_{sat} = 0.6108 \times \exp \left[\frac{17.269 T_{ws}}{T_{ws} + 237.3} \right] \tag{2.12}$$

$$e_a = e_s \times \frac{RH}{100.0} \tag{2.13}$$

$$e_s = 0.6108 \exp \times \left[\frac{17.269 T_a}{T_a + 237.3} \right] \tag{2.14}$$

where T_a and T_{ws} should be in $^\circ C$. To estimate latent heat flux in ms^{-1} the following equation can be used:

$$E^* = \frac{E}{\rho_w \lambda} \tag{2.15}$$

where ρ_w (in kgm^{-3}) is water density and given by Henderson-Sellers (1986):

$$\rho_w = 1000.0 \times \left(1 - 1.9549 \times 10^{-5} |T_{ws} - 3.84|^{1.68} \right) \tag{2.16}$$

where the water surface temperature (T_{ws}) is in $^{\circ}C$.

Heat and mass transfer coefficients are influenced by the atmospheric stability conditions over the lake and therefore it could be affected by the gradients of temperature and humidity over the water surface as well as the wind speed values. In the following section, an algorithm is proposed to calculate the transfer coefficients adjusted to the site-specific measurements and modify them according to the stability conditions over the water surface. The proposed framework is based on the algorithms that are commonly used for estimating sensible and latent heat fluxes from oceans and large lakes (Zeng et al., 1998; Fairall et al., 1996; Renfrew et al., 2002). These methods rarely have been used to estimate evaporation from small lakes in arid and semi-arid regions. The proposed algorithm is able to: 1) take into account the roughness lengths of momentum, water vapor and temperature (Brutsaert, 1982); 2) adjust the air density, water density, water vapor pressure and other parameters included for local conditions; 3) consider the effects of different parameters and their interactions; 4) start with neutral transfer coefficients and then adjust them for different stability conditions; and 5) use land-based measurements to estimate heat fluxes from small water surfaces where measuring these parameters are rarely available.

The input parameters required for the model are: water surface temperature (T_{ws} [$^{\circ}C$]), air temperature (T_a[$^{\circ}C$]), wind speed measured at height z (typically 2.0 or 10.0 m) above the surrounding land (measured by land-based weather station) ($U_z[ms^{-1}]$), relative humidity (RH[%]) and air pressure ($P_{atm}[Pa]$). These parameters can be measured by land-based weather stations installed surrounding the water surface (Figure 2.1). Water surface temperature can be used in the model either from the measured values or by applying the proposed model in this study.

2.5. NEUTRAL TRANSFER COEFFICIENTS

Comparing the actual (include the stability effects) and neutral (assuming neutral conditions, N) heat fluxes from small water surfaces gives a clear idea on the effects of atmospheric stability conditions on heat fluxes. In this study, firstly the neutral heat fluxes were computed and then have been adjusted for stability conditions. Neutral transfer coefficients for momentum and heat fluxes in atmospheric boundary layer are determined from:

$$C_{DN} = \left(\frac{u_*}{U_z}\right)^2 = \left(\frac{\kappa}{\ln(z/z_{0m})}\right)^2 \tag{2.17}$$

$$C_{EN} = \frac{\kappa^2}{\ln(z/z_{0m}).\ln(z/z_{0q})} = \frac{\kappa C_{DN}^{1/2}}{\ln(z/z_{0q})} \tag{2.18}$$

Under near neutral conditions the transfer coefficients for sensible heat (C_{HN}) and latent heat (C_{EN}) are assumed equal (Zeng et al., 1998; Verburg and Antenucci, 2010);

$$C_{HN} = C_{EN} \tag{2.19}$$

where C_{DN} is neutral drag (momentum) coefficient (dimensionless), C_{EN} neutral latent heat transfer coefficient (dimensionless), C_{HN} the neutral transfer coefficient for sensible heat (dimensionless), κ is the non-dimensional von Karman constant (≈ 0.41), z the

measurement height of climate variables (2.0 m above the land surface), z_{0m} is roughness length of momentum (m), z_{0q} is roughness length for water vapor (m) and g is the gravitational acceleration ($\approx 9.81\, ms^{-2}$). Air shear velocity (friction velocity, u_*) in ms^{-1} is obtained from

$$u_* = \left(C_D U_z^2\right)^{1/2} = \frac{\kappa U_z}{\ln(z/z_{0m})} \tag{2.20}$$

and the functional form of Smith (1988) is implemented to estimate momentum roughness length (z_{0m}) (Zeng et al., 1998; Smith, 1988):

$$z_{0m} = \alpha\left(\frac{u_*^2}{g}\right) + \beta\left(\frac{\nu}{u_*}\right) \tag{2.21}$$

where α represents the Charnock constant ($\alpha = 0.013$) (Zeng et al., 1998) and β is a constants ($\beta = 0.11$). The roughness length of humidity (and temperature) is giving by the functional form of Brutsaert (1982):

$$\ln\frac{z_{0m}}{z_{0q}} = b_1 Re_*^{1/4} + b_2 \Rightarrow z_{0q} = z_{0m} exp\left(b_1 Re_*^{1/4} + b_2\right) \tag{2.22}$$

where $b_1 = -2.67$ and $b_2 = 2.57$ are constant and Re_* is roughness Reynolds number calculated by:

$$Re_* = \frac{u_* z_{0m}}{\nu} \tag{2.23}$$

Kinematic viscosity of air ($\nu[m^2 s^{-1}]$) can be obtained as

$$\nu = \frac{\mu}{\rho_a} \tag{2.24}$$

where dynamic viscosity of air ($\mu[N\, s\, m^{-2}]$) is computed from a linear function of air temperature (T_a in $^\circ C$) (Verburg and Antenucci, 2010):

$$\mu = 4.94 \times 10^{-8} T_a + 1.7184 \times 10^{-5} \tag{2.25}$$

In neutral conditions the roughness length for temperature (z_{0h}) is assumed to be the same as that for water vapor (z_{0q}) (Zeng et al., 1998; Verburg and Antenucci, 2010);

$$z_{0h} = z_{0q} \tag{2.26}$$

As mentioned previously, in the proposed algorithm the neutral transfer coefficients are estimated at the first step and then modified for the atmospheric stability conditions. To start the computation procedure an initial value for friction velocity (u_*) is needed. Therefore the computation was started with an initialized u_* using Amorocho and De Vries (1980) equation with wind speed at 10.0 m (U_{10}):

$$u_* = U_{10}\left(0.0015\left[1 + \exp\left[\frac{U_{10} + 12.5}{1.56}\right]^{-1}\right] + 0.00104\right)^{-2} \tag{2.27}$$

where U_{10} is wind speed at 10.0 m above the land surface which can be estimated from U_z by (Schertzer et al., 2003; Verburg and Antenucci, 2010):

$$U_{10} = U_z\left(\frac{10}{z}\right)^{(1/7)} \tag{2.28}$$

after obtaining z_{0m} by

$$U_{10} = U_z \frac{\ln(10/z_{0m})}{\ln(z/z_{0m})} \tag{2.29}$$

Using this initial value of u_* with Equations (2.20) and (2.21) a simple iteration loop is performed to calculate the momentum roughness length to get the desired convergence criteria (within 0.001% of the previous value). After calculating the z_{0m} using this algorithm, the neutral transfer coefficients can be estimated.

2.6. MODIFYING TRANSFER COEFFICIENTS FOR ATMOSPHERIC STABILITY CONDITIONS

An unstable atmosphere can enhance heat and mass transfer over the water surface. To consider the effects of atmospheric stability on heat fluxes, the heat and mass transfer coefficients are modified regarding the atmospheric stability conditions. This is done using stability functions (Brutsaert, 1982; Dyer, 1967; Businger et al., 1971). There are many stability functions (Ψ) for stable and unstable conditions of atmospheric boundary layer. In this study the following stability functions were used:

- for stable conditions ($\zeta > 0$), all transfer stability functions for momentum, heat and mass, respectively (Ψ_M , Ψ_T and Ψ_E) are assumed to be equal (Dyer, 1967; Businger et al., 1971) and given by:

$$\Psi_M = \Psi_T = \Psi_E \begin{cases} -5\zeta & \text{if} \quad 0 < \zeta \leq 0.5, \\ 0.5\zeta^{-2} - 4.25\zeta^{-1} - 7\ln\zeta - 0.852 & \text{if} \quad 0.5 < \zeta \leq 10, \\ \ln\zeta - 0.76\zeta - 12.093 & \text{if} \quad \zeta > 10, \end{cases} \tag{2.30}$$

- for unstable atmospheric boundary layer ($\zeta < 0$) the equations below could be used:

$$\Psi_M = \ln\left[\frac{(1+x^2)}{2}\right] + 2\ln\left[\frac{(1+x)}{2}\right] - 2\arctan(x) + \frac{\pi}{2} \tag{2.31}$$

$$\Psi_T = \Psi_E = 2\ln\left[\frac{1+x^2}{2}\right] \tag{2.32}$$

where

$$x = (1 - 16\zeta)^{1/4} \tag{2.33}$$

Using the atmospheric stability functions, the modified transfer coefficients can be written as:

$$C_D = \frac{\kappa^2}{[\ln(z/z_{0m}) - \Psi_M]^2} \tag{2.34}$$

$$C_E = \frac{\kappa^2}{[\ln(z/z_{0m}) - \Psi_M] \times [\ln(z/z_{0q}) - \Psi_E]} = \frac{\kappa C_D^{1/2}}{[\ln(z/z_{0q}) - \Psi_E]} \tag{2.35}$$

$$C_H = C_E \tag{2.36}$$

2.7. WATER SURFACE TEMPERATURE

In Section (2.4) the proposed approach for computing the heat fluxes from water surfaces was explained. As it can be seen, water surface temperature is a crucial parameter for sensible heat flux estimation. In addition, this parameter is required in advance to determine the atmospheric stability conditions for modifying the transfer coefficients (Section (2.6)). However, in most inland water surfaces especially for small shallow ones in developing regions, due to the logistical difficulties and economic issues in operating measurements over the lakes, water surface temperature measurements are rarely available. In order to address this issue, a simple correlation model was used in this study. This model contains only the over land measured micrometeorological parameters. As the water surface temperature as well as the standard meteorological parameters were available during the study period, the correlation matrix is established to find the main variables influencing the water surface temperature. The correlation coefficients between the water surface temperature and micrometeorological variables measured on land are presented in Table 2.2. As shown in Table 2.2, the water surface temperature is mainly influenced by the air temperature (T_a), relative humidity (RH) and incoming short-wave radiation (R_s) respectively whereas the effect of wind speed which mostly was low could be ignored.

Table 2.2: Correlation matrix of (measured) water surface temperature values in Lake Binaba with micrometeorological parameters measured in nearby land station.

Parameter	$T_a[^\circ C]$	$T_{ws}[^\circ C]$	$U_2\,[ms^{-1}]$	RH [%]	$R_s\,[Wm^{-2}]$
Air Temperature (T_a)	1.000	0.458	0.529	-0.503	0.617
Water Surface Temperature (T_{ws})	**0.458**	**1.000**	**-0.006**	**0.300**	**0.130**
Wind Speed (U_2)	0.529	-0.006	1.000	-0.467	0.708
Relative Humidity (RH)	-0.503	0.300	-0.467	1.000	-0.578
Incoming Short-wave Radiation (R_s)	0.617	0.130	0.708	-0.578	1.000

After evaluating the different regression models to find the best fit to the measured values (using R software), the following equation was obtained:

$$T_{ws} = \left[2.187 \times T_a - 0.0631 \times T_a^2 + 0.001 \times T_a^3\right] + [0.006 \times R_s] + \left[0.377 \times RH - 0.005 \times RH^2\right] - 6.159; \qquad R^2 = 0.690 \tag{2.37}$$

where T_{ws} is water surface temperature in $^\circ C$, T_a is air temperature in $^\circ C$, R_s is incoming short-wave radiation in Wm^{-2} and RH is relative humidity (%).

To test the performance of the water surface temperature model, it was applied for another small lake in the study area, Lake Winkogo ($10^\circ 42' 48'' N$, $00^\circ 51' 32'' W$) (the distance between these two lakes is around 60.0 km and the meteorological conditions are the same). Similar to the Lake Binaba, the water surface temperature values as well as the micrometeorological parameters measured over the surrounding land were available in Lake Winkogo (Annor et al., 2016). Several measures of the (water surface temperature) model performance evaluation are presented in Table 2.3 for Lake Binaba as well as the Lake Winkogo.

According to the evaluation measures presented in Table 2.3, the calculated water surface temperature values are in satisfactory agreement with the measured ones (Ali

506469-L-sub01-bw-Abbasi
Processed on: 9-11-2016

Table 2.3: Evaluation of water surface temperature model performance. This model was validated for two similar lakes in the study area, Lake Binaba and Lake Winkogo (MAE: mean absolute error; $RMSE$: root mean square error; d: index of agreement, R^2: Coefficient of determination; E: Nash-Sutcliff coefficient).

Study Lake	$RMSE\,[^\circ C]$	$MAE\,[^\circ C]$	E	R^2	d	$Bias$
Lake Binaba	1.029	0.850	0.651	0.713	0.880	-0.271
Lake Winkogo	1.582	1.302	0.453	0.584	0.800	-0.604

et al., 2015) and can be used in the estimation of heat fluxes from water surfaces (Section (2.4)).

2.8. MODEL ALGORITHM

In Equation (2.1), Obukhov length (L) is a function of sensible (H) and latent (E) heat fluxes. Therefore stability functions are functions of sensible and latent heat fluxes over the water surface. The calculating procedure is initiated with neutral transfer coefficients for momentum, heat and mass, respectively (C_{DN}, C_{HN} and C_{EN}) and followed by the neutral sensible and latent heat fluxes (H_N and E_N). Utilizing the neutral values, an iteration loop on L is established. In each iteration, air shear velocity (u_*), roughness lengths for momentum, temperature and water vapor (z_{0m}, z_{0h}, z_{0q}), modified transfer coefficients (C_D, C_H, C_E), sensible (H) and latent (E) heat fluxes are recalculated and applied to recalculate L and the stability functions (Ψ). These iterations are continued until L converges to within 0.0001% of the previous value of L. The framework of the model is depicted in 2.3.

2.9. MODEL VERIFICATION AND VALIDATION

The main advantage of the new model developed in this study is to estimate evaporative heat flux as well as the sensible heat flux from the small water surfaces. This model needs only standard micrometeorological parameters measured over the land surrounding the inland water surface. In addition, water surface temperature can be used in the model either from measurements or from the proposed approach (as described at Section (2.7)) in this study. In Lake Binaba, beside the standard meteorological parameters over the land, sensible heat fluxes were measured over the water surface during the study period using 3-D sonic anemometer (Section (2.3)). The observed sensible heat fluxes were used to validate the estimated convective heat fluxes from the water surface. Regarding the footprint of heat fluxes over the water surface, the measured heat fluxes should be filtered before being used in model validation.

2.9.1. HEAT FLUX DATA FILTERING

In this study,the measured sensible heat flux values were used to validate the calculated heat fluxes (sensible heat flux, H) from the water surface. Due to the non-sufficient (finite) dimensions of the lake Binaba in wind direction to be sure that the fluxes come only from the water surface, the heat fluxes data taken over the water surface should be processed before being used in validation process. The measured fluxes by represent

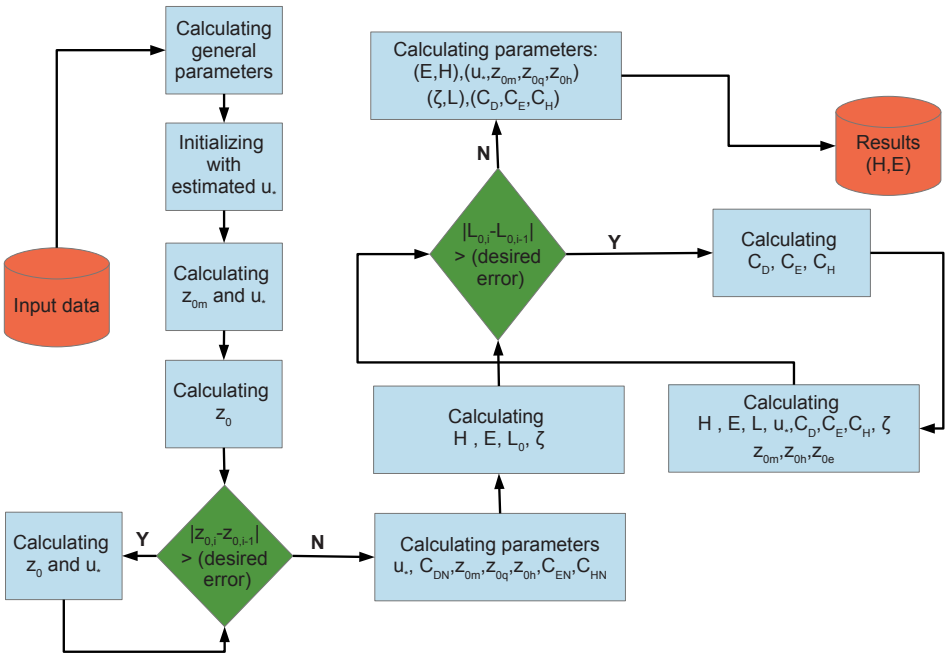


Figure 2.3: Proposed framework to estimate heat fluxes from water surface considering atmospheric stability conditions.

the upwind area fluxes which called footprint (FP). The dimensions and location of the measured heat flux footprints depend on the height of measurement, wind speed and its direction, surface properties, and atmospheric stability conditions (Vesala et al., 2008). For small lakes with limited dimensions (e.g. lake Binaba with less than 500 m) in predominant wind direction, footprint analyzing of the heat flux measurements is a crucial concept. To select the reliable fluxes which represent the fluxes from only the water surface the following steps were used to filter the sensible heat flux measurements (after processing the raw data as mentioned in Section (2.3)):

1. Different ranges for wind direction were defined. For these ranges, the upwind distances (X_{ud} in m) which include only the water surface were determined according to the geometry of the lake and its shape as well. The extensions of this area which includes only fluxes coming from the water surface is shown with blue lines in Figure 2.1.

2. Using the prepared Python code, for each ranges of wind direction, by using the values of X_m (in m) and the X_{ud} values which have been determined in previous step, the data points where $X_m \leq X_{ud}$ were extracted. In this study, the X_m is the source areas (distance) of 80% of the integrated flux (footprint) in m. According to Kljun et al. (2015), in most cases 80% of the footprint area includes the main impact of the measurement (it should be noted that 100% of the footprint area is

infinite). X_m was computed by the Alteddy software (version 3.90) and is applied here for sensible heat data-filtering to use for validation of the model.

3. For selected time frame from filtered heat flux data, the heat flux footprint area (length) is calculated. For footprint prediction (FPP), the method developed by Kljun et al. (2015) for footprint parameterization was used (Figure 2.4).

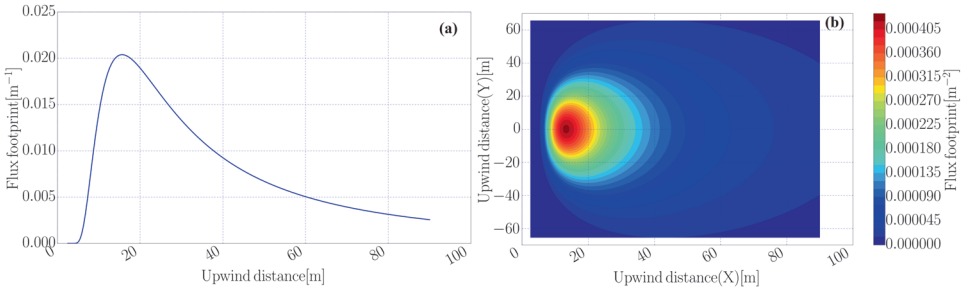


Figure 2.4: Footprint representations for selected time frame (November 24, 2012 at 19:30) in the study period. At this time frame the atmosphere was unstable with L (Obukhov length)=-1.05 m; h (atmospheric boundary layer height) = 1930.7 m; u^* (friction velocity) = 0.043 ms^{-1} and measurement height was 1.90 m above water surface. The 3-D Sonic anemometer is located at (0,0) m and the $X-$axis points towards main wind direction: **(a)** footprint length estimate in main wind direction (1-D); and **(b)** footprint contour lines (2-D).

After data-filtering, 559 (of 1392) half-hourly heat flux data points (43% of the initial data set) remained for model validation. To investigate the model performance, the remained data points were classified according to the atmospheric stability conditions using the ratio of z/L (or ζ where z is the height of measurement (m), L is Obukhov length (m) and $\zeta = z/L$ is stability parameter (unitless)). The summation of the data sets' properties which have been used in this study are presented in Table 2.4.

Table 2.4: Atmospheric stability condition investigation of measured heat flux data. Stability conditions of different data sets which used in this study are reported in this table (**EC-NF**: initial data point; **EC-F**: filtered data using proposed algorithm; **M-Tws-Obs-NF**, **F**: data used in model by using measured water surface temperature. Due to lack of some input parameters (e.g. water surface temperature) number of data point is less than initial data points (**F**:Filtered, **NF**: non-filtered); **M-Tws-Mod-NF**, **F**: data used in model by using the simulated water surface temperature).

Data Set	Total Data		Stable Conditions		Unstable Conditions	
	Number of points	Percent	Number of points	Percent	Number of points	Percent
EC-NF	1327	100	366	27.58	961	72.42
EC-F	559	100	4	0.72	555	99.28
M-Tws-Obs-NF	1287	100	433	33.64	854	66.36
M-Tws-Obs-F	552	100	25	4.53	527	95.47
M-Tws-Mod-NF	1328	100	438	32.98	890	67.02
M-Tws-Mod-F	559	100	23	4.11	536	95.89

2.9.2. VALIDATING THE CALCULATED SENSIBLE HEAT FLUXES

As mentioned in Section (2.9.1), the filtered measured values of sensible heat flux from the 3-D sonic anemometer installed over the water surface were used to validate the model. The validation process was carried out for different stability conditions to check the performance of the proposed model in different stability conditions. In Table 2.5 the measures of model performance are presented. According to the suggestion of Legates and McCabe Jr. (1999), to assess the performance of the model, four common quantitative evaluation criteria, namely, the root mean squared error ($RMSE$), mean absolute error (MAE), index of agreement (d) and the bias ($Bias$) were used in this study. The values of index of agreement (d) varies between 0.0 and 1.0, where 0.0 indicates no agreement and 1.0 represents perfect agreement for measured and estimated values (Ali et al., 2015; Legates and McCabe Jr., 1999).

In Figure 2.5 comparisons of simulated and observed sensible heat fluxes from water surface for stable and unstable atmospheric conditions are shown. The number of points in Figure 2.5(a) is low due to the filtering of the measured sensible heat fluxes over water surface (Section(2.9.1)). After filtering the heat flux data (regarding the footprint values explained before) approximately all validation data points (99%) belong to the unstable atmosphere conditions and therefore, validating the results for stable conditions is not accurate. However, as shown in the Table 2.4, in most times (72.5%) the atmosphere is unstable over the Lake Binaba. It means that if the model works well in unstable conditions, it would cover most times and conditions available over the water surface. The performance of the model, as shown in Figure 2.5(b) and Table 2.5, according to the evaluation parameters is satisfactory. To investigate the performance of the model for all atmospheric stability conditions (especially for stable conditions) collecting long-term (including sufficient stable and unstable conditions after data filtering) heat fluxes measurements over the water surface as well as microclimate variables on the land is crucial.

2.10. RESULTS OF THE MODEL AND DISCUSSION

The proposed approach was run for Lake Binaba in Ghana, for the study period from November 23, 2012 to December 22, 2012. The input data to the model was provided by the on-ground automatic weather station (AWS) in the shore of the water body as shown in Figure 2.1. The effects of atmospheric stability conditions on the transfer coefficients and consequent heat fluxes from the water surface are discussed below.

2.10.1. ATMOSPHERIC STABILITY

According to the Monin-Obukhov Similarity Theory (MOST), stability parameter ζ can be used as an indicator for the atmospheric stability. ζ depends on both the difference between the air and water surface virtual temperature (ΔT_v) and horizontal wind speed. $|\zeta|$ is large when wind speed is low. The ζ values computed for the study period show that the atmosphere was unstable 72.5% of the study time period at Lake Binaba (Table 2.4). The stability parameter (ζ or z/L) usually is unknown in most small lakes. Applying the proposed method, the value of L and consequently, the stability parameter (ζ) will be computed and the atmospheric stability conditions can be indicated to apply the correct

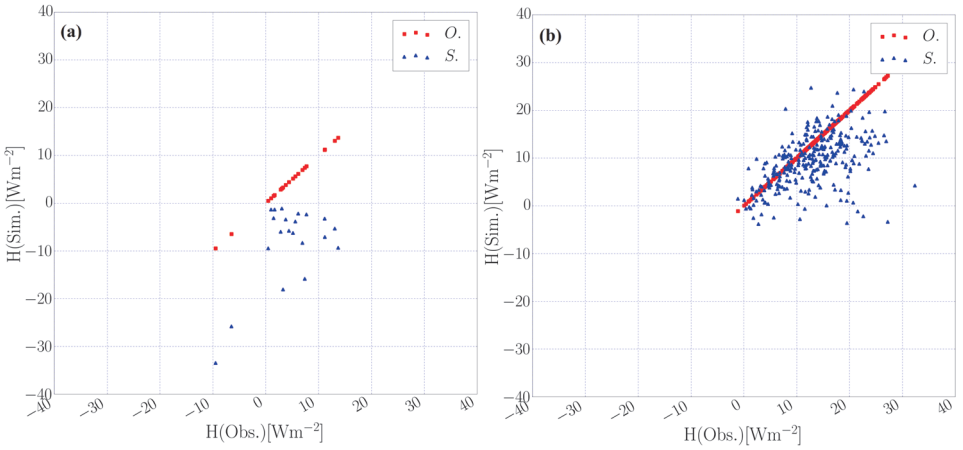


Figure 2.5: Comparison of simulated (Sim.) and observed (Obs.) sensible heat flux values over water surface. Observed raw heat flux data was processed, corrected and footprint filtered. Red square points correspond to 1:1 relationship; **(a)** for atmospheric stable conditions; **(b)** for unstable atmospheric conditions.

stability functions (Section (2.6)).

2.10.2. ROUGHNESS LENGTHS

The average roughness lengths of momentum and heat (or water vapor) are $5.51\times10^{-5}\,m$ and $1.49\times10^{-4}\,m$ respectively. Figure 2.6(a) illustrates that the roughness length of momentum (z_{0m}) decreased for velocities up to 2.5 ms^{-1} and for higher values of horizontal wind speeds ($U_z > 2.5\,ms^{-1}$) its values increased gradually with wind speed. However, the trend of the heat (or water vapor) roughness length is different. The $z_{0h}(= z_{0q})$ does not vary significantly for wind speeds more than 2.5 ms^{-1} as shown in Figure 2.6(b).

Comparing the computed roughness lengths over the water surface shows that unlike for the land surfaces, the heat (and water vapor) roughness length is larger than the momentum roughness length. For small lakes with low to moderate wind speeds ($U_2 < 5\,ms^{-1}$), the water surface can be considered as a smooth surface. Unlike for the land surfaces (rough surfaces), for smooth surfaces z_{0q} and z_{0h} are larger than z_{0m}. Over the rough surfaces (such as land areas) the heat (z_{0h}) and water vapor (z_{0q}) roughness lengths are considerably smaller than the momentum roughness length (z_{0m}) (Brutsaert, 1982). This large differences in roughness lengths can be related to the different mechanism for momentum and heat or water vapor transfer. Over the rough surfaces, momentum transfer is enhanced by the effective drag including local pressure gradients beside the viscous shear. The heat and water vapor transfer are controlled primarily by molecular diffusion (Brutsaert, 1982). At lower wind speeds, the momentum exchanges over the water surface (smooth surface) are mainly affected by the non-atmospheric factors such as swell on water surface (Vercauteren et al., 2011). However, The interaction between turbulent atmosphere and an inland water surface (specifically for small shallow lakes) is complex and includes a number of complicated physical processes and hence, the pre-

Table 2.5: Calculated metrics of model (of heat flux calculation) performance (**MAE**: mean absolute error; **RMSE**: root mean square error; **d**: index of agreement; **Bias**: bias) for calculated sensible heat fluxes for different atmospheric stability conditions. In this table different data sets are presented: **Tws-Obs-30m**: using observed water surface temperature values in 30-min intervals; **Tws-Mod-30m**: using calculated water surface temperature values in 30-min intervals; **Tws-Obs-H**: using hourly observed water surface temperature values; **Tws-Mod-H**: using hourly calculated water surface temperature values.

Data	Stability Condition	$RMSE\,[^{\circ}C]$	$MAE\,[^{\circ}C]$	d	$Bias$
Tws-Obs-30m	Total Data	10.40	6.29	0.54	-3.22
	Stable Conditions	15.24	13.45	0.47	-13.46
	Unstable Conditions	10.12	5.95	0.49	-2.74
Tws-Mod-30m	Total Data	11.63	9.8	0.49	-9.50
	Stable Conditions	16.32	14.3	0.48	-14.30
	Unstable Conditions	11.38	9.61	0.47	-9.29
Tws-Obs-H	Total Data	8.73	5.82	0.64	-3.71
	Stable Conditions	14.44	12.73	0.49	-12.73
	Unstable Conditions	8.18	5.34	0.60	-3.08
Tws-Mod-H	Total Data	11.30	9.71	0.51	-9.49
	Stable Conditions	15.69	13.66	0.50	-13.66
	Unstable Conditions	10.97	9.46	0.47	-9.23

diction of z_{0m} as well as the z_{0h} and z_{0q} over the inland water surfaces is still subject to some uncertainty (Brutsaert, 1982).

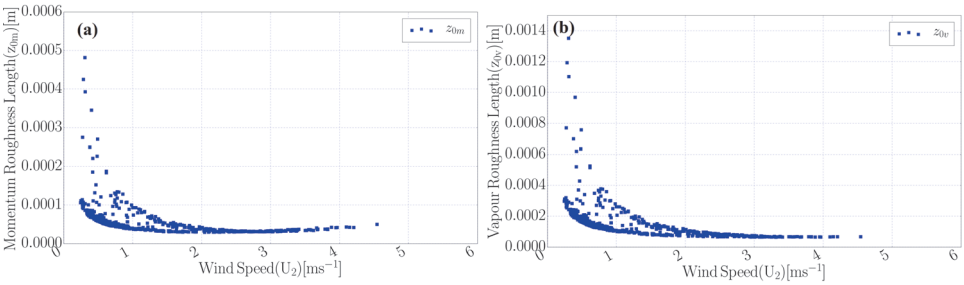


Figure 2.6: Relationship between the horizontal wind speed (measured over surrounding land) and **(a)** momentum roughness length; **(b)** heat (or water vapor) roughness length.

2.10.3. TRANSFER COEFFICIENTS

In Figure 2.7(a) the relationships between the wind speed and the neutral transfer coefficients are shown. As it can be seen, the average of the neutral drag coefficients is 1.60×10^{-3}. It decreased for wind speeds up to 2.0 ms^{-1} and increased approximately linearly for higher wind speeds ($U_2 > 2\,ms^{-1}$). The general trend of the neutral heat (or water vapor) transfer coefficient (with an average value of 1.76×10^{-3}) is the same as the drag coefficient but its value decreases for wind speeds up to 3.0 ms^{-1} (this point is 2.0 ms^{-1} for drag coefficient). For wind speeds more than 2.0 ms^{-1} it increased with a very smooth rate, less than the change rate of the neutral drag coefficient.

506469-L-sub01-bw-Abbasi
Processed on: 9-11-2016

Using the stability functions to adjust the transfer coefficients, increased the average of the drag coefficient and heat (or water vapor) transfer coefficients by 25.9% and 48.3% to 2.02×10^{-3} and 2.61×10^{-3} respectively. The effect of stability conditions on the transfer coefficients is largest for low wind speeds (as shown in Figure 2.7(b)) and for large values of (virtual) air-water surface temperature difference (ΔT_v or ΔT) (where $\zeta < 0$ as shown in Figure 2.7(c)) which happened in unstable atmospheric boundary layers (Figure 2.7(d)). This effect enhanced the transfer coefficients and consequently the sensible and latent heat fluxes from the water surface. The modified transfer coefficients for a non-neutral atmosphere converge to neutral values (C_{DN} ,C_{HN}) with an increase in wind speed with ζ converging to zero (Figure 2.8(a) and Figure 2.8(b)).

The ratio of the stability adjusted transfer coefficients to the neutral coefficients C_E/C_{EN} and C_D/C_{DN} were larger than 1.0 when ΔT_v was positive and the atmospheric boundary layer was unstable (Figure 2.7(c)). The rate of change of the modified transfer coefficients with ζ was fast for values of ζ close to zero and attenuated for increasing $|\zeta|$ (Figure 2.8(a) and Figure 2.8(b)). The ratio C_E/C_{EN} in unstable conditions was larger than the ratio C_D/C_{DN} and therefore, the effects of atmospheric stability conditions were higher for water vapor (heat) transfer rather than the drag forces.

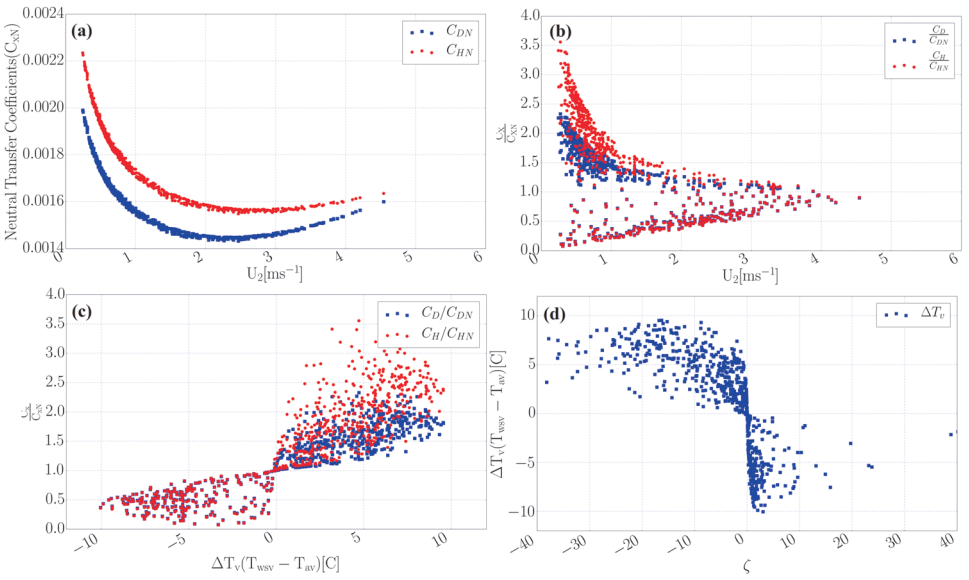


Figure 2.7: Relationship between wind speed values and: **(a)** neutral transfer coefficients; **(b)** changes of ratio of transfer coefficients to their neutral values; **(c)** effect of virtual air-surface temperature difference on the transfer coefficients; **(d)** relationship between virtual air-surface temperature difference and stability parameter values.

2.10.4. SENSIBLE AND LATENT HEAT FLUXES

In this study, the heat fluxes from small inland water surfaces were calculated taking into account the atmospheric stability conditions. To this aim, the heat (C_H) and mass (wa-

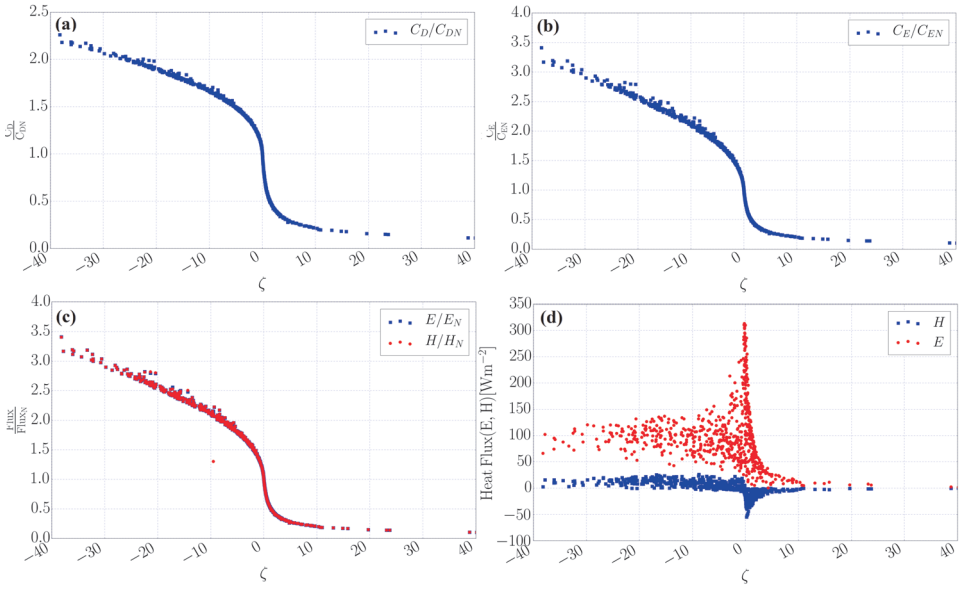


Figure 2.8: Relationship between the stability parameter and: **(a)** ratio of momentum transfer coefficient to corresponding neutral values; **(b)** ratio of heat (or water vapor) transfer coefficient to corresponding natural values; **(c)** ratio of heat fluxes to their neutral values; and **(d)** sensible and latent heat fluxes.

ter vapor) transfer coefficients (C_E) were modified to take the stability conditions into consideration. When stability functions were used to calculate sensible heat and latent heat fluxes from the water surface, the average estimated latent (evaporation) heat flux increased by 44.7% compared with estimates using the neutral atmospheric boundary layer (Figure 2.8(c)). This rate is lower than the increase in the average value of C_E which was 48.3% because the atmospheric stability effects on C_E is largest at lower wind speed values, while the E values are smaller for lower wind speeds.

While the effects of stability on the transfer coefficients were largest at high $|\zeta|$, large latent heat flux values happened when stability parameter (ζ) converged to zero due to the high wind speeds effect (Figure 2.8(d)). When the sensible and latent heat fluxes from the water surface is high, the water surface temperature is generally low. As the changes of the transfer coefficients cancel out by dividing the sensible heat flux by latent heat flux, the stability condition of the atmospheric boundary layer does not impact the Bowen ratio (Bowen ratio is dimensionless ratio of sensible heat flux to latent heat flux). Bowen ratio (β) values in the study period varied in range of $[-0.4, 0.3]$. These low values of Bowen ratios show that most of the heat from the water surface were released by the evaporative fluxes. However, in the study lake sensible heat fluxes should be taken into account in the total heat fluxes from the water surface due to the effect of sensible heat fluxes on atmospheric stability conditions.

Using the method developed in this study with considering the effect of atmospheric stability conditions, the sensible and latent heat fluxes from the (small) water surface

506469-L-sub01-bw-Abbasi
Processed on: 9-11-2016

were calculated and shown in Figure 2.9 and Figure 2.10. To show the effects of time scales on the results (especially in evaluating the performance of the model) both hourly and daily averaged heat fluxes are illustrated in Figure 2.9 and Figure 2.10 respectively. In addition for both time scales, the heat fluxes with and without considering the atmospheric stability conditions are presented. As shown in Figure 2.9 as well as in Figure 2.10 the effects of stability conditions on sensible heat fluxes are less than the latent heat flux values. However, the sensible heat flux values are smaller than the latent heat fluxes, but they cannot be ignored. Regarding the framework of the model as shown in Figure 2.3, to estimate the atmospheric stability conditions, the sensible heat flux values are needed (e.g. Equation (2.1)). Therefore, to consider the effect of stability conditions on heat fluxes from the water surface (especially for evaporative fluxes) sensible heat fluxes should be calculated accurately.

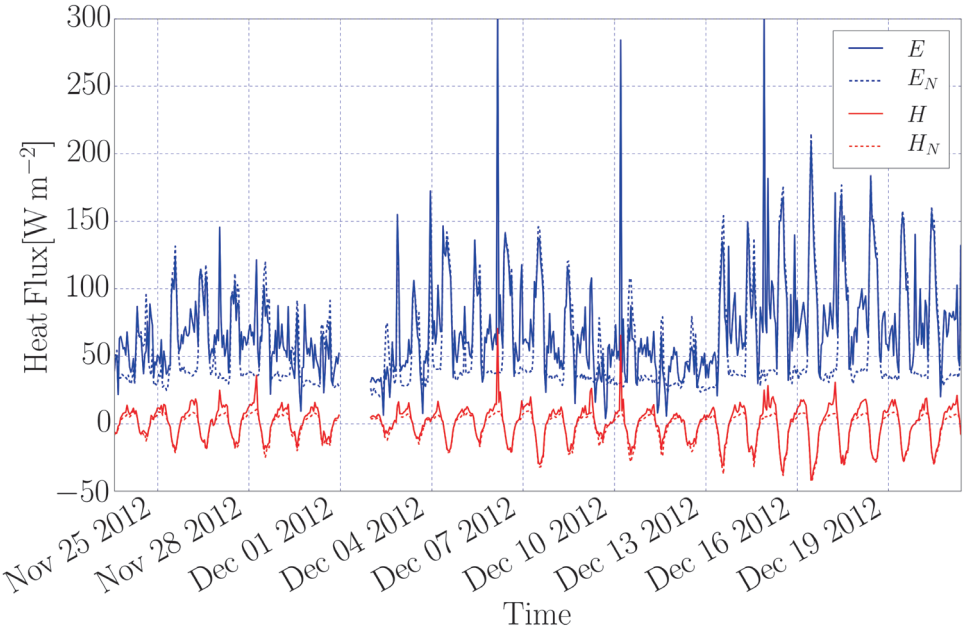


Figure 2.9: Calculated hourly averaged heat fluxes from Lake Binaba by using proposed approach. Index N, indicates heat fluxes without considering the effects of atmospheric stability conditions on fluxes. Discontinuity in the graphs is due to malfunction of the weather station during these times.

During the study period, the actual (with considering the stability conditions) and neutral (with assumption of natural atmospheric stability conditions) daily averaged evaporation values from the water surface were 2.5 mmd^{-1} (or 69.6 Wm^{-2}) and 2.0 mmd^{-1} (55.6 Wm^{-2}) respectively. These values for sensible heat fluxes were 0.65 Wm^{-2} and -2.6 Wm^{-2} respectively (Figure 2.10).

Following the concept of mass transfer method (Equations (2.5) and (2.6)) which was used in this study, the correlation between the sensible heat flux (H) with the product

506469-L-sub01-bw-Abbasi
Processed on: 9-11-2016

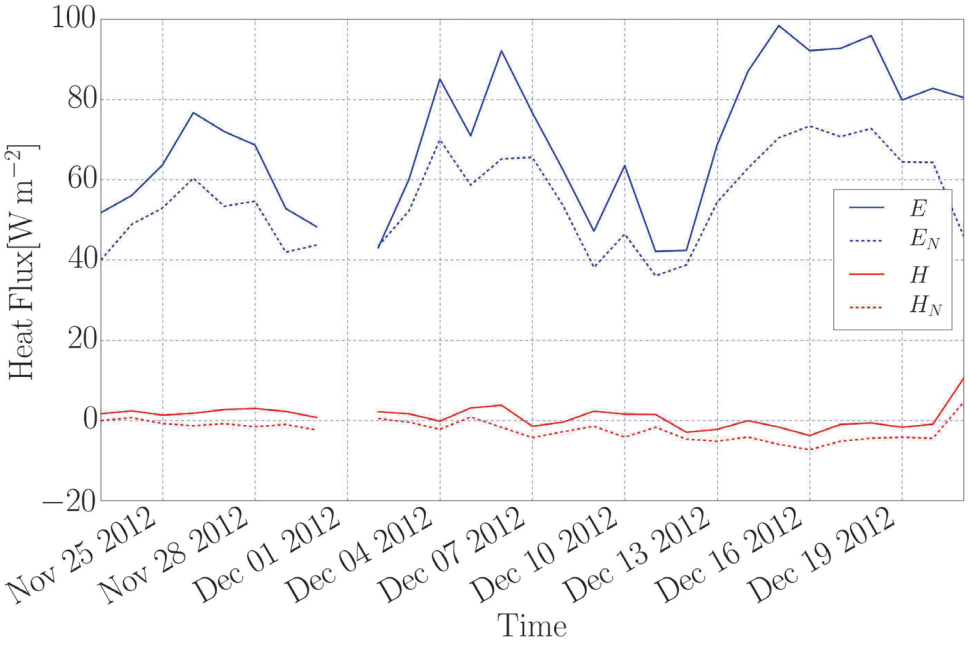


Figure 2.10: Calculated daily averaged heat fluxes from Lake Binaba by using proposed approach for two different conditions: without considering the effects of atmospheric stability conditions on heat fluxes (N) and with considering the atmospheric stability on heat fluxes.

of wind speed (U_2) and difference in water surface temperature and air temperature ($\Delta T = T_{ws} - T_a$) is investigated. As shown in Figure 2.11(a), H was well correlated to $U_2(T_{ws} - T_a)$. This correlation can be described by the heat transfer coefficient (C_H) as shown in Equations (2.5). This correlation for $U_2(T_{ws} - T_a) \leq 0$ (where $T_{ws} < T_a$ and mostly stable conditions) seems to be linear. However, for $U_2(T_{ws} - T_a) > 0$ and for $T_{ws} > T_a$ (in unstable conditions) the correlation seems to be nonlinear. Therefore, for sensible heat flux from small water surfaces the heat transfer coefficient (C_H) can be approximated as a linear function for stable conditions, whereas this transfer coefficient is nonlinear for unstable conditions and should be calculated carefully. In addition, due to the small wind speed values in the study site, the term of $U_2(T_{ws} - T_a)$ was dominated by changes in T_a and therefore, its values should be collected accurately. Similar correlation analysis is executed for the values of E and $U_2(e_s - e_a)$. As shown in Figure 2.11(b) the correlation of latent heat flux (E) with $U_2(e_s - e_a)$ is more complex than the correlation of H and $U_2(T_{ws} - T_a)$ which was explained before. For large values of $U_2(e_s - e_a)$ (i.e. $U_2(e_s - e_a) \geq 2.0$) the relationship can be assumed to be linear whereas for small values (i.e. $U_2(e_s - e_a) < 2.0$) the relationship is mostly nonlinear. It means that using a single water vapor transfer coefficient (or mass transfer coefficient commonly called wind function) for all wind speeds to estimate latent heat fluxes from water surfaces could generate large errors in the calculated values, especially for the water bodies when the wind speeds are low ($U_2 < 1.0\, ms^{-1}$). As a conclusion from these analyses, for small wa-

506469-L-sub01-bw-Abbasi
Processed on: 9-11-2016

ter surfaces with low wind speeds the wind function (which is commonly used in mass transfer methods to estimate evaporation from water surface) should be justified for free convection situations. As this issues is beyond the aims of this study the reader is referred to some literature such as Edson et al. (2007); Huang (2003); Sill (1983) for more details.

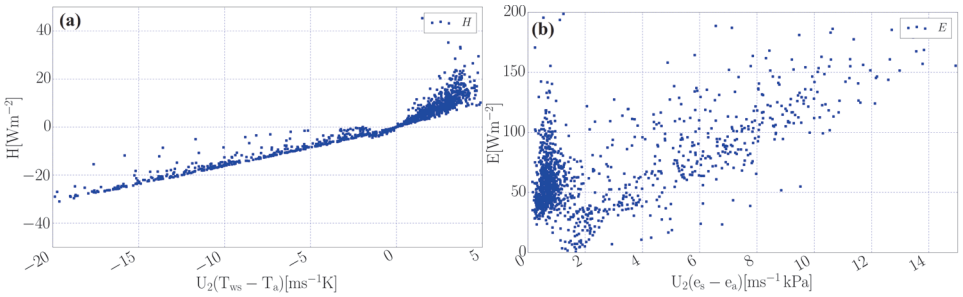


Figure 2.11: **(a)** Calculated sensible heat flux from water surface as a function of product of wind speed and difference between water surface temperature and air temperature; **(b)** Calculated latent heat flux as a function of product of wind speed and difference between water-air interface vapor pressure and vapor pressure of overlying air.

2.11. CONCLUSION

The atmospheric stability conditions over small and shallow lakes in arid and semi-arid regions have been shown to be important in estimating evaporation from open water bodies. In the model developed in this study, only standard micrometeorological parameters measured over the lands are required to estimate heat fluxes from water surface considering the atmospheric stability conditions. Using the Monin-Obukhov Similarity Theory (MOST), stability conditions were used to estimate latent and sensible heat fluxes. The bulk aerodynamic transfer method was improved by using the stability parameter from MOST and the atmospheric stability adjusted transfer coefficients. From the modeling results, atmospheric instability occurred more than 72.5% of the time in the study period hence enhanced the evaporation from water surface by 44.7% on average. Using the developed method, the calculated daily average evaporation from lake Binaba during the study period was 2.5 mmd^{-1}. The effect of atmospheric instability on the drag coefficient and heat (or water vapor) transfer coefficient were found to be 23.9% and 48.3% respectively. The correlation of the computed sensible heat fluxes with the measured ones was satisfactory especially for the unstable atmosphere. Analysing the sensible and latent heat fluxes from lake Binaba showed that air temperature was the dominant microclimate variable for the sensible heat flux whereas the latent heat flux (evaporation) can be controlled by the vapor pressure of the overlying air for moderate to high wind speeds. For low wind speeds estimating the latent heat flux needs to take into account free convection concept. For small water surfaces with low to moderate wind speeds, considering the free convection conditions would improve the heat flux estimation.

506469-L-sub01-bw-Abbasi
Processed on: 9-11-2016

506469-L-sub01-bw-Abbasi
Processed on: 9-11-2016

3

A CFD-BASED APPROACH FOR ESTIMATING WATER SURFACE EVAPORATION

3.1. INTRODUCTION

Evaporation from free water surface is a major component of the hydrological cycle (Vidal-López et al., 2012). Estimating these losses are needed for a wide range of subjects such as water resources planning, water quality of fresh water resources, irrigation management, ecosystem modelling, water sustainability, climate change, etc. (Ali et al., 2008; Gianniou and Antonopoulos, 2007; Carter et al., 1999; Xu and Singh, 2000). In arid and semi-arid regions, annual evaporation losses from lakes and reservoirs could rise up to 50% of the accumulated stored water (Fowe et al., 2015; Gokbulak and Ozhan, 2006; Mugabe et al., 2003; Craig and Aravinthan, 2007; Martínez-Granados et al., 2011; Gallego-Elvira et al., 2012). The significance of estimating evaporation accurately increases for water resources accounting of arid and semi-arid areas (Ali et al., 2008) especially for developing countries where economic water scarcity is a major problem. Evaporation in lakes is a function of wind speed, solar and atmosphere radiation, air temperature, water surface temperate, vapor pressure deficit, atmosphere stability conditions, and the lake surrounding environment (fetch) (Ali et al., 2008). The complex interaction and dependency of evaporation on many parameters makes it unique for each lake hence inhibits theoretical methods for its' estimation (Gianniou and Antonopoulos, 2007).

The parameters that affect evaporation rate from water surface can be grouped into two categories, including: 1) climatological and meteorological factors such as wind speed, temperature, relative humidity, etc.; and 2) geology and physiography of water bodies such as shape, depth, water quality, size, circulation in water body, advective and

This chapter is based on Abbasi et al. (2015a): Abbasi, A.; Annor, F.O.; van de Giesen, N.: Developing a CFD-based Approach to Estimate Evaporation from Water Surfaces in (Semi-)Arid Regions. Hydrological Processes (Manuscript re-submitted for publication), 2015.

506469-L-sub01-bw-Abbasi
Processed on: 9-11-2016

storage energy sources and sinks, and even the location. Water surface (the lake surface area) determines the effect of advective energy from the surrounding environment. The water depth is critical for heat storage and release (Gianniou and Antonopoulos, 2007; Abtew and Melesse, 2013).

There are many models available for estimating evaporation from open water surfaces. These methods use two general approaches to estimate evaporation amount which include: 1) direct measuring of evaporation like evaporation pan (Fu et al., 2009, 2004) and Eddy Correlation (EC) (Assouline et al., 2008; Blanken et al., 2000; McGloin et al., 2014; Stannard and Rosenberry, 1991); and 2) calculating (indirect) evaporation using the meteorological parameters. The indirect methods can be put into four categories, mainly through the approach they use in calculating evaporation using the meteorological inputs, which include: water budget (balance) method; aerodynamic or mass transfer method (Singh and Xu, 1997b); energy balance and combination methods (Gianniou and Antonopoulos, 2007; Rosenberry et al., 2007; Delclaux et al., 2007); and radiation- and temperature-based methods (Xu and Singh, 2001, 2000).

Direct measurement of evaporation rate at the air-water interface using Eddy Covariance (EC) system is often very expensive. This method is usually applied for short-term observations and has to be designed carefully to obtain reliable data. Although, evaporation pan method is convenient and cost-effective and widely used in estimating evaporation, due to the practical issues and relatively large errors in the measured evaporation amounts it is not an applicable method especially in case of small and shallow lakes.

In the mass balance method, evaporation is computed as the change in volume of water stored and the difference between the inflows and outflows of the lake. This method theoretically is simple but practically it needs some inputs that they are not measured easily. In this method, the relative importance of the components depends on the physiographical and hydrological settings (Finch and Calver, 2008). The energy balance and combination methods have been seen to be reliable in providing precise estimation of evaporation (Ali et al., 2008; Rosenberry et al., 2007) but these methods need a wide range of data sets as input parameters such as net radiation, conduction heat flux, and heat storage of the water body, etc. which should be measured for a long time period to generate reliable evaporation estimation (Gallego-Elvira et al., 2012; Vidal-López et al., 2012). Temperature- and radiation-based methods usually need less input parameters (mainly they need air temperature or radiation components) in comparing with other methods, but their estimations are not reliable for small inland water surfaces. To find more details on the algorithm, pros and cons of each method and comparing the estimated evaporation obtained from different methods, especially for small water surfaces in (semi-) arid regions the reader is referred to the work which is under revision by Annor et al. (2016).

The mass-transfer approach, which is the foundation of the method developing in the current study, needs moderate data as input. This method correlates evaporation amount to the vapour pressure deficit between the water surface and its atmosphere above, through a mass-transfer coefficient, usually considered as a linear function of wind speed referred to as the "wind function". A wide range of empirical mass-transfer formulae have been applied by researchers (McJannet et al., 2012; Singh and Xu, 1997b). Some of them (Harbeck, 1962; Brutsaert, 1982; McJannet et al., 2012) attempted to pro-

506469-L-sub01-bw-Abbasi
Processed on: 9-11-2016

pose generalizable wind functions by correlating the mass transfer coefficient to the surface area of the water body, but these proposed formulae usually are applicable only to the conditions similar to the places the formulae or functions were parameterized (Martínez Alvarez et al., 2007; Vidal-López et al., 2012).

In most of the above described methods, the models' parameters are specific to a given water body under the prevailing surrounding environment and for a specific climate which are valid only for the specific ranges of parameters (reservoir size, temperature difference, humidity, atmosphere conditions, etc.) that are used in the designed experiment (Vinnichenko et al., 2011). This therefore means these coefficients may not provide satisfactory estimation for other regions (Sartori, 2000).

Considering this limitations and the urgent need to estimate evaporation from water surfaces in semi-arid and arid regions, it was deemed helpful to establish a cost effective and generalisable approach to determine reliable wind functions for desired water bodies. Computational Fluid Dynamics (CFD) is a very powerful tool for this. This is due to the fact that by using CFD for modeling the heat transfer in the atmospheric boundary layer (ABL), it is possible to derive convective heat and mass-transfer coefficients for a given water body. Results from CFD models could be used to analyse the spatial and temporal variations of the evaporation rate over the water surface and determine the effects of advection on heat fluxes from water surfaces under arid and semi-arid conditions. These analyses are not possible when using traditional methods (Craig, 2006). Most of the methods used to estimate evaporation from water surfaces are "one dimensional" with areal homogeneity assumption. Therefore, these methods are not able to account for the sideways movement of energy due to the different energy (temperature) and aerodynamic characteristics of differing land-water surfaces (advection). In arid regions, the evaporation from small water surfaces would be impacted by upwind hot dry air flows over the water body (Craig, 2006; Jacovides et al., 1988).

The current study aims mainly is to present a new applicable computational method based on CFD for calculating convective heat flux and mass transfer coefficients and consequently estimating evaporation rate from water surface using the estimated mass-transfer coefficient. Using results of CFD simulations and heat and mass transfer analogy, a wind function which includes the water body specifications, environmental and meteorological conditions is extracted. To evaluate the performance of the approach developed, the calculated sensible heat flux obtained using derived synthetic wind functions was compared with sensible heat fluxes measured with a 3-D sonic anemometer for Lake Binaba, a small and shallow lake in semi-arid Upper East Region of Ghana. Finally, by utilizing the derived heat and mass transfer coefficients the sensible and latent heat fluxes from the water surface were computed. Additionally, the spatial distributions of convective and evaporative heat fluxes over the water surface provided by CFD simulation are presented and discussed.

3.2. DESCRIPTION OF STUDY SITE AND DATA COLLECTION

The Upper East Region of Ghana is classified as one of the poorest in the country. Most of the inhabitants of the region (mostly rural areas) are farmers and rely on rainfed agriculture. To improve their livelihoods and enhance food security a number of small reservoirs (more than 160) with surface areas between 1.0 to 100.0 hectares (Abbasi et al.,

2016a; Annor et al., 2009) were constructed for them by the Ghana government and development partners in the late 1980s and early 1990s. These were constructed to promote dry season farming (crop and livestock), fishing and domestic water uses. Their closeness to the point of use made them very attractive (Abbasi et al., 2016a; Keller et al., 2000). However with recent changes in climate (climate change), the small reservoirs which were to increase the resilience of the communities which use them are at risk from high evaporation losses from them. Binaba dam, a small and shallow reservoir located in this region ($10°53'20''N$, $00°26'20''W$) was studied to determine the rate of evaporation in small lakes in this climate. The Binaba reservoir has an average surface area of 31 ha with a maximum depth of 4.0 m. The average depth is about 1.1 m at full storage level (Figure 3.1). To monitor the meteorological parameters, a floating measurement station was installed over the water surface (Figure 3.2(a)). Measurements taken included atmospheric parameters (wind speed at 2.0 m above the water surface, relative humidity, air temperature, wind speed and its direction), incoming short-wave radiation, water temperature profile, and sensible heat flux using a 3-D sonic anemometer which was used to validate the model. The installed 3-D sonic anemometer recorded sensible heat flux over the water surface at 10.0 Hz and translated this into 30-minutes intervals. The raw eddy correlation data measured by the 3-D sonic anemometer was processed (calculating mean values, variances, applying corrections, calculating corrected fluxes, etc.) by Alteddy version 3.90, a visual Fortran program developed in Alterra research institute of Wageningen University in the Netherlands (Elbers, 2016, 2002). As processing raw measured eddies is beyond the aims of this study, the reader is referred to Annor et al. (2016) to find more details on it. Atmospheric measurements and water thermistor string (to measure water surface temperature that was needed in the model) were situated near the dam body, where the lake depth is around 4.0 m (Figure 3.1). The water temperature profiles were measured with thermistor string and HOBO tidbit v2 temperature loggers with nominal accuracy of $\pm 0.2°C$. In addition, the meteorological parameters were measured on land surrounding the lake at a height of 2.0 m above the land surface (Figure 3.2(b)). The measurements taken from these land-based station were used to prepare the boundary and initial conditions in the model developed in this study. In Figure 3.1 location of floating measurement platformover the water surface and the on-ground station are shown.

The above described measurements were done from November 23, 2012, to December 22, 2012. Investigating the measured values showed that the air temperature fluctuated from 18.0 to $40.0°C$ with an average of $28.7°C$ while the water surface temperature varied between $24.0°C$ and $32.5°C$ with an average of $27.5°C$ during the measurement period. Figure 3.3 shows the diurnal changes of air temperature and water surface temperature, with daily variations of approximately $10.0°C$ and $3.5°C$ respectively. Figure 3.4 shows the measured wind speed values on both land and water surface. The maximum wind speeds recorded during the study were 3.5 and 4.5 ms^{-1}, respectively over the land and water surface with the South-Western (SW) direction being the most dominant direction.

506469-L-sub01-bw-Abbasi
Processed on: 9-11-2016



Figure 3.1: Shape of Lake Binaba and its surroundings (Google, 2015). Approximate location of over water measurements is shown by filled red square and land-based station is shown by filled blue circle.



Figure 3.2: **(a)** Floating measurement station over the water surface; and **(b)** land-based station near Lake Binaba.

3.3. HEAT AND MASS TRANSFER IN ATMOSPHERIC BOUNDARY LAYER

Most evaporation studies try to predict evaporation rates using mass transfer method. Evaporation from an open water surface utilizing the mass transfer approach can be de-

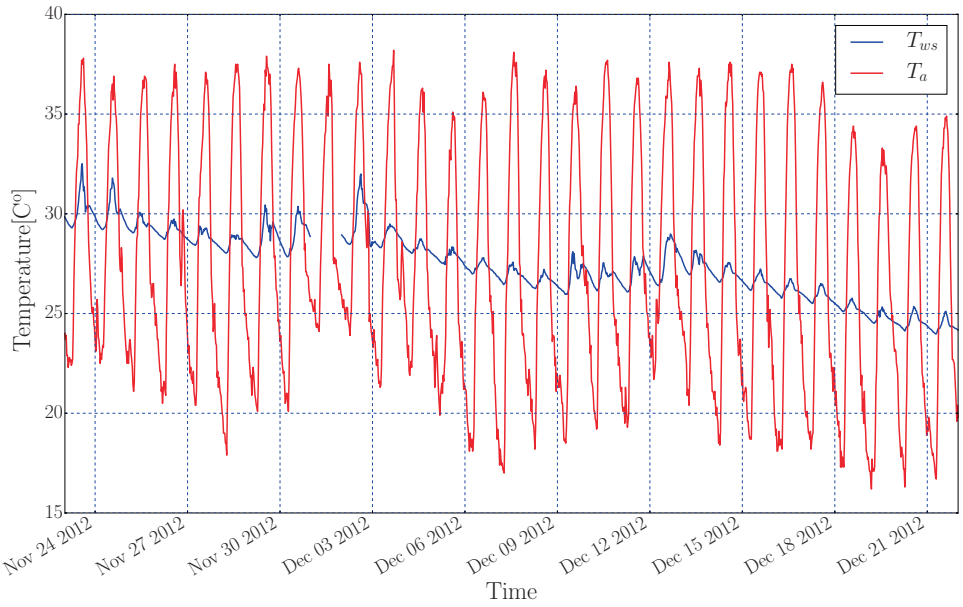


Figure 3.3: Measured water surface and air temperature values at 2.0 m above water surface used in the simulations.

scribed as (Singh and Xu, 1997b):

$$E = f(\bar{u})(e_s - e_a) \tag{3.1}$$

where E ($mm\,d^{-1}$) is the evaporation rate, $f(\bar{u})$ is the wind function which depends on the mean wind speed ($\bar{u}$), e_s (kPa) is saturation vapor pressure at the temperature of water surface (T_{ws}), e_a (kPa) is vapor pressure at air temperature (T_a) and $\bar{u}$ is the mean wind speed measured at a reference height above the water surface. Assuming a linear relation of wind function with wind speed measured at a height of 2.0 m above the water surface, typically the following formula is used as a wind function ($f(\bar{u})$) in evaporation estimation:

$$f(\bar{u_2}) = a + b\bar{u_2} \tag{3.2}$$

where a and b are fitting constants, calibrated using observed field data (Bower and Saylor, 2009). More details on the mass-transfer coefficient can be found in the literature (Sartori, 2000; Warnaka and Pochop, 1988).

The main disadvantage of Equations (3.1) and (3.2) for parameterizing evaporation is the fact that other processes that affect evaporation are excluded in the wind function. Constants a and b vary with lake size, incoming short-wave radiation, climate condition, season, geographical location, etc. (Bower and Saylor, 2009; Sartori, 2000). Although full-scale experimental measurements can result in realistic wind functions for specific water bodies, the obtained ones are usually case-specific and are not always reliable for other types of water surfaces due to the wide range of variations in lake characteristics and their climate conditions (Defraeye et al., 2011).

506469-L-sub01-bw-Abbasi
Processed on: 9-11-2016

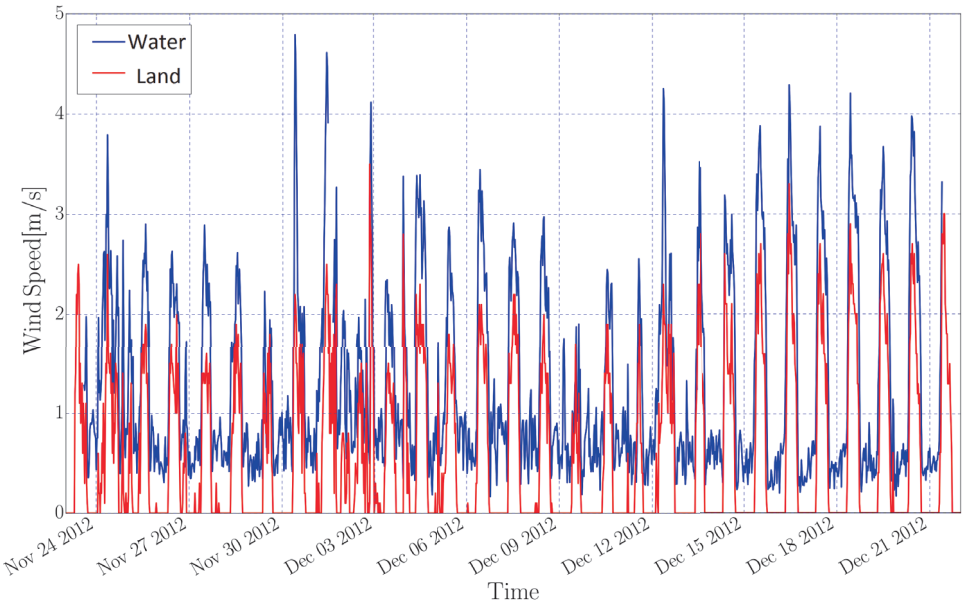


Figure 3.4: Measured wind speed values at 2.0 m above land surface (Land) and over water surface (Water) during the simulation period.

It is assumed that air with velocity U_2 (wind speed at height 2.0 m above the water surface) and temperature T_a flows over an inland water surface of arbitrary area and shape. The water surface temperature is presumed to be uniform (T_{ws}) but changes with time. If the air temperature and water surface temperature are not equal ($T_a \neq T_{ws}$), the convective heat transfer will occur between the water surface and the atmospheric boundary layer which can be expressed as follows (Vidal-López et al., 2012):

$$H_s = h_s \times (T_{ws} - T_a) \tag{3.3}$$

where H_s ($W\,m^{-2}$) is convective heat flux (positive if it is away from the water surface) and h_s ($Wm^{-2}K^{-1}$) is the average convection coefficient for the entire water surface. Equation (3.3) relates the convective heat flux normal to the water surface (H_s) to the difference between the water surface temperature (T_{ws}) and surrounding air temperature (T_a).

A similar equation can be obtained for convection mass transfer over the water surface:

$$H_m = h_m \times \rho_a (X_s - X_a) \tag{3.4}$$

where H_m (Wm^{-2}) is the convective mass transfer (positive if it is away from the water surface), h_m ($Wm^{-2}K^{-1}$) is the convective mass-transfer coefficient, ρ_a is air density ($\approx 1.225\,kgm^{-3}$), and X_a and X_s are water vapour mixing ratio of air and water surface, respectively ($kg(water)/kg(dry\,air)$).

Determining transfer coefficients (for both heat and mass) is not simple. This is due to the fact that the coefficients depend on air properties such as specific heat, thermal

conductivity, viscosity and density, as well as on water surface geometry, the fetch and air flow conditions. For mixed or forced convective flow regimes, usually there is a linear or power-law correlation between the convective heat transfer coefficient and wind speed at a reference location (usually at a height of 2.0 m above water surface). The correlation can be determined by experiments (measurements) on water surface or by the wind tunnel experiments on a flat plate, or even more recently by using Computational Fluid Dynamics (CFD) (Defraeye et al., 2010). Many of the existing relations provide only a single value for the study surface and do not take the distribution of heat fluxes over the water surface, the effects of turbulent fluctuations and the effects of wind direction on the heat fluxes into consideration (Defraeye et al., 2011). The convective heat transfer coefficient can be used to compute the mass transfer coefficient or the wind function in a mass transfer approach to estimate evaporation.

3.4. HEAT AND MASS TRANSFER ANALOGY

Using dependent dimensionless parameters, heat and mass transfer equations can be rewritten as follows:

$$H_s = \frac{Nu \times k}{L} \times (T_{ws} - T_a) \tag{3.5}$$

$$H_m = \frac{Sh \times D}{L} \times \rho_a (X_s - X_a) \tag{3.6}$$

where Nu (dimensionless) is the Nusselt number, k is the thermal conductivity of air ($\approx 0.0242\, W m^{-1} K^{-1}$), D is the molecular diffusion coefficient for water vapour in air ($\approx 2.2 \times 10^{-5}\, m^2 s^{-1}$), ρ_a is the air density ($kg m^{-3}$), and L (m) is the characteristic length(a horizontal dimension in this study) of the water body.

Two or more processes are defined analogous if they have dimensionless governing equations of the same form. Equations (3.5) and (3.6) show that there is an exact analogy between the mass and heat transport processes (Incropera and DeWitt, 1996). The heat and mass transfer analogy allows for the estimation of the mass transfer coefficient directly out of the heat transfer or vice versa.

Sherwood Number (Sh) is equal to the dimensionless concentration gradient at the surface and it provides a measure of the convection mass transfer occurring at the surface. Assuming heat and mass transfer analogy for the current geometry, the Sherwood Number is written as (Gallego-Elvira et al., 2012; Defraeye et al., 2012):

$$Sh = Nu \left(\frac{Sc}{Pr} \right)^m \tag{3.7}$$

where $Pr = \mu C_p / k$ is Prandtl number (dimensionless), C_p is specific heat of air at constant pressure ($\approx 1006.43\, J kg^{-1} K^{-1}$), μ is dynamic viscosity of air ($\approx 1.7895 \times 10^{-5}\, kg m^{-1} s^{-1}$), $Sc = \nu / D$ is the Schmidt number (dimensionless), and ν is air kinematic viscosity ($m^2 s^{-1}$). For free and mixed convection conditions the value of the exponent is assumed, $m = 1/3$ (Incropera and DeWitt, 1996; Jacobs and Verhoef, 1997; Pauken, 1999; Bower and Saylor, 2009; Gallego-Elvira et al., 2012). Nusselt Number (Nu) (dimensionless) provides a measure of the convective heat transfer occurring at the water surface

506469-L-sub01-bw-Abbasi
Processed on: 9-11-2016

and can be expressed as following which is based on the heat and mass transfer analogy (Gallego-Elvira et al., 2012):

$$Nu = \frac{h_s L}{k} \tag{3.8}$$

where h_s (Wm^2K^{-1}) is the convective heat transfer coefficient. Using Equation (3.7) and the definition of Sherwood (Sh) and Nusselt (Nu) numbers, the convective heat transfer coefficient can be written as:

$$\frac{Nu}{Pr^m} = \frac{Sh}{Sc^m} \Rightarrow h_m = \frac{Sh \times D}{L} = \frac{Nu \times Sc^m \times D}{L \times Pr^m} = \frac{h_s \times Sc^m \times D}{k \times Pr^m} \tag{3.9}$$

By using Equation (3.9), the mass transfer coefficient (h_m) can be extracted from the heat transfer coefficient (h_s) and consequently evaporation can be estimated from water surface with the following equation (Incropera and DeWitt, 1996; Jacobs and Verhoef, 1997; Pauken, 1999; Bower and Saylor, 2009; Gallego-Elvira et al., 2012):

$$E_{lake} = \frac{Sh \times D \times \rho_a (X_s - X_a)}{L} \tag{3.10}$$

where E_{lake} is evaporation from the water surface in $mm\,s^{-1}$.

3.5. APPLICATION OF COMPUTATIONAL FLUID DYNAMICS

With the limitations in estimating and using the correct wind function or mass transfer coefficient highlighted above, it was useful to develop a general CFD-based approach to find this coefficient. The main advantages of using this approach are outlined: 1) different and complex configurations of lake and its surroundings can be investigated; 2) the transfer coefficients can be obtained in desired high spatial resolution; 3) the effects of different Atmospheric Boundary Layer (ABL) conditions can be considered (Defraeye et al., 2011); and 4) by defining the wide range of scenarios according to the meteorological conditions (steady simulations), it is possible to ignore the costly time-dependent (unsteady) simulation and reduce the computational resources required for the CFD simulations.

3.5.1. SIMULATION AIR FLOW OVER WATER SURFACE

Air flow and heat transfer over the water surface is simulated by solving flow equations (conservation of continuity, momentum and energy) using Reynolds Averaged Navier Stokes (RANS) approach. By neglecting the pressure work, the following conservation equations can be derived (Defraeye et al., 2012):

CONTINUITY EQUATION

Continuity equation can be written as

$$\frac{\partial u_j}{\partial x_j} = 0 \tag{3.11}$$

MOMENTUM EQUATION

The constant-density (except in the gravity term) momentum equations using the Boussinesq approach can be written as:

$$\frac{\partial u_i}{\partial t} + \frac{\partial}{\partial x_j}(u_j u_i) - \frac{\partial}{\partial x_j}\left\{\nu_{eff}\left[\left(\frac{\partial u_i}{\partial x_j} + \frac{\partial u_j}{\partial x_i}\right) - \frac{2}{3}\left(\frac{\partial u_k}{\partial x_k}\right)\delta_{ij}\right]\right\} = -\frac{1}{\rho_k}\frac{\partial p}{\partial x_i} + g_i\left[1 - \beta(T - T_{ref})\right] \tag{3.12}$$

TEMPERATURE EQUATION

The temperature (instantaneous internal energy) in the ABL can be calculated from the energy conservation equation for incompressible flows (Ferziger and Perić, 2002; White, 1991) as:

$$\frac{\partial T}{\partial t} + \frac{\partial}{\partial x_j}(T u_j) - \alpha_{eff}\frac{\partial}{\partial x_k}(\frac{\partial T}{\partial x_k}) = 0 \tag{3.13}$$

where T is temperature in ABL (K) and α_{eff} is effective heat transfer coefficient ($m^2 s^{-1}$). Effective heat transfer coefficient in ABL can given by:

$$\alpha_{eff} = \frac{\nu_t}{Pr_t} + \frac{\nu_0}{Pr} = \alpha_t + \alpha_0 \tag{3.14}$$

where u_i is the velocity component (ms^{-1}), p pressure (Pa), T temperature (K), $\nu_{eff} = \nu_0 + \nu_t$ is the effective kinematic viscosity ($m^2 s^{-1}$), with ν_0 and ν_t denoting molecular and turbulent viscosity respectively ($m^2 s^{-1}$), g_i the gravity acceleration vector (ms^{-2}), T_{ref} a reference temperature ($T_{ref} = 293.15\ K$), β the coefficient of expansion with temperature of the fluid ($Jkg^{-1}K^{-1}$), δ is the delta of Kronecker (dimensionless), α_0 and α_t are molecular and turbulent heat transfer coefficient respectively ($m^2 s^{-1}$), and ρ_k is effective kinematic density (dimensionless). The Boussinesq approximation is valid under the assumption that density differences are sufficiently small to be neglected, except where they appear in a term multiplied by g_i (Fredriksson, 2011). In the model, for incompressible flows the density was calculated as a linear function of temperature as

$$\rho_k = 1 - \beta\left(T - T_{ref}\right) \tag{3.15}$$

$$\beta = -\left(\frac{1}{\rho_0}\right)\frac{\partial \rho}{\partial T} \tag{3.16}$$

where ρ_k is the effective (driving) kinematic density (dimensionless) and ρ_0 is air density at reference temperature ($kg\,m^{-3}$). These three-dimensional conservation equations were numerically solved with `OpenFOAM` CFD toolbox using a finite volume method. To describe the turbulence of the flow, the standard $k-\varepsilon$ closure model was used (Vidal-López et al., 2012).

3.5.2. BOUNDARY CONDITIONS

The boundary conditions as shown in Figure 3.5 are presented below:

- Inlet (Inflow) boundary: as the available observations on the land-based station are not sufficient to determine the velocity field at the inflow boundary, for u_i, k

506469-L-sub01-bw-Abbasi
Processed on: 9-11-2016

and ε, the profiles shown in Equations (3.17), (3.18) and (3.19) respectively were used as they represent the characteristics of the upwind terrain in neutral atmospheric condition (Blocken et al., 2007; Joubert et al., 2012):

$$u = \frac{u_*}{\kappa} \ln\left(\frac{z+z_0}{z_0}\right); \qquad v = 0; \qquad w = 0 \tag{3.17}$$

$$k = \frac{u_*^2}{\sqrt{C_\mu}} \sqrt{C_1 \times \ln\left(\frac{z+z_0}{z_0}\right) + C_2} \tag{3.18}$$

$$\varepsilon = \frac{u_*^3}{\kappa(z+z_0)} \sqrt{C_1 \times \ln\left(\frac{z+z_0}{z_0}\right) + C_2} \tag{3.19}$$

where u_* is the friction velocity (ms^{-1}) given by:

$$u_* = \frac{u_{ref}\kappa}{\ln\left(\frac{z_{ref}+z_0}{z_0}\right)} \tag{3.20}$$

- Outlet (Outflow) boundary: at outlet boundary, the flow is usually not known before solving the airflow. In most ABL simulations, zero-normal gradient conditions are applied on the outflow boundary for all variables except for the pressure, where a fixed value of zero is set (Benjamin et al., 2011):

$$\frac{\partial}{\partial x}(u, v, w, k, \varepsilon) = 0; \qquad p = 0; \qquad \frac{\partial}{\partial x}(T) = 0 \tag{3.21}$$

- Bottom boundary includes terrain (land) boundary and water surface boundary is modelled as no-slip boundary using standard wall functions. For temperature boundary condition over the bottom surface, the measured temperature can be used as water surface boundary conditions. For surrounding land the zero gradient condition was assumed for temperature.

- Lateral boundaries are assumed slip boundaries (free slip):

$$v = 0; \qquad \frac{\partial}{\partial y}(u, w, k, \varepsilon) = 0; \qquad \frac{\partial}{\partial y}(T) = 0 \tag{3.22}$$

- Top boundary (free atmosphere) assumed is slip (free slip):

$$w = 0; \qquad \frac{\partial}{\partial z}(u, v, k, \varepsilon) = 0; \qquad \frac{\partial}{\partial z}(T) = 0 \tag{3.23}$$

In these equations, u ,v and w are the components of velocity in $x-$, $y-$, and $z-$direction respectively (ms^{-1}), k is turbulent kinetic energy (m^2s^{-2}), ε is turbulent dissipation rate (m^2s^{-3}), u_* is the ABL friction velocity (ms^{-1}), z_{ref} is the measurement height above the land surface (m), u_{ref} is the horizontal velocity measured at the height of z_{ref} in ms^{-1}, z is the height above the ground level (m), κ is the dimensionless von Karman

506469-L-sub01-bw-Abbasi
Processed on: 9-11-2016

constant (≈ 0.41), z_0 is the aerodynamic roughness length (m) and C_1 and C_2 are constants where $C_1 = -0.01$ and $C_2 = 1.23$ (ÓSullivan et al., 2011). As the measurements of roughness length were not available and due to the low to moderate wind speed values, the changes of roughness length with wind velocity over the surrounding lands was ignored (Prospathopoulos et al., 2012). Considering the type of crops around the water surface, the average roughness length was assumed $z_0 = 0.13\,m$, which represents a land surface with sparse vegetation (Wieringa, 1992; Bagayoko et al., 2007). For the water surface, the roughness length was assumed $z_0 = 10^{-4}\,m$ which seems to be appropriate on this type of water surfaces with low to moderate wind speed (Vercauteren, 2011).

Vertical velocity associated with gradual decrease of the water level due to evaporation can be neglected because it is several orders of magnitude less than convective velocity of the air (Vinnichenko et al., 2011).

3.5.3. COMPUTATIONAL GRIDS

In order to perform reliable CFD computations in a complex geometry which includes a lake or reservoir, the generation of a good computational grid is essential. Concentration of grid points near the lake's boundary is more clustered to cover the sharp gradients in resolved parameters. Computational domain was extended by 4200 m in the $x-$direction; 3200 m in the $y-$direction and more than 500 m upwards in order to avoid interaction between boundary conditions and the developing flow (Vinnichenko et al., 2011). In this work, the computational grid was generated with the `snappyHexMesh` utility available in `OpenFOAM`. `snappyHexMesh` is a powerful script-driven, unstructured mesh generator. After testing different mesh densities, the generated computational grid composed of 1216837 grid points; 1029591 cells, resulting in 987725 hexahedra elements and 41703 polyhedra elements. The mesh was refined sufficiently with smaller cell sizes near the lake boundary and the water surface as well in order to solve precisely the sharp changes in surfaces' properties from land to water surface or vice versa. The computational domain which included Lake Binaba and its surroundings is presented in Figure 3.5. As shown in Figure 3.5 the computational grids near the water surface and the border of land and water are more dense to be able to catch the sharp changes in surfaces' properties.

3.5.4. NUMERICAL SETUP

The governing equation of flow in ABL were solved using the `OpenFOAM` CFD package. `OpenFOAM` includes a set of efficient `C++` modules that could be used to establish solvers. Due to the collocated and polyhedral numerics implemented in `OpenFOAM` it can be used in both structured and unstructured meshes with the advantage of being easily extendable to run in parallel. The solver used to simulate the heat transfer in ABL is steady state and incompressible heat transfer that considers buoyancy effects in the momentum equation. The standard $k-\varepsilon$ closure (SKE) was used to simulate the turbulence in the model. The `SIMPLE` method was used for pressure-velocity coupling.

3.5.5. CFD SCENARIOS

As unsteady simulation of the ABL needs high computational resources and it would make the model inapplicable for estimating evaporation from inland water surfaces, a

506469-L-sub01-bw-Abbasi
Processed on: 9-11-2016

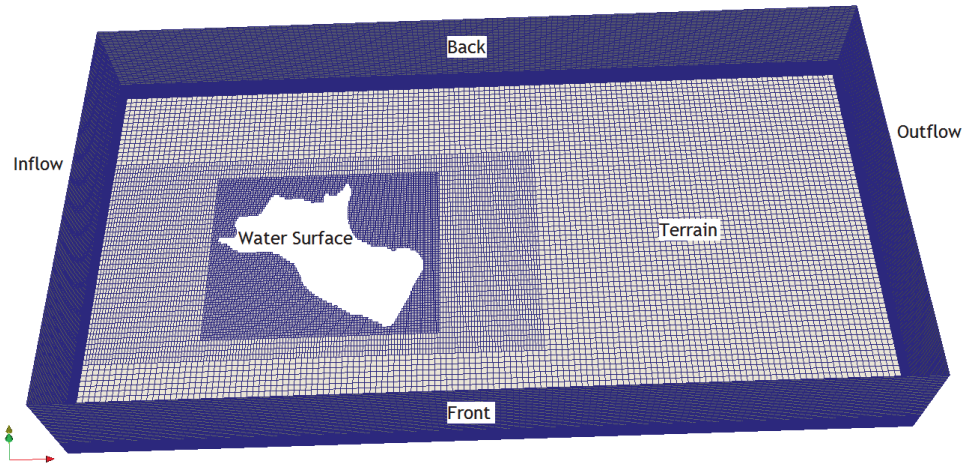


Figure 3.5: Computational domain of ABL model with boundaries and generated grid.

set of different steady state simulations were defined to simulate ABL flow. These scenarios were generated from considering the most important parameters in convective heat and mass transfer processes over the water surface. In addition, these generated scenarios should cover the whole range of the variations of the important parameters in evaporation. With regards to evaporation from the water surface, the important parameters considered in the CFD simulations (scenarios) were: a) water surface temperature (T_{ws}); b) air temperature (T_a); c) wind speed (U_2) over the water surface; and d) the atmospheric stability parameter (to take into account the stability conditions on evaporation). Using CFD simulations the convective heat flow over the water surface were computed for the different defined scenarios. The input data to the model are summarized in Table 3.1. For each established scenario, CFD simulation provides the convective heat transfer (heat flux) between the water surface and atmosphere:

$$H_s = \alpha_{eff} \times \rho_a \times C_p \frac{\partial T}{\partial z} \tag{3.24}$$

where α_{eff} is effective heat transfer coefficient of air ($m^2 s^{-1}$), T is temperature (K), C_p is specific heat of air ($Jkg^{-1}K^{-1}$) and ρ_a is air(fluid) density ($kg\,m^{-3}$). By using Equation (3.24), the convective heat flux can be calculated for each computational grid and consequently, the total heat flux between the water surface and the above atmosphere can be computed from the cell values. As the main goal of this study is to develop a generalizable and cost-effective model to estimate evaporation from water surfaces, the averaged values over the water surface would be used instead of the point-values to calculate heat and mass transfer coefficients.

Applying the calculated total convective heat fluxes (Equation (3.24)), the water surface temperature (T_{ws}) and air temperature (T_a) (in Equation (3.3)), the averaged convective heat transfer coefficients for each scenario were computed. A plot of the calculated averaged convective heat transfer coefficients against the measured wind speed

506469-L-sub01-bw-Abbasi
Processed on: 9-11-2016

Table 3.1: Defined scenarios for CFD simulations

CFD Scenario	T_a [°C]	T_{ws} [°C]	RH [%]	$U_2[ms^{-1}]$	ζ[–]	q_s	q_a
CFDEvap-01	40.02	31.74	28	1.230	-0.047	0.029947	0.012873
CFDEvap-02	17.87	23.98	41	0.582	-1.965	0.018712	0.005157
CFDEvap-03	39.97	32.51	31	1.278	-0.224	0.031345	0.014239
CFDEvap-04	18.24	23.98	35	0.603	-20.41	0.018712	0.004502
CFDEvap-05	32.35	28.20	51	4.792	0.0190	0.024218	0.015460
CFDEvap-06	24.47	24.58	23	0.166	-3.734	0.019422	0.004332
CFDEvap-07	21.53	28.05	76	0.537	-126.3	0.024003	0.012136
CFDEvap-08	39.06	26.60	10	2.714	0.6500	0.021979	0.004307
CFDEvap-09	27.07	27.80	24	2.831	-0.007	0.023464	0.005282
CFDEvap-10	39.36	28.92	18	1.933	-0.005	0.025294	0.007923
CFDEvap-11	32.63	25.21	11	3.507	-126.3	0.020189	0.003322
CFDEvap-12	29.10	25.43	13	4.205	0.6500	0.020641	0.003211
CFDEvap-13	21.53	28.05	76	5.500	———	0.024003	0.012136
CFDEvap-14	39.06	26.60	10	5.500	———	0.021979	0.004307
CFDEvap-15	32.35	28.20	51	4.792	0.0190	0.024218	0.015460
CFDEvap-16	18.24	23.98	35	0.603	-20.41	0.018712	0.004502
CFDEvap-17	39.06	26.60	10	2.714	0.0650	0.021979	0.004307
CFDEvap-18	21.53	28.05	76	0.537	-126.32	0.024003	0.012136
CFDEvap-19	24.47	24.58	23	0.166	-3.734	0.0194220	0.004332
CFDEvap-20	17.87	23.98	41	0.582	-1.965	0.018712	0.0051570

(U_2) over the water surface, produces a linear relationship: $h_s = g(U_2)$. Eventually, assuming heat and mass transfer analogy (Equation (3.9)), and using the averaged calculated heat transfer coefficients (h_s), the averaged convective mass transfer coefficient could be derived as a function of wind speed ($h_m = f(U_2)$). Using Equation (3.10) and the computed mass transfer coefficient, the evaporation rate from the water surface was estimated. The proposed framework for estimating heat fluxes using CFD approach (CFD-Evap Model) is depicted in Figure 3.6.

3.6. NUMERICAL RESULTS AND DISCUSSION

Regression analysis was done for the modelled heat fluxes from the water surface.

3.6.1. WIND FUNCTION

According to the different combinations of T_{ws}, T_a, U_2 and atmospheric stability conditions (ζ), a total of 20 different scenarios were generated for the CFD simulations (Table 3.1). The atmospheric boundary layer in six scenarios were stable ($\zeta > 0$), and unstable ($\zeta < 0$) for the rest. Due to the significant effects of stability conditions on evaporation from water surface (Abbasi et al., 2016a), stable and unstable conditions are considered separately to evaluate the performance of the model in different stability conditions (approach 1 which uses different equations for stable (Equation (3.25)) and unstable (Equation (3.26)) conditions). Figures 3.7(a) and 3.7(b) show the linear regression between the heat transfer coefficient (h_s) values over the lake and the wind speed (U_2) values in the defined scenarios presented in Table 3.1 in stable and unstable atmospheric conditions,

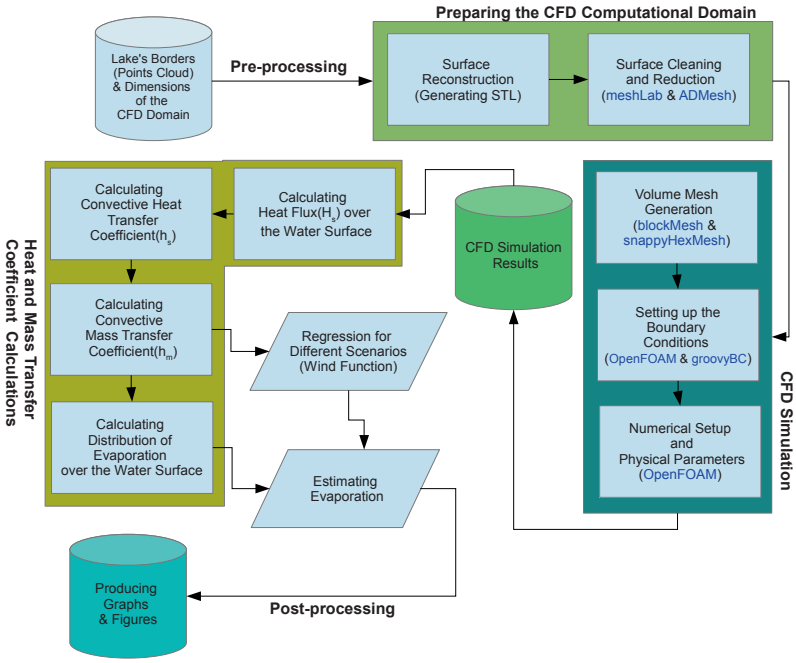


Figure 3.6: Proposed CFD-based simulation (CFDEvap Model) to calculate evaporation from water surface.

respectively. The calculated heat transfer coefficients are given by:

$$Stable \quad Condition \Rightarrow \quad h_s = \quad 2.49270 \times U_2 + 1.33900; \qquad R^2 = 0.817 \quad (3.25)$$

$$Unstable \quad Condition \Rightarrow \quad h_s = \quad 2.35780 \times U_2 + 0.89800; \qquad R^2 = 0.982 \quad (3.26)$$

As in most lakes in the study area, the stability conditions (stability parameters) are not

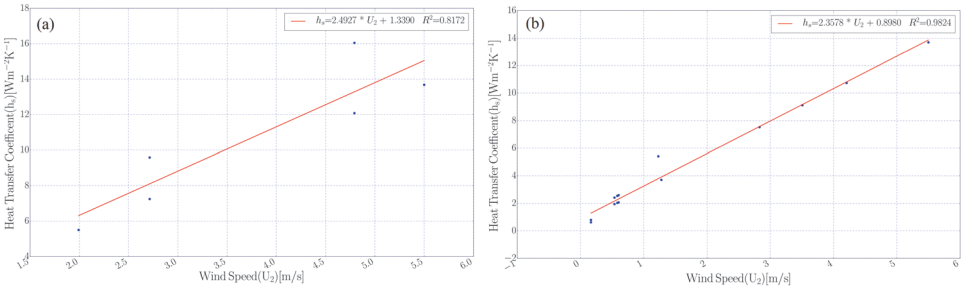


Figure 3.7: Calculated heat transfer coefficient function for different U_2 values in different atmospheric stability conditions: **(a)** stable conditions; and **(b)** unstable conditions.

known, it could be more practical to develop the model independent of stability parame-

ter (approach 2 using a single equation for all atmospheric stability conditions (Equation (3.27))). In Figure 3.8(a) the linear regression of heat transfer coefficient for all scenarios is depicted. It can be given by:

$$h_s = 2.50510 \times U_2 + 0.85200; \qquad R^2 = 0.953 \tag{3.27}$$

where h_s is in $(Wm^{-2}K^{-1})$ and U_2 in (ms^{-1}) respectively. The obtained heat transfer coefficients from both approaches will be used to estimate sensible and latent heat fluxes from the studied lake in Sections (3.6.3) and (3.6.4). Regarding the extracted equation for convective heat flux from the water surface, the sensible heat flux is not only a function of wind speed but also depends on the other parameters (such as temperature difference between the air and water surface) which is summarized in the constant term in Equations (3.25) through (3.27).

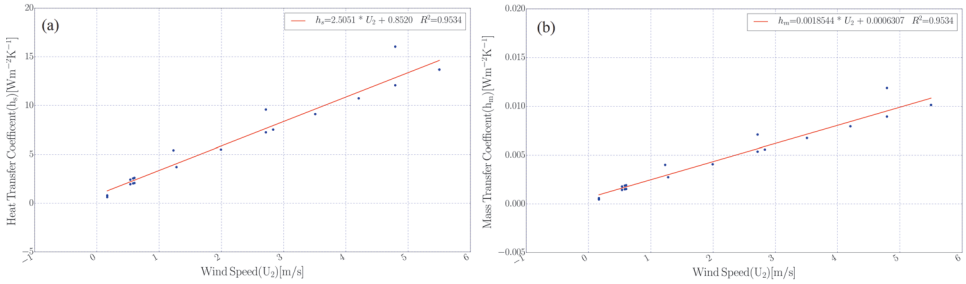


Figure 3.8: Calculated transfer coefficient functions for different U_2 values for total scenarios regardless the stability conditions: **(a)** heat transfer coefficient function; and **(b)** mass transfer coefficient function.

Using the heat and mass transfer analogy as shown in Equation (3.9), the mass transfer coefficient in approach 1 can be given by:

$$Stable \quad Condition \Rightarrow \quad h_m = \quad 0.00184 \times U_2 + 0.00099 \tag{3.28}$$

$$Unstable \quad Condition \Rightarrow \quad h_m = \quad 0.00175 \times U_2 + 0.00066 \tag{3.29}$$

and for whole conditions, regardless of the stability conditions it gives by the following (Figure 3.8(b)):

$$h_m = 0.00185 \times U_2 + 0.00063 \tag{3.30}$$

where h_m is in (ms^{-1}) and U_2 in (ms^{-1}) respectively. Equations (3.28) through (3.30) show that even when the wind speed is very low or in very calm conditions the evaporation values could be non-zero.

However, the equations for sensible (Equations (3.25) through (3.27)) and latent (Equations (3.28) through (3.30)) heat fluxes are extracted using Lake Binaba's properties and its related parameters, the proposed approach is generalizable and with applying minor modifications, it can be used for other water surfaces with different meteorological and geometrical properties.

506469-L-sub01-bw-Abbasi
Processed on: 9-11-2016

3.6.2. MODEL VERIFICATION AND VALIDATION

In Lake Binaba, beside the standard meteorological parameters, sensible heat fluxes were measured during the study period using a 3-D sonic anemometer. The observed sensible heat fluxes were used to validate the estimated convective heat fluxes from the water surface. As the stability conditions are known in Lake Binaba, both obtained transfer coefficients using different approaches (approaches 1 & 2) could be applied to estimate heat fluxes. On one hand, due to the lack of measurements of stability conditions in most lakes, it is preferred to apply the approach 2. In the other hand, comparing the results shows that there are no significant differences between two approaches. In Figure 3.9 the calculated sensible heat fluxes over the water surface are compared with the measured values by using approach 1. The same comparison is illustrated in Figure 3.11 for calculated sensible heat fluxes using approach 2. In both approaches, the estimated values of sensible heat flux are in good agreement with observed ones especially for unstable atmospheric conditions where sensible heat fluxes (H_s) are positive. In Figure 3.10 and Figure 3.12 the calculated and measured sensible heat fluxes are depicted in different times to show the performance of the model in different times. In the stable atmospheric conditions (negative values of H_s), the model overestimated the sensible heat flux values. Regarding the defined CFD scenarios (Table 3.1), in most of scenarios, the atmosphere was unstable. This could be due to the number of stable and unstable atmospheric conditions modelled which gives the impression that the model has a better performance for unstable atmospheric conditions. The accuracy of the model could be improved by defining some extra stable CFD scenarios, improving the CFD simulations by enhanced turbulence models to take into account the buoyancy effects and doing unsteady simulation implementing time-dependent meteorological parameters (Abbasi et al., 2015c). According to the results of Abbasi et al. (2015c), the performance of the ABL model is better in unstable atmospheric conditions rather than the stable conditions and therefore, it could input some errors in the computed sensible heat fluxes especially for stable atmospheric conditions. In Lake Binaba, due to the frequency of unstable conditions (more than 65%) (Abbasi et al., 2016a) the proposed model can be used to estimate evaporation with acceptable level of accuracy. Agreement between the model and measurements reveals that the CFD-based method proposed in this study can provide reliable estimations of the convective heat and mass transfer coefficients especially for unstable atmospheric conditions.

3.6.3. EVAPORATION PREDICTION

In Section (3.4), the convective mass transfer coefficient was derived as a function of the wind velocity. The evaporation rate from the water surface was calculated using the estimated mass transfer coefficient. The evaporation values were obtained by using the mass transfer coefficient for all defined scenarios. Figure 3.13 shows the estimated evaporation values in hourly intervals and the daily averaged values of evaporation as well. The results show that the minimum, average and maximum values of evaporation from Lake Binaba during the study period were 2.75, 4.30 and 5.90 $mm\,d^{-1}$ respectively. The estimated evaporation values are a little higher than ones estimated by Abbasi et al. (2016a) using bulk aerodynamic method by considering atmospheric stability conditions (the minimum, average and maximum values were reported 1.8, 3.6 and

506469-L-sub01-bw-Abbasi
Processed on: 9-11-2016

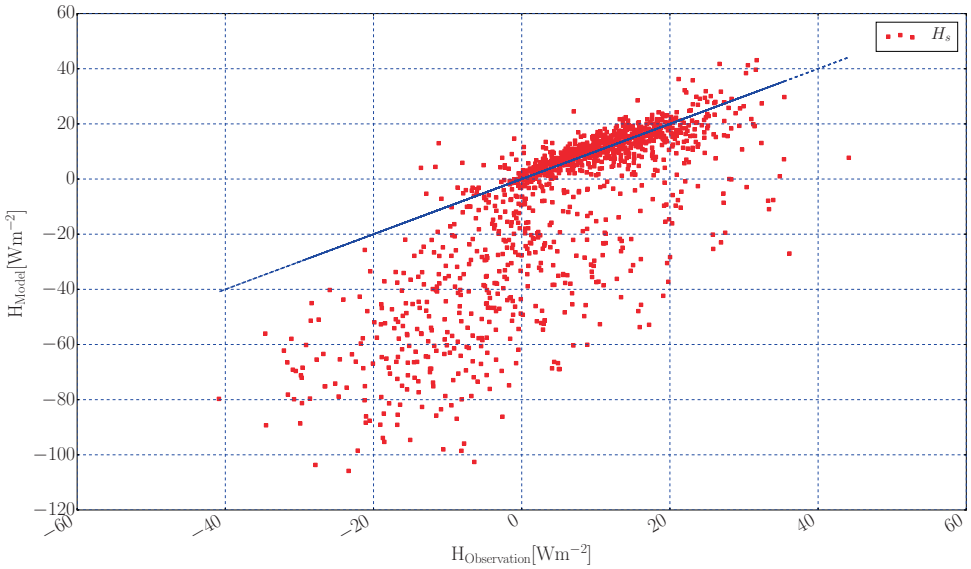


Figure 3.9: Comparison of calculated (CFDEvap Model) and measured (3-D sonic anemometer) sensible heat flux values over twater surface considering stability conditions (approach 1). Dashed line corresponds to the 1:1 relationship.

6.2 mmd^{-1}, respectively). The difference between the evaporation amounts obtained from the CFDEvap Model (this chapter)and the values from Abbasi et al. (2016a) (0.95, 0.7 and −0.3 mmd^{-1} in minimum, average and maximum values, respectively) can be related to the performance of the CFDEvap Model in stable atmospheric conditions (in the Lake Binaba around 35% of time during the measuring period the atmosphere was stable) which overestimates evaporation amount.

In comparison with other methods especially mass transfer methods, the model developed in this study can be applied straightforward to calculate relatively acceptable evaporation amounts from small water surfaces in (semi-)arid regions. The accuracy of estimated evaporation could be improved by increasing the number of steady scenarios to include wide range of effective parameters in evaporation which are used in ABL simulations.

3.6.4. SPATIAL DISTRIBUTION OF EVAPORATION

Using the distribution of transfer coefficients it was possible to estimate the spatially distributions of sensible and latent heat fluxes over the water surface. In Figure 3.14(a) the spatial distribution of sensible heat flux is shown for a selected scenario (CFDEvap-08 in Table 3.1). In this scenario the atmosphere is stable ($\zeta = 0.65$) and the magnitude of the difference between the water surface temperature and air temperature is maximum ($|T_{ws} - T_a| = 12.5$). It can be seen that in the upwind edges of water surface perpendicular to the wind direction, the sensible heat flux has maximum values and its value decrease towards the downwind edges of lake. Therefore the distribution of sensible heat flux

506469-L-sub01-bw-Abbasi
Processed on: 9-11-2016

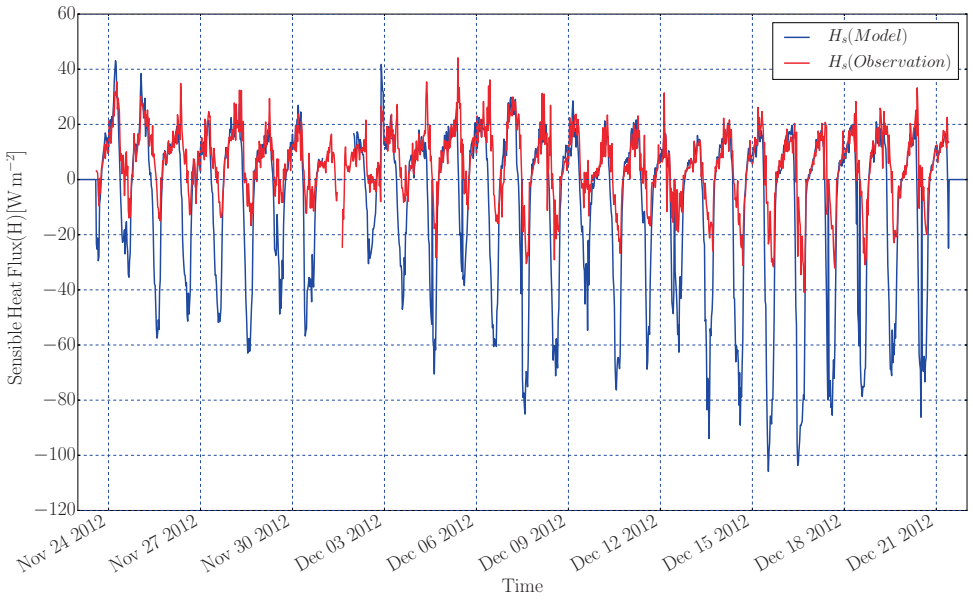


Figure 3.10: Calculated sensible heat fluxes and observed ones over water surface during study period considering stability conditions (approach 1). Negative values of sensible heat flux indicates stable atmospheric conditions.

from the water surface are affected with wind direction and its values. Figure 3.14(b) shows the spatial distribution of evaporation (latent heat flux) from the water surface for the selected scenario (CFDEvap-02 in Table 3.1). This scenario was selected because of its conditions: unstable atmosphere ($\zeta = -1.965$), minimum air temperature ($T_a = 17.87°C$) and its time (07:00:00 in the morning). As it can be seen in Figure 3.14(b), the distribution of evaporation from the lake can be affected by the shape and direction of the water surface's edges. The evaporation values are maximum near the upwind edges perpendicular to the wind direction. However, in the selected scenario (CFDEvap-02) the wind speed is very low ($U_2 = 0.6\,ms^{-1}$) and the incoming short-wave radiation can be ignored, the evaporation value is not zero.

Considering the ability of the proposed approach in modelling the air flow and wind over the water surfaces taking into account the lake's geometry and meteorological parameters, it allows one to investigate the advection aspects and oasis effect over the water surface.

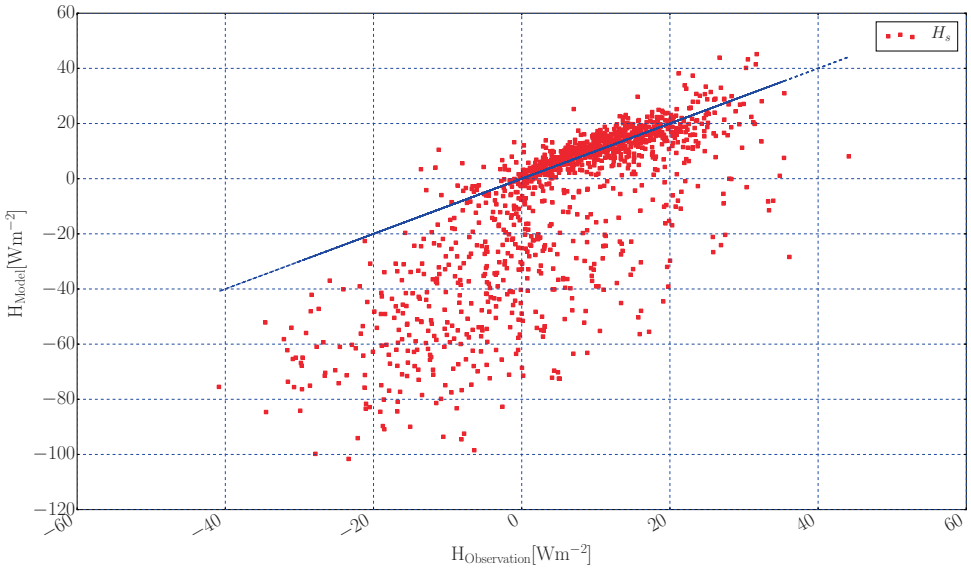


Figure 3.11: Comparison of calculated (CFDEvap Model) and measured (3-D sonic anemometer) sensible heat flux values over water surface regardless of stability conditions (approach 2). Dashed line corresponds to 1:1 relationship.

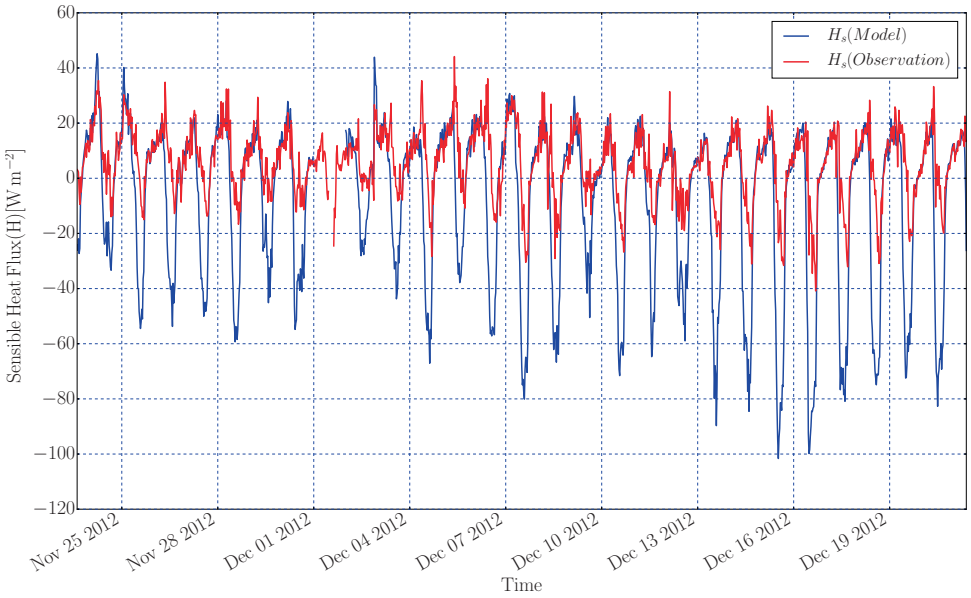


Figure 3.12: Calculated and observed sensible heat fluxes over water surface during study period regardless of stability conditions (approach 2). Negative values of sensible heat flux indicates stable atmospheric conditions.

506469-L-sub01-bw-Abbasi
Processed on: 9-11-2016

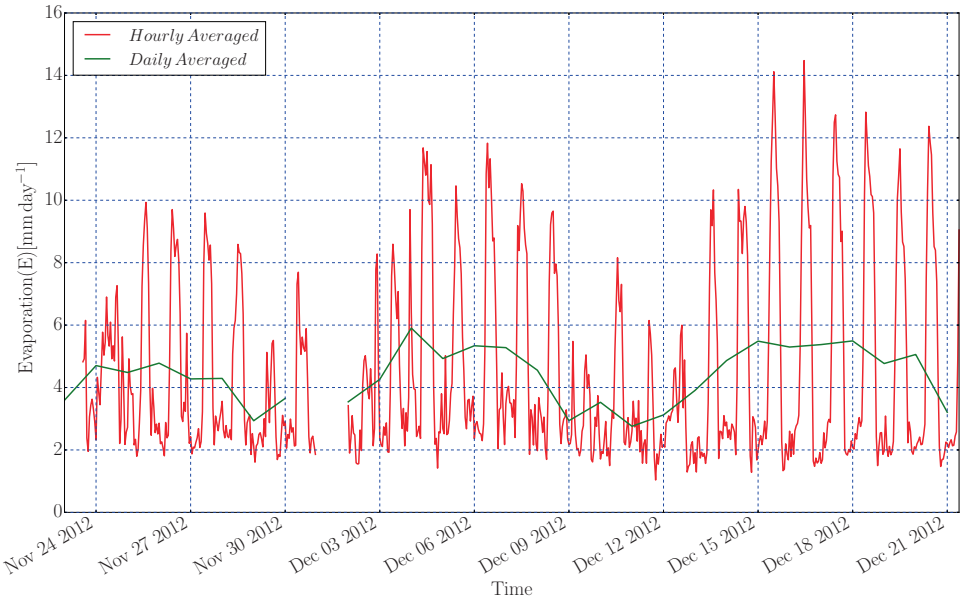


Figure 3.13: Estimated hourly and daily evaporation values from water surface using wind function extracted from CFDEvap Model.

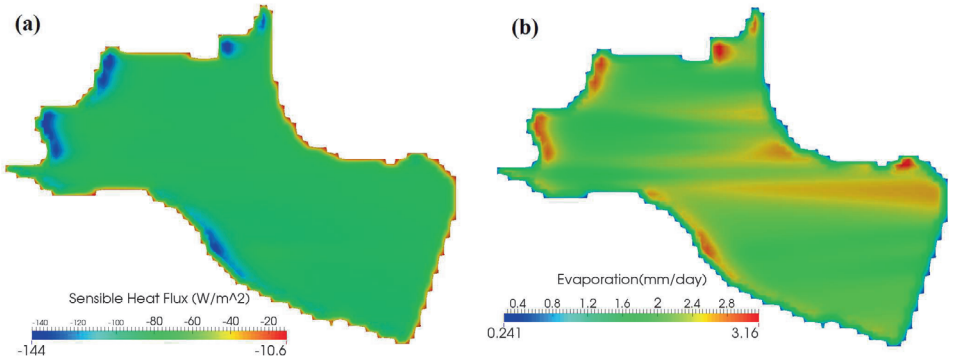


Figure 3.14: Spatial distribution of heat fluxes over water surface: **(a)** sensible heat flux in scenario "CFDEvap-08"; and **(a)** latent heat flux in scenario "CFDEvap-02". Wind direction is from west (left).

506469-L-sub01-bw-Abbasi
Processed on: 9-11-2016

3.7. CONCLUSION

In this study, a CFD-based approach has been developed to determine the heat and mass transfer coefficients over the water surface of a semi-arid shallow and small lake. Using this method, the mass transfer coefficients that are usually used in aerodynamic mass transfer method in estimating evaporation from the water surface, could be estimated and used for evaporation evaluation from the water surface. To determine the heat and mass transfer coefficients, different scenarios based on most important parameters in evaporation from water surfaces include air temperature, water surface temperature, wind speed over the water surface and the atmospheric stability conditions were defined. These scenarios were established in a way that handle the possible changes in values of the effective parameters. According to the determined scenarios, a set of the turbulent ABL airflow simulations were executed to determine the values of airflow variables in the computational domain. Using the heat and mass transfer analogy assumption, the heat (sensible heat flux) and mass (latent heat flux) transfer coefficients were determined (their average values as well as their spatial distributions over the water surface) and consequently, the spatial distributions of sensible and latent heat fluxes over the water surface were computed. The sensible heat flux values estimated by the proposed approach were compared with the measured ones over the lake. The CFDEvap Model developed in this study predicted sensible heat fluxes accurately for unstable atmospheric conditions but overestimated convective heat flux in stable (and neutral) atmospheric boundary layer.

The proposed methodology (CFDEvap approach) represents a useful framework for estimating evaporation from water bodies in (semi-) arid regions where there is an urgent need to find the water losses due to evaporation from stored waters. This approach seems promising specially in regions where advection, oasis and atmospheric instability effects on evaporation are considerably high and the one dimensional models (which are used widely in calculating evaporation) are not capable to give a precise estimation of evaporation amounts. In addition, due to the fully three-dimensional algorithm implemented in the proposed framework, it can generate the map of spatial distribution of evaporation rate and the sensible heat fluxes over the open water surface to evaluate the fetch effects of water surface on evaporation. Although, there are some minor differences between the estimated evaporation values using the developed model in this study with measurements, this model is easily applicable and cost effective. Regarding the available measurements and the accessible computational resources to run ABL simulation, it would be possible to improve the performance of the proposed approach by either including a wider range of scenarios or unsteady modelling of ABL.

506469-L-sub01-bw-Abbasi
Processed on: 9-11-2016

4

A Framework to Simulate Small and Shallow Reservoirs

4.1. Introduction

Inland water bodies (especially small lakes and reservoirs) are usually built to store water during periods with high runoff in order to increase the availability of water in dry seasons. Efficient management of reservoirs depends largely on updated (real-time) information on the water quantity and water quality of the stored water as well as the projected water demand. Flow field and distributions of water temperature and other compositions such as salinity in inland water bodies are crucial parameters that strongly affect water quality. Studying the flow field and temperature dynamics in water bodies requires the use of models to analyze the mathematical equations that govern the processes of circulation and stratification. During the last decades a large number of models with wide range of complexity from simple one-dimensional models to fully three-dimensional circulation models have been produced. In most of these models, the flow equations are solved by using the shallow water assumptions where the diffusion equations for the energy transfer or other constituents are included.

Most reservoir dynamics models assume one-dimensionality conditions, where the scale of heat and momentum changes in vertical (depth) direction is commonly much larger than in the horizontal directions. Although this simplification make the model more straightforward, some significant complex processes occurring in the water bodies especially in shallow ones are ignored. However, one-dimensional models remain attractive due to their appropriateness, simplicity and convenience for studying the flow and temperature dynamics in reservoirs especially for deep and large lakes (Abeysinghe et al., 2005). There is a wide range of one-dimensional models with different assumptions, numerical methods and performance abilities in simulating inland water bodies.

This chapter is based on Abbasi et al. (2015b): Abbasi, A.; Annor, F.O.; van de Giesen, N.: A Framework to Simulate Small and Shallow Inland Water Bodies in Semi-arid Regions. Advances in Water Resources (Manuscript re-submitted for publication), 2015.

506469-L-sub01-bw-Abbasi
Processed on: 9-11-2016

Han et al. (2000) applied Dynamic Reservoir Simulation Model (DYRESM) to simulate the hydrodynamics of Sau Reservoir in the North-Eastern Spain. The one-dimensional Dynamic Reservoir Simulation Model (DYRESM) is widely used to predict the temperature and density distributions in reservoirs considering time varying environmental factors and the watershed characteristics mostly for long-term (seasonal and inter-annual) analyses (Abeysinghe et al., 2005).

Herb and Stefan (2005) and Herb and Stefan (2005) modelled the vertical turbulent diffusion and the stratification process in a shallow lake (Otter Lake) with submersed macrophytes, in the USA. The results of their one-dimensional model showed that thermal stratification is enhanced by macrophytes and wind mixing dependent on the mixed-layer thickness. Hondzo and Stefan (1993) generalized the temperature model for various types of lakes taking the meteorological conditions into account in which vertical turbulent diffusion, surface wind mixing, and heat fluxes were incorporated into the model through regression analysis of the field data. Kirillin (2002) developed a one-dimensional model of temperature evolution in the water bodies considering the general mechanisms of vertical heat exchange in a lake. He tested the model against observations in the Lake Müggelsee, Berlin and showed that the proposed 1-D parameterization model could describe promisingly the structure of the stratification and the temperature profiles in the water body for long-term studies. Kirillin (2010) coupled a global climate model with a one-dimensional lake temperature model, FLake, to evaluate impacts of global warming on two study lakes in Berlin, Germany. Gooseff et al. (2005) developed a temperature model for the Lower Madison River, to investigate the effects of global climate change on extreme water temperature evolutions in aquatic ecosystems using assumption of well-mixed water body. Most of these studies discussed above were done for large and deep lakes where the impacts of the boundary conditions on the flow field and temperature dynamics could be ignored. In addition, they mostly studied long-term effects of large-scale climate on the lakes which are difficult to do for small lakes due to the spatial resolution used in the models. For small reservoirs, detailed hydro-climatological field measurements are needed to validate the model.

In spite of the simplicity and attraction of 1-D models due to their physical realism and computational economy, they cannot be used to predict thermal stratification in shallow water bodies where the horizontal advective term cannot be neglected.

For many shallow water flows, it is sufficient to consider the depth-averaged equations, referred to as the shallow water equations, which are two-dimensional in the horizontal plane, since the length scale of the vertical direction is much smaller than that of the horizontal directions (Lee, 2007). Many two-dimensional models (Naithani et al., 2007; Lap and Mori, 2007; Kim and Cho, 2006) have been proposed for analyzing the vertical mixing, circulation, and wind-induced currents in lakes and reservoirs. Two-dimensional models are based on depth-averaged equations commonly known as shallow water equations. In two-dimensional models, it is assumed that vertical length scale is much smaller than that in the horizontal direction hence the hydrostatic pressure distribution is assumed which significantly simplifies the numerical formulation and computational implementation (Lee, 2007). Lei and Patterson (2001, 2002) investigated the natural convection in a reservoir sidearm subjected to solar radiation using two-dimensional Navier Stokes equations and energy equation with Boussinesq assumption.

506469-L-sub01-bw-Abbasi
Processed on: 9-11-2016

They showed that the 2-D models can be used for quantifying the flow details with some level of confidence. Bednarz et al. (2008, 2009) investigated the response of transient flow to diurnal cycles of heating and cooling at the water surface in a reservoir by using the 2-D RANS (Reynolds Averaged Navier Stokes) equations using the Boussinesq assumption. According to their findings, temperature dynamics (diurnal cycles) in reservoirs has significant environmental and ecological impacts.

It has been recognised that the vertical direction plays a significant role in the circulation of shallow water bodies which one- and two-dimensional models are unable to simulate in lakes (Vreugdenhil, 1994). The flow parameters in shallow water bodies typically have three-dimensional structures due to the effects of complex bathymetry and temperature (density) stratification (Lee, 2007). According to the field measurements by Sweeney (2004) the water bodies with one meter depth or even less can become thermally stratified.

A number of commercial packages have been developed and used by some authors to study the three-dimensional flow structures of shallow water bodies such as waste water stabilization ponds (WSPs) or shallow lakes (Ta and Brignal, 1998; Sweeney, 2004). One of the big challenges in using these packages is the small aspect ratios of depth to horizontal grid increments found in shallow water bodies and complex interactions between the water surface and the atmospheric boundary layer which are the most important forcing terms for vertical mixing and temperature dynamics in the water body. In addition, most of these models do not include the effects of temperature on the flow field in the water body. Although some numerical models (Hodges et al., 2000b; Svensson, 1998) implement the temperature induced circulation in lakes and oceans, most of these models use the hydrostatic pressure approximation. According to the findings of some researchers (Casulli and Cheng, 1992; Casulli, 1999, 1997; Chen, 2003a,b; Chen et al., 2003), vertical velocity calculated using the hydrostatic pressure approximation can lead to numerical errors especially for the scalar transport equation in shallow water bodies.

To study wind-induced circulation with non-hydrostatic distribution of pressure in water bodies with complex bathymetry, Koçyigit and Falconer (2004b) simulated the three-dimensional structure of water flow in Lake Esthwaite, a shallow homogeneous lake in Cumbria, UK. According to their findings, hydrodynamic pressure distribution had some impacts on the vertical velocity profiles especially in the near shorelines where the topography changed sharply. Lee et al. (2009) applied a three-dimensional non-hydrostatic circulation model known as MITgcm which integrates the incompressible Navier Stokes equations using the Boussinesq approximation to analyse the temperature dynamics and water circulation of Yachiyo Lake, Japan (Marshall et al., 1997). Laval et al. (2003) simulated the water circulation in Lake Kinneret taking the impacts of spatial and temporal wind speed fluctuations into consideration by using the three-dimensional Estuary and Lake Computer Model (ELCOM) and validated the model results with some field observations. ELCOM solves the Reynolds Averaged Navier Stokes equations with the hydrostatic pressure approximation using TRIM's algorithm, with slight modifications for the advection terms (Hodges and Dallimore, 2014). Their numerical application indicated that the model can predict diurnal temperature variations accurately. Appt et al. (2004) used three-dimensional model ELCOM to study wind-induced water cir-

506469-L-sub01-bw-Abbasi
Processed on: 9-11-2016

culation in Upper Lake Constance situated in Europe (Germany, Switzerland and Austria) near the Alps. The high-resolution thermal structure of Lake Biwa was examined by Yamashiki et al. (2003) by applying a three-dimensional model based on Large Eddy Simulation (LES). Lee (2007) developed a three-dimensional model using finite difference method to study temperature dynamics and non-hydrostatic distribution of pressure in Torrens Lake in Adelaide, South Australia and showed that the typical thermal variations could be simulated accurately by the 3-D model. Fan and Furbo (2012) used a three-dimensional mathematical model to simulate horizontal and vertical distribution of water temperature of the Fenhe Reservoir, Shanxi province, China and validated the model with field data. They showed that the proposed model could be applicable for long-term studies of large reservoirs. Liu et al. (2012) performed and applied a transient three-dimensional hydrodynamic model to the subtropical alpine Yuan-Yang Lake in Taiwan. Their model was based on Finite Element Method (FEM) and they were able to model the surface elevation and water temperature in a reasonable agreement with field observations of these parameters.

Recently, some well validated commercial codes (e.g. ANSYS FLUENT, STAR-CD, FIDAP, FLOW3D, PHOENICS) have become available and several studies have been conducted using these CFD codes to obtain the hydrodynamic characteristics of shallow water bodies. Politano et al. (2008) used a commercial CFD code FLUENT to undertake a fully three-dimensional non-hydrostatic simulation model of temperature distribution at McNary Dam, US. They used heat flux boundary condition for temperature on the free water surface. Haque et al. (2007) examined the flow structure and temperature distribution within the powerhouse units of McNary Dam on the Columbia River by applying a three-dimensional RANS model implemented in FLUENT. In general, these commercial packages can be used for simulating general fluid flow problems utilizing the Reynolds Averaged Navier Stokes equations. Besides some limitations in modifying, developing and applying commercial software due to the need for the licenses, the small aspect ratio of the computational grid may lead to excessive computational time, instability, and storage requirements in shallow water flow simulations (Lee, 2007).

In comparison with deep and large lakes, several difficulties are encountered in the modeling process for inland shallow lakes and are mainly sources of error in the results. In deep lakes generally the lake-bed contours have little influence on the overall flow pattern in the water body. However, in shallow water lakes, lake-bed variations have a stronger influence on the flow patterns due to their proximity to the surface and should be considered accurately. Therefore accurate bathymetry of these water bodies should be used in their simulations.

Due to the small dimensions of shallow water bodies investigated in this study (maximum 1000 m in horizontal plane, i.e. in $x-$ and $y-$directions), most of the models were developed mainly for large and deep lakes (e.g. DELFT3D and TELEMAC3D) are not applicable (TELEMAC, 2016; DELFT3D, 2016). In addition, in spite of the importance of utilizing the real physical boundary conditions in the simulations, implementing complex and time varying boundary conditions in most of the available models is very challenging.

Considering these restrictions, a framework is developed in this study to simulate the flow field and heat transfer in small and shallow water bodies taking into account the real

506469-L-sub01-bw-Abbasi
Processed on: 9-11-2016

bathymetry, complex boundary conditions based on the available field observations and buoyance effects. This framework is totally based on open-source software and covers all steps needed in the simulation from generating applicable geometry to visualizing the results.

The framework consists of three main components and some sub-components depicted in Figure 4.1. Since the main goal of the study was to develop a model based on open-source toolboxes, all software used are open-source and allow continuous community-based improvement of the model without any requirement for software licenses. The main toolkit used is `OpenFOAM` (OpenFOAM, 2015), a powerful CFD simulation toolkit, which uses the finite volume numerical schemes to solve the governing equations.

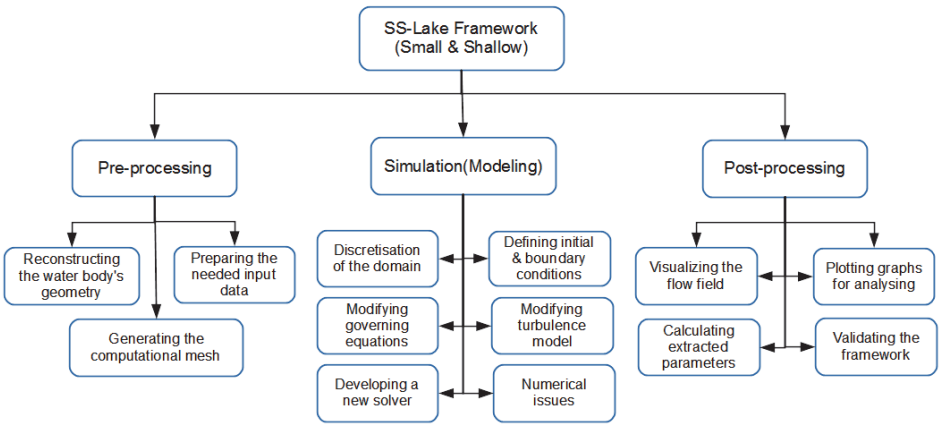


Figure 4.1: Components of the proposed framework (SS-Lake Framework) for simulating small and shallow reservoirs.

4.2. PRE-PROCESSING PHASE

The pre-processing stage which is the first step in the framework as shown in Figure 4.1, has two main issues that should be handled. The first one is preparing the input files needed by the model to read constants, and time-dependent parameters (such as measured values for water surface temperature, short-wave radiation, relative humidity, wind speed, etc.). All model input parameters are prepared by a home-made code using `python`. This code reads the measured values, analyses and validates them and checks the quality of the input data before making it readable in CFD simulations (e.g. in grid generation or modelling by `OpenFOAM`). The generated input files (text files) will be used in the model as the time varying boundary conditions or as time-dependent source/sink terms in turbulence model and flow equations (Sections (4.3.2) and (4.3.4)). The second issue which should be dealt with in this phase is generating the computational grid which is described in more details in Section (4.2.2). The general overview of pre-processing phase tasks are illustrated in Figure 4.2.

506469-L-sub01-bw-Abbasi
Processed on: 9-11-2016

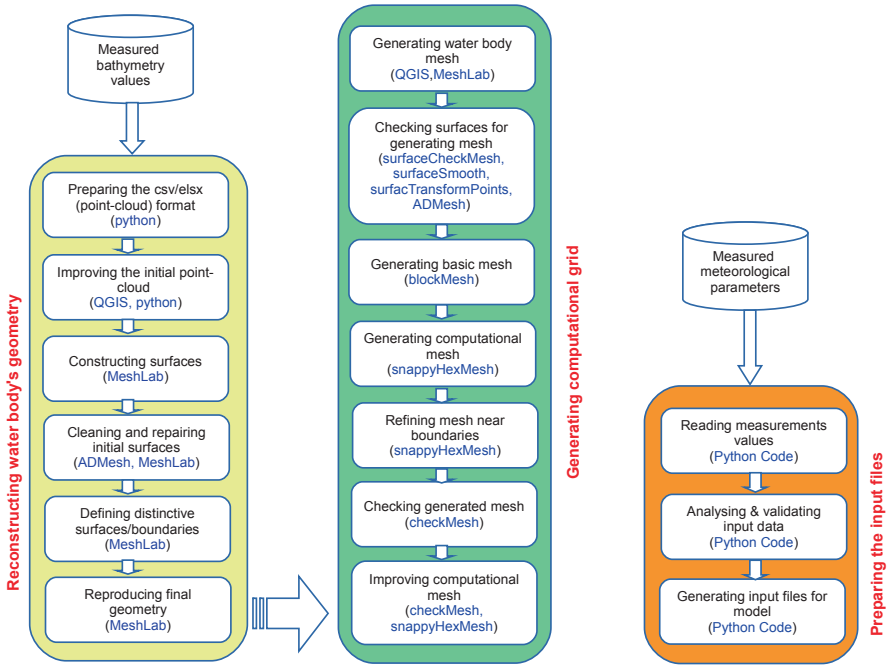


Figure 4.2: Details of pre-processing phase of proposeed framework. Used tools and software to handle each task are presented in the parentheses.

4.2.1. RECONSTRUCTING WATER BODY'S GEOMETRY

In most small and shallow inland water bodies there is no high-quality measurements of the bathymetry or sufficient data to build the geometry of the computational domain applicable in CFD modelling. It could be related to the logistical difficulties or maybe due to the high cost of doing measurements over these water surfaces. Again, most available tools and software used to generate surface (for all surfaces in the domain: water surface, bottom and sides of the reservoir) fail mainly due to the small ratio of the depth to the horizontal dimensions (H/L where H is the depth and L is the length) of these water bodies (in this study this ratio, H/L, varies from 0.0002 to 0.004). The initial measured bathymetry is a point-cloud which contains a set of $x-$, $y-$ and $z-$coordinates of measured points. Using this rough point-cloud the generated surfaces were very poor and not applicable in the model. To resolve this problem, a robust, straightforward and generalizable approach was developed in this framework to reconstruct the water surface, bottom and side surfaces of the water body using the roughly measured bathymetry depicted in Figure 4.4(a,b). Using the open-source tools mentioned previously in Figure 4.2, the initial point-cloud was improved to generate acceptable and applicable surfaces for CFD simulations. The method presented in this study to improve the measured bathymetry focuses on small and shallow lakes, although the developed procedure could be applicable for similar problems. Reconstructing the surfaces (geometry) of inland wa-

ter bodies includes the following steps:

1. Reading the initial bathymetry data which contains the $x-$, $y-$ and $z-$coordinates of measured points at the bottom and sides of the lake (1838 points for an example for lake Binaba), separated with a tab, called initial point-cloud. This initial point-cloud had some problems in generating an applicable geometry for being used in CFD simulations due to: a) this point-cloud doesn't have adequate resolution. In some regions there is no point to generate the surface (accessibility constraints during measuring may leave some regions devoid of data); b) it has no point sets to define the water surface boundary. The measured points with highest elevation (or z-values) do not represent the water surface and it is necessary to define this boundary (surface) in the point cloud; c) there are some points in the point-cloud that do not belong to the lake bathymetry (some points in the dry region in the shoreline that should not be included in the geometry of lake); d) the vertical scale compared with the horizontal lengths is very small (around $2:1000$) and causes significant errors in generating the geometry; and e) the point samples may not be uniformly distributed over the model surface.

2. Improving the initial point-cloud by adding some extra points using the interpolation methods which is done by using `QGIS` (Open Source Geographic Information System) (QGIS, 2015). The improved point-cloud contains 42412 points which could be sufficient to produce smooth surfaces applicable in the modelling.

3. Generating a `csv` (comma-separated values) file containing the points' coordinates is interpretable by `MeshLab` (an open-source and extensible toolkit for generating, editing and processing unstructured 3D triangular meshes) (MeshLab, 2015) to generate surfaces of the water body.

4. Reading the improved point-cloud, checking, modifying and generating an `STL` (STereoLithography / Standard Triangle Language) file by using `MeshLab` which could be handled by mesh generator toolboxes. In an `STL` file, multiple objects can be represented as a list of triangles that conform to their surfaces. It should be noted that in this step the normal vectors of point-sets and the quality of generated surfaces should be checked. Due to the very small ratio of the depth to the horizontal dimensions, prior to generating `STL` file, the dimensions should be scaled up in $z-$direction (depth) to generate an acceptable surface. The method used to get an applicable surface from the improved point-cloud, should be able to infer the topology of the surfaces, accurately fit the noisy data, and fill holes reasonably. From several trails to construct surfaces, it was found that the 'Poisson' method (implemented in `MeshLab`) could be a befitting pick for reconstructing the surface from the point-cloud. Poisson Surface Reconstruction is one of the approaches to obtain smooth and watertight surface. As the final task after generating the surfaces (`STL` files), it is strictly suggested to do some repairing and cleaning processes (such as merging close vertices, removing duplicate faces, remove duplicate vertex, etc.).

5. To be able to assign the right boundary conditions to the surfaces (boundaries) in the model, distinctive surfaces should be defined in the reconstructed `STL` file. In

506469-L-sub01-bw-Abbasi
Processed on: 9-11-2016

most inland water bodies models there are mainly two different surfaces: a) a surface that represents the water surface; and b) a surface that represents the bottom and sides. Defining extra surfaces such as inlet and outlet boundaries could be done easily in the proposed approach.

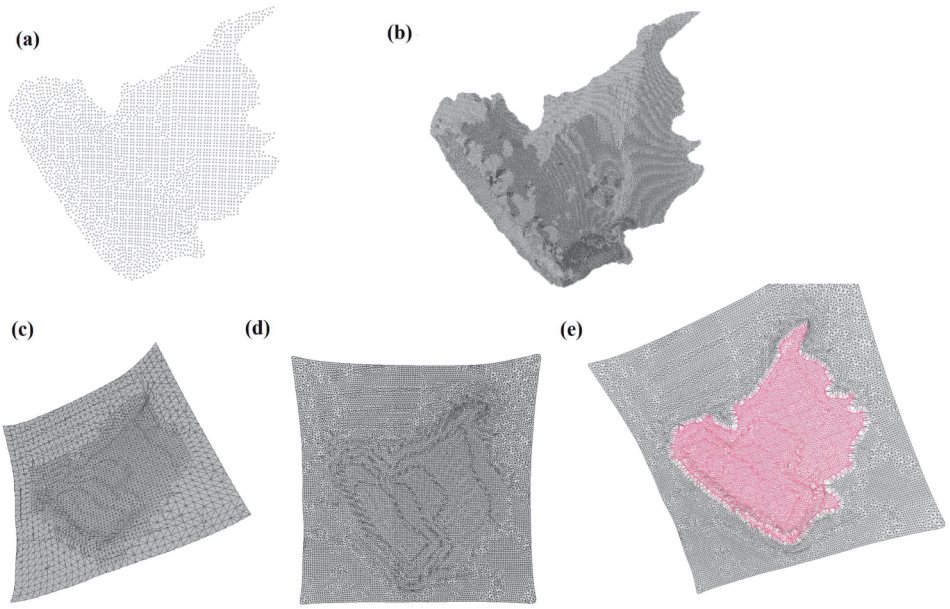


Figure 4.3: Chained processes of generating surfaces (in STL format) from an initial point-cloud: **(a)** plan view of initial point-cloud **(b)** improved point-cloud using proposed approach to generate water body's geometry **(c)** initially generated surface **(d)** refining and reconstructing initial generated surface; and **(e)** separating surfaces and removing unneeded parts.

4.2.2. GENERATING THE COMPUTATIONAL GRID

In Section (4.2.1) an approach to generate the necessary surfaces which represent the boundaries in the model was presented. The next step through the presented framework is to translate the physical domain into a numerical domain, or computational mesh. The generated mesh must accurately represent the shape of the water body. The quality of the computational grid has a clear impact on the accuracy of the CFD simulations and influences significantly the convergence speed of the simulation. In spite of the importance of the computational grid in CFD simulations, generating an appropriate high quality grid (i.e. low skewness, low orthogonality, aspect ratio near 1, etc.) remains a big challenge while using inappropriate grids will lead to large errors.

The proposed framework uses a right hand coordinate system (typically used in simulations), with the $z-$axis positive in the upward direction (normal to the water surface) and $z = z_{ws}$ represents the maximum depth of lake, corresponding to the water surface. The origin is located in the lower left-hand corner of the mesh, when viewed in

506469-L-sub01-bw-Abbasi
Processed on: 9-11-2016

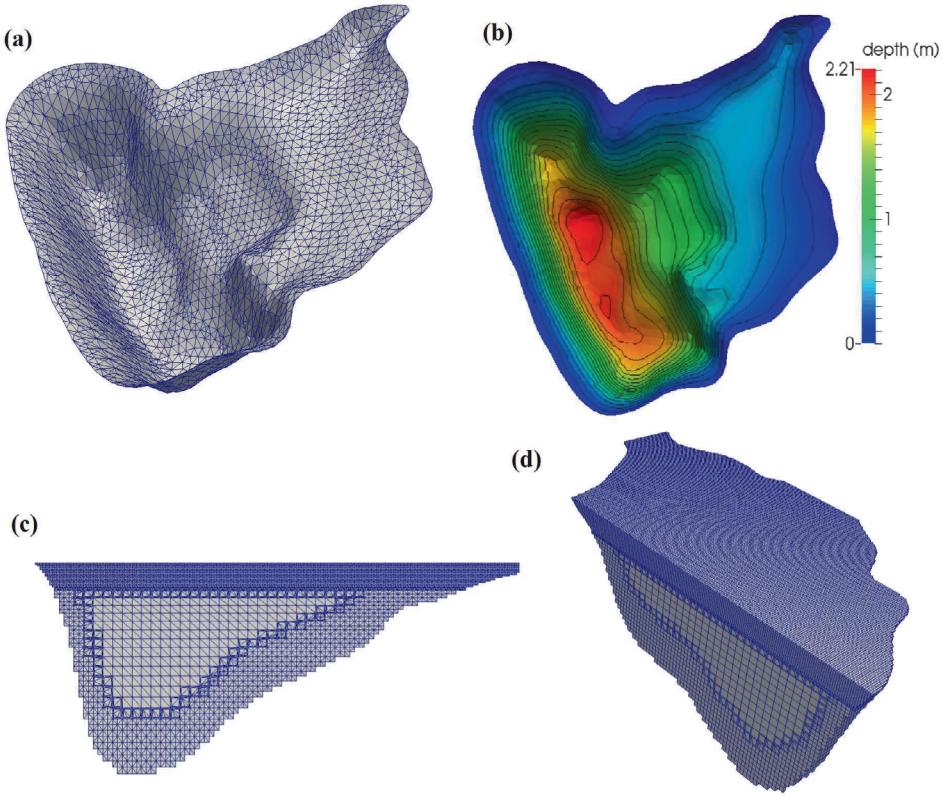


Figure 4.4: **(a)** Example of final generated surface (in STL format) of a water body which is used in generating computational mesh **(b)** 3-D view of water body's geometry and the depth contours **(c)** vertical section of generated computational grid of water body and **(d)** 3-D view of computational grids (vertical dimension is exaggerated by 50).

the $xy-$plane. Keeping with this convention in the model, the $x-$axis is aligned to be positive in the easterly direction, with the $y-$axis positive in the north direction.

Horizontal grids are generated depending on the geometrical boundaries conforming to improve measured bathymetric data. For the vertical direction, when turbulence models are included the vertical grid points are clustered near the free surface to resolve the flow field and capture temperature distributions and shear stress distribution in the most dynamic zone. Figure 4.4(c,d) shows details of the generated grid. The typical cell size in the lake (in this study) is 10 m and 0.1 m in the horizontal and vertical directions respectively. Near the free water surface, refining the grid is essential especially in vertical direction (cell heights are about 0.01-0.02 m) to capture the strong temperature and velocity gradients which exist at the air-water interface due to the impacts of atmospheric conditions (Haque et al., 2007).

Generating a good mesh is very challenging for shallow water bodies due to the high

506469-L-sub01-bw-Abbasi
Processed on: 9-11-2016

aspect ratio cells which commonly exist in some regions. In generating the computational grids there is always a trade-off between run time and good results (mainly from a good grid resolution in the vertical direction). This results in high aspect ratios and long flat cells. Generally, generating computational grid for non-uniform geometries (in which one of the directions is much smaller than the others) seems problematic for most available grid generators which generally deliver optimum results ensure good convergence for aspect ratios near one. This problem could be resolved by scaling/rescaling the dimensions in the desired direction (Brockhaus, 2011). It is strongly suggested that the adequacy of the grids is investigated by comparing the results of the model using different mesh sizes. Commonly, using fine mesh in simulations produces better agreement in some regions of studied domain, however it needs more computational resources and more run time hence some judgments should be made on the desired accuracy and the required computational resources.

The grid generation was done with an `OpenFOAM`-utility `snappyHexMesh(sHM)` (SnappyHexMesh, 2015). Unlike most commercial and automatic grid generators `sHM` is a script-driven tool used to generate unstructured computational grid containing hexaedra and split-hexaedra meshes (Brockhaus, 2011). `sHM` proved to be very flexible with different domain configurations. `sHM` allows to use `STL` files which represent the domains' topography in complex geometries.

In general, the process of generating computational grids includes the following steps:

1. Checking the quality of reconstructed surfaces (`STL` file) and cleaning or repairing the surfaces which involves: a) checking the surface by using `surfaceCheck` utility; b) smoothing the surfaces by using `surfaceSmooth` utility; c) rotating the surface to decrease the non-orthogonality of the generated mesh by using `surfaceTransformPoints` utility; and finally, d) cleaning and repairing the final surface by using `ADMesh` (a program for processing triangulated solid meshes) (ADMesh, 2015). The finally cleaned, repaired and improved surface could be used to generate the computational grids afterwards;

2. Generating a background block structured mesh which contains the outlines of the computational domain. The quality of finally generated mesh is significantly affected by the aspect ratio, fineness, orientation and other properties of the initial mesh used;

3. Generating the computational grid using the `snappyHexMesh(sHM)` utility. `sHM` uses a non-interactive approach to generate the grid hence could be considered as an almost ideal tool for automatized mesh generation (Brockhaus, 2011). Notwithstanding this advantage, it must be mentioned that this tool does not have a graphical interface and everything should be controlled from its dictionary by commands;

4. Refining the mesh near the boundaries to resolve high gradients in flow parameters using the available options in `sHM` ; and

5. Checking the quality (maximum aspect ratio, non-orthogonality, skewness, etc.) of the mesh by using `checkMesh` utility and improving the grids if necessary.

506469-L-sub01-bw-Abbasi
Processed on: 9-11-2016

4.3. SIMULATION PHASE

4.3.1. GOVERNING EQUATIONS

The flow field in morphometrically complex small and shallow water bodies is governed by the conservation laws of mass, momentum and energy. Combining the flow simulation and heat transfer in the water body alongside the complex geometry of lake introduces extra complexities to the model. In water bodies, the wind shear stress due to air flow and changes in water density due to temperature evolution are considered as driving forces. Even though the thermodynamical properties of water are assumed to be constant, the buoyancy body force term in the momentum equation is added allowing one to relate density changes to temperature. The flow is assumed to be three-dimensional, incompressible Newtonian fluid using Boussinesq approach (Tsanis, 2006; Tritton, 2007). Based on these assumptions the Reynolds Averaged Navier Stokes (RANS) equations are written as (Ferziger and Perić, 2002; White, 1991; Massel, 1999):

$$\frac{\partial u_j}{\partial x_j} = 0 \tag{4.1}$$

$$\frac{\partial u_i}{\partial t} + \frac{\partial}{\partial x_j}(u_j u_i) - \frac{\partial}{\partial x_j}\left\{\nu_{eff}\left[\left(\frac{\partial u_i}{\partial x_j} + \frac{\partial u_j}{\partial x_i}\right) - \frac{2}{3}\left(\frac{\partial u_k}{\partial x_k}\right)\delta_{ij}\right]\right\} = -\frac{1}{\rho_k}\frac{\partial p}{\partial x_i} + g_i\left[1-\beta(T-T_{ref})\right] \tag{4.2}$$

$$\frac{\partial T}{\partial t} + \frac{\partial}{\partial x_j}(Tu_j) - \alpha_{eff}\frac{\partial}{\partial x_k}(\frac{\partial T}{\partial x_k}) = S_T(t,x_k) \tag{4.3}$$

where u_i is the velocity component in x_i-direction (ms^{-1}), t is time (s), p pressure (Pa), T temperature (K), $\nu_{eff} = \nu_0 + \nu_t$ is the effective kinematic viscosity $(m^2 s^{-1})$, with ν_0 and ν_t denoting molecular and turbulent viscosity, respectively, g_i the gravity acceleration vector (ms^{-2}), T_{ref} a reference temperature (K), β the coefficient of expansion with temperature of the fluid $(Jkg^{-1}K^{-1})$ and δ is the delta of Kronecker (dimensionless), α_0 and α_t are molecular and turbulent heat transfer coefficient respectively $(m^2 s^{-1})$, ρ_k is effective kinematic density (dimensionless) and S_T is the heat source term (Ks^{-1}) in the lake due to the penetrated solar radiation. The Boussinesq approximation is valid under the assumption that the density differences are sufficiently small to be neglected, except where they appear in the term multiplied by g_i (Fredriksson, 2011; Corzo et al., 2011). According to White (1991) and Ferziger and Perić (2002), the Boussinesq approximation introduces errors less than 1% for temperature variations of $2\,K$ for water or $15\,K$ for air. In the model, for incompressible flows the water density is computed as a linear function of temperature as

$$\rho_k = 1-\beta\left(T-T_{ref}\right) \tag{4.4}$$

$$\rho = \rho_k \times \rho_0 \tag{4.5}$$

where ρ is the temperature dependent density (kgm^{-3}), and ρ_0 is water density at reference temperature (kgm^{-3}). Heat transfer conductivity in water body is given by:

$$\alpha_{eff} = \alpha_t + \alpha_0 = \frac{\nu_t}{Pr_t} + \frac{\nu_0}{Pr} \tag{4.6}$$

506469-L-sub01-bw-Abbasi
Processed on: 9-11-2016

where ν_0 molecular kinematic viscosity ($m^2 s^{-1}$), ν_t turbulent kinematic viscosity ($m^2 s^{-1}$), Pr is Prandtl number (a dimensionless number defined as the ratio of momentum diffusivity to thermal diffusivity which controls the relative thickness of the momentum and thermal boundary layers), Pr_t turbulent Prandtl number (unitless). Changes in temperature in water bodies might occur mainly due to the heat exchange across the air-water interface. Accurate estimation of the heat fluxes is largely required in the simulation of temperature dynamics in the water body (Politano et al., 2008). Atmospheric heat fluxes include incoming short-wave (solar) and long-wave (atmosphere) radiations, outgoing long-wave radiation, conductive heat at the free surface and evaporative heat flux. Computationally, all of the heat flux components except for incoming short-wave radiation are considered as boundary condition at the water surface.

Including the incoming short-wave radiation in the temperature source term (S_T) allows the radiation to penetrate and be absorbed through a specific depth of the water column rather than only at the air-water interface (Losordo and Piedrahita, 1991; Wood et al., 2008). The heat source term using Lambert-Beer low is written as:

$$S_T(z^*, t) = \frac{1}{\rho_0 C_p} \frac{\partial Q_{Rs}^{z^*}}{\partial z} \tag{4.7}$$

$$Q_{Rs}^{z^*} = Q_{Rs}^0 \sum_{i=1}^{7} f_i \exp\left(-\eta_i z^*\right) \tag{4.8}$$

$$S_T(z^*, t) = \frac{Q_{Rs}^0}{\rho_0 C_p} \sum_{i=1}^{7} \eta_i f_i \exp\left(-\eta_i z^*\right) \tag{4.9}$$

where z^* is downward vertical distance from the water surface (m), C_p specific heat of lake water ($Jkg^{-1}K^{-1}$), $Q_{Rs}^{z^*}$ is heat flux due to penetrated solar radiation at a depth z^* within the water (Wm^{-2}), Q_{Rs}^0 is the net solar radiation at the air-water interface (Wm^{-2}), f_i is the fraction of energy contained in the i^{th} bandwidth (dimensionless), and η_i is the composite attenuation coefficient of the i^{th} bandwidth (m^{-1}) (Branco and Torgersen, 2009; Momii and Ito, 2008). The values of f_i and η_i are presented in Table 4.1. The attenuation coefficient (light extinction coefficient) for visible light theoretically is a function of wave length, temperature and water turbidity (Politano et al., 2008; Losordo and Piedrahita, 1991) and typically ranges from 0.02 to 31.60 for inland shallow waters (Politano et al., 2008; Smith and Baker, 1981; Losordo and Piedrahita, 1991; Goudsmit et al., 2002; Bigham Stephens et al., 2015). In inland water bodies, usually the extinction coefficient is computed by using a linear function of the Secchi depth (Idso and Gilbert, 1974; Politano et al., 2008). According to Henderson-Sellers (1984), value of η is largely affected by water turbidity and macrophyte population in the water body. Based on measured Secchi disc (a device to measure water turbidity) depth, Williams et al. (1981) suggested that, under non-eutrophic conditions, η can be represented by (Lee, 2007; Williams et al., 1981):

$$\eta = 1.1 \times d_s^{-0.73}, \tag{4.10}$$

where d_s is the Secchi disc depth (m). To calculate η accurately, detailed measurements of macrophyte population are necessary; these are normally not available. For this study,

506469-L-sub01-bw-Abbasi
Processed on: 9-11-2016

Table 4.1: Short-wave radiation bandwidth fractions of the total energy (f) and composite attenuation coefficients (η) (adopted from Branco and Torgersen (2009)

Wavelength(nm)	f	$\eta(m^{-1})$
< 400 (UV)	0.046	assume same as VIS
400-700 (VIS)	0.430	Obtained from measurements (here assumed 3.0)
700-910	0.214	2.9
910-950	0.020	20.4
950-1090	0.089	29.5
1090-1350	0.092	98.4
> 1350	0.109	2880.0

the attenuation coefficient was assumed to be 3.0 ($\eta = 3.0\,m^{-1}$). The net solar radiation at the air-water interface (Q^0_{Rs}) is given by the following equation (Subin et al., 2012):

$$Q^0_{Rs} = (1 - r_{ws})\, R_s \tag{4.11}$$

where R_s is the incoming short-wave radiation at the water surface ($W m^{-2}$) and r_{ws} is the reflection coefficient of solar radiation from water surface (dimensionless).

4.3.2. TURBULENCE MODEL

In order to model the turbulent flows using the RANS approach requires a turbulence model to compute the Reynolds stresses and close the system of mean flow equations. According to the number of additional transport equations which should be solved along with the RANS equations, a wide range of turbulence models has been proposed (e.g. zero, one, two or seven equation models).

From literature reviewed, standard $k-\varepsilon$ (SKE) and realizable $k-\varepsilon$ (RKE) models are widely used in most CFD simulations. The semi-empirical standard $k-\varepsilon$ model contains transport equations for the turbulence kinetic energy (k) and the dissipation rate of kinetic energy (ε). Various two-equation models (such as $k-\omega$) similar to the standard $k-\varepsilon$ model are available which need extra input parameters. However the standard $k-\varepsilon$ model is mostly used for circulation models with free surface variation. In simulating water flow alongside heat transfer in inland water bodies, it was found that the realizable $k-\varepsilon$ model provides better results than the standard or other traditional $k-\varepsilon$ models (Shih et al., 1995; Wang, 2013). In this model, dissipation rate of fluctuations is approximated by the dynamic vorticity equation. In addition, the realizable $k-\varepsilon$ model has been shown to enhance the numerical stability in turbulent flow simulations (Shih et al., 1995). In this model, the turbulent kinetic energy (k in $m^2 s^{-2}$) and the dissipation rate of turbulent kinematic energy (ε in $m^2 s^{-3}$) were obtained from:

$$\begin{aligned} \frac{\partial k}{\partial t} + u_j \frac{\partial k}{\partial x_j} &= \frac{\partial}{\partial x_j}\left[\left(\frac{\nu_t}{\sigma_k}\right)\frac{\partial k}{\partial x_j}\right] + \nu_t\left(\frac{\partial u_i}{\partial x_j} + \frac{\partial u_j}{\partial x_i}\right)\frac{\partial u_i}{\partial x_j} - \varepsilon \\ &+ G_k + G_b + S_k \end{aligned} \tag{4.12}$$

$$\begin{aligned} \frac{\partial \varepsilon}{\partial t} + u_j \frac{\partial \varepsilon}{\partial x_j} &= \frac{\partial}{\partial x_j}\left(\frac{\nu_t}{\sigma_\varepsilon}\frac{\partial \varepsilon}{\partial x_j}\right) + C_1 S\varepsilon - C_{\varepsilon 2}\frac{\varepsilon^2}{k+\sqrt{\nu\varepsilon}} \\ &+ C_{\varepsilon 1} C_{\varepsilon 3}\frac{\varepsilon}{k} G_b + S_\varepsilon \end{aligned} \tag{4.13}$$

506469-L-sub01-bw-Abbasi
Processed on: 9-11-2016

where ν_t is the turbulent kinematic viscosity ($m^2 s^{-1}$), G_k is the production of turbulent kinetic energy by the mean velocity gradient ($m^2 s^{-3}$), G_b is the production of turbulent kinetic energy by the buoyancy ($m^2 s^{-3}$), S_k (in $m^2 s^{-3}$) and S_ε (in $m^2 s^{-4}$) are the source terms which include the effects of wind on k and ε equations respectively. The parameter $C_{\varepsilon 3}$ (dimensionless) is the ratio of the velocity functions in the vertical and longitudinal directions and is not constant but instead depends on the flow conditions (Lee, 2007):

$$C_{\varepsilon 3} = \tanh|\frac{w}{u_h}| \tag{4.14}$$

where u_h and w are the components of the flow velocity perpendicular and the components of the flow velocity parallel to the gravitational vector, respectively (ms^{-1}). The coefficient C_1 is evaluated as (Shih et al., 1995):

$$C_1 = max\left(0.43, \frac{\zeta}{\zeta+5}\right) \tag{4.15}$$

$$\zeta = S\frac{k}{\varepsilon} \tag{4.16}$$

$$S = \sqrt{2S_{ij}S_{ij}} \tag{4.17}$$

$$S_{ij} = \frac{1}{2}\left(\frac{\partial u_i}{\partial x_j} + \frac{\partial u_j}{\partial x_i}\right) \tag{4.18}$$

and the turbulent kinematic viscosity is given by

$$\nu_t = C_\mu \frac{k^2}{\varepsilon} \tag{4.19}$$

$$C_\mu = \frac{1}{A_0 + A_s\frac{kU^*}{\varepsilon}} \tag{4.20}$$

$$U^* = \sqrt{S_{ij}S_{ij} + \overline{\Omega_{ij}}\,\overline{\Omega_{ij}}} \tag{4.21}$$

$$A_s = \sqrt{6}\cos\phi \tag{4.22}$$

$$\phi = \frac{1}{3}cos^{-1}(\sqrt{6}W) \tag{4.23}$$

$$W = \frac{S_{ij}S_{jk}S_{ki}}{\widetilde{S}^3} \tag{4.24}$$

$$\widetilde{S} = \sqrt{S_{ij}S_{ij}} \tag{4.25}$$

where $\overline{\Omega_{ij}}$ is the mean rate-of-rotation tensor. The production of turbulent kinetic energy by the mean velocity gradient (G_k) is written as

$$G_k = \nu_t S^2 \tag{4.26}$$

When a temperature gradient and a non-zero gravity field are present simultaneously (such as for the current model), the k and ε equations include the generation of k due to

buoyancy (G_b in Equation (4.12)), and the corresponding contribution to the production of ε (G_b in Equation (4.13)). The buoyancy-induced turbulence is given by

$$G_b = \beta g_i \frac{\nu_t}{Pr_t}\left(\frac{\partial T}{\partial x_i}\right) \tag{4.27}$$

where g_i is the component of the gravitational vector in the i-th direction and Pr_t is the turbulent Prandtl number. The default value of Pr_t for water used in the standard and realizable $k-\varepsilon$ models is 0.85 (Fluent, 2006; Wang, 2013). In unstable stratification $G_b > 0$ and turbulence kinetic energy tends to be higher. For stable stratification, $G_b < 0$ and the buoyancy force tends to disrupt the turbulence. While the effects of buoyancy on the generation of k are relatively well understood and are commonly included in the turbulence models when there are both a non-zero temperature (or density) gradient and a non-zero gravity field, the buoyancy effect on ε is less clear (Fluent, 2006). However, in the model prepared, the buoyancy effects on ε are given by Equation (4.26) which is used in the transport equation for ε (Equation (4.13)). The degree to which ε is influenced by the buoyancy is estimated by the non-constant parameter $C_{3\varepsilon}$.

Standard values of the model constants of the realizable $k-\varepsilon$ turbulence approach in the model equations are (Shih et al., 1995):

$$C_\mu = 0.09; \quad C_{\varepsilon 1} = 1.44; \quad C_{\varepsilon 2} = 1.92; \quad \sigma_k = 1.0; \quad \sigma_\varepsilon = 1.3; \quad A_0 = 4.0 \tag{4.28}$$

Depending on the approach used to implement the effects of wind velocity over the water surface in the model (Sections 4.3.2 and 4.3.2), the source/sink terms (in Equations (4.12) and (4.13)) can be determined.

WIND EFFECTS INCLUDED AS SOURCE/SINK TERMS IN TURBULENCE EQUATIONS

In shallow and small inland water bodies, turbulence produced by wind can be critical. The momentum input at the water surface can be caused by water surface (skin) friction, wave-induced pressure fluctuations and wave and drift-related current interactions (Wang, 2013). Below the wave-affected surface layer, the vertical profiles of the horizontal velocity follow the law-of-the-wall. The classical logarithmic-layer characteristic is thus applicable (Craig and Banner, 1994). The effects of wind speed on the water body can be considered as source/sink terms in the turbulence model's equations (Wüest and Lorke, 2003; Wang, 2013). In this approach the effects of wind shear stress over the flow was implemented in turbulence equations using source/sink terms (S_k and S_ε). Using this method water surface is modeled using a rigid-lid approach. In this approximation, the free surface deformations are ignored (Tsanis, 2006). Assuming a flat surface with zero shear stress, a slip boundary condition (normal component of velocity, u_z is zero and tangential components, u_x and u_y are zero gradient) is used for velocity on the water surface boundary:

$$u_x \neq 0; \qquad \frac{\partial u_x}{\partial z} = 0 \tag{4.29}$$

$$u_y \neq 0; \qquad \frac{\partial u_y}{\partial z} = 0 \tag{4.30}$$

$$u_z = 0 \tag{4.31}$$

506469-L-sub01-bw-Abbasi
Processed on: 9-11-2016

and effects of wind stress on k and ε can be parameterized as source/sink terms in Equation (4.12) and Equation (4.13) as (Wüest and Lorke, 2003):

$$S_k = \frac{u_*^3}{\kappa z^*} \tag{4.32}$$

$$S_\varepsilon = C_{1\varepsilon}\frac{\varepsilon}{k}S_k \tag{4.33}$$

It means that the vertical velocity profile near the water surface following the law of the wall and the usual logarithmic function can be applied (Craig and Banner, 1994). In these equations, κ is the von Karman constant (dimensionless), z^* is the vertical distance from the free surface (m), u_* is the friction velocity (ms^{-1}) given by

$$u_* = \sqrt{\frac{\tau_0}{\rho_0}} \tag{4.34}$$

and the wind stress (τ_0 in $kgm^{-1}s^{-2}$) can be parameterized as follows:

$$\tau_0 = \rho_a C_D U_{10}^2 = \rho_a u_*^2 \tag{4.35}$$

where ρ_a is the air density (kgm^{-3}), C_D is the empirical dimensionless drag coefficient (unitless) which mainly depends on wind speed and water surface waves, U_{10} is the mean wind speed at 10 m height (ms^{-1}) and u_* is the surface wind friction velocity (ms^{-1}). For strong winds ($U > 5 \quad ms^{-1}$) a relationship between C_D and U_{10} is given by a variation of Charnock's law (Charnock, 1955; Wüest and Lorke, 2003; Markfort et al., 2010):

$$C_{D,10} = \left[\kappa^{-1}\ln\left(\frac{10g}{C_{D,10}U_{10}^2}\right) + 11.3\right]^{-2} \tag{4.36}$$

where g is the gravitational acceleration (ms^{-2}), U_{10} is the mean velocity at a height of 10 m and $C_{D,10}$ is surface drag coefficient at a height of 10 m above the water surface. The implicit function presented in Equation (4.36) converges quickly after a few iterations (Wüest and Lorke, 2003).

For small and shallow lakes, wind speed is typically low (commonly $U_{10} < 5\,ms^{-1}$) and measurements of the drag coefficient are relatively scarce. Confusingly, in literature the values of $C_{D,10}$ vary over a wide range and is associated with large scatters (Wüest and Lorke, 2003; Goudsmit et al., 2002; Falconer et al., 1991). For this study, the following empirical relationship for low wind speeds measured at a height of 10 m is used (Wüest and Lorke, 2003; Markfort et al., 2010):

$$C_{D,10} = 0.0044 \times U_{10}^{-1.15} \tag{4.37}$$

In small inland water bodies such as the one studied, the wave field is typically not fully developed due to the small fetches and consequently, the wind-induced turbulence obtained from Equation (4.32) through (4.37) will be underestimated. To include the effects of wind velocity on the flow field, some modifications should be applied in the original turbulence model. These include time varying source/sink terms (Equations (4.32)

506469-L-sub01-bw-Abbasi
Processed on: 9-11-2016

and (4.33)) which could introduce more complexity to the model. Assuming constant wind speed values and using this approach would be straightforward to do and will require less simulation time (Wang, 2013). The most noticeable advantage of this approach could be simplifying the assigned velocity boundary condition over the water surface.

WIND EFFECTS CONSIDERED AS BOUNDARY CONDITION

As stated in Section (4.3.2) it is possible to consider the effects of wind velocity as source/sink terms in k and ε equations in turbulence model. The second and most common approach is considering the wind effects as a boundary condition over the water surface (Section 4.3.4). In this situation the source/sink terms (S_k and S_ε) can be ignored in the turbulence model equations (Equations (4.12) and (4.13)):

$$S_k = 0; \qquad S_\varepsilon = 0 \tag{4.38}$$

4.3.3. INITIAL CONDITIONS

In most small and shallow lakes simulations it is assumed that at *t=0* (initial condition), the water is at rest with a given temperature distribution homogeneous or stratified. Although the initial values of flow parameters (for starting the simulation) have no effect on the results, assigning the real initial conditions in the model could accelerate the converging of numerical computations hence reduces the required simulation time especially for the first time steps. As for most reservoirs there is often no sufficient data to generate the initial distribution of temperature and velocity, the measured temperature profile at the start time of simulation (T at $t = 0$) throughout the entire lake could be used as initial condition. For the velocity, it is assumed that there is no current and zero flow is assumed. If measurements are available for other parameters in the water body, they could be easily applied as initial conditions in the model. The initial conditions (simple or complex) are set by using `funkySetField`, a tool available in `swak4Foam` libraries (Gschaider, 2015b), with python-based functions applicable with `OpenFOAM` platform. To prevent numerical instabilities in the model, a weak (non-zero value) initial turbulence is assumed in the simulation (Verdier-Bonnet et al., 1999).

4.3.4. BOUNDARY CONDITIONS

In the CFD simulation of small and shallow inland water bodies, assigning the physical real conditions on the boundaries are significantly important and the results of the simulation can be directly affected by them (Elo, 2007). The boundary conditions in the lake models are mostly time varying and are complicated. Water surface temperature and circulation in the water body are strongly influenced by time varying meteorological conditions. Depending on the available data (measurements) different types of boundary conditions could be applied for the reservoirs in the current framework.

FREE WATER SURFACE BOUNDARY CONDITIONS

Generally, in water bodies, physical and chemical properties (such as kinetic energy, momentum, heat, etc.) exchanges occur in the Surface Boundary Layer (SBL) which is known as the most dynamic zone and is mostly driven by wind- and heat flux-induced turbulence. Therefore, assigning correct boundary conditions on the water surface is a

506469-L-sub01-bw-Abbasi
Processed on: 9-11-2016

fundamental step in simulating the flow in lakes (Etemad-Shahidi et al., 2010; Craig and Banner, 1994).

Velocity Boundary Condition:
Wind is one of the most important forces which drives free surface movement. Wind over water surface affects lake currents, sensible and latent heat fluxes and turbulence as well as surface waves. The wind drag coefficient is significantly affected by the water surface wave development. Waves produce additional roughness and consequently increases the friction at the free water surface. This mechanism enhances transferring momentum flux from air to water (Wang, 2013). Circulation in the lake is mainly driven by wind shear on the water surface (Liu et al., 2012). The wind-induced circulation significantly affects the dynamics of water temperature and consequently water quality and ecosystem in the inland shallow water bodies. The generated circulation in the water body is very complicated and this study is far from solving all details of it. It is assumed that wind induced circulation in a closed basin occurs when stresses due to winds are applied at the free surface as a boundary condition. The exchanged momentum from atmospheric boundary layer to the water surface by the wind blowing across the water surface has typically been modeled using a stress boundary condition, which is a function of the viscosity (v). In this study, the effects of wind shear stress over the flow was considered through two approaches which use different boundary conditions for velocity (U) on the water surface:
I) Shear Stress over the Water Surface: in this approach the effects of wind shear stress over the flow was considered as time-dependent shear stress boundary condition over the water surface and given by

$$\left[(\nu_0+\nu_t)\frac{\partial u}{\partial z}\right]=\frac{\tau_{sx}}{\rho_0} \tag{4.39}$$

$$\left[(\nu_0+\nu_t)\frac{\partial v}{\partial z}\right]=\frac{\tau_{sy}}{\rho_0} \tag{4.40}$$

where

$$\tau_{sx}=\rho_a C_D u_w\sqrt{u_w^2+v_w^2} \tag{4.41}$$

$$\tau_{sy}=\rho_a C_D v_w\sqrt{u_w^2+v_w^2} \tag{4.42}$$

and C_D (dimensionless) was calculated using Equation (4.37). The normal component of velocity over the water surface boundary is calculated by:

$$u_z=0 \tag{4.43}$$

Therefore on the water surface the following conditions are applied as velocity boundary condition:

$$\frac{\partial u_x}{\partial z} = \frac{C_D\times\rho_a\times|U|}{\rho_w\times(\nu_0+\nu_t)}\times u_x \tag{4.44}$$

$$\frac{\partial u_y}{\partial z} = \frac{C_D\times\rho_a\times|U|}{\rho_w\times(\nu_0+\nu_t)}\times u_y \tag{4.45}$$

$$u_z = 0 \tag{4.46}$$

Without the wind shear stresses, Equations (4.44) and (4.45) lead to no flux conditions along the water surface boundary.
II) Sink/Source Terms in Turbulence Equations: as described in Section (4.3.2), for this type of boundary condition, the effects of wind speed are implemented in the turbulence equations and consequently slip (for a scalar, it can be replaced by a zero-gradient condition and for a vector it is equal to zero fixed value and zero fixed gradient for the normal and tangential components respectively) condition is assumed for velocity. This approach is suggested for high wind speeds or approximately uniform wind speeds.

Turbulence Boundary Conditions:
At large scales, it is generally assumed that wind creates a boundary-layer close to the upper surface (Craig and Banner, 1994; Verdier-Bonnet et al., 1999) where a constant shear stress is assumed and consequently the vertical velocity profile follows the law-of-the-wall. The production of turbulent kinetic energy in this logarithmic region can be computed by the wind-induced vertical gradient of energy flux. In this study, the effects of wind surface waves in turbulence was ignored due to low wind speeds hence the standard wall functions (which are generally required for modelling the effects of roughness length in the flow near the walls typically based on the velocity) were applied to the turbulent parameters k and ε on the water surface boundary.

Temperature Boundary Conditions:
For the simulation period, meteorological parameters and water surface temperature measurements were available. The proposed framework is flexible in working with different temperature boundary conditions on the water surface. The type of boundary for temperature on the free surface depends on the available (measured) parameters such as water surface temperature.
I) Using Measured Water Surface Temperature as Boundary Condition: if the measured water surface temperature values are available this type of boundary condition can be applied on the free water surface (Dirichlet type):

$$T(t) = T_m(t) \tag{4.47}$$

where $T_m(t)$ is the measured water surface temperature varying with time. This type of boundary condition is less practical in small and shallow water bodies simulations due to the requirement for additional measurements of temperature over the water surface which are rarely available for most small lakes. However, the big advantage of using this boundary condition is the avoidance of uncertainties in computing the heat flux components over the water surface (Goudsmit et al., 2002).
II) Heat Fluxes as Boundary Condition: heat exchanges across the air-water interface which consist of long-wave and short-wave radiations, sensible and latent heat fluxes impact the temperature changes in the water body. Although precise estimation of the heat flux components is important in the simulation of flow dynamics in a water body (Politano et al., 2008), the parameterization of these terms is complex and contains a large amount of uncertainties because they are controlled mainly by time varying meteorological conditions. In this study, the heat flux over the water surface was divided into two categories: a) non-penetrative radiations which include sensible heat and latent

506469-L-sub01-bw-Abbasi
Processed on: 9-11-2016

heat fluxes and long-wave radiation, which affect only the water surface and considered as surface heat fluxes; b) penetrative radiation which contains short-wave radiation that can penetrate through the water column after passing through the water surface and distribute its heat contents through the water column in shallow waters. To take into account the distributed heat due to this heat flux, it is not included in the boundary condition, rather, this flux is considered as a heat source in the water body.

At the water surface the net surface heat flux (H_{net} in Wm^{-2}) which diffused away from the lake surface is expressed by the following equation (Neumann Type) (Goudsmit et al., 2002):

$$\rho_0 C_p \left(\alpha_{eff} \frac{\partial T}{\partial z}\right) = H_{net} \Rightarrow \frac{\partial T}{\partial z} = \frac{H_{net}}{\rho_0 C_p \alpha_{eff}} \tag{4.48}$$

The net heat transfer across the air-water interface includes four heat flux terms (Goudsmit et al., 2002; Ahsan and Blumberg, 1999):

$$H_{net} = H_{LA} - H_{LW} - H_S - H_E \tag{4.49}$$

where H_{LA} is the net long-wave (atmospheric) radiation from atmosphere, H_{LW} is the long-wave radiation from the water surface, H_S and H_E are the sensible and latent heat fluxes between the lake surface and the atmosphere, respectively (all terms in Wm^{-2}). As all these heat fluxes change in time, hence they should be updated at each time step. Out of these heat flux components, only the incoming short-wave radiation was measured and the rest were calculated within the model using standard formulations. As stated before, the H_{net} does not include the short-wave (solar) radiation as boundary condition but as a source term in the temperature equation (Equation (4.3)).

Long-wave radiation: the long-wave radiation is composed of energies emitted from the water surface and absorbed from the atmosphere. Atmospheric long-wave radiation is calculated from the Stefan-Boltzmann law (Goudsmit et al., 2002; Ahsan and Blumberg, 1999):

$$H_{LA} = (1 - r_a)\, \varepsilon_a \times \sigma\, T_a^4 \tag{4.50}$$

where H_{LA} is the net long-wave (atmospheric) radiation from the atmosphere per unit surface area (Wm^{-2}), r_a is the reflection coefficient of atmospheric radiation from water surface (unitless), ε_a emissivity of atmosphere and σ is Stefan-Boltzman constant, T_a is absolute air temperature in K. Similarly, long-wave radiation emits from the water surface estimated by (Goudsmit et al., 2002; Ahsan and Blumberg, 1999; Shufen et al., 2007b):

$$H_{LW} = \varepsilon_{ws} \times \sigma T_{ws}^4 \tag{4.51}$$

where ε_{ws} is the dimensionless emissivity of water whose numerical values vary from 0.96 to 0.97 (Lee, 2007) and T_{ws} is the absolute temperature of water surface in K. In Table 4.2 the values of constant parameters used are presented.

Sensible heat transfer: the sensible heat (H_S) is transferred with water vapor by convection and conduction. To estimate this heat transfer, the following equation is used:

$$H_S = h_s(T_{ws} - T_a) \tag{4.52}$$

where H_S is the convective heat transfer or sensible heat flux in Wm^{-2} (positive if it is away from the water surface), h_s is the convective heat transfer coefficient ($Wm^{-2}K^{-1}$)

Table 4.2: Values of model constants (water in $20\,^{\circ}C$)

Parameter	Definition	Unit	Value
r_a	reflection coefficient of atmospheric radiation from water surface	$[-]$	0.03
ε_a	emissivity of atmosphere	$[-]$	0.87
ε_w	emissivity of water surface	$[-]$	0.97
σ	Stefan-Boltzman constant	$[Wm^{-2}K^{-1}]$	5.669×10^{-8}
P_{atm}	atmospheric pressure	$[Pa]$	102′000
ρ_a	air density	$[kgm^{-3}]$	1.186
ρ_0	water density	$[kgm^{-3}]$	998.2336
Pr	Prandtl number	$[-]$	7.07
Pr_t	turbulent Prandtl number	$[-]$	0.85
κ	von Karman constant	$[-]$	0.41
C_p	specific heat of water	$[m^2\,s^{-2}\,K^{-1}]$	4.1818×10^3
T_{ref}	reference temperature	K	293.15
β	thermal expansion coefficient	K^{-1}	0.207×10^{-3}
ν_0	molecular viscosity	$[m^2\,s^{-1}]$	1.004×10^{-6}

which relates the convective heat flux normal to the water surface to the difference between the water surface temperature (T_{ws}) and surrounding air temperature (T_a). The convective heat transfer coefficient for the studied lake can be estimated by (Abbasi et al., 2015b):

$$h_s = 2.50510 \times U_2 + 0.85200 \tag{4.53}$$

where h_s is in $Wm^{-2}K^{-1}$ and U_2 in $m\,s^{-1}$, respectively. According to Abbasi et al. (2015b) this equation was obtained from a CFD-based approach (CFD-Evap Model) using heat and mass transfer analogy in the atmospheric boundary layer to calculate the heat and mass transfer coefficients over lake Binaba (Section (4.6)).
Latent heat flux: in general, latent heat flux (evaporation) is one of the most important parameters in heat dissipation, but its prediction is the most inaccurate. For the latent heat flux (H_E), the following formula is used (Abbasi et al., 2015b):

$$H_E = h_m \times \rho_a (X_{ws} - X_a) \times (24 \times 3600 \times 28.4) \tag{4.54}$$

where the evaporation rate is expressed in $[Wm^{-2}]$, X_a and X_{ws} are the water vapour mixing ratio of air and water surface ($kg(water)/kg(dry\,air)$), ρ_a is the air density ($kg\,m^{-3}$) and h_m is the mass transfer coefficient that is given by (Abbasi et al., 2015b):

$$h_m = 0.00185 \times U_2 + 0.00063 \tag{4.55}$$

where h_m is in ms^{-1} and U_2 is in ms^{-1} respectively. X_a and X_{ws} are calculated by:

$$X_a = \frac{0.622\,e_a}{P_{atm} - e_a} \tag{4.56}$$

$$X_{ws} = \frac{0.622\,e_s}{P_{atm} - e_s} \tag{4.57}$$

where P_{atm} is atmospheric pressure (kPa), e_s is the saturation vapor pressure at the temperature of the water surface (hPa) and e_a is the vapor pressure at the air temperature

506469-L-sub01-bw-Abbasi
Processed on: 9-11-2016

(hPa) given by (Goff, 1957)

$$e_a = \left(6.11 \times \exp\left(\frac{17.27 T_a}{237.3 + T_a}\right)\right) \times \frac{RH}{100} \tag{4.58}$$

$$e_s = 6.11 \times \exp\left(\frac{17.27 T_{ws}}{237.3 + T_{ws}}\right) \tag{4.59}$$

where RH is relative humidity (%) and water surface (T_{ws}) and air (T_a) temperatures are in $^\circ C$.

These heat fluxes are defined to be positive if heat flows from the water surface into the atmosphere. Heat fluxes induced by inlets and outlets and precipitation are generally disregarded (Livingstone and Imboden, 1989).

Determining correct heat fluxes for water surface boundary is often difficult. The main difficulty is that H_{net} is a function of various parameters, where each of them has to be computed by using its own formula, which depends on many uncertain parameters (Ahsan and Blumberg, 1999; Goudsmit et al., 2002). In addition, the heat fluxes on water surface include water surface temperature (T_{ws}) that should be calculated in each time step in advance by the model. Using this boundary condition, the model doesn't need to have the observed water surface temperature measurements.

In the current framework developed, the heat fluxes at the water surface that depend on water surface temperature, given by Equation (4.51) through (4.54), are implemented by using `groovyBC` library (Gschaider, 2015a) developed for handling the complex boundary conditions.

INFLOW AND OUTFLOW BOUNDARY CONDITIONS

The proposed framework is able to include the inflow and outflow boundaries in both flow and temperature simulation. In this case, the total river flow recharge or velocity and its temperature could be specified at the inflow and outflow sections. The velocities at the inflow and outflow sections are assumed to be uniformly distributed, and turbulent variables are assumed to be zero at the upstream and downstream end of the study domain. According to the measurements for the study case during the onset of the dry season, there is no inflow and almost no outflow during the simulation period (4 days).

LAKE-BED AND LAKE-SIDES BOUNDARY CONDITIONS

In shallow lakes the temperature boundary condition at the bottom and sides of lake could be very complex and need extra measurements before it could be used in the model. To simulate the effects of the bottom and sides of the lake, the absorbed and reflected parts of the penetrated short-wave radiation should be measured. In addition, the heat flux from these boundaries should be specified. Implementing the temperature gradient or heat flux from the bed and sides can improve the simulated flow field especially in shallow lakes. In spite of the importance of these parameters, measuring these values is not easy and needs extra instrumentations that commonly are not available for shallow lakes. The temperature boundary conditions at the bottom of the lake and side walls depending on the available measurements for the lake, are set to zero heat flux conditions (adiabatic condition) and can be given by (Shufen et al., 2007b):

$$\frac{\partial T}{\partial z} = 0 \tag{4.60}$$

506469-L-sub01-bw-Abbasi
Processed on: 9-11-2016

For velocity boundary condition, no flow condition is applied at the bottom and sides of the lake. Standard wall functions are used for turbulent equations in the model (Politano et al., 2008; Goudsmit et al., 2002).

4.4. NUMERICAL SIMULATION

The governing equations (Section (4.3.1)) using the described boundary and initial conditions in Sections (4.3.4) and (4.3.3) are solved by the control-volume open-source code `OpenFOAM`. The `OpenFOAM` (Open Source Field Operation and Manipulation) toolbox includes open source `C++` libraries released under the general public license (GPL) (OpenFOAM, 2015). Using the pre-configured built-in libraries, one can build his own numerical solvers for solving the specific fluid flow problems (Chen et al., 2014). In the present platform, these pre-configured solvers were modified before being applied. Implementing the unsteady source terms in the governing equations, including the wind source/sink terms and the buoyancy effects in turbulence equations are some examples of modifications in the standard available solvers.

In the current framework, a new CFD solver is developed based on `OpenFOAM`. The solver developed is a solver for heat transfer simulation considering transient temperature source terms called `LakebuoyantBoussinesqPimpleFoam`. Beside developing the new solver, a new turbulence model has been developed to include the effects of buoyancy in the flow field and wind-induced source/sink terms in turbulence.

The proposed model is an unsteady state, incompressible heat transfer solver based on the finite-volume scheme. To solve the flow, the entire desired domain (water body) should be discretized in the vertical and horizontal directions and a proper numerical solver chosen from the pre-configured built-in algorithms in `OpenFOAM` for each of the governing equations. In Table 4.3 the list of applied solvers is presented. These solvers are selected based on their stability, convergence and processing time after trying a number of simulations. Throughout this work, the `Euler` method was used to discretize the temporal term. This is a first-order, bounded implicit method and the `SmoothSolver` for the momentum, k, ε and T equations is used with a `GaussSeidel`smoother (Gauss refers to the standard finite volume discretization of Gaussian integration). The `GAMG` (Geometric-algebraic multi-grid) solver is chosen for pressure equation. This solver generates an initial quick solution using a coarse mesh with a small number of cells, and maps this solution onto a finer mesh. The quick solution is used as an initial guess to obtain an accurate solution on the fine mesh. Therefore, `GAMG` is generally faster than other standard methods. For the spatial discretization of differential operators, the `Gaussian` integration was used with various interpolation schemes: for gradient terms, the 2^{nd} order linear interpolation, for divergence terms, the 2^{nd} order upwind interpolation and for Laplacian terms, the 2^{nd} order linear interpolation with explicit non-orthogonal corrections. Table 4.4 shows the main numerical methods which could give stable and convergent solution in small shallow water body simulations.

To improve the stability of the computations, the relaxation parameters (which controls under-relaxation) were set to 0.3 for (dynamic) pressure and 0.5 for the other variables. Under-relaxation parameters control the variable changes from one iteration to the next.

The `PIMPLE` method was used for pressure-velocity coupling. The `PIMPLE` algorithm

506469-L-sub01-bw-Abbasi
Processed on: 9-11-2016

Table 4.3: Solution algorithms used in the framework developed for CFD calculations (Maric et al., 2014)

	Field	Task	Solver	Description
1	Pressure, corr. pressure pd	solver	PCG	Preconditioned conjugate gradient solver
		preconditioner	GAMG	Generalised geometric-algebraic multi-grid
2	Velocity	solver	PBiCG	Preconditioned bi-conjugate gradient solver
		preconditioner	DILU	Diagonal incomplete-LU
3	cell motion cellMotionU	solver	PCG	Preconditioned conjugate gradient solver
		preconditioner	DIC	Diagonal incomplete-Cholesky

Table 4.4: Numerical schemes chosen for CFD calculations of the SSL-framework (Maric et al., 2014)

	Item	Symbol	Keyword	Description
1	First and second time derivatives	$\frac{\partial}{\partial t}$	Euler	First order, bounded, implicit
2	Gradient	∇	faceLimited leastSquares 0.5	Limited, second order least squares
3	Divergence (velocity terms)	$\nabla.\vec{u}$	Gauss vanLeerV	Second order Gaussian integration, van Leer interpolation for face centres
4	Laplacian	∇^2	Gauss linear corrected	Second order, Gaussian integration, linear interpolation for face centres, conservative
5	Point-to-point interpolation		linear	Linear interpolation for general field
6	Gradient component normal to face	∇_{SN}	corrected	Explicit non-orthogonal correction

combines the SIMPLE (Semi-Implicit Method for Pressure-Linked Equations) algorithm and the PISO (Pressure Implicit with Splitting of Operators) algorithm to rectify the second pressure correction and correct both velocity and pressure explicitly. This algorithm allows one to use larger time steps than the PISO algorithm. Regarding the numerical stability criteria and the transient conditions of flow in the lake, an adaptive time-stepping technique was used in the simulations which is based on Courant-Friedrick-Levy-number (CFL) (Bechmann, 2006):

$$CFL = \Delta t_{max}\left(\frac{|u|}{\Delta x}, \frac{|v|}{\Delta y}, \frac{|w|}{\Delta z}\right) \leq 1 \tag{4.61}$$

where u , v and w are the velocity components (ms^{-1}) in $x-$, $y-$ and $z-$directions respectively. In this study after investigating the results of the model for different sets of CFL, the maximum value of global CFL was set to 0.2. For larger values of the Courant number the numerical computations were unstable in some points and in some time steps as well (Wang, 2013; Ferziger and Perić, 2002).

The solver developed here can be ran on parallel CPUs to accelerate the simulation. The challenges that could arise in solving these equations by running the model are memory related and simulation time (which is required to obtain a solution for a given set of conditions). As the core of the model is based on OpenFOAM, the framework offers parallelization features. With regards to the number of computational mesh and the simulation time, the model can be decomposed and run on a relatively large number of processors, either on supercomputers or HPC-Clouds.

4.5. POST-PROCESSING AND MODEL VALIDATION PHASE

At the post-processing stage, the boundary conditions, mathematical issues, computational grid, etc. are to be verified. In addition it is possible to extract desired parameters and functions which are needed for analysing the flow field and temperature distribu-

506469-L-sub01-bw-Abbasi
Processed on: 9-11-2016

tion.

One of the principle objectives in the current framework was to obtain general information on the direction and magnitude of the currents in the water bodies and the temperature dynamics, and how they vary over time. Once the simulations are validated, it is possible to use the model for different conditions that could be used to describe in general the most significant patterns in the water currents' variations over time. One of the big challenges in validating the lake models such as the one in this study is the fact that experimental data are rarely available and/or the measurement errors are commonly high (Callister, 2008).

Several assumptions are made in the development of the lake model regarding the input values. The results from the simulations are plotted against the measured data as a way to evaluate the validity of the model (Callister, 2008). To validate the model different cases are run to check the performance of different parts of the platform. Using different case studies with different conditions allows the user to find the problem easily in the model and be able to revise the model in a straightforward manner.

4.5.1. CONVECTION HEAT TRANSFER IN THE WATER BODY

Due to the long run time of the real geometry, it could be a reasonable choice to validate the model with some simple geometries to be sure about the performance of the model. It should be noted that in the described cases, the physics of the simulations and the general trends of the results are investigated which are very helpful in debugging the model.

The first case described here deals with a 2-D flow in a cavity shown in Figure 4.5. Using this case, the performance of the model in simulating heat transfer in the cavity (natural convection) was validated. To evaluate the performance of the model developed

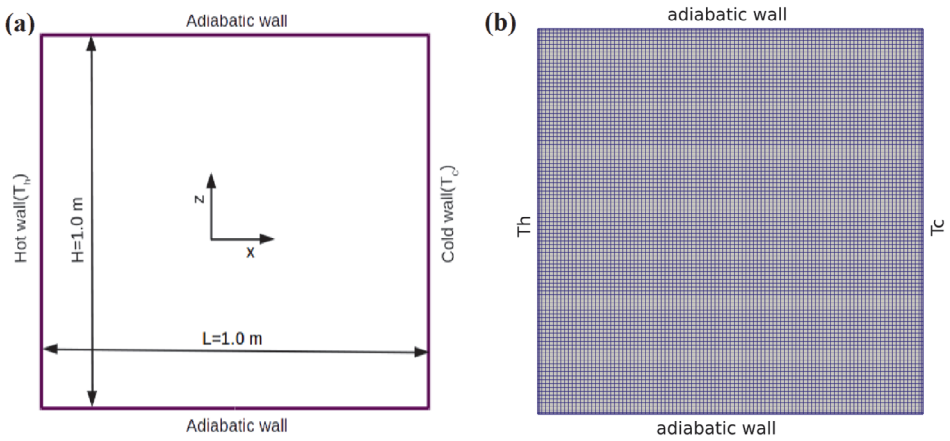


Figure 4.5: Detail of validation case (cavity) where $T_c = 303.15\,K$ and $T_h = 304.15\ K$: **(a)** geometry and model's conditions. **(b)** computational grid.

in this study, the results of the cavity model using the current approach were compared with some available flow parameters for the cavity model in similar conditions such as

the results of the simulation by Corzo et al. (2011) and the benchmark experimental measurements done by Le Quéré (1991). Figure 4.6(a) shows the horizontal velocity profile ($u = U_x/\alpha$) in the vertical mid-line. These results exhibit good agreement between the model with benchmark results. However, the quality of results are dependent on the computational grid and it is necessary to refine the grid in order to obtain an accurate solution. In Figure 4.6(b) the vertical profiles of the velocity is shown. Comparing the temperature distribution shown in Figure 4.6(c) with velocity profile shown in Figure 4.6(d) shows that the flow is limited to a narrow strip along the walls (left hot wall and right cold wall) where the velocity and temperature change suddenly.

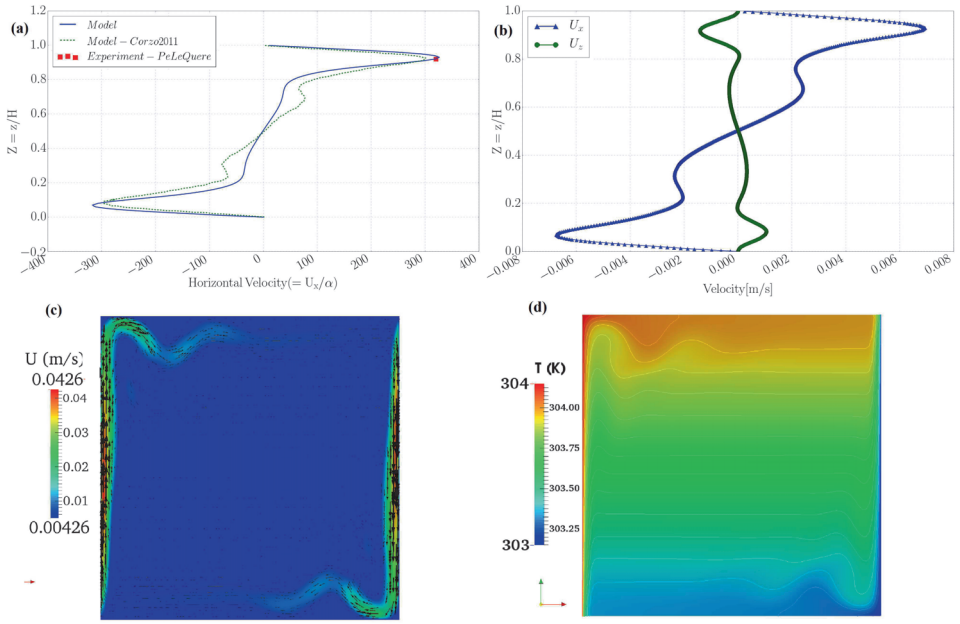


Figure 4.6: Results of model in the cavity **(a)** comparison of results of model (horizontal velocity profiles, $u = U_x/\alpha$, at x mid-plane where $Ra = 10^8$) with experimental values and other models and **(b)** simulated profiles of velocity components in the cavity **(c)** simulated velocity vectors with values and **(d)** temperature distribution and contours in the cavity.

4.5.2. SIMPLIFIED GEOMETRY OF WATER BODY

In this test case the ability of the framework in taking into consideration the effects of forced convection (heat transfer) in the water body is verified. As mentioned in Section (4.3.1) the temperature source term in the water is a function of the water turbidity. To check the performance of the model for different turbidity values and also to investigate the magnitude of the turbidity effects on the flow and temperature pattern in small and shallow water bodies, some simulations were done and the results analysed. In addition the influence of turbulence on the results was examined. The details of these cases are listed in Table 4.5. As shown in Table 4.5, two different geometries (S and L cases) are

506469-L-sub01-bw-Abbasi
Processed on: 9-11-2016

Table 4.5: Details of simplified case studies

Case ID	Dimensions $L \times W \times H$ [m]	Cells Number	Δx $[m]$	Δy $[m]$	Δz $[m]$	z_{min} $[m]$	aspect ratio	η $[m^{-1}]$	Secchi depth$[m]$	Remarks
S-01	$120 \times 100 \times 4$	6'000	10.0	10.0	0.2	0.2000	50.08	0.50	2.94	Laminar flow(no turbulence)
S-02	$120 \times 100 \times 4$	12'000	5.0	5.0	0.2	0.0125	800.00	1.82	0.50	Turbulent Flow
S-03	$120 \times 100 \times 4$	12'000	5.0	5.0	0.2	0.0125	800.00	3.56	0.20	Turbulent Flow
S-04	$120 \times 100 \times 4$	12'000	5.0	5.0	0.2	0.0125	800.00	5.17	0.12	Turbulent Flow
S-05	$120 \times 100 \times 4$	12'000	5.0	5.0	0.2	0.0125	800.00	4.20	0.16	Turbulent Flow
L-01	$1000 \times 800 \times 4$	46'000	20.0	20.0	0.2	0.0250	800.00	2.1	0.41	Turbulent Flow
L-02	$1000 \times 800 \times 4$	46'000	20.0	20.0	0.2	0.0250	800.00	4.2	0.16	Turbulent Flow
L-03	$1000 \times 800 \times 4$	46'000	20.0	20.0	0.2	0.0250	800.00	10	0.05	Turbulent Flow
L-04	$1000 \times 800 \times 4$	46'000	20.0	20.0	0.2	0.0250	800.00	2.1	0.41	Turbulent Flow, $S_T = 0$

considered to check the performance of the model in solving the flow field in the simple geometries with different dimensions of water bodies.

In Figure 4.7(a) the simulated temperature profiles in the water body (S cases) for different water turbidity values are shown. It shows that the effect of Secchi depth (water turbidity) in the shallow water bodies could be significant and should be considered in models. Figure 4.7(b) shows the temporal variations of temperature in the water body. The temperature distribution in the water correlates highly with the air temperature and at sometimes there is distinctive stratification in the lake. In Figure 4.7(c) the simulated temporal variations of temperature in the water body without considering the turbulence in the simulations is compared with Figure 4.7(d) which includes the turbulence in modelling. It shows that the effects of the turbulence in the flow field could be significant. Ignoring the turbulence in the simulation leads to unreliable results which gives no stratification in the water body. In the second simplified geometry case (L case), the larger dimensions similar to the real lake dimensions were chosen for the computational domain to investigate the performance of the platform in working with real dimensions. These real dimensions allowus to improve and handle the mathematical and computational issues such as selecting the proper numerical algorithm and required computational resources. Figure 4.8(a) shows the temperature profile in the case study for different values of water turbidity. According to the results, to have a better prediction on the stratification in the shallow lakes, it is important to measure the Secchi depth in some points in the water body. Using the measured water turbidity values in the model could increase the reliability of the results. In Figure 4.8(b) the distribution of the velocity's components in the water body are shown. It shows that in the water body, the velocity distribution is a function of the wind speed over the water surface and its direction as well. In addition, according to the velocity distributions in Figure 4.8(b), there are water flows in the water body in different directions and this phenomena could increase the circulation in the water body that could be of interest with regards to water quality issues. In Figure 4.8(c,d) the effects of water turbidity on the temporal distribution of temperature for L cases are shown. It can be seen that turbidity could affect the temperature distribution in the water body and its correct values which can be obtained from Secchi measurements should be used.

To check the performance of the model which includes the source/sink terms (that represent the wind velocity effects in turbulent equations (Equations (4.32) and (4.33)) some simulations were done. In Figure 4.9(a) and Figure 4.9(b) the velocity and temper-

506469-L-sub01-bw-Abbasi
Processed on: 9-11-2016

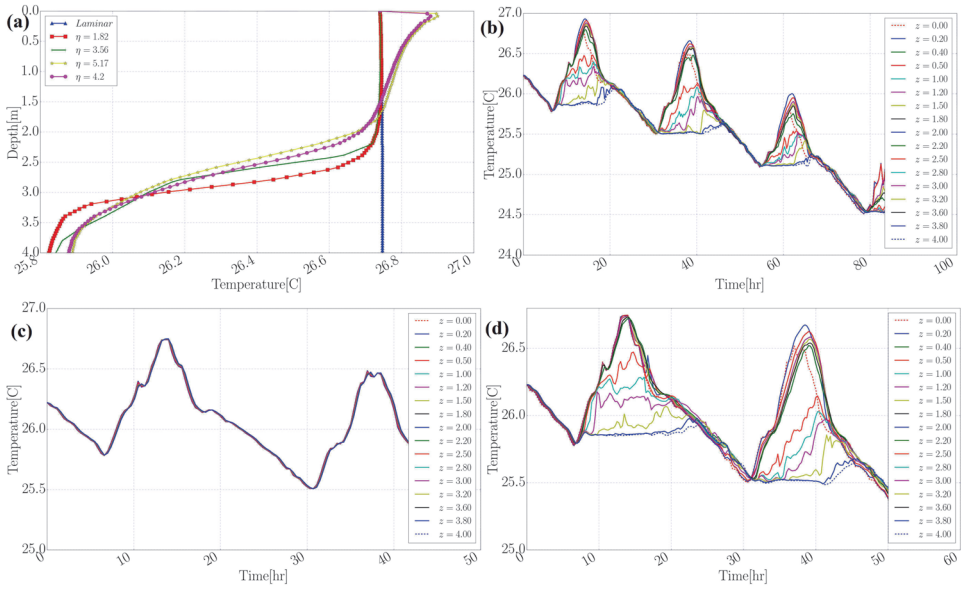


Figure 4.7: Results of the model for S cases: **(a)** effect of turbidity on vertical temperature profiles in the water body; **(b)** temporal variation of temperature for the selected turbidity value ($\eta = 3.56\,m^{-1}$); **(c)** simulated temporal temperature variations in the water body without turbulence implementation (laminar assumption); **(d)** simulated temporal temperature considering the turbulence in the simulation (where $\eta = 4.20\,m^{-1}$).

ature changes in different depths are shown respectively. As shown, the results are not so good compared with the validated model. The main reasons could be related to the low wind velocity values and the complex geometry of lake (Wang et al., 2013a). Therefore, in case of shallow lakes with low wind velocity values, this approach is not suggested.

Following the approach described in Section (4.3.4) the heat flux boundary condition was applied on the water surface and the changes of velocity and temperature are shown in Figure 4.9(c) and Figure 4.9(d) respectively. The differences between the temperature values in this simulation with validated case (using temperature values over the water surface) could be mainly due to the uncertainties that exist in estimating the heat fluxes values on the water surface as well as the dependency of the temperature gradient on the water-air interface to the flow parameters such as heat conductivity (Equations (4.6) and (4.48)). In this approach, the assigned right boundary conditions for turbulent equations are important and their values would affect the results of the model significantly.

4.6. MODEL APPLICATION FOR LAKE BINABA

Lake Binaba is a small and shallow man-made reservoir located in the Upper East Region of Ghana. Lake Binaba ($10°53'20''N$, $00°26'20''W$) is used for fishing, livestock watering, irrigation, construction, domestic uses and recreation (van Emmerik et al., 2013). The average area of the lake surface is 31 ha ($305534\,m^2$) with the average and maxi-

506469-L-sub01-bw-Abbasi
Processed on: 9-11-2016

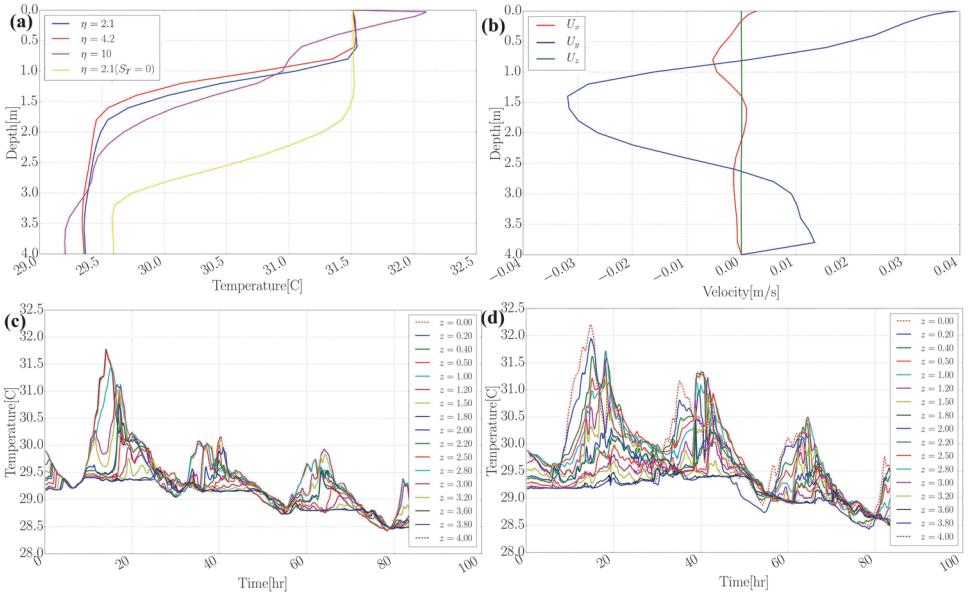


Figure 4.8: Results of the model L cases: **(a)** effect of turbidity on vertical temperature profiles in twater body; **(b)** velocity's components distribution in water body (where $\eta = 3.56\,m^{-1}$); **(c),(d)** simulated temporal variation of temperature in water body for different water turbidity values where $\eta = 2.1$ and $\eta = 10.0\,m^{-1}$ in (c) and (d) respectively.

mum depth of 1.1 m and 4.0 m, respectively (Abbasi et al., 2016a). The temperature profile in the water body as well as the meteorological parameters were measured at a floating measurement station over the water surface. The measurements include atmospheric parameters (air temperature, wind speed at 2.0 m above the water surface, wind direction and relative humidity), incoming short-wave radiation, and water temperature profile. These available measured parameters were used as transient boundary condition in the framework to simulate the flow and temperature in the lake. In the following graphs, the starting time of calculations was adapted to 00:00:00 a.m on December 24, 2012 (Abbasi et al., 2016b). Figure 4.10(a) shows the geometry (bathymetry) of lake Binaba generated by using the proposed approach in the current platform (Section (4.2.1)). In Figure 4.10(b) the computational grid of the lake is shown. The computational grid is refined near the water surface due to high gradients in the temperature and velocity over the water surface. The simulated velocity values and the temperature contours in 1.0 m beneath the water surface are shown in Figure 4.10(c) and Figure 4.10(c) respectively. The distribution of temperature (Figure 4.10(d)) at a depth of 1.0 m below the water surface is not homogeneous mainly due to the non-homogeneous distribution of velocity at this depth (Figure 4.10(c)). In Figure 4.11 the simulated velocity vectors on the water surface is depicted and shows the existence of inverse flow which enhances circulation in the water body. More details about the validation process can be found in Abbasi et al. (2016b).

506469-L-sub01-bw-Abbasi
Processed on: 9-11-2016

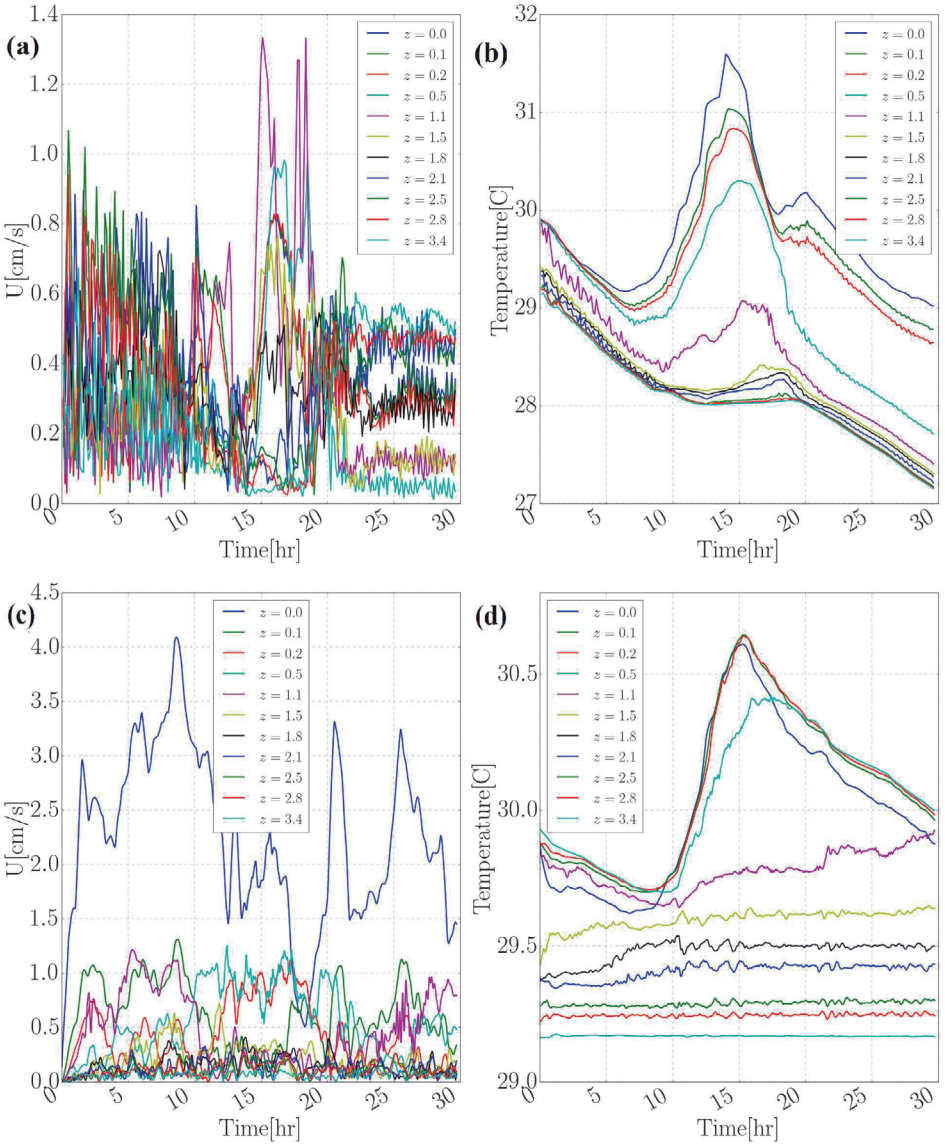


Figure 4.9: Results of model considering different approaches to include wind velocity effects: **(a),(b)** temporal distribution of velocity and temperature values respectively, when effects of wind are considered as source/sink terms in turbulence equations; **(c),(d)** temporal distribution of velocity and temperature values respectively, when effects of wind speed are considered as shear stress boundary condition over the water. In both cases, heat fluxes as temperature boundary condition are assumed over the water surface.

506469-L-sub01-bw-Abbasi
Processed on: 9-11-2016

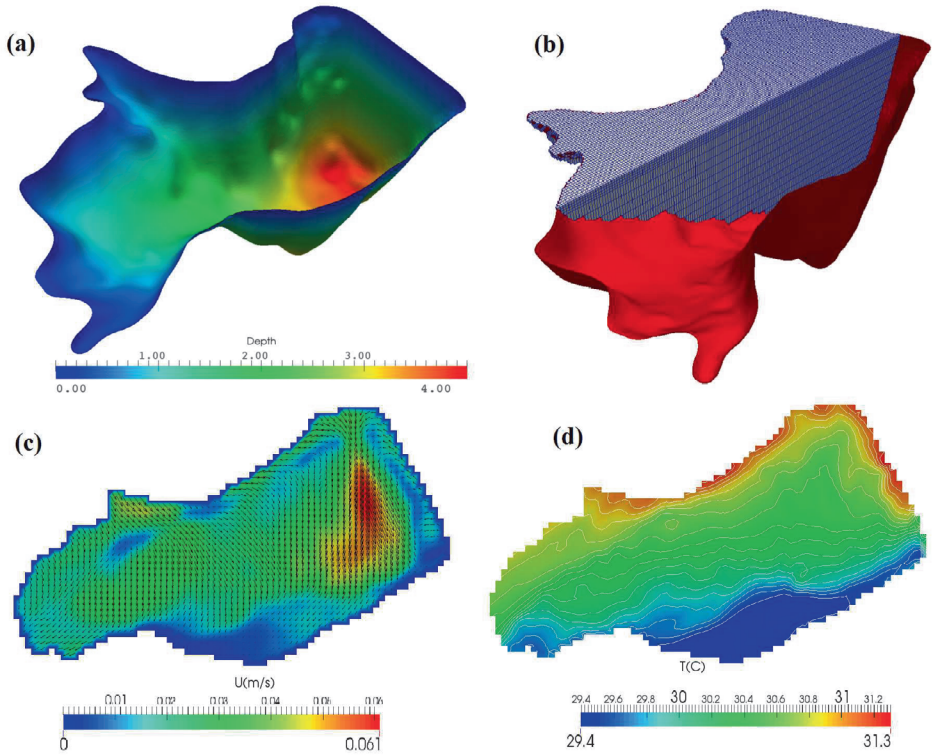


Figure 4.10: **(a)** Generated geometry of Lake Binaba with depth distributions; **(b)** computational grid in water body used in simulations (vertical exaggerated by 100); **(c)** simulated velocity field (stream lines); and **(d)** temperature field (values and contours) in 1 meter beneath water surface at $t = 13:00$ hr. The wind speed is 2.0 ms^{-1} from West.

506469-L-sub01-bw-Abbasi
Processed on: 9-11-2016

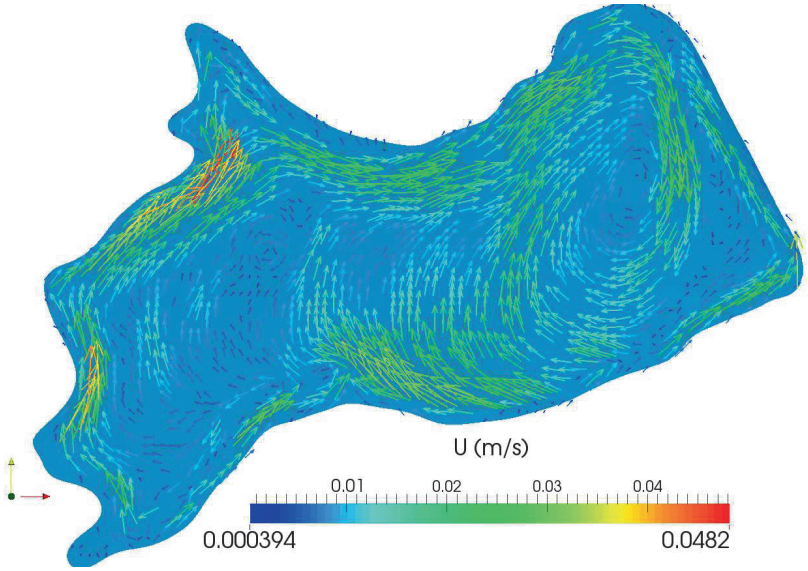


Figure 4.11: Simulated velocity vectors and velocity magnitudes over water surface at $t = 17:00$ hr. Wind speed is 2.1 ms^{-1} from South-Western.

4.7. CONCLUSION

In this study, a comprehensive framework for simulating small and shallow inland water bodies was developed. This framework includes all mandatory steps in lake and reservoir modeling which includes: creating bathymetry, generating computational grid, solving the flow field and temperature dynamics, plotting desired graphs, analysing the outputs, etc. In order to produce an acceptable bathymetry applicable in CFD simulations, a new simple approach using open-source tools has been developed which could be easily implemented in different models which require the geometry of the water body or similar computational domains to do simulations. Again, to consider the buoyancy effects in the water body, the turbulence model was improved to take into account the buoyancy effects. Considering the commonly available measurements for small water bodies, a wide range of boundary conditions are proposed that could be adapted to suit the measurements at hand over the water surface. To check the performance of the framework, several test cases and a real-world lake were simulated and compared with either field measurements or similar models results.

The results of the framework for different simulations has led to the following conclusions:

1. the model can estimate the temperature distribution as well as the flow field in water bodies;

2. the framework can work with a wide range of boundary conditions dependent on the available measured parameters;

3. the accuracy of the prepared model mainly depends on the errors and uncertainties in input meteorological parameters;

4. the temperature dynamics and the flow pattern in the water body at a given point are strong functions of the air temperature, incoming short-wave radiation and wind velocity over the water surface. The effects of other meteorological parameters are considered implicitly in heat fluxes over the water surface as boundary conditions;

5. the flow in the (small shallow) water body is fully 3-D and turbulent;

6. the influence of turbidity of water on the flow field could be significant in small and shallow water bodies;

7. one of the big challenges in modeling shallow lakes is implementing heat fluxes over the water surface accurately especially for the latent heat flux (evaporative heat flux);

8. the model is very sensitive to the resolution of the computational mesh. Making a reasonable balance between the computational mesh and the needed computational resources is a very important step in simulating lake-like domains;

9. due to the coupling of heat transfer processes with water flow in the lake, handling the numerical issues in the model is very crucial. To solve the model in a stable

506469-L-sub01-bw-Abbasi
Processed on: 9-11-2016

and precise way, appropriate numerical algorithms as suggested here should be chosen;

10. open-source and free of charge tools could be used to develop flexible and powerful frameworks to simulate inland water bodies.

Different approaches have been described in this study. Picking out the right turbulence model and boundary conditions are very important and can affect the results significantly. It is obvious that using methods with less uncertainties, if possible, are better in computing the parameters because they usually give better results.

The approach used in this study for temperature dynamics could be applied to water quality, biological and environmental simulations of shallow water bodies as well with the model developed.

506469-L-sub01-bw-Abbasi
Processed on: 9-11-2016

5

INVESTIGATION OF TEMPERATURE DYNAMICS IN LAKE BINABA

5.1. INTRODUCTION

Inland water bodies such as reservoirs and lakes are very important parts of the continental land surface (Shufen et al., 2007a). Reservoirs are typically built to store water for water supply, hydropower or flood control (Casamitjana et al., 2003). Knowledge of the mixing characteristics and temperature profile of a lake are important for its operation and management (Falconer et al., 1991). The thermal structure of water bodies, temperature stratification dynamics and changes in temperature values have a direct impact on the heat storage of lakes and their water quality (Antonopoulos and Gianniou, 2003; Babajimopoulos and Papadopoulos, 1986; Elo, 2007). Understanding the heat budget of lakes and reservoirs is crucial for estimating evaporation in the energy budget methods that are widely used (Brutsaert, 2005; Katul and Parlange, 1992; Priestley and Taylor, 1972; Vercauteren et al., 2011). However, measurements of heat exchange between the water surface and atmosphere are scarce. In most cases carrying out measurements for shallow and small inland water bodies is difficult and expensive and needs high level of expertise to obtain reliable measurements over the water surface even for measuring conventional meteorological parameters such as air temperature, wind velocity and so on. Although experimental temperature profiles in lakes are commonly available, the vertical resolutions are often not sufficient for assessing small-scale turbulence effects or investigating variations of water temperature induced by radiative forcing, air temperature as well as wind velocity in shallow waters (Vercauteren et al., 2011). As small shallow lakes and reservoirs respond to atmospheric conditions very quickly, precise estimation of the heat transfer between the atmosphere and their surface is extremely important to model the temperature dynamics and stratification in these water bodies (Ahsan and

This chapter is based on Abbasi et al. (2016b): Abbasi, A.; Annor, F.O.; van de Giesen, N.: Investigation of Temperature Dynamics in Small and Shallow Reservoirs, Case Study: Lake Binaba, Upper East Region of Ghana. Water 2016, 8, 84.

506469-L-sub01-bw-Abbasi
Processed on: 9-11-2016

Blumberg, 1999). In these water bodies, the near-surface water temperature commonly follows the radiative forcing (solar radiation) trend with an increase during the day and a decrease during the night. The gradient temperature can transport vertically into the water column by (effective) thermal diffusivity, which can be enhanced by the atmospheric parameters, water surface waves and the dynamics of the flow in the water body. Eddy diffusivity and thermal conductivity are important parameters in simulating the diurnal evolution of the temperature in the water bodies. Wind over the water surface affects lake currents, sensible and latent heat fluxes and turbulence as well as surface waves. The time-dependent effects of wind shear stress over the surface can change the flow pattern and thermodynamics of the lake. Therefore, considering the effects of heat transfer and wind-induced flow in small water bodies is so complicated and needs the use of high-resolution simulation to determine the flow parameters.

In the case of shallow and small inland water bodies, which have been used in this study, simulating the flow field requires an additional degree of complexity beyond simulation of a deep and large water body. Including the effects of the time-varying driving forces such as short-wave radiation, air temperature, wind speed and its direction, precipitation, cloud cover, water surface temperature, and variation in water composition (such as salinity and density) in a shallow water body simulation is difficult. In addition, implementing an appropriate approach to compute the heat fluxes through the water surface, the evaporative flux and the source heat due to the penetration of the incident short-wave radiation, which comes with a high degree of uncertainty, needs to be handled carefully. As these complexities introduce approximations and consequently modeling errors, developing a model which be able to simulate the flow variation in a small water body considering the aforementioned uncertainties is very promising. In this work, we have developed a fully three-dimensional and unsteady hydrothermal model that is capable of simulating the effects of wind and atmospheric conditions over a complex bathymetry to predict the circulation patterns as well as the temperature distribution in the water body. In this model, the atmospheric conditions, with particular attention to heat fluxes over the water surface (sensible and latent heat fluxes), are applied dynamically to reduce the model uncertainties. To verify the capabilities of the model developed in this study, it was applied to a small shallow reservoir in the Upper East Region of Ghana. To evaluate the performance of the model against the observed values of temperature, some quantitative metrics, include root mean square error (RMSE), the mean absolute error (MAE), the relative mean error (RME) and mean error (ME) were applied. From the metrics of model performance evaluation, the results show that the simulated temperature values are in good agreement with the observed values.

5.2. WATER BODIES MODELLING

In the last two decades, an increasing interest in predicting the temperature profiles in reservoirs and lakes has been high due to the correlation between temperature, water quantity and water quality (Koçyigit and Falconer, 2004a). Transport processes in water bodies are inherently three-dimensional, driven by wind, surface thermodynamics, and the topography of the lake. Hence, assessing the water temperature as well as water circulation, inherently requires transport modelling (Hodges et al., 2000a). Mathematical modelling of water temperature in lakes and reservoirs have been carried out over

the years to investigate thermal dynamics in water bodies (Dake and Harleman, 1969; Hostetler and Bartlein, 1990; Antonopoulos and Gianniou, 2003). However, in many real-world cases, it is not always possible to solve the water temperature equations analytically due to the non-linearity of some parameters at the air-water interface (Antonopoulos and Gianniou, 2003; Koçyigit and Falconer, 2004a) even though water temperature has been simulated in these models at various levels of complexity (Politano et al., 2008).

One-dimensional models (1-D) are extensively applied to estimate vertical temperature profiles in lakes in time. In 1-D models, variations in the lateral directions are assumed to be small with respect to variations in the vertical direction (Elo, 2007). In terms of a global or regional coupled atmosphere-lake modeling system for water bodies, 1-D models are the best choices since they require low computational resources and are sufficiently fast for long-term simulations (MacKay et al., 2009). Generally, one-dimensional models are not able to consider horizontal advection terms and this seems to be one of the disadvantages.

In the early 1980s, two-dimensional (2-D) laterally averaged models were used extensively to predict the flow field and temperature distribution in water bodies (Politano et al., 2008; Debolsky and Neymark, 1994; Lei and Patterson, 2002; Ferrarin and Umgiesser, 2005). Although these 2-D models are computationally efficient and easily implemented, they are not appropriate for simulating flow fields in shallow lakes because these 2-D models are not able to describe the fully three-dimensional flow field in shallow water bodies (Koçyigit and Falconer, 2004a).

Due to the inabilities of 2-D models in capturing mechanisms influencing mixing and temperature dynamics precisely, especially in morphometrically complex lakes and reservoirs, a number of three-dimensional models have recently been presented (Jin et al., 2002; Kennedy et al., 2006; Jin et al., 2000; Ahsan and Blumberg, 1999; Davies, 1982b,a; Haque et al., 2007; Koçyigit and Falconer, 2004a,b; Liu et al., 2012; Rueda and Schladow, 2003). Flow field prediction and consequently the temperature dynamics determination in water bodies are accomplishable only through fully 3-D models (Politano et al., 2008). Liu et al. (2012) developed and applied a three-dimensional finite element model to the subtropical alpine Yuan-Yang Lake (YYL) in northeastern region of Taiwan. Leon et al. (2007) evaluated the capability of the 3-D model (ELCOM) for coupling it with the Canadian Regional Climate Model (CRCM) on Great Slave Lake, Canada. Politano et al. (2008) solved a fully three-dimensional model to predict the temperature distribution at McNary Dam using the commercial code Fluent; and a later study by Wang et al. (2013b) developed a 3-D numerical model extending the approach of Politano et al. (2008) using the open-source code OpenFOAM.

While numerous 3-D models have been described to characterize thermal dynamics in lakes, they have usually been utilized for large and deep lakes where the representation of the boundary geometry is less important than for shallow small lakes (Falconer et al., 1991). Only a limited number of CFD simulations for temperature distribution in shallow and small inland water bodies can be found (Abbasi et al., 2015a).

5.3. DESCRIPTION OF STUDY SITE AND DATA COLLECTION

The Upper East Region of Ghana (UER) has more than 160 small and shallow reservoirs which have different surface areas ranging from 1 to 100 hectares (Annor et al.,

2009). These small reservoirs are operationally efficient with their flexibility, closeness to the point of use, and requirement for few parties for management (Keller et al., 2000). The studied lake is a small and shallow reservoir located in this region. Lake Binaba ($10°53'20''N$, $00°26'20''W$) is a man-made lake mainly used for irrigation, fishing, livestock watering, construction, domestic uses and recreation. As shown in Figure 5.1 a natural stream has been dammed, storing and supplying water for all these uses in Binaba, a small town in the sub-humid region of Ghana (van Emmerik et al., 2013). The average lake surface area is estimated around 31 ha with an average and maximum depth of 1.1 m and 4.0 m, respectively. To monitor the meteorological parameters, a floating measurement station was installed over the water surface. Measurements taken included atmospheric parameters (air temperature, wind speed at 2.0 m above the water surface, wind direction and relative humidity), incoming short-wave radiation, sensible heat flux using a 3-D sonic anemometer and water temperature profile. These parameters were used to validate the model. Atmospheric measurements and a water thermistor string were situated near the dam body, where the lake depth is around 4.0 m. The water temperature profile was measured with an Onset HOBO Tidbit v2 water temperature data logger with nominal accuracy of $\pm 0.21\,°C$ (HOBOTidbiT, 2015) and in the following depths: 0.100; 0.200; 0.500; 1.100; 1.550; 1.850; 2.150; 2.800; 3.465 m.



Figure 5.1: The shape of Lake Binaba and its surroundings (Google, 2015). Location of the thermistor chain is shown by a filled square over the lake.

The air temperature fluctuated from 18.0 to $40.0\,°C$ with an average of $28.7\,°C$ while the water surface temperature varied between $24.0\,°C$ and $32.5\,°C$ with an average of $27.5\,°C$ during the measurement period. Measurements were done between 23 November 2012 and 22 December 2012. A four-day period was selected from the observations to simulate the lake temperature and to validate the model as well. Figure 5.2(a) shows

506469-L-sub01-bw-Abbasi
Processed on: 9-11-2016

the diurnal changes of air temperature, with daily variations of approximately 16.0°C . Incoming short-wave (solar) radiation measurements from the atmosphere to the water surface are shown in Figure 5.2(b). The daily maximum value was recorded around 1:00 p.m. with a value above 800 Wm^{-2} for most of days. The measured values of relative humidity (RH) over the water surface are shown in Figure 5.2(c). The wind speed and directions, are shown in Figure 5.2(d) with South-Western direction being the most dominant direction with a maximum speed of 4.0 ms^{-1}. Since the wind speed values have been averaged over 30-min intervals (as for the other parameters), instantaneous wind speed may be larger. The variation of atmospheric pressure during the study period was very small and could be ignored. Therefore, the pressure was taken to be a constant 102 kPa for all of the simulations.

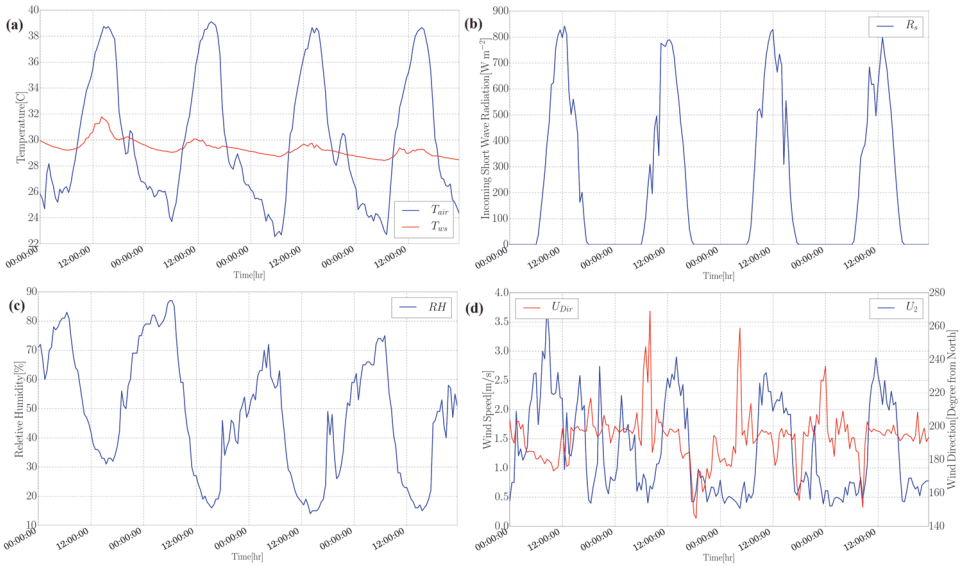


Figure 5.2: Measured meteorological parameters used in the simulation: **(a)** air and water surface temperature; **(b)** short-wave radiation; **(c)** relative humidity; and **(d)** wind speed and its direction.

5.4. MATHEMATICAL MODEL

5.4.1. GOVERNING EQUATIONS

The flow field was solved with the incompressible RANS (Reynolds Averaged Navier Stokes) equations. The water can be assumed to be incompressible (Tsanis, 2006), and the constant-density continuity equation can be written as:

$$\frac{\partial u_i}{\partial x_i} = 0 \tag{5.1}$$

The constant-density (except in the gravity term) momentum equations, using the Boussinesq approach, can be written as:

$$\frac{\partial u_i}{\partial t} + \frac{\partial}{\partial x_j}(u_j u_i) - \frac{\partial}{\partial x_j}\left\{\nu_{eff}\left[\left(\frac{\partial u_i}{\partial x_j} + \frac{\partial u_j}{\partial x_i}\right) - \frac{2}{3}\left(\frac{\partial u_k}{\partial x_k}\right)\delta_{ij}\right]\right\} = -\frac{1}{\rho_k}\frac{\partial p}{\partial x_i} + g_i\left[1 - \beta(T - T_{ref})\right] \tag{5.2}$$

where u_i is the velocity component in x_i direction (ms^{-1}); t is time (s); p pressure (Pa); T temperature (K); g_i the gravity acceleration vector (ms^{-2}); $\nu_{eff} = \nu_0 + \nu_t$ is the effective kinematic viscosity ($m^2 s^{-1}$), with ν_0 and ν_t denoting molecular and turbulent viscosity, respectively; ρ_k is the effective (driving) kinematic density (dimensionless), β the coefficient of expansion with temperature of the fluid (for water $\approx 0.207 \times 10^{-3} Jkg^{-1}K^{-1}$); T_{ref} reference temperature ($= 293.15\,K$); and δ is the delta of Kronecker (dimensionless). The Boussinesq approximation is valid under the assumption that density differences are sufficiently small to be neglected, except where they appear in the term multiplied by g_i (Fredriksson, 2011). In the model, for incompressible flows the density is considered as effective (driving) kinematic density and calculated as a linear function of temperature as (White, 1991; Ferziger and Perić, 2002):

$$\rho_k = 1 - \beta\left(T - T_{ref}\right) \tag{5.3}$$

and the density is calculated from

$$\rho = \rho_k \times \rho_0 \tag{5.4}$$

where ρ_0 is water density at reference temperature ($\approx 998.24\,kgm^{-3}$).

$$\frac{\partial T}{\partial t} + \frac{\partial}{\partial x_j}(Tu_j) - \alpha_{eff}\frac{\partial}{\partial x_k}\left(\frac{\partial T}{\partial x_k}\right) = S_T(t, x_k) \tag{5.5}$$

where T is temperature in water (K), α_{eff} heat transfer conductivity ($m^2 s^{-1}$) and S_T is the heat source term in lake due to the penetrating solar radiation (Ks^{-1}). Heat transfer conductivity can be given by:

$$\alpha_{eff} = \alpha_t + \alpha_0 = \frac{\nu_t}{Pr_t} + \frac{\nu_0}{Pr} \tag{5.6}$$

where ν_0 is the molecular kinematic viscosity (for water at reference temperature $\approx 1.004 \times 10^{-6}\ m^2 s^{-1}$), ν_t turbulent kinematic viscosity ($m^2 s^{-1}$), C_p specific heat of water ($\approx 4.1818 \times 10^3\ Jkg^{-1}K^{-1}$), Pr is Prandtl number (≈ 7.07), Pr_t turbulent Prandtl number (≈ 0.85) and α_{eff} is effective thermal conductivity ($m^2 s^{-1}$). Changes in temperature in water body might occur mainly due to heat exchange across the air-water interface. Accurate estimation of heat fluxes is extremely crucial in the simulation of temperature dynamics in the water body (Politano et al., 2008). Atmospheric heat fluxes include incoming short-wave (solar) and long-wave (atmosphere) radiations, outgoing long-wave radiation, conductive heat at the free surface and evaporative heat flux. Computationally, all these terms, except for incoming short-wave radiation, are considered at the water surface as boundary conditions.

506469-L-sub01-bw-Abbasi
Processed on: 9-11-2016

Incoming short-wave radiation is included in the source term (S_T) that allows radiation to be absorbed through a finite distance in the upper layers of the model water column rather than only at the air-water interface (Wood et al., 2008). The heat source term using Lambert–Beer law is written as:

$$S_T(z^*, t) = \frac{1}{\rho_0 C_p} \frac{\partial Q_{Rs}^{z^*}}{\partial z} \tag{5.7}$$

$$Q_{Rs}^{z^*} = Q_{Rs}^0 \sum_{i=1}^{7} f_i \exp\left(-\eta_i z^*\right) \tag{5.8}$$

$$S_T(z^*, t) = \frac{Q_{Rs}^0}{\rho_0 C_p} \sum_{i=1}^{7} \eta_i f_i \exp\left(-\eta_i z^*\right) \tag{5.9}$$

where z^* is downward vertical distance from the water surface (m), $Q_{Rs}^{z^*}$ is the heat flux due to penetrated solar radiation at a depth z^* within the water (Wm^{-2}), Q_{Rs}^0 is the net solar radiation at the air-water interface (Wm^{-2}), f_i is the fraction of energy contained in the i^{th} bandwidth (dimensionless), and η_i represents the composite attenuation coefficient of the i^{th} bandwidth (m^{-1}) (Branco and Torgersen, 2009; Momii and Ito, 2008). The values of f_i and η_i are presented in Table 5.1. The attenuation coefficient (light extinction coefficient) for visible light theoretically is a function of wave length, temperature and water turbidity (Politano et al., 2008; Losordo and Piedrahita, 1991) and typically ranges from 0.02 to 31.6 for inland shallow waters (Politano et al., 2008; Smith and Baker, 1981; Losordo and Piedrahita, 1991; Goudsmit et al., 2002; Bigham Stephens et al., 2015). Usually a linear relationship is applied to calculate the extinction coefficient value from observed Secchi depth in inland water bodies (Idso and Gilbert, 1974; Politano et al., 2008). For this study, the attenuation coefficient is assumed to be constant in the whole water body ($\eta = 3.0\ m^{-1}$). This value was computed from the turbidity measurements. By applying the approach proposed by Williams et al. (1981) and using the available measurements for Secchi depth values during the simulated period, the attenuation coefficient was calculated. The attenuation coefficient value was estimated only in one point and therefore, it is assumed that the distribution of the attenuation coefficient in the water body is homogeneous. The temperature profiles in a shallow lake are significantly sensitive to the attenuation coefficient and, hence, this parameter should be considered carefully in the simulation (Abbasi et al., 2015a).

The net solar radiation at the air-water interface (Q_{Rs}^0) is given by (Subin et al., 2012):

$$Q_{Rs}^0 = (1 - r_{ws})\, R_s \tag{5.10}$$

where R_s is the incoming short-wave radiation at the water surface (Wm^{-2}) and r_{ws} is the reflection coefficient of solar radiation from water surface (≈ 0.08) (Weinberger and Vetter, 2012).

5.4.2. TURBULENCE MODELLING

In this study, the turbulence is modeled with the realizable $k-\varepsilon$ (RKE) model. The results of the study done by Shih et al. (1995) has shown that the realizable $k-\varepsilon$ model performs

Table 5.1: Short-wave radiation bandwidth fractions of the total energy (f) and composite attenuation coefficients (η) (adopted from Branco and Torgersen (2009)

Wavelength(nm)	f	$\eta(m^{-1})$
<400 (UV)	0.046	assume same as VIS
400-700 (VIS)	0.430	3.0 (assumed)
700-910	0.214	2.9
910-950	0.020	20.4
950-1090	0.089	29.5
1090-1350	0.092	98.4
>1350	0.109	2880.0

better than the standard $k-\varepsilon$ (SKE) model or other traditional $k-\varepsilon$ models. In simulating flow field alongside heat transfer in the water body, it was found that the realizable $k-\varepsilon$ model is robust with reasonable accuracy and provides better results than the standard or other traditional $k-\varepsilon$ models (Shih et al., 1995; Joubert et al., 2012; Wang, 2013). In this turbulence model, the Reynolds stresses are limited by physical-based mathematical constraints (Rohdin and Moshfegh, 2007). In the SKE model, dissipation rate for fluctuation is approximated by the dynamic equation vorticity. In addition, the realizable $k-\varepsilon$ is expected to enhance the numerical stability in turbulent flow simulations. In this model, the turbulent kinetic energy (k in m^2s^{-2}) and the turbulent dissipation rate (ε in m^2s^{-3}) are obtained from:

$$\begin{aligned}\frac{\partial k}{\partial t}+u_j\frac{\partial k}{\partial x_j} &= \frac{\partial}{\partial x_j}\left[\left(\frac{\nu_t}{\sigma_k}\right)\frac{\partial k}{\partial x_j}\right]+\nu_t\left(\frac{\partial u_i}{\partial x_j}+\frac{\partial u_j}{\partial x_i}\right)\frac{\partial u_i}{\partial x_j}-\varepsilon \\ &+ G_k+G_b+S_k \qquad (5.11)\\ \frac{\partial \varepsilon}{\partial t}+u_j\frac{\partial \varepsilon}{\partial x_j} &= \frac{\partial}{\partial x_j}\left(\frac{\nu_t}{\sigma_\varepsilon}\frac{\partial \varepsilon}{\partial x_j}\right)+C_1S\varepsilon-C_{\varepsilon2}\frac{\varepsilon^2}{k+\sqrt{\nu\varepsilon}}+C_{\varepsilon1}C_{\varepsilon3}\frac{\varepsilon}{k}G_b+S_\varepsilon \qquad (5.12)\end{aligned}$$

where ν_t is the turbulent kinematic viscosity (m^2s^{-1}), G_k is the production of turbulent kinetic energy by the mean velocity gradient (m^2s^{-3}), G_b is the production of turbulent kinetic energy by the buoyancy (m^2s^{-3}), and S_k (m^2s^{-3}) and S_ε (m^2s^{-4}) are the source terms which include the effects of wind on k and ε equations respectively. The parameter $C_{\varepsilon3}$ (dimensionless) is not constant and depends on the flow conditions and is a function of the ratio of the velocity components in the vertical and longitudinal directions (Lee, 2007):

$$C_{\varepsilon3}=\tanh\left|\frac{w}{u_h}\right| \qquad (5.13)$$

where u_h and w are the components of the flow velocity perpendicular and parallel to the gravitational vector respectively (ms^{-1}). The coefficient C_1 (dimensionless) is evalu-

506469-L-sub01-bw-Abbasi
Processed on: 9-11-2016

ated as (Shih et al., 1995):

$$C_1 = max\left(0.43, \frac{\zeta}{\zeta+5}\right) \tag{5.14}$$

$$\zeta = S\frac{k}{\varepsilon} \tag{5.15}$$

$$S = \sqrt{2S_{ij}S_{ij}} \tag{5.16}$$

$$S_{ij} = \frac{1}{2}\left(\frac{\partial u_i}{\partial x_j} + \frac{\partial u_j}{\partial x_i}\right) \tag{5.17}$$

and the turbulent kinematic viscosity is given by

$$\nu_t = C_\mu \frac{k^2}{\varepsilon} \tag{5.18}$$

$$C_\mu = \frac{1}{A_0 + A_s\frac{kU^*}{\varepsilon}} \tag{5.19}$$

$$U^* = \sqrt{S_{ij}S_{ij} + \overline{\Omega_{ij}}\,\overline{\Omega_{ij}}} \tag{5.20}$$

$$A_s = \sqrt{6}\cos\phi \tag{5.21}$$

$$\phi = \frac{1}{3}cos^{-1}(\sqrt{6}W) \tag{5.22}$$

$$W = \frac{S_{ij}S_{jk}S_{ki}}{\widetilde{S}^3} \tag{5.23}$$

$$\widetilde{S} = \sqrt{S_{ij}S_{ij}} \tag{5.24}$$

where $\overline{\Omega_{ij}}$ is the mean rate-of-rotation tensor. G_k and G_b are written as

$$G_k = \nu_t S^2 \tag{5.25}$$

$$G_b = \beta g_i \frac{\nu_t}{Pr_t}\left(\frac{\partial T}{\partial x_i}\right) \tag{5.26}$$

where Pr_t (≈ 0.85) is the turbulent Prandtl number for energy (Wang et al., 2013a). The standard values of the model constants used for the realizable $k-\varepsilon$ turbulence approach in the model equations are given as (Shih et al., 1995):

$$C_\mu = 0.09; \quad C_{\varepsilon 1} = 1.44; \quad C_{\varepsilon 2} = 1.92; \quad \sigma_k = 1.0; \quad \sigma_\varepsilon = 1.3; \quad A_0 = 4.0 \tag{5.27}$$

Depending on the approach used to implement the effects of wind velocity over the water surface, the source/sink terms in Equations (5.11) and (5.12) can be parameterized (Abbasi et al., 2015a). In this study, the effects of wind velocity is considered as a shear stress boundary condition over the water surface and therefore, the source/sink terms are given by:

$$S_k = S_\varepsilon = 0 \tag{5.28}$$

506469-L-sub01-bw-Abbasi
Processed on: 9-11-2016

5.5. NUMERICAL SIMULATION

5.5.1. NUMERICAL GRID

In order to perform reliable Computational Fluid Dynamics (CFD) computations in complex geometries such as for lakes or reservoirs, the generation of a good computational grid (mesh) is essential. Numerical modeling of shallow water bodies is generally computationally expensive. In such domains the vertical length scale is much smaller than the horizontal scale. As a consequence, the vertical grid aspect ratio to the horizontal directions is small and numerical instability may be introduced. To avoid this instability, a large number of horizontal grid points are required to decrease the maximum aspect ratio of the grids. The extra grids will, however, increase the computational time significantly (Lee, 2007).

Lake Binaba is characterized by significant bottom slopes throughout its area. As the effects of morphometry are significant (Stepanenko et al., 2014), preparing the precise geometry (bathymetry) was important. Using the proposed approach by (Abbasi et al., 2015a) and the available (rough) bathymetry measurements, the lake geometry was generated (Figure 5.3(a)) and used in `snappyHexMesh` (SnappyHexMesh, 2015) utility available in `OpenFOAM` (OpenFOAM, 2015) to generate the computational mesh. `snappyHexMesh` is a powerful script-driven, unstructured mesh generator. This utility generates grids containing hexahedra and split-hexahedra (Brockhaus, 2011; Benjamin Martinez, 2011).

The computational mesh should follow the bathymetry of the lake. Horizontal grids were generated according to the geometrical boundaries. In the vertical direction (z), grid spacing was varied so it was concentrated only where the specific resolution was required (Figure 5.3(b)). Concentration of the vertical grid points near the boundaries, especially for water surface, was more clustered to cover the sharp gradients in resolved parameters.

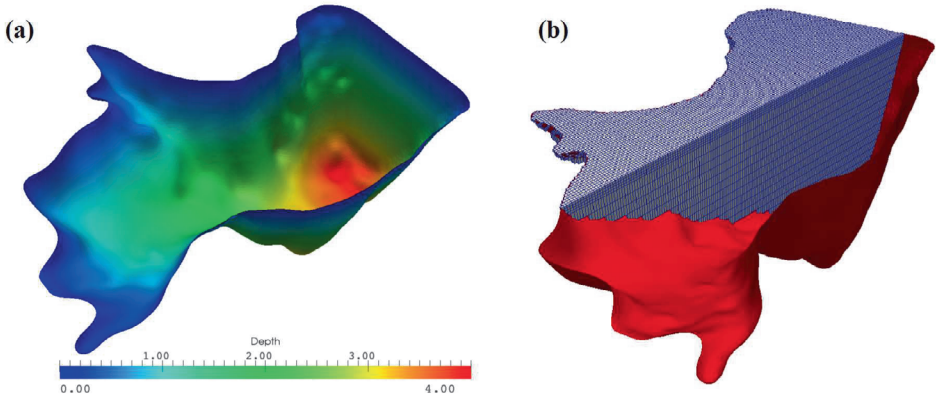


Figure 5.3: **(a)** The generated geometry of Lake Binaba with depth distributions; and **(b)** computational grid in the water body used in the simulation (vertical exaggerated by 100).

The generated computational grid was composed of 41400 grid points and 35617 cells. The computational grid for the lake was selected based on coarse and fine meshes to select the optimized number of cells. The selected mesh was refined sufficiently near

506469-L-sub01-bw-Abbasi
Processed on: 9-11-2016

the water surface to accommodate the high gradients, specifically in velocity and temperature.

5.5.2. NUMERICAL SETUP

The model improvements explained in Section (5.4), were implemented in `OpenFOAM` CFD package (OpenFOAM, 2015). `OpenFOAM` includes a set of efficient `C++` modules that could be used to establish solvers. Because of the collocated and polyhedral numerics implemented in `OpenFOAM`, it can be used in both structured and unstructured meshes with the advantage of being easily extendable to run in parallel. To respect the structure of the original code, a new turbulence model including the buoyancy effect and a new heat transfer solver were implemented. The solver is an unsteady state and incompressible heat transfer solver that considers buoyancy effects in the momentum equation. The `PIMPLE` method was used for pressure-velocity coupling. The `PIMPLE` algorithm combines the `SIMPLE` (semi-implicit method for pressure-linked equations) algorithm and the `PISO` (pressure implicit with splitting of operators) algorithm to rectify the second pressure correction and correct both velocity and pressure explicitly. This algorithm allows one to use larger time steps than `PISO` algorithm. Due to the transient conditions of flow in the lake, an adaptive time-stepping technique based on the Courant-Friedrick-Levy number (CFL) was used (Bechmann, 2006):

$$CFL = \Delta t_{max}\left(\frac{|\bar{u}|}{\Delta x}, \frac{|\bar{v}|}{\Delta y}, \frac{|\bar{w}|}{\Delta z}\right) \leq 1 \tag{5.29}$$

where $\bar{u}$, $\bar{v}$ and $\bar{w}$ are the velocity components in $x-$, $y-$ and $z-$directions, respectively (ms^{-1}). In this study, the maximum value of global CFL adopted was 0.2. For larger time steps numerical dissipation increases as the CFL-number increases and makes the model more unstable (Wang, 2013; Ferziger and Perić, 2002).

5.6. BOUNDARY CONDITIONS

5.6.1. TEMPERATURE

Meteorological and water temperature measurements were available (Figure 5.2) for the simulation period. At the atmosphere-water surface interface, the temperature gradient evaluated at the lake surface is described by the following equation (Neumann Type) (Goudsmit et al., 2002):

$$\rho_0 C_p\left(\alpha_{eff}\frac{\partial T}{\partial z}\right) = H_{net} \Rightarrow \frac{\partial T}{\partial z} = \frac{H_{net}}{\rho_0 C_p \alpha_{eff}} \tag{5.30}$$

The net heat exchange between the water surface and atmosphere (H_{net}) includes four heat flux terms (Goudsmit et al., 2002; Ahsan and Blumberg, 1999):

$$H_{net} = H_{LA} + H_{LW} + H_S + H_E \tag{5.31}$$

where H_{LA} is the net long-wave (atmospheric) radiation from atmosphere, H_{LW} is the long-wave (atmospheric) radiation from the water surface, H_S and H_E are the sensible and latent (evaporative) heat fluxes between the lake surface and atmosphere, respectively. Measurements of heat fluxes such as short-wave radiation, long-wave radiation,

506469-L-sub01-bw-Abbasi
Processed on: 9-11-2016

sensible heat flux, and latent heat flux are very difficult and expensive to take. Therefore, these heat fluxes are often parameterized using the most commonly available meteorological data (Ahsan and Blumberg, 1999). In the current study, the incoming short-wave radiation was the only surface heat transfer term that was directly measured. The rest of the surface terms were computed within the model at each time step using standard formulae. It should be mentioned that in the current model, H_{net} does not include the short-wave (solar) radiation. This term is included in temperature equations (Equations (5.5) and (5.9)) as the source term.

Atmospheric long-wave radiation was calculated from the Stefan-Boltzmann law (Ahsan and Blumberg, 1999; Goudsmit et al., 2002):

$$H_{LA} = (1 - r_a)\,\varepsilon_a \times \sigma\, T_a^4 \tag{5.32}$$

where r_a is the reflection coefficient of atmospheric radiation from water surface (≈ 0.03) (Perroud and Goyette, 2010; Lap and Mori, 2007), ε_a emissivity of atmosphere (≈ 0.87) (Henderson-Sellers, 1988), σ is Stefan-Boltzmann constant ($\approx 5.67 \times 10^{-8} [W m^{-2} K^{-1}]$), and T_a is absolute air temperature in K. Similarly, long-wave radiation from the water surface was estimated by (Goudsmit et al., 2002; Ahsan and Blumberg, 1999; Shufen et al., 2007a):

$$H_{LW} = -\varepsilon_{ws} \times \sigma T_w^4 \tag{5.33}$$

where ε_w is emissivity of water (≈ 0.97) (Hostetler and Bartlein, 1990; Yao, 2009), and T_w is the absolute temperature of water surface in K.

In general, latent heat flux (evaporation) is one of the most important parameters in heat dissipation, but its prediction is the most inaccurate. In most available methods for evaporation estimation, the models' parameters are specific to a given water body under the prevailing surrounding environment and for a specific climate which are valid only for the specific ranges of parameters (reservoir size, temperature difference, humidity, atmosphere conditions, etc.) that are used in the designed experiment. This therefore means these coefficients may not provide satisfactory estimation for other regions. In this study, for sensible heat (H_S) and latent heat (H_E) fluxes, the following formulae were used. These equations were obtained from a CFD-based approach (CFDEvap Model) applied for Lake Binaba (Abbasi et al., 2015b). The convective heat transfer between a water surface and the atmospheric boundary layer can be expressed as follows:

$$H_S = -h_s(T_s - T_a) \tag{5.34}$$

where H_S is the convective heat transfer or sensible heat flux in $W m^{-2}$ (positive if it flows from the atmosphere into the water surface) and h_s is the convective heat transfer coefficient ($W m^{-2} K^{-1}$), which relates the convective heat flux normal to the water surface to the difference between the water surface temperature (T_{ws}) and surrounding air temperature (T_a). The convective heat transfer coefficient can be estimated by (Abbasi et al., 2015b):

$$h_s = 2.50510 \times U_2 + 0.85200 \tag{5.35}$$

Using the analogy between the heat and mass transfer, the convective mass transfer coefficient was derived as a function of wind velocity. The evaporation rate from the

506469-L-sub01-bw-Abbasi
Processed on: 9-11-2016

water surface could then be calculated using the estimated mass transfer coefficient:

$$H_E = -h_m \times \rho_a (X_{ws} - X_{air}) \times (24 \times 3600 \times 28.4) \tag{5.36}$$

where the evaporation rate is expressed in Wm^{-2}, X_{air} and X_{ws} are the water vapor mixing ratio of air and water surface, respectively ($kg(water)/kg(dry\,air)$), ρ_a is the air density, assumed constant in this study $\approx 1.186\,kgm^{-3}$, the coefficient (24×3600) is used for converting the latent heat flux to $mm\,d^{-1}$ and the coefficient of (28.4) converts it to Wm^{-2} to be consistent with the rest heat flux components over the water surface, and h_m is the mass transfer coefficient given by (Abbasi et al., 2015b):

$$h_m = 0.00185 \times U_2 + 0.00063 \tag{5.37}$$

where h_m is in ms^{-1} and U_2 in ms^{-1} and the respective constant values in the sensible and latent heat flux equations specific to the studied lake obtained from CFDEvap model (Abbasi et al., 2015b), X_{air} and X_{ws}, were calculated by:

$$X_{air} = \frac{0.622\,e_a}{P_{atm} - e_a} \tag{5.38}$$

$$X_{ws} = \frac{0.622\,e_s}{P_{atm} - e_s} \tag{5.39}$$

where P_{atm} is atmospheric pressure ($= 102\,kPa$), e_s is the saturation vapor pressure at the temperature of the water surface (hPa) and e_a is the vapor pressure at the air temperature (hPa) given by (Goff, 1957):

$$e_a = \left(6.11 \times \exp\left(\frac{17.27 T_a}{237.3 + T_a}\right)\right) \times \frac{RH}{100} \tag{5.40}$$

$$e_s = 6.11 \times \exp\left(\frac{17.27 T_{ws}}{237.3 + T_{ws}}\right) \tag{5.41}$$

where RH is relative humidity (%) and water surface (T_{ws}) and air (T_a) temperatures are in $^\circ C$.

These heat fluxes are defined to be positive if heat flows from the atmosphere into the water surface. Heat fluxes induced by inlets and outlets and precipitation are generally neglected (Livingstone and Imboden, 1989).

Determining the correct heat fluxes for a water surface boundary is often difficult. The main difficulty is that H_{net} is a function of various parameters, where each of them has to be computed by using its own formula and sets of coefficients as well (Goudsmit et al., 2002). Therefore estimation of H_{net} needs a great deal of judgment in adopting the suitable formula, which depends on many uncertain parameters (Ahsan and Blumberg, 1999). In addition, some components of the net heat flux depend on unknown water surface temperature values (T_{ws}), which creates an implicit boundary condition that should be calculated in each time step in advance by the model. Although using a heat flux boundary condition over the water surface needs more computational resources, it needs no costly observed water surface temperature. This temperature boundary condition, which includes heat fluxes at the water surface, given by Equations (5.33) through

(5.37), was implemented in the current model by using the `groovyBC` (Gschaider, 2015a) library developed for complex boundary conditions.

Another alternative, but less practical, temperature boundary condition on the water surface uses measured water surface temperature values as boundary condition (Dirichlet type) for temperature. Using observed values of water surface temperature as water surface boundary condition has the advantage of avoiding the uncertainties in the net heat flux estimation (Goudsmit et al., 2002) but the model needs extra measurements over the water surface that is rarely available in most small lakes. The disadvantage of using measured water surface temperature is that using this boundary condition assumes homogeneous temperature at the open water surface which introduces error in the simulation.

In shallow lakes, the temperature boundary condition at the bottom and sides are very complex and need extra measurements to implement in the model. To simulate the effects of bottom and sides, the absorbed and reflected penetrated short-wave radiation should be measured. In addition, the heat flux from these boundaries has to be specified. In spite of the importance of these parameters, measuring their values is not easy and needs extra equipment. Regarding the available measurements, the boundary condition at the bottom of lake and side walls were set to zero heat flux conditions (adiabatic condition) and given by (Shufen et al., 2007a):

$$\frac{\partial T}{\partial z} = 0 \tag{5.42}$$

where T is temperature in K . The measured temperature profile at start time (on 24 November 2012 at 12:00:00 a.m.) was used as the initial condition for temperature for the simulation.

5.6.2. VELOCITY

Wind over the water surface affects lake currents, sensible and latent heat fluxes and turbulence, as well as surface waves. The effects of wind shear stress over the flow was considered as a time-dependent shear stress boundary condition over the water surface. The shear stress over the water surface is given by:

$$\left[\nu_{eff}\frac{\partial u}{\partial z}\right] = \frac{\tau_{sx}}{\rho_0} \tag{5.43}$$

$$\left[\nu_{eff}\frac{\partial v}{\partial z}\right] = \frac{\tau_{sy}}{\rho_0} \tag{5.44}$$

where

$$\tau_{sx} = \rho_a C_D u_w \sqrt{u_w^2 + v_w^2} \tag{5.45}$$

$$\tau_{sy} = \rho_a C_D v_w \sqrt{u_w^2 + v_w^2} \tag{5.46}$$

where C_D is the drag coefficient (unitless), ρ_a is the air density (kgm^{-3}), τ_{sx} and τ_{sy} are horizontal shear stress components over the water surface ($kgm^{-1}s^{-2}$), u_w and v_w are horizontal components of the mean wind speed over the water surface (ms^{-1}), and

506469-L-sub01-bw-Abbasi
Processed on: 9-11-2016

ν_{eff} is the effective kinematic viscosity ($m^2 s^{-1}$). The empirical dimensionless drag coefficient (C_D) depends to large extent only on wind speed and the state of wave development or wave age. For small shallow lakes, wind speed is generally low $U_{10} < 5\, ms^{-1}$, where U_{10} is wind speed at height 10 m above the water surface (Figure 5.2(d)) and measurements of the drag coefficient are relatively scarce. Confusingly, in the literature, the values of C_D vary over a wide range and it is associated with large scatter (Falconer et al., 1991; Goudsmit et al., 2002; Wüest and Lorke, 2003). In this study, the following empirical relationship for low wind speeds measured at a height of 10 m is used (Markfort et al., 2010; Wüest and Lorke, 2003):

$$C_{D,10} = 0.0044 \times U_{10}^{-1.15} \tag{5.47}$$

where C_D is the drag coefficient (unitless) and U_{10} is the wind velocity at height 10 m above the water surface (ms^{-1}). In this study, the wind speeds were measured at a height of 2 m from the water surface hence the observed values were converted to its values at 10 m using logarithmic distribution function for wind speed. The normal component of velocity over the water surface boundary was calculated by:

$$u_z = 0 \tag{5.48}$$

On the other boundaries, the non-slip conditions for velocity and zero heat flux for temperature and the standard wall functions were imposed (Goudsmit et al., 2002; Politano et al., 2008).

5.7. NUMERICAL RESULTS AND DISCUSSION

A large number of simulations were run during the model development. The simulation was run for four days (345600 s) where the starting time of calculations was at 12:00:00 a.m. on 24 November 2012. The simulated flow field in the water body shows the existence of an unsteady and three-dimensional flow for most times due to the effects of the reservoir geometry, dynamic atmospheric conditions and the coupling of energy (temperature) changes with the flow field.

To validate the model, the distribution of simulated temperature in the water body was compared with observations as shown in Figure 5.4. For each depth where the temporal temperature profile is depicted in Figure 5.4, the mean error ($ME = T_M - T_S$ where T_M and T_S are measured and simulated temperature values, respectively) or relative mean error ($RME = |T_M - T_S| / T_M \times 100$) are provided as a measure of the bias of the simulated values. The calculated values of ME and RME for each depth are presented in Table 5.2. As shown in Table 5.2, the maximum difference between the simulated and observed values is -1.60 where the minus sign means the model overestimated the temperature. Alongside the ME and RME, the root mean square error ($RMSE = \left(\sum_{i=1}^{n} (T_{Si} - T_{Mi})^2 / n\right)^{1/2}$) and the mean absolute error ($MAE = \frac{1}{n} \sum_{i=1}^{n} |T_{Si} - T_{Mi}|$) are provided as the measures of the overall goodness-of-fit of the simulations to the observations. The values of $RMSE$ between the simulated and observed values of temporal temperature profiles at different depths range from 0.11 to 0.44 $^\circ C$ with an average value of 0.33 $^\circ C$. Similarly, the calculated MAE ranges from 0.03 to 0.31 $^\circ C$ with an average of 0.21 $^\circ C$. As was expected considering the depicted temperature profiles in Figure 5.4,

506469-L-sub01-bw-Abbasi
Processed on: 9-11-2016

the $RMSE$ as well as the MAE are increasing in greater depths. A good agreement between simulated and observed temperatures demonstrate the capability of the model to represent temperature dynamics in the small and shallow inland water bodies. These results clearly indicate the variability in the temperature and velocity distributions and the daily thermal cycle predicted by the model for the studied meteorological conditions. Although deviations between modeled and observed temperature profiles at some depths, especially at greater depths were relatively large, general trends and daily temperature fluctuations due to heat transfer are reasonably reproduced by the model. These large deviations between the simulated and observed values are mainly due to the existing uncertainties in thermal boundary condition assigned to the bottom and sides of lake considering the available data or applicable measurements. As shown by Suárez et al. (2010), in shallow water bodies the thermal interaction between the reservoir bottom, which includes both the bottom and the sides, and the sediment beneath the reservoir significantly affects the reservoir thermal structure. In addition, ignoring the variations of turbidity in the water column and changes of the extinction coefficient of water in this simulation can be considered as the error sources, especially at greater depths (Suárez et al., 2010; Jacobs et al., 1997; Losordo and Piedrahita, 1991). To evaluate the effects of upper thermal boundary condition (on the water surface) on the temperature profiles, both boundary conditions for temperature described above were considered. In both simulations, the same differences were found between the simulated and observed temperature values at greater depths.

In Figure 5.4, the simulated water temperature (S.) and observed values (M.) at different depths are depicted. These temporal profiles of temperature were generated by using the heat flux as the temperature boundary condition (Section (5.6.1)) on the water surface. These profiles show that in each day of simulation, two different time periods can be detected. In the first time period, which commonly (in the four-day simulated period) ranges from 12:00:00 till 6:00:00 a.m., the simulated temperature matched the observed ones. In this period, due to the good agreement between the modeled and observed temperatures the model can predict the heat budget of the lake precisely. In the second time period, which commonly expands from 6:00:00 a.m. till 12:00:00 a.m., the model overestimated the temperature and consequently the heat content of the lake. As these time periods occur periodically in the simulated period, it seems that the model's excess heat during the second time period (from 6:00:00 a.m. till 12:00:00 a.m.) is matched by excess cooling at the first period. Therefore, in spite of the uncertainties and errors discussed above, the model could be applied precisely for estimating heat budget of lakes through a one-day time step. This aspect of the model can be promising in energy budget method for evaporation estimation where ignoring the heat content of the lake usually makes significant error in the estimated evaporation from the water surfaces (Vercauteren et al., 2011; Katul and Parlange, 1992).

To analyze the simulated temperature profiles with respect to the incoming shortwave radiation, by following the proposed approach by Vercauteren et al. (2011), the amplitude and the phase shift of the observed and the simulated daily temperature variations (24 November 2012) as a function of the depth are plotted in Figure 5.5. As Figure 5.5 shows the model overestimated both the amplitude and the phase shift in all depths and the differences between the simulated and measured values are increased

506469-L-sub01-bw-Abbasi
Processed on: 9-11-2016

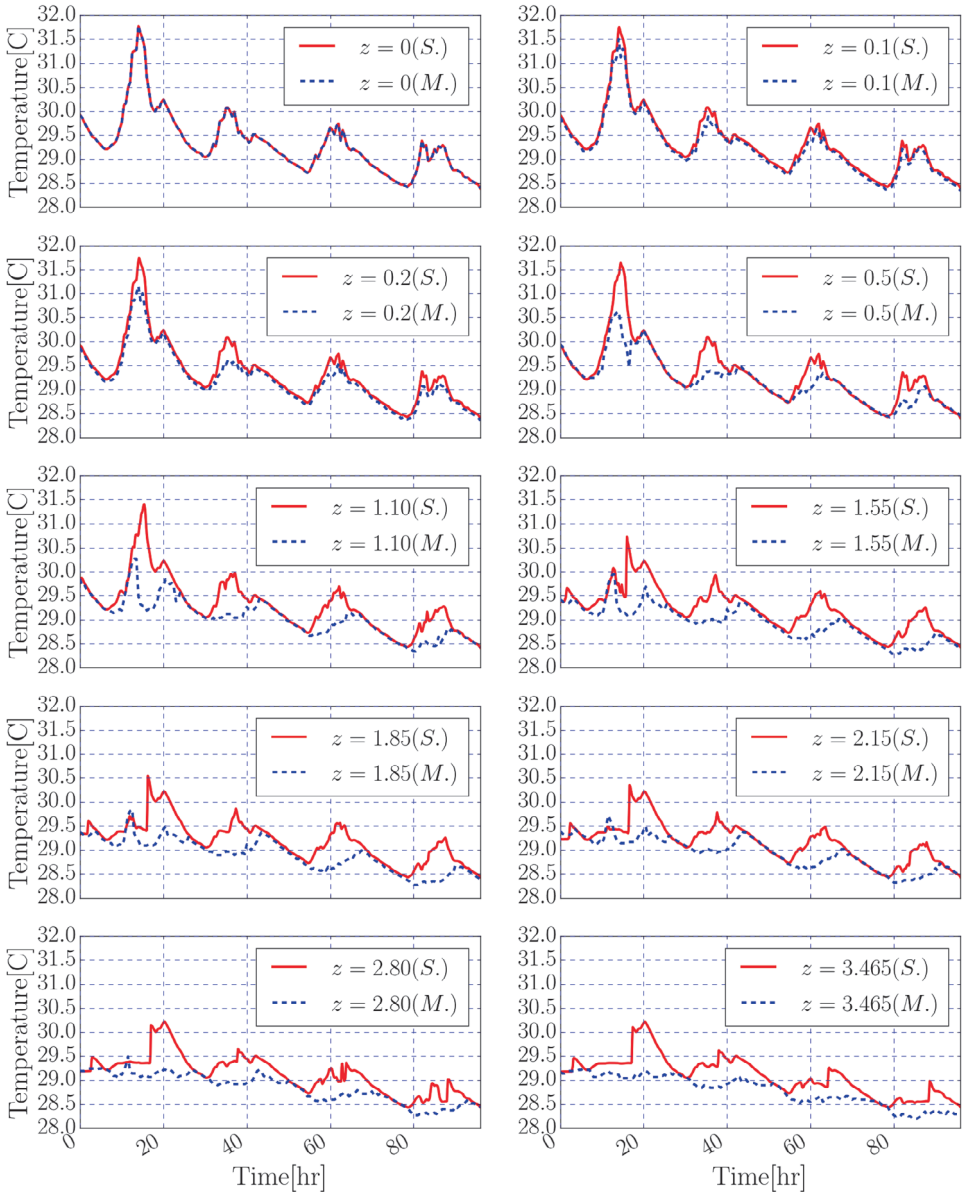


Figure 5.4: Simulated water temperature (S.) and observed values (M.) at different depths (at water surface as well as depths of 0.100, 0.200, 0.500, 1.100, 1.550, 1.850, 2.150, 2.800 and 3.465 m).

with depth. Although the applied model in this study is fully 3-D and considers the horizontal flows, analyzing the amplitude and phase shift of the temperature signals helps to find the order of the importance of radiation as well as the turbulent diffusivity (or heat

506469-L-sub01-bw-Abbasi
Processed on: 9-11-2016

Table 5.2: Calculated metrics of model performance (MAE: mean absolute error; $RMSE$: root mean square error; ME: mean error; RME: relative mean error) for simulated temporal temperatures at different depths.

Depth	MAE	$RMSE$	Mean Error [$^\circ C$]			RME[%]		
(m)	($^\circ C$)	($^\circ C$)	max	min	ave	max	min	ave
0.0	0.029	0.043	0.2053	-0.1985	0.0032	0.6556	0.0017	0.0969
0.1	0.079	0.110	0.0650	-0.4645	-0.0773	1.4922	0.0000	0.2659
0.2	0.117	0.172	0.0023	-0.7523	-0.1166	2.4385	0.0076	0.3960
0.5	0.169	0.297	0.0760	-1.4065	-0.1402	4.6780	0.1038	0.5764
1.10	0.258	0.442	0.0335	-1.6010	-0.2541	5.4021	0.0009	0.8870
1.55	0.282	0.407	0.0340	-1.5325	-0.2816	5.2681	0.0075	0.9770
1.85	0.298	0.415	0.1960	-1.2730	-0.2931	4.3723	0.0094	1.0320
2.15	0.253	0.360	0.2560	-1.0185	-0.2277	3.4922	0.0009	0.8750
2.80	0.283	0.374	0.1123	-1.0593	-0.2780	3.6444	0.0009	0.9800
3.465	0.308	0.385	0.0425	-1.0400	-0.3057	3.5659	0.0043	1.0690
Total	**0.208**	**0.329**	**0.2560**	**-1.6010**	**-0.1972**	**5.4021**	**0.0000**	**0.7162**

conductivity) on temperature profiles.

As on the selected day (24 November 2012), the wind speed was low (Figure 5.2(d)), it is expected that incoming short-wave radiation has the dominant effect (in comparison with the turbulent diffusivity) on the temperature profiles. The overestimated amplitude and phase shift of temperature signals show that the model overestimated the radiation effects especially on the calm days and consequently radiation can lead to an overestimation of the turbulent heat transfer conductivity (Vercauteren et al., 2011). It can be concluded that the optical properties of the water bodies should be considered carefully in shallow lake models to enable one predict the temperature signals due to the significant effects of radiation on both the amplitude of the temperature oscillations as well as the phase shift.

The vertical simulated temperature distribution through the water body, in seven distinctive time frames were plotted in Figure 5.6. These time frames were chosen in a way that they cover both the heating and cooling phases in the lake. To show the performance of the model with respect to the vertical temperature profiles, the measured vertical temperature profiles are plotted as well in Figure 5.6 with dotted lines for the same time frames. At the beginning part of the simulation (from 12:00:00 a.m. to 7:00:00 a.m.) the water surface is cooling and the value of temperature source (S_T) is equal to zero. During the cooling time, the wind speed over the water surface is low (less than 1.0 ms^{-1}). Looking at the simulated temperature profile, during the cooling phase (at $t = 7\,h$) there are very small differences at different depths and the lake could be considered as a well-mixed water body (Figure 5.6). This condition could be useful in making some simplifications in calculating the heat budget of the lake to calculate evaporation from the water surface in energy budget methods. As the radiative heating intensifies, the water temperature in the top layers near the water surface increase as a consequence of the penetrating short-wave radiation from the water surface. It should be mentioned that during the heating phase (from 7:00:00 a.m. to 6:00:00 p.m.) the values of H_{net} over

506469-L-sub01-bw-Abbasi
Processed on: 9-11-2016

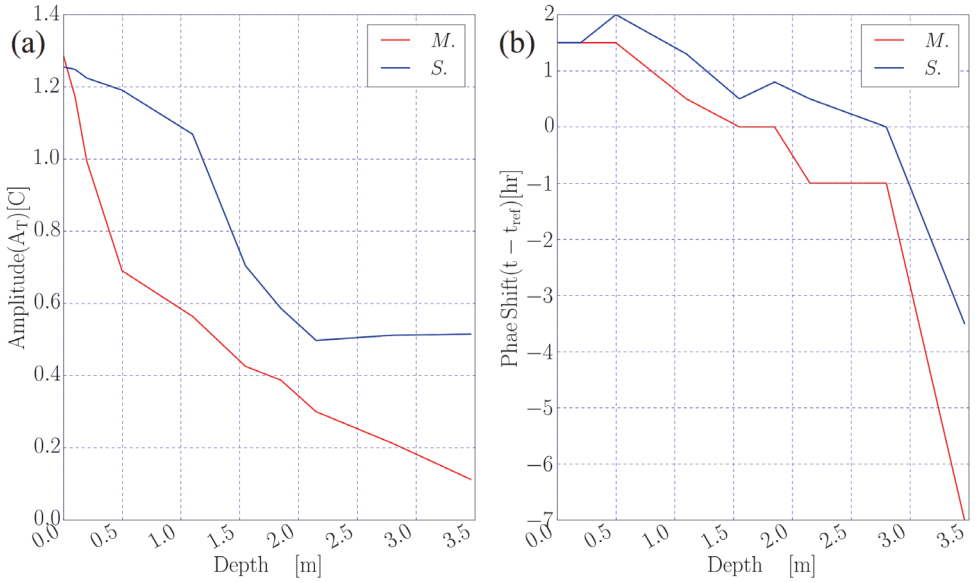


Figure 5.5: Analysis of the simulated (S.) and observed (M.) temperature values on the selected day (24 November 2012). **(a)** Amplitude of the daily temperature variations as a function of depth. Amplitude is defined as the half-temperature fluctuations (the difference between the maximum and minimum temperature values in each depth); **(b)** The phase shift with respect to the maximum short-wave radiation value as a function of depth where t and t_{ref} are the times of the maximum temperature and short-wave radiation respectively.

the water surface remain negative. Due to the effects of absorbed radiation, applied as source term in temperature equation, the temperature increases especially in the top layers near the water surface from 7:00:00 a.m. until 2:00:00 p.m. where the incoming short-wave radiation is increasing. As the incoming short-wave radiation decreases on the water surface from 2:00:00 p.m. to 12:00:00 a.m., the temperature decreases in the top layers to reach to the well-mixed condition (at $t = 24\,h$). The behavior of the water body in the heating phase is completely different from the cooling phase. In the heating phase the water body is not well-mixed; hence, to estimate the heat budget applicable in the evaporation calculation, the non-uniform simulated distribution of temperature is used.

According to Equation (5.2) in the governing equations of the model, the flow was coupled with energy in the lake. Therefore, changes in temperature impact the flow field. The velocity distribution at different depths and stream lines in the lake show the transient boundary conditions over the water surface and complex bathymetry of lake which make the flow in the lake unsteady and fully 3-D. Assuming that the top grid cells near the free water surface represent the temperature and velocity at the free surface, the horizontal distributions of velocity field at the water surface are presented in Figure 5.7.

Figure 5.7 and Figure 5.8 present the velocity fields at two different depths, at the water surface and at 1.0 m beneath the water surface at 1:00 p.m. As expected, there were

506469-L-sub01-bw-Abbasi
Processed on: 9-11-2016

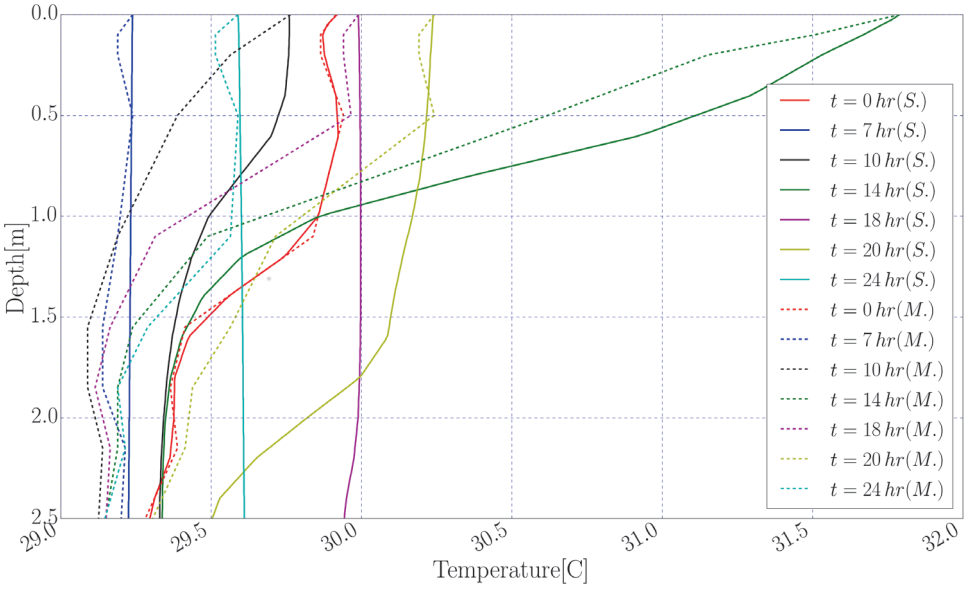


Figure 5.6: Simulated vertical temperature profiles (S.) and observed values (M.) at selected time frames.

return currents at this depth. The simulated vertical velocity profiles show non-uniform distributions, where flow near the bottom and sides tend to follow the bathymetry.

As shown in Figures 5.9 and 5.10, the higher wind speeds caused more mixing in the water column in the vertical direction and consequently lead to higher return flows, which were generated between the surface and deeper layers. Wind induced circulation mainly affects the region near the free water surface and its effects are negligible near the bottom of the lake. In deep regions, this process consequently separates the bottom layer from the top mixed layer and leads to stratification. However, in shallow regions, winds at the water surface can generate circulation throughout the whole depth, from the surface to the bottom of the lake, and therefore in the shallow parts there was no significant stratification most of the time (Figure 5.13). In general, as can be seen in Figure 5.8 and Figure 5.11, the velocity distributions in the horizontal section are greatly dependent on wind speed and its direction at the water surface. Higher wind velocities induce strong horizontal circulation as corroborated by Lee (2007).

Figure 5.12 shows the simulated temperature values in a horizontal section at 1 m beneath the water surface. As can be seen, the temperature distribution is not uniform and the temperature difference between the points at similar depth is around $1.4\,^{\circ}C$. The vertical distribution of temperature in a vertical section is illustrated in Figure 5.13, which shows that the behavior of shallow and deep parts are different, and shallow parts respond faster to air heating. Since surface temperature is a complex function of several parameters, such as wind speed, incoming short-wave (solar) radiation, wind direction, humidity, air temperature, etc., it is difficult to detect a general clear pattern in water temperature. However, generally, the simulated results indicate that heating during the

506469-L-sub01-bw-Abbasi
Processed on: 9-11-2016

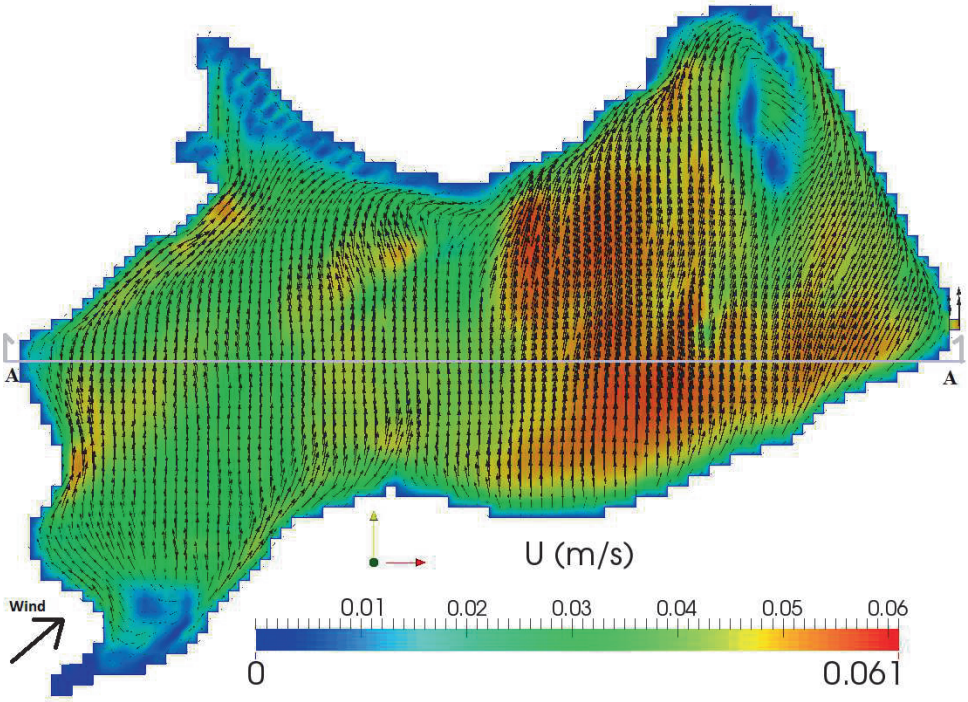


Figure 5.7: Simulated velocity vectors and their magnitudes over the water surface at t = 1:00 p.m. where $U_2 = 1.0\, ms^{-1}$. Line A-A is the vertical section illustrated in Figure 5.13.

day is normally related to incoming solar radiation, while cooling at night is more complicated and is more a function of wind speed and its direction. Water in the surface layer starts to warm after sunrise as incoming solar radiation increases (around 7:00:00 a.m.), and this increase continues until short-wave radiation reduces (at 3:00 p.m.), after which surface water temperatures reduce gradually.

Apart from the wind effects on flow field in water bodies, the coupling energy and momentum equations drive the circulation. As solar radiation increases, the temperature in the top layers increases. This increase extends vertically by effective thermal conductivity to the bottom of the lake. With an increase in wind during the day, the velocities at the surface also increases, but no significant vertical circulation is seen throughout the water because of the existence of stable stratification. Water temperature in the top layer is more sensitive to the meteorological conditions. Steeper temperature gradients in the top layers near the water surface are correctly predicted by the model due to the high heat fluxes at the water-air interface.

The main sources of error in the results could be related to the following:

1. Estimating heat fluxes over the water surface as boundary condition is very uncertain especially for latent heat flux. The location, climate, shape, depth, bathymetry, atmospheric stability conditions, etc. make it difficult to estimate evaporation ac-

506469-L-sub01-bw-Abbasi
Processed on: 9-11-2016

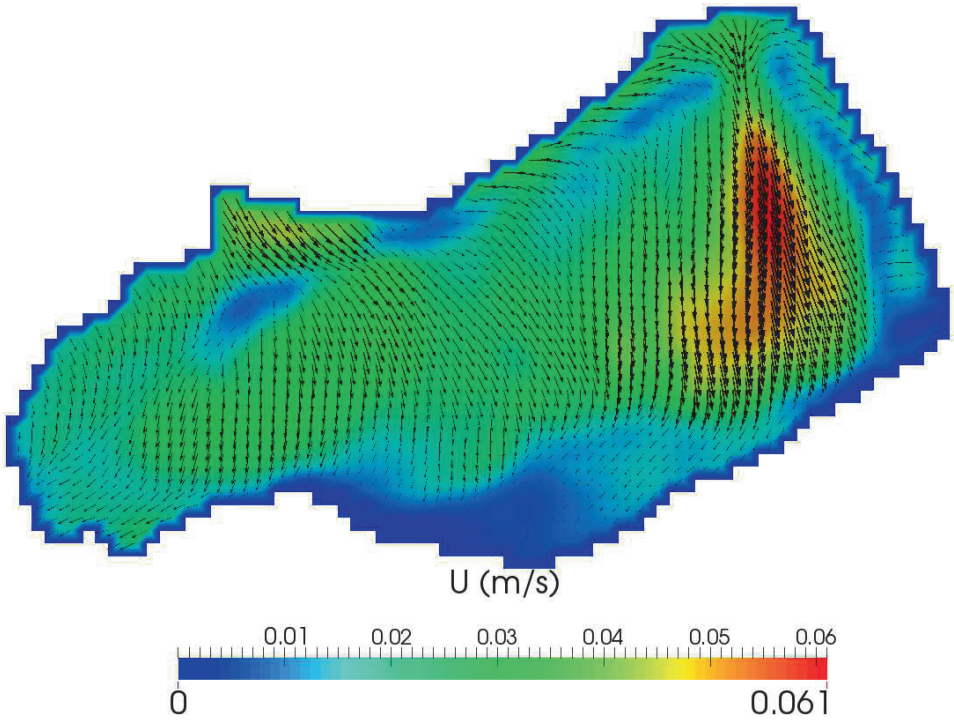


Figure 5.8: Simulated velocity vectors and theirs magnitudes at 1 meter beneath the water surface at t = 1:00 p.m. where $U_2 = 1.0\, ms^{-1}$.

curately from the water surface.

2. There are no measurements for some important parameters that can affect the flow field and temperature in the water body, such as turbidity, and heat fluxes at the bottom and side walls where using simplified temperature boundary conditions could be considered as a source of error.

3. The measurements were taken only at one point. This means that the distribution of parameters over the water surface was assumed homogeneous. For shallow and small lakes with limited fetch, this assumption could produce a large error in the results.

4. Coupling the turbulent flow and heat transfer in a shallow water body is complex and computational issues such as numerical errors, mesh dependency and residuals control should be considered.

5. Errors in field measurements on the water surface especially for water surface temperature or heat fluxes.

Due to the limitation of computational resources, it is not possible to use a finer mesh or very small time steps. In this study different settings for numerical schemes

506469-L-sub01-bw-Abbasi
Processed on: 9-11-2016

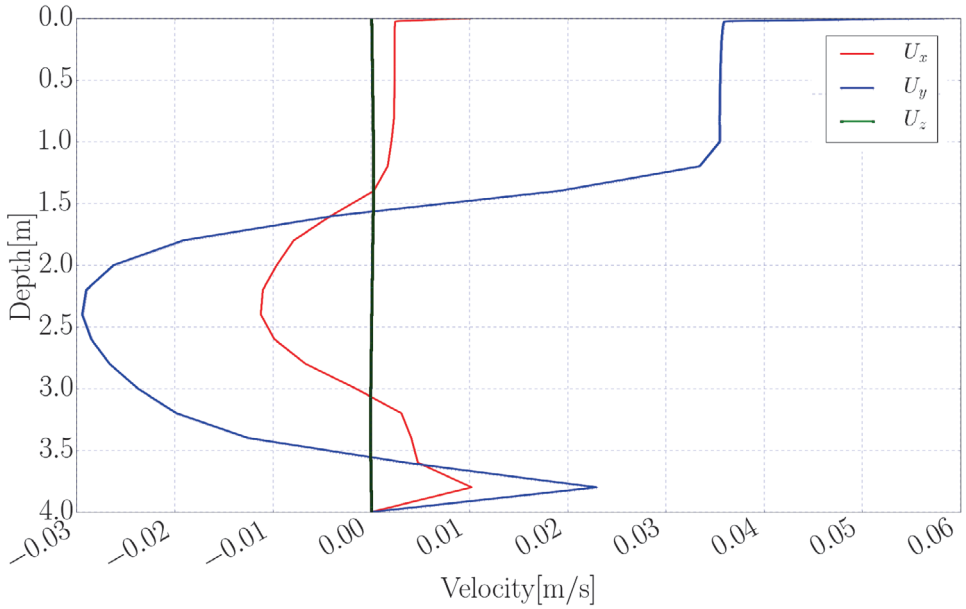


Figure 5.9: Simulated vertical distribution of velocity components in the water body where $U_2 = 3.0\,ms^{-1}$.

and mesh sizes as well as the time steps were considered to find the optimum situation to make a balance between the needed computational resources and the desired accuracy according to the aims of simulations. For the computational grid used alongside the implemented adaptive time-stepping technique (Section (5.5.2)), different time step values ($0.1 \leq \Delta t \leq 10$ seconds) were used in this simulation to prevent numerical stability issues. Four days of simulations, as described in this paper, took about 20 h on the HPC Cloud-based virtual machine with 12 Intel processors at 2.7 GHz and 96 GB RAM (Collaborative Organisation for ICT in Dutch Higher Education and Research, 2015).

506469-L-sub01-bw-Abbasi
Processed on: 9-11-2016

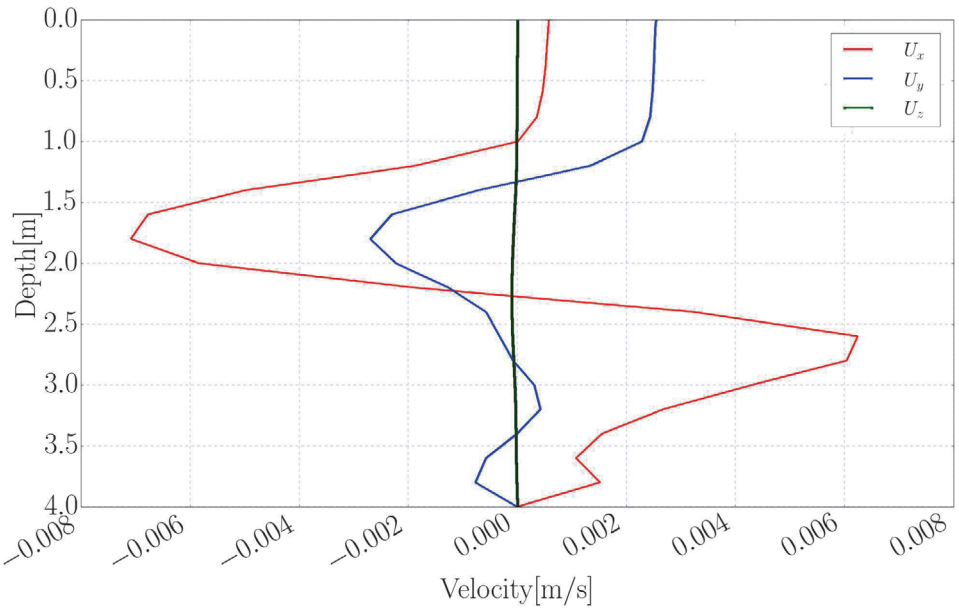


Figure 5.10: Simulated vertical distribution of velocity components in the water body where U_2 = 0.7 ms^{-1}.

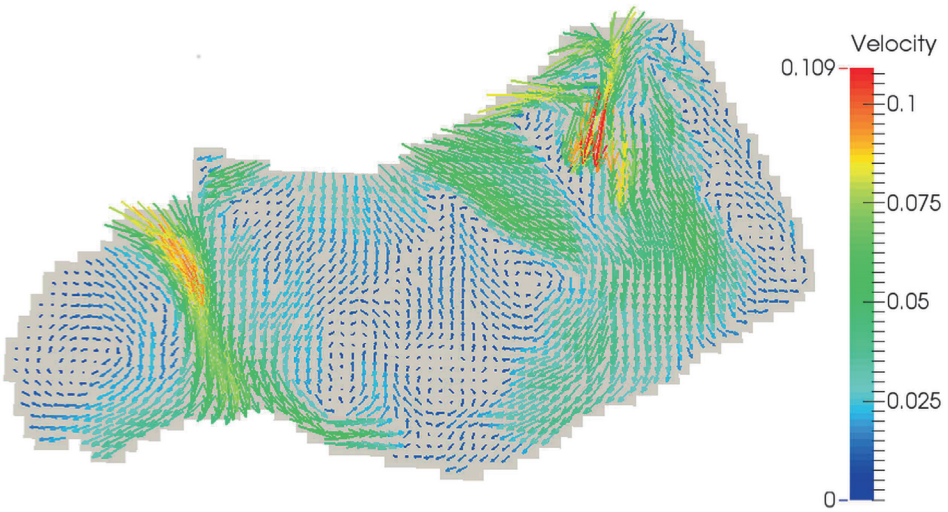


Figure 5.11: Simulated velocity field (stream lines) at 1 m beneath the water surface at t = 9:00 a.m. where $U_2 = 3.8\,ms^{-1}$.

506469-L-sub01-bw-Abbasi
Processed on: 9-11-2016

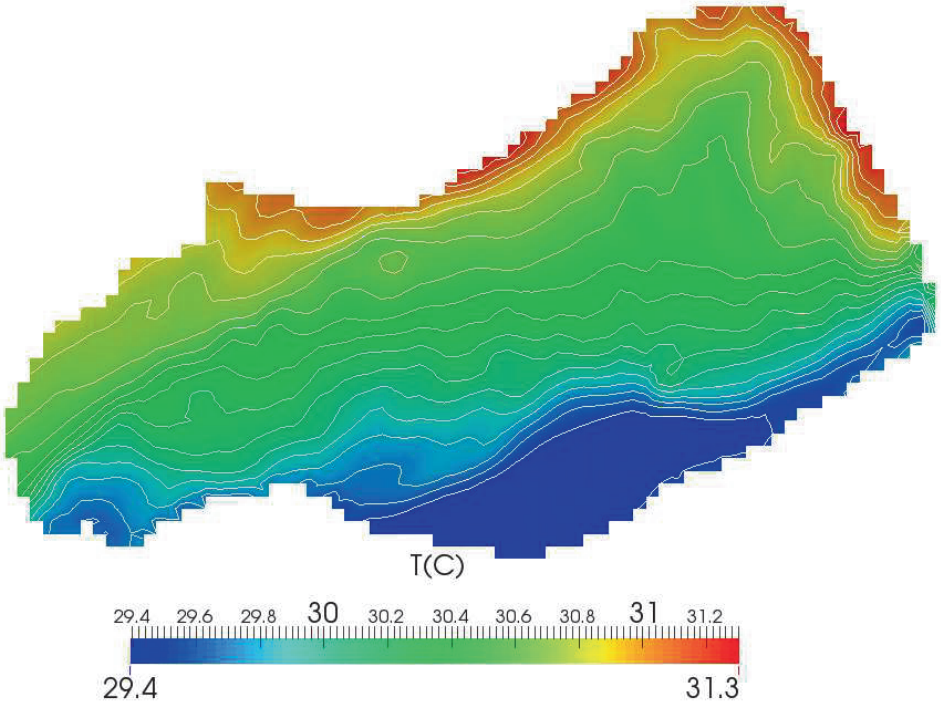


Figure 5.12: Simulated temperature field (values and contours) at 1 m beneath the water surface at t = 1:00 p.m.

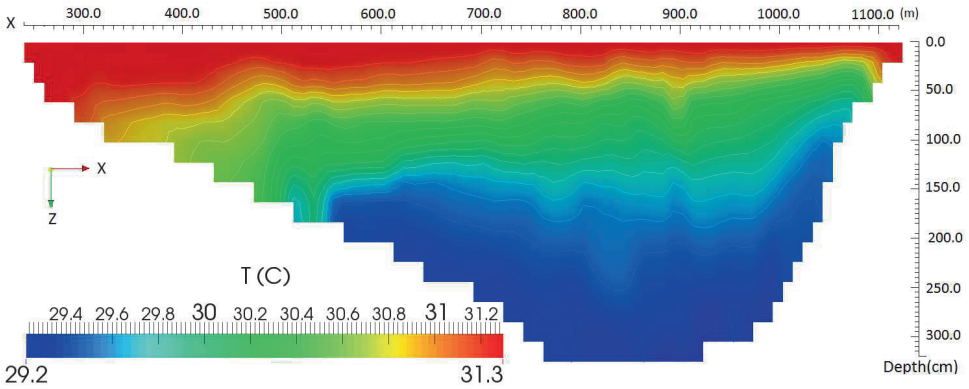


Figure 5.13: Simulated temperature field (values and contours) in a vertical section of the lake shown as line A-A in Figure 5.7 at t = 1:00 p.m. (vertical exaggerated by 100).

5.8. CONCLUSION

The temperature profile in a shallow and small lake in a semi-arid region was simulated. The main aim of the simulation was to find how the flow field and temperature distribution vary spatially and temporally in the shallow inland water body. As the flow in the water body is fully 3-D and turbulent, the full 3-D modified equations of the flow considering the temperature in the water body were solved by a CFD approach using OpenFOAM. The results for Lake Binaba show that the model overestimates the temperature distribution in the water body. This could be related to using boundary conditions with a high degree of uncertainties. The accuracy of the model mainly depends on the error in input meteorological parameters. The profile temperatures and flow pattern in water bodies have been found to have strong correlations with the air temperature, incoming short-wave radiation and wind velocity over the water surface. The effects of other meteorological parameters were considered implicitly in the heat fluxes over the water surface as boundary conditions. One of the big challenges in modeling very shallow lakes is implementing heat fluxes over the water surface accurately especially for the latent heat flux (evaporative heat flux).

According to the results, the lake model could be improved in the following ways: (1) improving the temperature boundary condition on the bottom and sides of the lake by considering heat fluxes through the sediments; (2) improving the methods to estimate heat fluxes over the water surface as temperature boundary condition; (3) considering the effects of the reflected penetrated short-wave radiation in the water body as an extra source term in the lake; and (4) an optimization method to find the optimized number of cells and the regions that should be refined in the lake.

The developed approach could be used for water quality, biological and environmental simulations of shallow water bodies as well.

506469-L-sub01-bw-Abbasi
Processed on: 9-11-2016

6

SMALL WATER SURFACES AND ATMOSPHERIC BOUNDARY LAYER INTERACTIONS

6.1. INTRODUCTION

In the regional hydrological cycle, small water bodies represent a significant part of the water budget. However, in most of the current mesoscale and global atmospheric models, the influences of small inland water bodies in the surface parametrization are neglected (Swayne et al., 2005). The most important issue of inland water bodies is the lake-atmosphere exchange process which should be considered through water surface fluxes such as momentum, heat convection and evaporation of water (Vercauteren, 2011). In comparison to land surfaces, inland water surfaces such as small lakes and reservoirs have different interactions with the atmospheric boundary layer above them with regards to evaporation, wind speed and heat exchanges over the water surfaces (Swayne et al., 2005). However, implementing these effects in Atmospheric Boundary Layer (ABL) models introduces extra complexities in the ABL simulations especially, in regions with huge numbers of small water surfaces. One complexity of the water-atmosphere interaction in regional climate model comes from the fact that the presence of lakes has significant effects on the atmosphere dynamics due to the change of roughness length, moisture contents and temperature of water versus that of land (Beniston, 1986). The distribution of the sensible and latent heat fluxes can affect the flow on small, regional and global scales (Giorgi and Avissar, 1997; Avissar and Pielke, 1989; Gao et al., 2008; Lyons and Halldin, 2004) where the exchanges of water vapor, heat and momentum over grid cells should be improved for water surface (Pielke and Uliasz, 1998; Wu et al., 2009).

This chapter is based on Abbasi et al. (2015c): Abbasi, A.; Annor, F.O.; van de Giesen, N.: The Effects of Small Water Surfaces on Turbulent Flow in the Atmospheric Boundary Layer: URANS Approach Implemented in OpenFOAM. Environmental Modelling & Software (Manuscript submitted for publication), 2015.

506469-L-sub01-bw-Abbasi
Processed on: 9-11-2016

Understanding and modelling the correlation of the atmospheric boundary layer with its underlying water surface is crucial for a wide range of scientific research such as developing inland water surface evaporation models, atmosphere simulations, and investigating the climate change influences on inland water bodies (Edson et al., 2007; Parlange et al., 1995). Due to the logistical difficulties and economic issues in operating measurements over water surfaces especially for small reservoirs, water-atmosphere interaction commonly has been studied less than land-atmosphere interaction (DeCosmo et al., 1996; Heikinheimo et al., 1999; Sun et al., 2001; Vickers and Mahrt, 2010).

The effect of roughness changes on the atmospheric boundary layer flow has been studied extensively by several researchers, especially in micro-meteorology. Some of these research examined the air flow and flux exchange in ABL by using theoretical analyses (e.g. Bradley (1968); Jackson (1976); Petersen and Taylor (1973); Raupach et al. (1980, 1996)) and some of them used field measurements or wind tunnel studies (e.g. Cao and Tamura (2006); Nadeau et al. (2011); Rider et al. (1964); Dyer and Crawford (1965); Davenport and Hudson (1967); Lang et al. (1974, 1983); Lettau and Zabransky (1968); Panofsky and Townsend (1964); Panofsky and Petersen (1972); Petersen and Taylor (1973); Munro and Oke (1975); Figuerola and Berliner (2005)) to understand the problem of sharp changes in the roughness length. However, measurements of spatial variations in the ABL are challenging and require the use of several pieces of equipment (Mahrt et al., 1994). Most of these research mainly focused on momentum and heat exchange above land.

Previous research works investigated airflow over heterogeneous surfaces such as complex terrains and rural and urban type environments which consist of different surfaces. Vercauteren (2011) investigated the lake-atmosphere process by using the Lake-Atmosphere Turbulent EXchange (LATEX) field measurement over Lake Geneva. Pendergrass and Arya (1984) simulated the effects of sharp roughness changes of rural and urban type surfaces on the development of the Internal Boundary Layer (IBL) under a neutral condition. Fesquet et al. (2009) investigated the influences of different atmospheric stability conditions and fetch effects on ABL turbulent airflow over heterogeneous terrains. They showed that the local turbulence variables such as momentum fluxes are significantly affected by the land surface complexity (Fesquet et al., 2009). By using a three-dimensional Large Eddy Simulation (LES) model, Fesquet et al. (2009) studied the effects of surface inhomogeneities on the ABL flow structure.

A big challenge in simulations of atmospheric boundary layer over the heterogeneous surfaces (for instance a surface consists of land and water surface) is that there are sharp changes of the surfaces' properties from land to water surface and vice versa. In addition, small inland water bodies usually have a limited fetch and dependent on the fetch values, the airflow over the lakes has time or not to adjust to its underlying water surface. In these cases, the horizontal inhomogeneity can be very important and the effect of this limited fetch still needs to be assessed (Vercauteren, 2011; Brutsaert, 1982). Such strong spatial differences in surface characteristics (temperature, wetness and the roughness) affect the airflow and transfer processes of heat and water vapor, specifically the evaporation rates. In response to these changes, an internal boundary layer develops that characterizes the region influenced by the wet surface.

Following rapid changes in surface properties from land to water or vice versa down-

wind of the step change location, an Internal Boundary Layer (IBL) develops which is strongly dependent on the surface below. In this situation, only the lowest parts of the atmosphere may be affected by the underlying surface conditions and the flow structure in higher levels is usually mainly dependent on the upwind surface conditions (Pendergrass and Arya, 1984).

Measuring airflow parameters on the water surface usually is costly and time consuming. Hence, due to the lack of measurements over the water surface, especially for small and shallow lakes (which are rarely available or usually confined to a single point), modelling the atmospheric boundary layer (ABL) flow would be promising for spatial information of air flow passing from different surfaces. Computational Fluid Dynamics (CFD) simulations help to understand the interactions of inland water bodies with the surrounding atmosphere. CFD as a robust tool can provide the temporal and spatial distribution of airflow parameters in the computational domain, which is difficult to achieve using experimental measurements, to investigate the effects of the water surfaces on the above atmosphere.

The atmospheric boundary layer flow is usually turbulent and fully developed. Studying the turbulent flow in ABL alongside the size of atmospheric domains is an ongoing challenge to simulate realistic atmospheric flows. To simulate the turbulent flow dynamics in the lower atmosphere, the Reynolds Averaged Navier Stokes (RANS) approach has been widely utilized (e.g. Solazzo et al. (2009); Majdoubi et al. (2009); Milashuk and Crane (2011); Anagnostopoulos and Bergeles (1998); Foudhil et al. (2005); Pattanapol et al. (2008); Luna et al. (2003); Liu et al. (1996); Prospathopoulos et al. (2012); Hsieh et al. (2007); Huser et al. (1997)). Although, recently due to the significant growth in computing tools and consequently decreasing the simulation cost, more accurate methods with more computational needs, such as Large Eddy Simulation (LES) is becoming more applicable in ABL studies (e.g. Benjamin Martinez (2011); Flores et al. (2013); Beyers et al. (2010); Hertwig et al. (2011); Chamecki et al. (2008); Albertson and Parlange (1999); Porté-Agel et al. (2014); Cancelli et al. (2014); Porté-Agel et al. (2011); Maronga et al. (2013); Esau and Lyons (2002); Bou-Zeid et al. (2004); Vercauteren et al. (2008)). The water surface and land fluxes of momentum, heat and water vapor determine the state of the atmosphere to a large extent. Their accurate parametrization has been recognized as a big challenge to make CFD a more reliable tool for simulation of airflow over the heterogeneous surfaces which include small water surfaces (Cabot and Moin, 1999; Piomelli and Balaras, 2002; Piomelli, 2008). A review of numerical studies of flow over wet surfaces can be found for example in Crosman and Horel (2010).

Considering the dimensions of the computational domain, the global and mesoscale models of atmospheric flow are not applicable to study the small waters effects on airflow because of the hydrostatic pressure assumption and their inabilities in resolving the variations in topography in vertical direction and consequently roughness variations in the simulation (Kim et al., 2000). Fully 2-D and 3-D atmosphere models can be used to provide reliable predictions considering various conditions to investigate the airflow in the ABL. Although, adding the third dimension to the model, usually makes the model more complex and expensive due to the high computational requirements, these three-dimensional models provide accurate airflow predictions over the complex terrain which is not possible with one- or two-dimensional simulations (Joubert et al., 2012).

506469-L-sub01-bw-Abbasi
Processed on: 9-11-2016

In the present research, the state of the airflow in the atmosphere as it passes from a dry land surface to a wet (water) surface is considered. The effect of a surface transition and sharp changes in surfaces properties (such as roughness length, wetness and temperature) on the flow are investigated. In addition, the atmospheric stability conditions are considered in the simulation to study the effect of stability conditions on the airflow over a non-homogeneous surface. The RANS approach is used to study the airflow and heat fluxes above a small inland water surface surrounded by arid lands.

6.2. MODEL STRUCTURE

In atmospheric boundary layer (ABL), the flow is represented by the conservation laws of mass, momentum and energy. Combining the airflow and heat transfer in the ABL introduces extra complexities to the simulation. Even though the thermodynamic properties of air are assumed to be constant, the buoyancy body force term in the momentum equation is added allowing one to relate density changes to temperature in ABL. In the model developed in this study, it is assumed that the ABL airflow is incompressible and fully three-dimensional.

The RANS approach has been applied to simulate the ABL flow due to its computational feasibility. Although, using other approaches such as Direct Numerical Simulation (DNS) or Large Eddy Simulation (LES) methods would generate more precise results, they are not applicable in most of ABL airflow modelling because applying these approaches for real-life complex geometries needs a very fine computational grid and consequently, high computational resources (Wakes et al., 2010). Based on the turbulence model used, the numerical scheme, and the discretization technique, wide range of RANS models with different complexity levels have been developed in ABL modeling. In using the RANS approach to resolve the turbulence of the airflow, some (zero, one, two or even more) additional equations must be solved alongside the flow equations (Prospathopoulos et al., 2012; Tsanis, 2006; Tritton, 2007).

The different phases of the ABL modelling framework developed in this study is illustrated in Figure 6.1.

6.2.1. GOVERNING EQUATIONS

The Navier Stokes equations, as a widely used approach, are solved to model the airflow, heat (temperature) and water vapor (specific humidity) transfer over the inland water surface and its surrounding lands. With the assumption of the pressure work being negligible, the following conservation equations can be derived for mass, momentum and energy respectively (Defraeye et al., 2012; Ferziger and Perić, 2002; White, 1991; Massel, 1999; Zhang et al., 2005):

$$\frac{\partial u_i}{\partial x_i} = 0 \tag{6.1}$$

$$\frac{\partial u_i}{\partial t} + \frac{\partial}{\partial x_j}(u_j u_i) - \frac{\partial}{\partial x_j}\left\{\nu_{eff}\left[\left(\frac{\partial u_i}{\partial x_j} + \frac{\partial u_j}{\partial x_i}\right) - \frac{2}{3}\left(\frac{\partial u_k}{\partial x_k}\right)\delta_{ij}\right]\right\} = -\frac{1}{\rho_k}\frac{\partial p}{\partial x_i} + g_i\left[1 - \beta\left(T - T_{ref}\right)\right] \tag{6.2}$$

506469-L-sub01-bw-Abbasi
Processed on: 9-11-2016

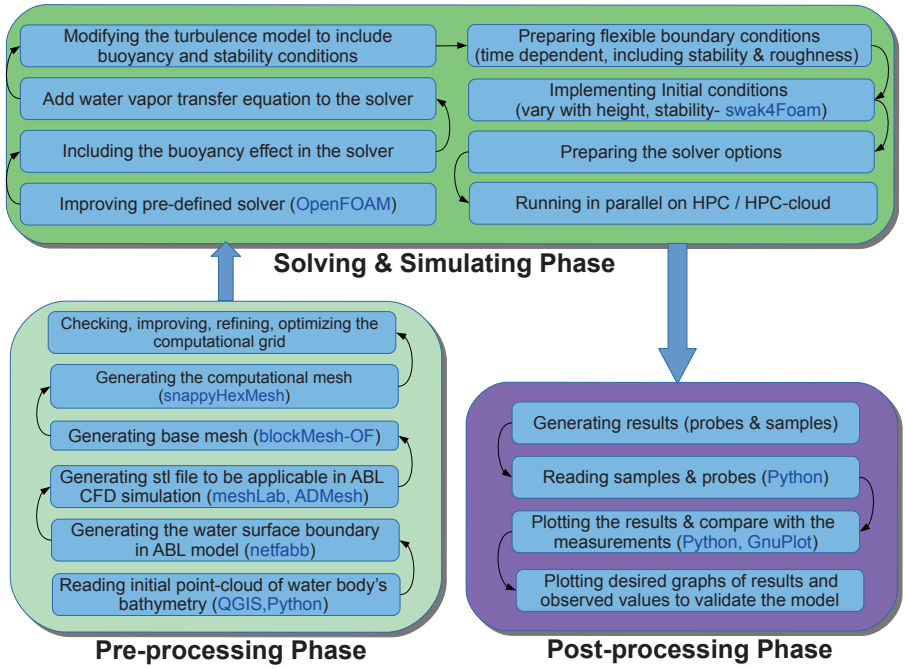


Figure 6.1: General framework of ABL simulation used in this study.

$$\frac{\partial T}{\partial t} + \frac{\partial}{\partial x_i}(Tu_i) - \alpha_{eff}\frac{\partial}{\partial x_k}(\frac{\partial T}{\partial x_k}) = 0 \tag{6.3}$$

$$\frac{\partial q}{\partial t} + \frac{\partial}{\partial x_i}(qu_i) - \chi_{eff}\frac{\partial}{\partial x_k}(\frac{\partial q}{\partial x_k}) = 0 \tag{6.4}$$

where u_i is the velocity component in x_i direction (ms^{-1}), p is pressure (Pa), T is temperature (K), q is specific humidity ($g\,kg^{-1}$), $\nu_{eff} = \nu_0 + \nu_t$ is the effective kinematic viscosity ($m^2 s^{-1}$), with ν_0 and ν_t denoting molecular and turbulent viscosity, respectively, g_i the gravity acceleration components (ms^{-2}), T_{ref} reference temperature (= 293.15 K), β the coefficient of expansion with temperature of the air ($Jkg^{-1}K^{-1}$) and δ is the delta of Kronecker (dimensionless), $\alpha_{eff} = \alpha_0 + \alpha_t$ is effective heat transfer conductivity ($m^2 s^{-1}$), with α_0 and α_t denoting molecular and turbulent thermal conductivity of air, respectively, ρ_k is the effective (driving) kinematic density (dimensionless) and χ_{eff} effective water vapor transfer coefficient (in this study it is assumed that $\chi_{eff} = \alpha_{eff}$). The Boussinesq approximation is valid under the assumption that density differences are sufficiently small (as this study) to be neglected, except where they appear in the term multiplied by g_i (Fredriksson, 2011; Corzo et al., 2011). According to White (1991) and Ferziger and Perić (2002), the Boussinesq approximation introduces errors less than 1% for temperature variations of 15 K for air. In the model developed here, for incompressible flows the density of air is calculated as a linear function of temperature changes

506469-L-sub01-bw-Abbasi
Processed on: 9-11-2016

as

$$\rho = \rho_k \times \rho_0 \tag{6.5}$$
$$\rho_k = 1 - \beta\left(T - T_{ref}\right) \tag{6.6}$$
$$\beta = -\left(\frac{1}{\rho_0}\right)\frac{\partial \rho}{\partial T} \tag{6.7}$$

In the current model, a constant value for β (it is assumed air is an ideal gas) is used. Heat transfer conductivity in atmosphere can be given by:

$$\alpha_{eff} = \alpha_t + \alpha_0 = \frac{\nu_t}{Pr_t} + \frac{\nu_0}{Pr} \tag{6.8}$$

where Pr_t is turbulent Prandtl number and Pr is Prandtl number.

6.2.2. TURBULENCE MODEL FORMULATION

In ABL simulation, turbulence is not negligible and plays an important role (Crasto, 2007). Different turbulence models have been developed and applied in ABL simulations. The turbulence closures are applied in order to solve the Reynolds stresses and the scalar transport terms in the RANS approach. Investigation of different turbulence models used in RANS is beyond the aims of this study and the comprehensive study of the turbulence models can be found in Computational Fluid Dynamics books (e.g. Cebeci (2004); White (1991); Ferziger and Perić (2002), etc.).

Standard $k-\varepsilon$ (SKE) and realizable $k-\varepsilon$ (RKE) models are used widely in most of CFD simulations. These turbulence approaches due to the relatively low computational needs, are considered as promising turbulence models in wide-range of applications (Silvester et al., 2009). The semi-empirical standard model introduces two more transport equations for the turbulence kinetic energy (k) and the dissipation rate of kinetic energy (ε) in the flow equation system. Kim et al. (1997) and Kim and Patel (2000) showed that in comparison with other two-equation turbulence models, the $k-\varepsilon$ model requires less computational resources and can solve the airflow in ABL without loss of accuracy. Various two equation models (such as $k-\omega$) similar to the standard $k-\varepsilon$ model are available which need extra input parameters. In these models, the transport equation for k is derived mathematically while ε is based upon empirical definition (Silvester et al., 2009). According to Silvester et al. (2009), the standard $k-\varepsilon$ performs poorly for flows with steep pressure gradients and in cases with complex flows. The poor performance of $k-\varepsilon$ model mainly relates to imprecision in the ε equation (Hussein and El-Shishiny, 2009). However, the standard $k-\varepsilon$ model is mostly used for atmospheric boundary layer models. In simulating airflow alongside heat transfer in the regional atmosphere, it was found that the realizable $k-\varepsilon$ model is robust with reasonable accuracy and provides better results than the standard or other traditional $k-\varepsilon$ models (Shih et al., 1995; Wang, 2013; Joubert et al., 2012). In this turbulence model, the Reynolds stresses are limited by physical-based mathematical constraints (Rohdin and Moshfegh, 2007). In the RKE turbulence model, dissipation rate for fluctuation is approximated by the dynamic equation vorticity. In addition, the RKE is expected to accurately predict the flow variables and likely to enhance the stability of employed numerical schemes in ABL turbulent flow simulations

506469-L-sub01-bw-Abbasi
Processed on: 9-11-2016

(Shih et al., 1995). In the RKE model, the turbulence kinetic energy (k) and the turbulent dissipation rate (ε) are obtained from:

$$\begin{aligned}\frac{\partial k}{\partial t}+\frac{\partial}{\partial x_j}(k\,u_j) &= \frac{\partial}{\partial x_j}\left[\left(\frac{\nu_t}{\sigma_k}\right)\frac{\partial k}{\partial x_j}\right]+\nu_T\left(\frac{\partial u_i}{\partial x_j}+\frac{\partial u_j}{\partial x_i}\right)\frac{\partial u_i}{\partial x_j}-\varepsilon \\ &+ G_k+G_b \end{aligned} \tag{6.9}$$

$$\begin{aligned}\frac{\partial \varepsilon}{\partial t}+\frac{\partial}{\partial x_j}(\varepsilon\,u_j) &= \frac{\partial}{\partial x_j}\left(\frac{\nu_t}{\sigma_\varepsilon}\frac{\partial \varepsilon}{\partial x_j}\right)+C_1 S\varepsilon-C_{\varepsilon 2}\frac{\varepsilon^2}{k+\sqrt{\nu\varepsilon}} \\ &+ C_{\varepsilon 1}C_{\varepsilon 3}\frac{\varepsilon}{k}G_b \end{aligned} \tag{6.10}$$

where k is the turbulence kinetic energy, ε is the dissipation rate of turbulence kinetic energy, ν_0 and ν_t are molecular and turbulent viscosity respectively, G_b is the production of turbulent kinetic energy by the buoyancy, and G_k is the production of turbulent kinetic energy by the mean velocity gradient. The parameter $C_{\varepsilon 3}$ is the ratio of the velocity functions in the vertical and longitudinal directions and is not constant but instead depends on the flow conditions (Lee, 2007):

$$C_{\varepsilon 3}=\tanh\left|\frac{w}{U_h}\right| \tag{6.11}$$

where U_h and w are the components of the airflow velocity perpendicular and parallel to the gravitational vector, respectively. The coefficient C_1 is evaluated as (Shih et al., 1995):

$$C_1=max\left(0.43,\frac{\zeta}{\zeta+5}\right) \tag{6.12}$$

$$\zeta=S\frac{k}{\varepsilon} \tag{6.13}$$

$$S=\sqrt{2S_{ij}S_{ij}} \tag{6.14}$$

$$S_{ij}=\frac{1}{2}\left(\frac{\partial u_i}{\partial x_j}+\frac{\partial u_j}{\partial x_i}\right) \tag{6.15}$$

and the turbulent kinematic viscosity is given by

$$\nu_t=C_\mu\frac{k^2}{\varepsilon} \tag{6.16}$$

$$C_\mu=\frac{1}{A_0+A_s\dfrac{kU^*}{\varepsilon}} \tag{6.17}$$

$$U^*=\sqrt{S_{ij}S_{ij}+\overline{\Omega_{ij}}\,\overline{\Omega_{ij}}} \tag{6.18}$$

$$A_s=\sqrt{6}\cos\phi \tag{6.19}$$

$$\phi=\frac{1}{3}cos^{-1}(\sqrt{6}W) \tag{6.20}$$

$$W=\frac{S_{ij}S_{jk}S_{ki}}{\widetilde{S}^3} \tag{6.21}$$

$$\widetilde{S}=\sqrt{S_{ij}S_{ij}} \tag{6.22}$$

506469-L-sub01-bw-Abbasi
Processed on: 9-11-2016

$\overline{\Omega_{ij}}$ represents the mean rate-of-rotation tensor to capture rotational effects on the flow field. The production of turbulent kinetic energy by the mean velocity gradient (G_k) is written as:

$$G_k = \nu_t S^2 \tag{6.23}$$

In the current ABL airflow modelling, due to the existence of temperature gradient alongside the non-zero gravity field, the production of turbulent kinetic energy by the buoyancy is included in the k and ε equations (G_b in Equation (6.9) and Equation (6.10)). The generation of turbulence due to buoyancy is given by

$$G_b = \beta g_i \frac{\nu_t}{Pr_t}\left[\left(\frac{\partial T}{\partial x_i} - \frac{g_i}{C_p}\right)\right] \tag{6.24}$$

where Pr_t is the turbulent Prandtl number (a dimensionless number defined as the ratio of momentum diffusivity to thermal diffusivity where controls the relative thickness of the momentum and thermal boundary layers). For standard and realizable $k-\varepsilon$ models, default value of Pr_t for air is 0.71 (Fluent, 2006). g_i is gravitational vector components, C_p is specific heat of air and T is (air) temperature. In unstable atmospheric conditions $G_b > 0$ and according to k equation (Equation (6.9)) the turbulence kinetic energy tends to be increased. In contrast to the unstable conditions, for stable stratification in ABL where $G_b < 0$, buoyancy force disrupts the turbulence intensity. To investigate the influence of atmospheric stability conditions on the airflow in ABL, the buoyancy terms in the k and ε should be implemented in turbulence model. While the process of generation of turbulence due to buoyancy on turbulent kinetic energy (k) is relatively clear, the effect of buoyancy on the dissipation rate of kinetic energy (ε) is less understood (Fluent, 2006). In the current model, the buoyancy effects on both k and ε are included in turbulence model given by Equation (6.24). To take into account the buoyancy effects on ε, the non-constant parameter $C_{\varepsilon 3}$ is used as defined in Equation (6.11).

Exploring a wide-range of turbulent flow experiments (e.g. Shih et al. (1995) and Pieterse (2013)), values of the model constants of the realizable turbulence approach in the Equation (6.9) and (6.10) are:

$$C_{\varepsilon 1} = 1.176; \quad C_{\varepsilon 2} = 1.92; \quad \sigma_k = 1.0; \quad \sigma_\varepsilon = 1.3; \quad A_0 = 4.0 \tag{6.25}$$

6.3. ATMOSPHERIC STABILITY CONDITION

The turbulent airflow in ABL is strongly influenced by the atmospheric stability conditions (Garratt, 1994). Some attempts have been made to take into consideration the stability effects in simulating the turbulent ABL (Alinot and Masson, 2005; Huser et al., 1997; Meissner et al., 2009; Pontiggia et al., 2009). In non-neutral conditions, the applied turbulence model should account for both shear and buoyancy produced turbulence terms. To consider the effects of atmospheric stability conditions in the ABL flow, the conservation of energy (or temperature), is included in the governing equations and coupled with the momentum equation. The buoyancy forces are taken into consideration using the Boussinesq approximation for buoyancy, and density variations are introduced only into the gravity terms of the momentum equations (Alinot and Masson, 2005; Meissner et al., 2009; Pontiggia et al., 2009). Additionally to buoyancy forces, thermal stratification in ABL has a significant impact on the turbulence characteristics. Therefore, the

506469-L-sub01-bw-Abbasi
Processed on: 9-11-2016

turbulence model has to be modified to take into account the generation and destruction of turbulence due to buoyancy. This is typically done via buoyancy term in k and ε equations. For determining the buoyancy related term in turbulence equations different approaches exist in the literature, and their formulations differ greatly (Huser et al., 1997; Sogachev et al., 2012; Vendel et al., 2010).

Generally, two different approaches can be applied for considering the atmospheric stability conditions in the ABL simulations. In the first approach, the stability conditions are implemented in the vertical profiles of temperature and other parameters at the inflow boundary (free stream stability approach). To prepare these vertical profiles at the inflow, the stability conditions should be prescribed. This method is applied in Section (6.6). In the second approach, the stability conditions are implemented in time and location varying surface (skin) temperature or time-dependent non-uniform heat fluxes on the surface (surface stability approach) (Koblitz et al., 2013). In comparison with heat fluxes, using (measured) temperature values on the surfaces is more straightforward and introduces less uncertainties in the simulations. Due to the transient nature of ABL flow, in both approaches the applied boundary conditions at the inflow and bottom boundaries are unsteady and vary with height and time (Section (6.5)).

6.3.1. SOLVER SPECIFICATIONS

Steady-state solvers have been applied in many ABL simulation cases to predict the mean flow characteristics (Prospathopoulos et al., 2012). However, in some cases such as the current study, the steady flow assumption is not strictly valid and would make large errors in the simulations, even in the micro-scale. Abrupt changes in the surface characteristics, time-dependent meteorological parameters, combining heat transfer with wind flow simulation, and unsteady (transient) boundary conditions especially over the water surface make it necessary to develop an unsteady solver to estimate flow parameters in this study.

The developed solver in the current study solves the governing equations in the model described in Section (6.2.1) alongside the turbulence model equations described in Section (6.2.2) using the described boundary and initial conditions (Section (6.5.1)). The ABL airflow equations are discretized using the Finite Volume Method (FVM) in open-source code `OpenFOAM`. The `OpenFOAM` (Open Source Field Operation and Manipulation) toolbox includes open source `C++` libraries released under the general public license (GPL). Using pre-configured built-in libraries, one can build his own numerical solvers for solving the desired ABL airflow problems (Chen et al., 2014). The pre-configured solvers were modified and used for the current study. Considering the buoyancy effects in turbulence equations is an example of modification in the standard available solvers and libraries.

Furthermore, and unlike most of the commercial codes now available (e.g. `ANSYS-FLUENT`, `FIDAP`, `PHOENICS`, `STAR-CD`, etc.), the pre-configured solvers and utilities in `OpenFOAM` could be extended to generate strictly customized tools and boundary conditions (BC). As `OpenFOAM` is available free and open-source, it would be a promising tool for research due to its adaptability to specific case studies. In addition, in contrast to the commercial CFD packages, using `OpenFOAM` does not need any expensive licenses neither for industrial or academic purposes (Benjamin et al., 2011). The free availabil-

506469-L-sub01-bw-Abbasi
Processed on: 9-11-2016

ity of this open source CFD software alongside its robustness could be a very attractive motivation to use it in developing countries (Balogh et al., 2012).

The developed OpenFOAM-based incompressible solver in the current context computes the airflow variables in the atmospheric boundary layer over a non-homogeneous surface. The presented solver has been built on the built-in solver in OpenFOAM called buoyantBoussinesqPimpleFoam, and some corrections, improvements and additions have been done to adapt it to the specific case study. This unsteady finite volume solver was used in this study to simulate airflow and heat transfer in the atmospheric boundary layer.

SOLVING ALGORITHM

One of the main advantages of OpenFOAM is that allows one to employ desired specific solver for each of the governing equations. According to the results of some similar simulations, throughout this work, the Euler blended Crank-Nicholson method was used to discretize the temporal term. This is a first-order, bounded implicit method and the SmoothSolver for the momentum, k, ε, T and q equations is used with a GaussSeidel smoother (Gauss refers to the standard finite volume discretization of Gaussian integration). For solving the pressure equation, the GAMG (Geometric-algebraic multi-grid) solver is employed. Multi-grid solvers (such as GAMG) decrease the computational time and show appropriate performance in problems of airflow over the complex terrains. This solver is specially convenient and fast in highly dense domains. It first generates a quick solution on a coarser mesh (with a small number of cells) and then maps the resolved field data onto a finer mesh to obtain an accurate solution. Regarding the spatial discretization, gradient terms were solved by the 2^{nd} order linear interpolation (Gaussian), divergence terms were solved by the 2^{nd} order upwind interpolation (Gaussian) and Laplacian terms were solved by the 2^{nd} order linear interpolation with explicit non-orthogonal corrections. To improve the stability of the computations, the relaxation parameters (which limit the variable changes from one iteration to the next iteration) are set to 0.3 for pressure and 0.5 for the other variables.

The PIMPLE method was employed for pressure-velocity coupling. PIMPLE algorithm combines the PISO (pressure implicit with splitting of operators) and SIMPLE (semi-implicit method for pressure-linked equations) algorithms to rectify the second pressure correction and correct both velocity and pressure explicitly. This algorithm allows one to use larger time steps than the PISO algorithm. Due to the transient conditions of flow in the ABL, an adaptive time-stepping technique based on Courant-Friedrick-Levy-number (CFL-number) is used (Bechmann, 2006):

$$CFL = \Delta t_{max}\left(\frac{|u|}{\Delta x}, \frac{|v|}{\Delta y}, \frac{|w|}{\Delta z}\right) \leq 1 \tag{6.26}$$

where CFL is Cournat-Friedrick-Levy-number, u, v and w are the velocity components in $x-$, $y-$ and $z-$directions respectively. In this study, the maximum value of global CFL is adopted to 0.5. For larger time steps, numerical dissipation increases as the CFL-number increases and the model will be more unstable (Wang, 2013; Ferziger and Perić, 2002).

The problems that arise in solving these equations are memory related issues and also the run time (to obtain a solution) when running the model. As stated earlier on,

506469-L-sub01-bw-Abbasi
Processed on: 9-11-2016

the core of the model is based on `OpenFOAM` and, therefore the framework offers parallelization features. Hence, the model can be decomposed and ran on a relatively large number of processors, either on supercomputers or HPC clouds to reduce the simulation time.

6.4. COMPUTATIONAL DOMAIN

Computational domain is extended 3500 m in $x-$direction, 1850 m in $y-$direction and more than 500 m upwards ($z-$direction) in order to allow the flow to settle and avoid interaction between boundary conditions and the developing flow (Joubert et al., 2012; Prospathopoulos and Voutsinas, 2006; Vinnichenko et al., 2011). As shown in Figure 6.2, the extension of the computational domain downwind of the water body is larger than the upwind distance to minimize the effects of outflow boundary on the airflow. The shape of the water surface is the primary input for building the computational domain in the current simulation. The water surface shape, though relatively small, induces complex 3D flow in ABL. During the simulation time (one day), changes of the water level with an average value of 0.006 m were ignored and a constant level was assumed for the water surface. The water surface shape was generated from the roughly measured bathymetry using the approach proposed by Abbasi et al. (2015a).

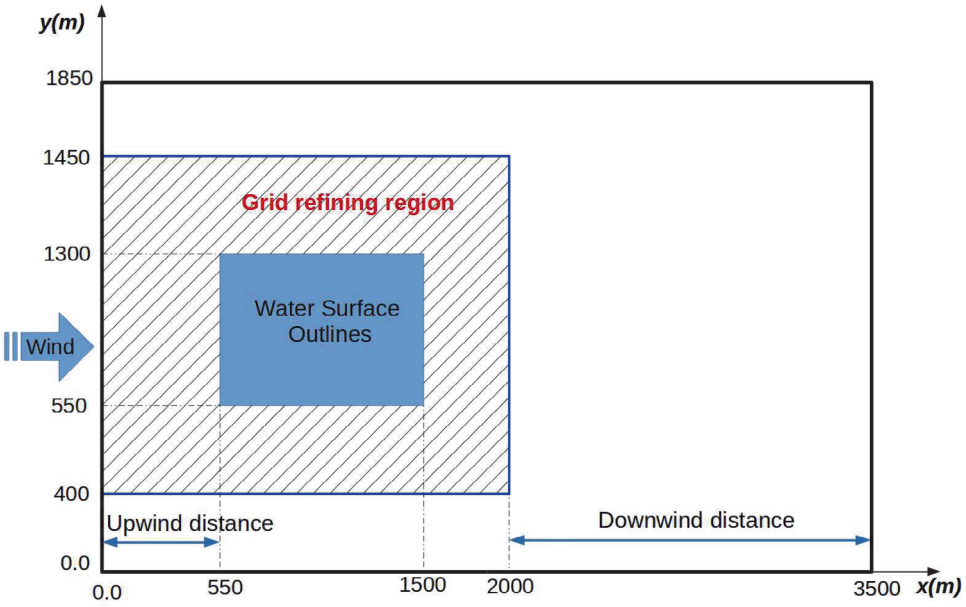


Figure 6.2: Plan view of computational domain, water surface outlines and grid refining region.

6.4.1. MESH GENERATION

Generating and applying a good computational grid is a very important step in performing reliable CFD simulations especially in complex terrains. Generally, in ABL simu-

506469-L-sub01-bw-Abbasi
Processed on: 9-11-2016

lations, grid generation remains a significant challenge for CFD simulations. Using a computational grid with highly skewed, non-orthogonal differential cells will produce significant errors in solving the governing equations. Indeed, meshing complex terrains is not straightforward and is very case-sensitive especially for heterogeneous surfaces with sharp changes in their properties. The generated mesh must accurately represent the shape of the water surface and its surrounding terrain. To improve the generated computational grid, concentration of grid points near the lake's boundary and near the bottom boundary (wall) are more clustered to cover the sharp changes in surface properties. Refining the computational mesh only at specific regions can reduce significantly the computational cost (Prospathopoulos et al., 2012). In addition, refining the grid at regions with abrupt changes in surface characteristics increases the representation accuracy of the terrain and the predictions accuracy as well. The quality of the mesh which, in turns, have a clear impact on the accuracy of any CFD simulations (Rhoads, 2014) and affects significantly the convergence speed and the accuracy of the modelling.

The proposed framework uses a right hand coordinate system (typically used in simulations), with the $z-$axis positive in the upward direction (normal to the water surface). The origin is located in the lower left-hand corner of the mesh when viewed in the $xy-$plane. Keeping with this convention in the model, the $x-$axis is aligned to be positive in the easterly direction, with the $y-$axis positive in the northerly direction. Horizontal grids are generated by following the geometrical boundaries (water surface and land) available in the computational domain. For the vertical direction the grid points are clustered near the water surface and at the location of abrupt changes to resolve the turbulent flow field and capture flow parameters such as temperature and shear stress distributions in the most dynamic zones. Figure 6.3 shows the generated grid's details. The vertical grids near the lower surface should be sufficiently fine to be able to capture the large thermal and velocity gradients present in this region.

In this work, the computational grid was generated with `snappyHexMesh` (`sHM`) utility available in `OpenFOAM`. `sHM` as a powerful script-driven tool, which generates unstructured mesh containing hexahedra and split-hexahedra cells (Brockhaus, 2011). `snappyHexMesh` proved to be very flexible with different domain configurations. `sHM` allows to use `STL` (STereoLithography / Standard Triangle Language) files which represent the small water surfaces in complex heterogeneous surfaces. Although using unstructured meshes allows for local mesh refinement and facilitates the transition between regions with different mesh densities, they are more costly than structured meshes. Unstructured meshes are being used widely in ABL simulations due to their flexibility and the adaptation capability (Kim and Boysan, 1999). The final mesh used in this simulation consists primarily of hexahedral cells (1144900 cells) with some polyhedral cells (17268 cells). The choice of mesh size is based on the available computational resources and the resolution required to get accurate results as well. This mesh should be refined sufficiently near the bottom boundary (Abbasi et al., 2015a). The final computational grid is shown in Figure 6.4. In the current simulation, the effect of the roughness of surfaces is applied by using wall functions which introduce some restrictions on the minimum height of the first cell above the bottom surface. This requires the first cell center adjacent to the wall should not be smaller than the roughness height (it means it should be placed within the logarithmic region of the boundary layer) (Joubert et al., 2012; Wakes

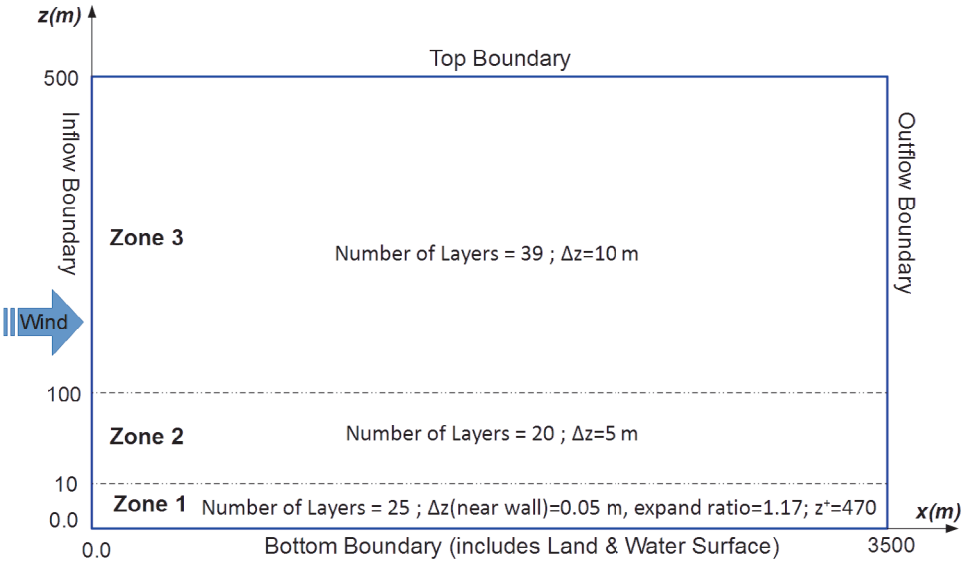


Figure 6.3: Defined different zones in height ($z-$direction) to generate computational grid. Properties of generated mesh in each zone are presented.

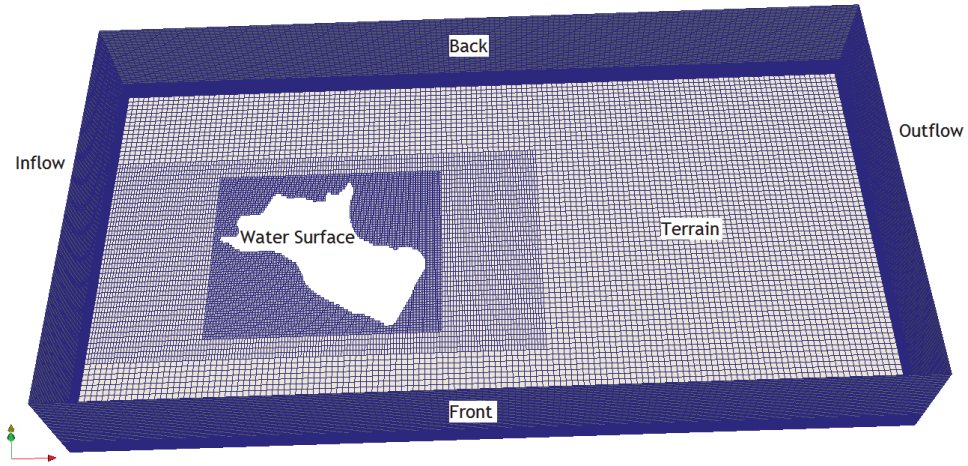


Figure 6.4: Computational grid and boundaries of model. Top boundary and water surface are not shown to make a better view.

et al., 2010). According to the roughness lengths of the bottom surfaces (land and water surface) the height of the first cells near the wall could be very large (a cell size of 3.5 and 0.25 m should be chosen for the cells adjacent to the land and water surface respectively) and with this cell size, there would be big errors in simulations. To conquer this

problem, the first cell is placed on top of the roughness elements and the boundary conditions will be modified. Displacing the first model level by z_0 (where z_0 is the surface roughness length) has the advantage that in the case of large roughness changes (e.g. land) there are no minimum height restrictions for the first cells (Koblitz et al., 2013).

6.5. INITIAL AND BOUNDARY CONDITIONS

6.5.1. INITIAL CONDITIONS

The initial conditions have no effect on the results of the simulations, however, it is strictly suggested to assign real initial conditions in the model. Implementing correct initial conditions in the model could be useful in converging the simulations and reduce the simulation time specially for first time steps. As in most cases, often there is no sufficient data to generate the initial distribution of airflow parameters, therefore the vertical profiles in the inflow at the start time of simulation (at $t = 0$) are applied throughout the entire domain as initial condition (Section (6.6)). Implementing the initial condition (simple or complex) is done by `funkySetField` tool available in `swak4Foam` libraries, which are `python`-based functions applicable alongside `OpenFOAM`. To prevent the numerical instabilities, for turbulence parameters, it is suggested to impose a weak initial turbulence level (a non-zero turbulence condition) in ABL simulations (Verdier-Bonnet et al., 1999).

6.5.2. BOUNDARY CONDITIONS

As shown in Figure 6.4, the modelled computational domain has seven defined physical boundaries: Inflow boundary as the upwind boundary; Outflow as the downwind boundary; two boundaries parallel to the wind direction (Back and Front); two walls to represent the water surface (Water Surface) and the surrounding terrain (Terrain); and the Top boundary as the vertical extension of the domain.

INFLOW BOUNDARY

As the available measurements in most ABL studies are not sufficient to determine the velocity field at the inflow boundary of the computational domain, assuming neutral atmospheric conditions, the logarithmic law is used for the vertical distribution of the inflow velocity. The vertical profiles should represent the characteristics of upstream terrain (Blocken et al., 2007; Prospathopoulos and Voutsinas, 2006). The implementation of the logarithmic velocity profile in this region where the inflow and bottom boundary meet would improve the stability of simulation. Inflow boundary conditions for u_i, k and ε respectively are given by the following equations (Blocken et al., 2007; Joubert et al., 2012; Yang et al., 2009):

$$u = \frac{u_*}{\kappa} \ln\left(\frac{z+z_0}{z_0}\right); \qquad v = 0; \qquad w = 0 \tag{6.27}$$

$$k = \frac{u_*^2}{\sqrt{C_\mu}} \sqrt{C_1' \times \ln\left(\frac{z+z_0}{z_0}\right) + C_2'} \tag{6.28}$$

$$\varepsilon = \frac{u_*^3}{\kappa(z+z_0)} \sqrt{C_1' \times \ln\left(\frac{z+z_0}{z_0}\right) + C_2'} \tag{6.29}$$

where u_* is the friction velocity $[ms^{-1}]$ given by:

$$u_* = \frac{u_{ref}\kappa}{ln\left(\frac{z_{ref}+z_0}{z_0}\right)} \tag{6.30}$$

where u , v and w are velocity components in $x-$, $y-$ and $z-$directions respectively, κ is the von Karman constant (≈ 0.4187), z_0 is the aerodynamic roughness length $[m]$, z is the vertical distance above the bottom surfaces $[m]$, C_1', C_2' and C_μ are constant where $C_1' = -0.01$, $C_2' = 1.23$ and $C_\mu = 0.033$ (ÓSullivan et al., 2011), and u_{ref} is the wind speed measured at the reference height (z_{ref}). In the described vertical profiles of the mean horizontal wind speed U, turbulent kinetic energy k and turbulent dissipation rate ε, it is assumed that the ABL is neutral condition (i.e. the turbulence originates from friction and shear forces and the effect of thermal stratification is ignored) (Yang et al., 2009). If the measurements of the atmospheric stability conditions are available, the profiles could be modified to take into account the real conditions at inflow boundary (Section (6.6)). In this study, the roughness length for terrain surrounding the water surface (lake) is assumed $z_0 = 0.13\,m$, which represents a land surface with sparse vegetation (Bagayoko et al., 2007).

TOP BOUNDARY

The top boundary is positioned high enough (about 500 m) above the top of the boundary layer and the no-flux condition can be imposed for the velocity field (Churchfield, 2013; Prospathopoulos and Voutsinas, 2006). Physically in this boundary condition, the velocity is tangential to the boundary:

$$u = U_\infty; \qquad v = w = 0; \qquad \frac{\partial k}{\partial z} = 0; \qquad \frac{\partial \varepsilon}{\partial z} = 0; \qquad \frac{\partial q}{\partial z} = 0; \qquad T = T_\infty \tag{6.31}$$

where u , v and w are velocity components in $x-$, $y-$ and $z-$directions respectively, U_∞ prescribing the value corresponding to the inflow velocity profile at the height of the top boundary , and T_∞ prescribing the value corresponding to the inflow temperature profile at the height of the top boundary. For other flow variables, it is assumed that the fluxes across the top of the domain are zero and hence a symmetry condition (no-gradient) is used.

OUTFLOW BOUNDARY

At outlet boundary, the flow that leaves the domain is typically not known before solving the flow. However, in most ABL simulations fully developed flow conditions (zero-normal gradient condition) are imposed on the outflow boundary which introduces errors (Benjamin et al., 2011; Hussein and El-Shishiny, 2009). As the flow in homogeneous ABL is not fully developed, this assumption introduces some errors in the flow parameters. To minimize the errors due to this assumption, the outflow boundary is placed far downstream of the area of interest (water surface) (Koblitz et al., 2013). The following conditions are assumed as boundary conditions at the outflow:

$$\frac{\partial u}{\partial x} = 0; \qquad \frac{\partial v}{\partial x} = 0; \qquad \frac{\partial w}{\partial x} = 0; \qquad \frac{\partial k}{\partial x} = 0; \qquad \frac{\partial \varepsilon}{\partial x} = 0; \qquad \frac{\partial q}{\partial x} = 0; \qquad \frac{\partial T}{\partial x} = 0 \tag{6.32}$$

506469-L-sub01-bw-Abbasi
Processed on: 9-11-2016

LATERAL BOUNDARIES

For the lateral boundaries (Back and Front) which are oriented parallel to the wind direction, slip boundary condition is imposed which represents the fully developed flow conditions on the lateral boundaries Prospathopoulos and Voutsinas (2006):

$$\frac{\partial u}{\partial z} = 0; \qquad v = 0; \qquad \frac{\partial w}{\partial z} = 0; \qquad \frac{\partial k}{\partial z} = 0; \qquad \frac{\partial \varepsilon}{\partial z} = 0; \qquad \frac{\partial q}{\partial z} = 0; \qquad \frac{\partial T}{\partial z} = 0 \tag{6.33}$$

As shown in Equation 6.33, slip boundary represents a zero-gradient condition for scalar parameters (such as k and ε) and for the tangential components of velocity vector (i.e. u and v) and defines fixed value (zero) for the normal component (i.e. w) of velocity.

BOTTOM BOUNDARY

In the desired computational domain, the bottom boundary encompasses two surfaces with different properties, land surface and water surface. Heterogeneous surfaces which contain different surfaces, make the airflow over the surface complex. Wind flow over the heterogeneous surfaces is strongly affected by the surfaces' roughness length. In order to simulate airflow over the water surface and its surrounding accurately, the boundary conditions for bottom surfaces must be correctly selected (Luna et al., 2003; Wakes et al., 2010). The lower boundary conditions (water and land surfaces) use wall functions. Using the wall functions, the airflow is not solved explicitly in the immediate vicinity of the bottom surface and the effects of surfaces on the airflow are modelled through wall function by using proper aerodynamic roughness length (z_0) values (Foudhil et al., 2005).

Using a wall function besides RANS method for the ABL has the limitation of inconsistency in the turbulence model, the fully developed inflow and the standard wall boundary conditions (Balogh et al., 2012). Generally, to solve this limitation, it is required that the vertical distance of the first cell's center point (z_p) of the wall-adjacent cell (bottom boundary) should be larger than the physical roughness height (k_s) of the surface (Blocken et al., 2007). It is therefore suggested that the position of the center point of the first cell near the wall should be larger than or at least equal to the physical roughness height ($z_p \gtrsim k_s$). Physically, It is not meaningful to have grid cells within the physical roughness height (Benjamin Martinez, 2011; Blocken et al., 2007).

The physical roughness height (k_s) is a function of the aerodynamic (momentum) roughness length (z_0) of the surface and can be computed as following Prospathopoulos and Voutsinas (2006):

$$k_s = \frac{E}{C_s} z_0 \tag{6.34}$$

where E represents the empirical constant (≈ 9.793) and C_s is the roughness constant which contains the type of roughness. Due to the lack of specific guidelines on determining the value of roughness constant, generally its default value for sand-grain roughened pipes and channels (≈ 0.5) is used (Blocken et al., 2007).

Using standard wall functions in one hand, requires a refinement of the mesh near the rough wall to capture the high gradients in flow parameters and in the other hand, introduces the constraint of placing the first computational node (at least k_s away from the wall). To solve this contradictory, the roughness height (z_0) is included in the vertical profiles of the inflow boundary conditions presented in Equation (6.27) through

506469-L-sub01-bw-Abbasi
Processed on: 9-11-2016

Equation (6.30). By employing these inflow boundary conditions, the first cell can be displaced on top of the roughness elements (z_0) and therefore, in the case of large roughness changes (e.g. water to land) there are no minimum height restrictions for the first cell (Koblitz et al., 2013).

Changes in surface roughness (from dry land to water surface) cause the local profiles of wind speed, temperature and turbulence to be out of equilibrium and make the flow fully three-dimensional and more complex than flow over a flat terrain. For the land surrounding the lake, by ignoring the changes of roughness with wind speed due to the low to moderate wind speed values (Prospathopoulos et al., 2012), and considering the type of crops around the water surface, the average roughness length assumed $z_0 = 0.13\,m$, which represents a land surface with sparse vegetation (Bagayoko et al., 2007). For the water surface, the roughness length was assumed $z_0 = 10^{-4}\,m$ which seems to be appropriate on this type of water surfaces with low to moderate wind speed (Vercauteren, 2011).

For temperature boundary condition over the bottom surface, the measured surfaces temperature (for both water and land surface) can be used directly (Dirichlet boundary condition), or the heat flux values as the cooling or warming forces can be specified (Neumann boundary condition). Changes in temperature of bottom surface might occur mainly due to the heat exchange across the bottom surface and air interface. Accurate estimation of heat fluxes is extremely important in the simulation of temperature dynamics over the ground (bottom) surface. In this study, both approaches for temperature boundary conditions stated above are used to compare the performance of the suggested boundary conditions. Obviously, using the Dirichlet boundary condition for temperature on the bottom surface has less uncertainties and could decrease the computational time. For the last approach and its details, especially over the water surface, the reader is referred to a paper currently submitted for publish (Abbasi et al., 2015a).

6.6. VALIDATION OF THE MODEL

The main aim of using numerical models in ABL simulations is to provide predictions that represent the real air flow field with a reasonable accuracy (Wakes et al., 2010). Generally, to validate a numerical simulation, accurate measured data from full-scale observations are necessary. In ABL modelling, because of the practical difficulties in taking full-scale measurements, these measurements are rare (Kim and Patel, 2000). In the current study, to validate the solver developed, turbulence models for different atmospheric stability conditions and the performance of implemented boundary and initial conditions, three models with different stability conditions according to Pieterse (2013) were selected. The details of the validated cases are summarized in Table 6.1. To validate the model using the pre-described parameters in Table 6.1, the computational mesh, initial conditions, and turbulence model equations were adopted from Pieterse (2013). As in these cases the stability parameters are known, the first approach (free stream stability approach) described in Section (6.3) was used to implement stability conditions in the simulations hence, the inlet profiles were modified as below:

$$u(z) = \frac{u_*}{\kappa}\left[\ln\left(\frac{z+z_0}{z_0}\right) - \Phi_m(\zeta)\right] \tag{6.35}$$

$$T(z) = \frac{T_*}{\kappa}\left[\ln\left(\frac{z+z_0}{z_0}\right) - \Phi_h(\zeta)\right] + T_0 - z\frac{g}{C_p} \tag{6.36}$$

where $\zeta = \frac{z}{L}$ is the stability parameter, L is the Monin-Obukhov length and is defined as:

$$L = \frac{u_*^2 T_0}{\kappa g T_*} \tag{6.37}$$

where C_p is the specific heat of air, g is the gravity acceleration, T_0 is the temperature at ground level and T_* is the scaling temperature defined as

$$T_* = \frac{-q_0}{\rho C_p u_*} \tag{6.38}$$

where q_0 is the heat flux from the surface, ρ is air density, Φ_h and Φ_m are the integrated forms of the similarity functions and are given by

$$\Phi_h = \Phi_m = -5\frac{z}{L} \qquad L > 0 \tag{6.39}$$

$$\Phi_m = \ln\left[\left(\frac{1+x^2}{2}\right)\left(\frac{1+x}{2}\right)^2\right] - 2\tan^{-1}x + \pi/2 \qquad L < 0 \tag{6.40}$$

$$\Phi_h = 2\ln\left(\frac{1+x^2}{2}\right) \qquad L < 0 \tag{6.41}$$

where:

$$x = \left(1 - 16\frac{z}{L}\right)^{1/4} \tag{6.42}$$

For turbulence parameters, the inlet profile considering the stability conditions could be written as

$$\varepsilon(z) = \frac{u_*^3}{\kappa z}\varphi_\varepsilon\left(\frac{z}{L}\right) \tag{6.43}$$

$$k(z) = \sqrt{\frac{\nu_t \varepsilon}{\rho C_\mu}} - 5.48u_*^2\sqrt{\frac{\varphi_\varepsilon(z/L)}{\varphi_m(z/L)}} \tag{6.44}$$

where ν_t is turbulent kinematic viscosity and φ_ε is given by:

$$\varphi_\varepsilon\left(\frac{z}{L}\right) = \begin{cases} 1 - \frac{z}{L} & \text{if} \quad L < 0 \\ \varphi_m\left(\frac{z}{L}\right) - \frac{z}{L} & \text{if} \quad L > 0 \end{cases} \tag{6.45}$$

φ_h and φ_m are the similarity functions and are given by:

$$\begin{cases} \varphi_m = \varphi_h = 1 + 5\frac{z}{L} & \text{if} \quad L > 0 \\ \varphi_m^2 = \varphi_h = \left(1 - 16\frac{z}{L}\right)^{-1/2} & \text{if} \quad L < 0 \end{cases} \tag{6.46}$$

As the bottom boundary is homogeneous, the prescribed cases for the validation were run in 2D. It is assumed that there is an equilibrium ABL which implies horizontal homogeneity, this implies the streamwise gradients of all parameters should be zero (Yang

506469-L-sub01-bw-Abbasi
Processed on: 9-11-2016

Table 6.1: Parameters describing different stability conditions in validating cases (adopted from Pieterse (2013))

ABL state	$z_0[m]$	$u_r[ms^{-1}]$	$z_r[m]$	$q_0[Wm^{-2}]$	$T_0[^\circ C]$	$L[m]$	$u_*[ms^{-1}]$	$\kappa[-]$	$k_s[m]$
Neutral	0.002	10	10	0.0	25.0	∞	0.481	0.41	0.015
Stable	0.002	10	10	-30.0	10.0	309.5	0.472	0.41	0.015
Unstable	0.002	10	10	100.0	40.0	-108.1	0.497	0.41	0.015

et al., 2009). It also means that by comparing the imposed profiles at the inflow boundary and the predicted profiles in different positions streamwise, it is possible to validate the model. Theoretically, the vertical profiles should be maintained throughout a computational domain without an obstacle. Using the assumption of equilibrium ABL, the vertical profiles of airflow's parameters in each prescribed validation case are plotted. The streamwise flow parameters under neutral condition are illustrated in Figure 6.5. It can be seen that the vertical profiles of the flow are maintained throughout the downstream distance. There are some slight differences which are consistent with the observation of previous studies (e.g. Blocken et al. (2007); Hargreaves and Wright (2007); Pieterse (2013)). A comparison of the homogeneity error at a height of 10 m, relative to the inlet conditions under neutral atmosphere is shown in Figure 6.6. It illustrates clearly that the temperature profile is well maintained. The maintenance of the velocity is also particularly good, with less than 10% error at a height of 10 m, the point in the domain where some of the largest inhomogeneity were observed (Pieterse, 2013). The relative streamwise large gradients in the k and ε profiles could be mainly due to the use of wall functions and has been investigated by many researchers (e.g. Blocken et al. (2007); Hargreaves and Wright (2007); Parente et al. (2011)). The streamwise gradients of flow parameters under stable and unstable atmosphere are shown in Figure 6.7 and Figure 6.9 respectively. Similar to the neutral simulation, the comparison of the homogeneity error at a height of 10 m, relative to the inlet conditions under stable and unstable atmosphere is shown in Figure 6.8 and Figure 6.10 respectively. As shown in these graphs, the model performance is better in the non-neutral atmosphere. Generally, the performance of the model regarding the stability conditions is good and could be used in simulating the airflow in ABL considering stability conditions. For more details about the validating process and the results refer to Pieterse (2013).

6.7. DESCRIPTION OF STUDY SITE AND DATA COLLECTION

The Upper East Region of Ghana is classified as one of the poorest in the country. Most of the inhabitants of the region (mostly rural areas) are farmers and rely on rainfed agriculture. To improve their livelihoods and enhance food security a number of small reservoirs (more than 160) with surface areas between 1 to 100 hectares (Abbasi et al., 2016b; Annor et al., 2009) were constructed for them by the Ghana government and development partners in the late 1980s and early 1990s. These were constructed to promote dry season farming (crop and livestock), fishing and domestic water uses. Their closeness to the point of use made them very attractive (Abbasi et al., 2016a; Keller et al., 2000). However with recent changes in climate (climate change), the small reservoirs which

506469-L-sub01-bw-Abbasi
Processed on: 9-11-2016

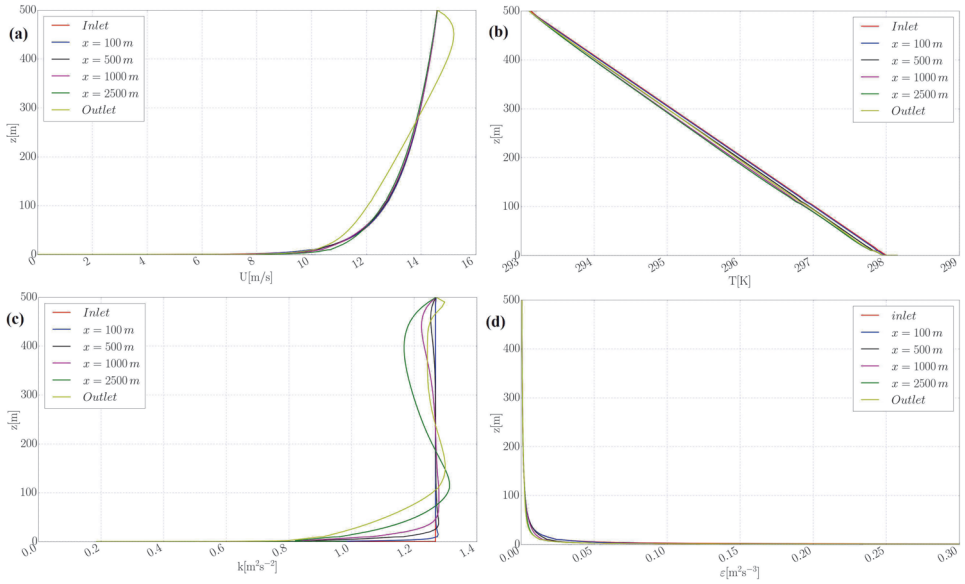


Figure 6.5: Neutral model results illustrating streamwise gradients for **(a)** wind speed; **(b)** temperature; **(c)** turbulent kinetic energy; and **(d)** turbulent dissipation rate.

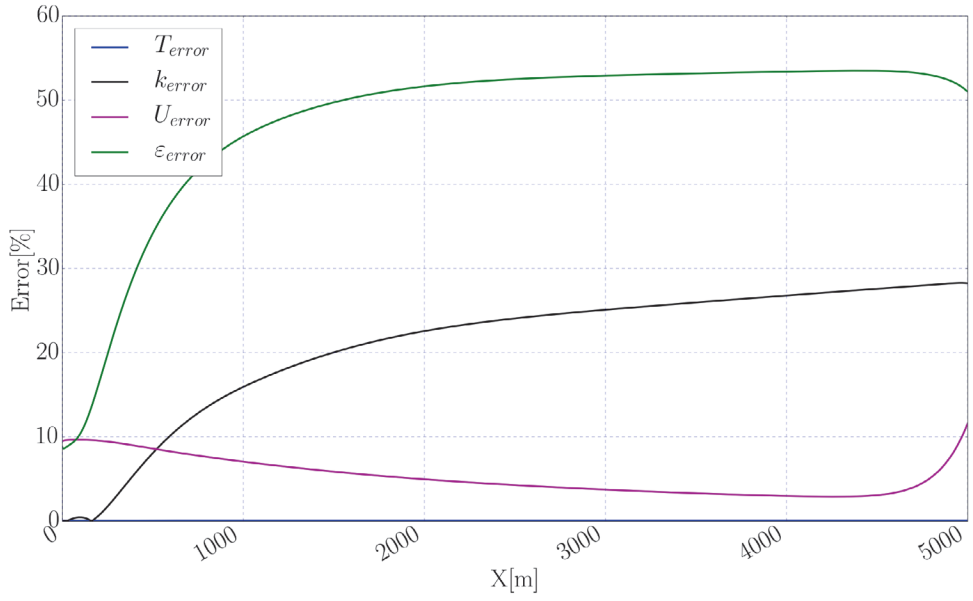


Figure 6.6: Relative change of flow parameters in neutral condition relative to inlet values.

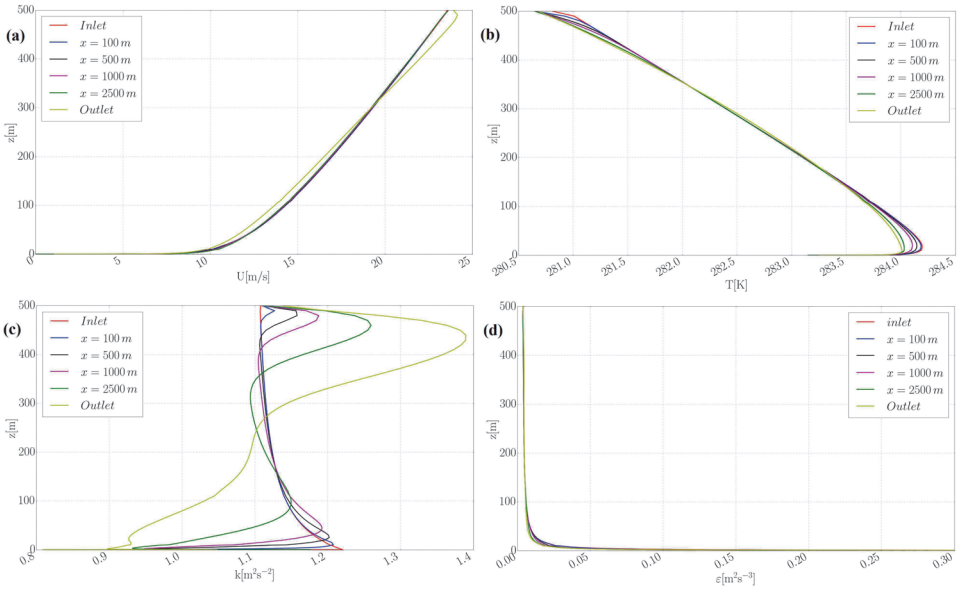


Figure 6.7: Model results for stable atmospheric condition illustrating streamwise gradients for **(a)** wind speed; **(b)** temperature; **(c)** turbulent kinetic energy; and **(d)** turbulent dissipation rate.

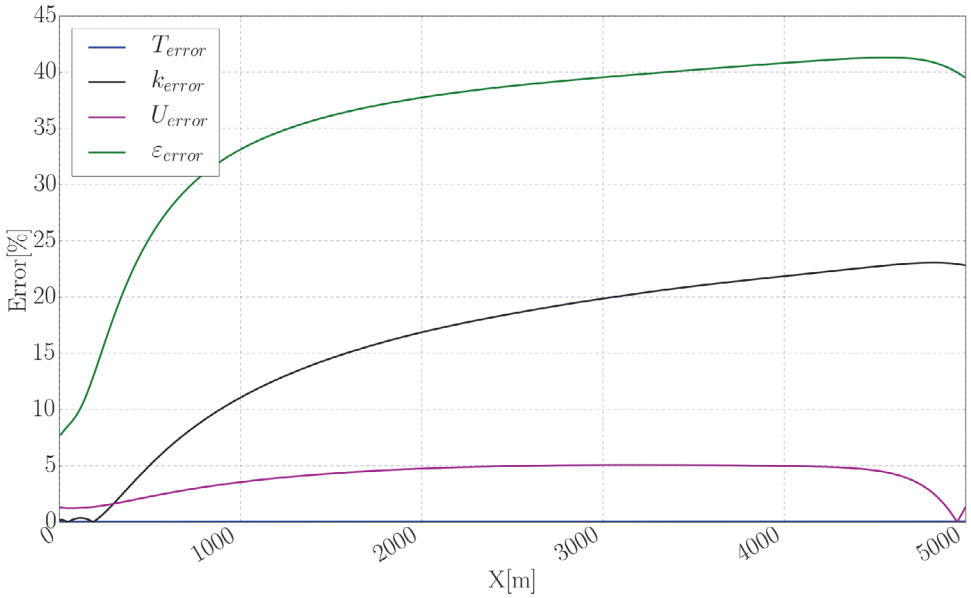


Figure 6.8: Relative change of flow parameters in stable atmospheric condition relative to inlet values.

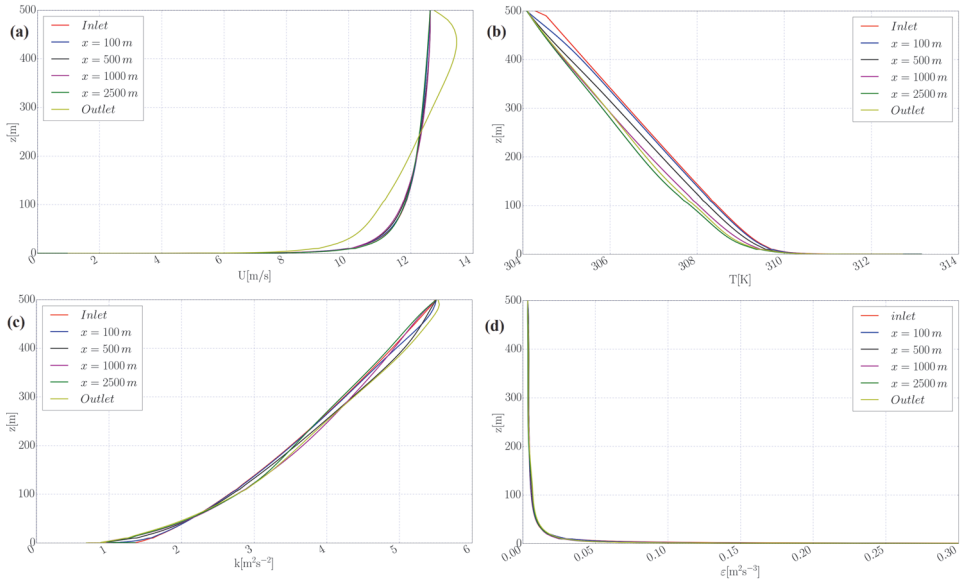


Figure 6.9: Model results for unstable atmospheric condition illustrating streamwise gradients for **(a)** wind speed; **(b)** temperature; **(c)**turbulent kinetic energy; and **(d)** turbulent dissipation rate.



Figure 6.10: Relative change of flow parameters in unstable atmospheric condition relative to inlet values.

were to increase the resilience of the communities which use them are at risk from high evaporation losses from them. Binaba dam, a small and shallow reservoir located in this region ($10°53'20''N$, $00°26'20''W$) was studied to determine the rate of heat fluxes in small lakes in this region. The Binaba reservoir has an average surface area of 31 ha with a maximum and average depth of 4.0 m and 1.1 m respectively, at full storage level (Figure 6.11). To monitor the meteorological parameters, a floating measurement station was installed over the water surface. Measurements taken included atmospheric parameters (air temperature, wind speed at 2 m above the water surface, wind direction and relative humidity), incoming shortwave radiation, water temperature profile, and sensible heat flux using a 3-D sonic anemometer. The installed 3-D sonic anemometer recorded sensible heat flux over the water surface at 10 Hz and accumulated over 30-minutes intervals. The air temperature fluctuated from 18.0 to 40.0 $°C$ with an average of 28.7 $°C$ while the water surface temperature varied between 24.0 $°C$ and 32.5 $°C$ with an average of 27.5 $°C$ during the measurement period. Measurements were done from November 23, 2012, to December 22, 2012. Figure 6.12(a) shows the diurnal changes of air temperature, with daily variations of approximately 10.0 $°C$. The maximum wind speed recorded during the study was 4.5 ms^{-1} (Figure 6.12(b)) with the South-Western direction being the most dominant direction.



Figure 6.11: Lake Binaba and its surroundings.

6.8. RESULTS AND DISCUSSION

To simulate the transient behavior of ABL and the influence of water surface on the airflow, unsteady RANS (URANS) was used (Equation (6.1) through (6.4)). In the following section, by using the results of the model, the effects of water surface on the flow features in ABL is discussed. To this end, the flow parameters such as velocity, temperature and water vapour concentration over the water surface and its surroundings are analysed.

506469-L-sub01-bw-Abbasi
Processed on: 9-11-2016

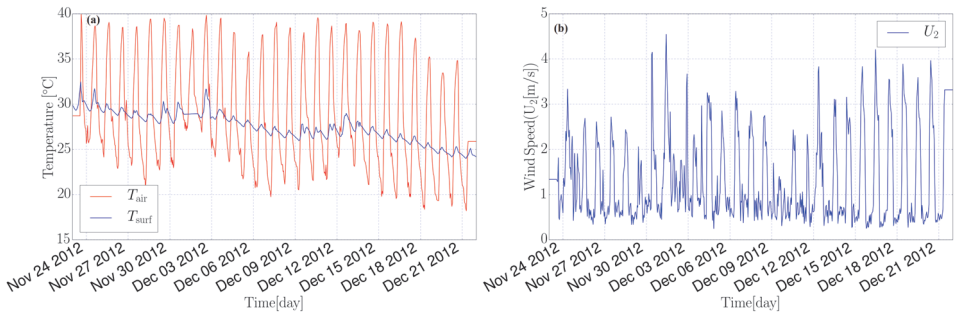


Figure 6.12: **(a)** Measured water surface and air temperature at 2 m above water surface; **(b)** measured wind speed at 2 m above water surface during the simulation period.

In the modelled complex domain, the airflow encounters sudden changes in surface roughness, temperature and wetness. These sharp changes modify the velocity, humidity and temperature profiles in a layer near the bottom boundary which is commonly referred to as the Internal Boundary Layer (IBL) (Bou-Zeid et al., 2004; Józsa et al., 2007).

In Figure 6.13 the flow parameters in streamwise ($x-$)direction which includes both land (upstream and downstream) and water surface at different times are plotted. As shown in velocity graph (Figure 6.13(a)) the flow velocity has sharp changes after passing the land-water border and in passing the water-land border as well. The main reason for these sharp changes could be related to the big difference between the water surface roughness ($z_0 = 0.0001\,m$) and the land surface ($z_0 = 0.13\,m$). With atmospheric stability condition (Table 6.2), in the unstable conditions, the airflow has sharp changes in passing from land through water surface or vice versa. However, for stable conditions ($t = 12:00$ and $t = 15:00\,hr$), the velocity profile has no clear pattern in the transition zones. Investigating the streamlines at these times shows that in stable conditions there are some inverse flows in the domain which could change the velocity values when compared with the effect of roughness changes. Therefore, in stable conditions the effect of buoyancy on the air flow could be dominant and should be considered in the model. Including the buoyancy effect in the momentum equation could be another reason for the changes in flow parameters (Equation (6.2)). As shown in Table 6.2 at $t = 12:00\,hr$ and $t = 15:00\,hr$, the ABL is stable and the buoyancy effect could be maximum due to the highest values of differences between the reference (T_{ref}) and air temperature (T_a). For temperature, (Figure 6.13(b)) its shape in streamwise ($x-$)direction in stable conditions is different from unstable conditions. In stable conditions, there are some sharp changes (either increasing or decreasing) in temperature profiles. For unstable conditions, the changes in temperature profile are small and, in general, the change in temperature due to the water surface in ABL is smaller than its effects on the velocity profile. Canvassing the airflow properties illustrated in Figure 6.13 and Figure 6.14 shows that the water surface generally can change the airflow parameters distribution in streamwise. These changes have different shapes in different stability conditions due to the effect of buoyancy.

To study the distribution of airflow parameters with respect to the bottom surface

506469-L-sub01-bw-Abbasi
Processed on: 9-11-2016

Table 6.2: ABL condition in different simulated times (ζ is stability parameter, T_a is air temperature, T_{ws} is water surface temperature, and T_{ref} is reference temperature)

Time$[hr]$	$\zeta[-]$	$T_a[K]$	$T_{ws}[K]$	$T_a - T_{ws}[K]$	$T_{ref}[K]$	$T_a - T_{ref}[K]$	Stability Condition
1	-1.13	301.81	302.02	-0.21	293.15	8.81	Unstable
2	-3.48	301.58	301.94	-0.36	293.15	8.58	Unstable
8	-2.95	301.21	301.82	-0.61	293.15	8.21	Unstable
12	2.11	310.4	303.72	6.68	293.15	17.4	Stable
15	4.75	313.08	305.15	7.93	293.15	20.08	Stable
19	-3.17	304.13	303.64	0.49	293.15	11.13	Unstable
24	-9.5	297.99	301.74	-3.75	293.15	4.99	Unstable

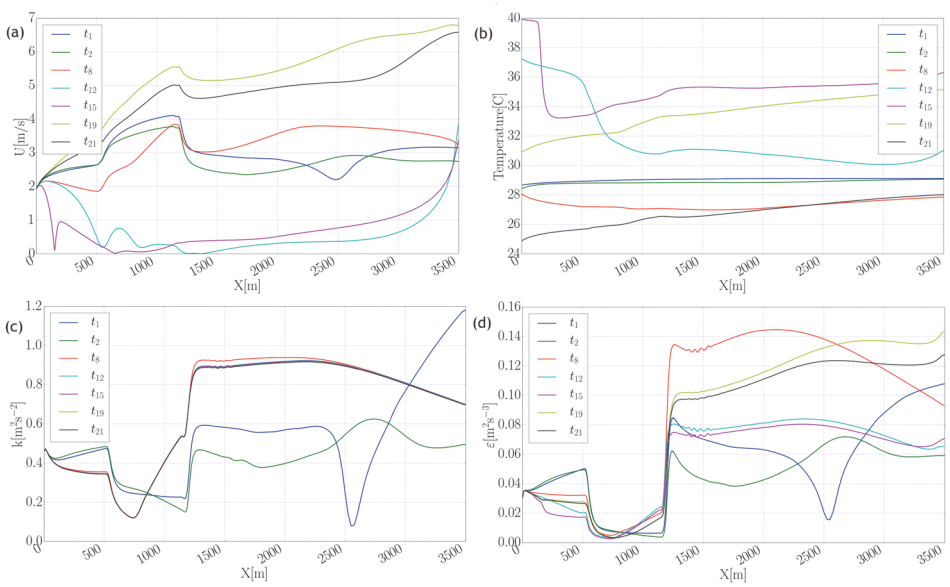


Figure 6.13: Simulated flow parameters at height 2 m above the bottom surface in streamwise ($x-$)direction include land and water surface. Water surface extends from $x \approx 550$ to $x \approx 1200\,m$. Results are plotted for seven different times: $t_1 = 01:00$, $t_2 = 02:00$, $t_8 = 08:00$, $t_{12} = 12:00$, $t_{15} = 15:00$, $t_{19} = 19:00$ and $t_{21} = 24:00\,hr$: **(a)** velocity; **(b)** temperature; **(c)** turbulent kinematic energy; and **(d)** dissipation rate of turbulent kinetic energy.

effects on the ABL flow, the simulated airflow parameters are depicted over the four different lines streamwise in Figure 6.15 and Figure 6.16 at two selected times. Two lines (x_5 and x_8) pass only from the land surface and the rest (x_6 and x_7) are located on both land and water surface. In addition, due to the transient ABL flow, the simulated results are shown in two different times ($t = 02:00$ and $t = 15:00\,hr$) where at $t = 02:00\,hr$ the ABL is unstable and in $t = 15:00\,hr$ it is stable and it could be possible to study the effect of stability conditions on the ABL flow passing through different surfaces. It is clear that the position of the water surface in the computational domain is an important parameter in the airflow in the ABL, especially in unsteady flow simulation. Examining the

506469-L-sub01-bw-Abbasi
Processed on: 9-11-2016

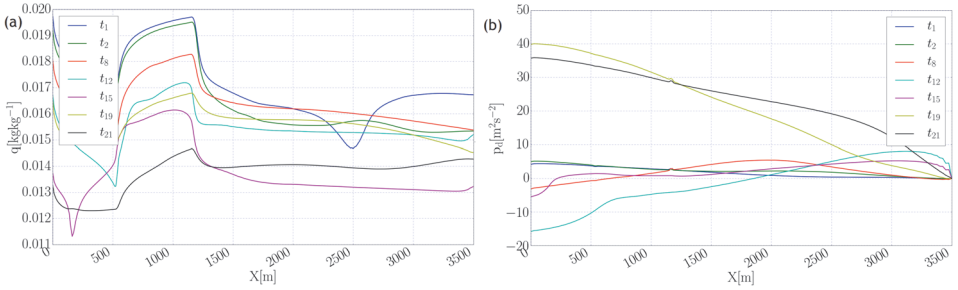


Figure 6.14: Simulated flow parameters at height 2 m above the bottom surface in streamwise ($x-$)direction include land and water surface. Water surface extends from $x \approx 550$ to $x \approx 1200\,m$. Results are plotted for seven different times: $t_1 = 01:00$, $t_2 = 02:00$, $t_8 = 08:00$, $t_{12} = 12:00$, $t_{15} = 15:00$, $t_{19} = 19:00$ and $t_{21} = 24:00\,hr$: **(a)** specific humidity; and **(b)** dynamic pressure ($P_d = P_{total} - P_{static}$).

shape of the flow parameters (for instance q in Figure 6.15(f)) shows that different locations of the water surface (for line x_6 the water surface extends from 900 to 1300 m and for the x_7 it extends from 550 to 1200 m) could generate different distributions of airflow parameters.

In Figure 6.17, Figure 6.18 and Figure 6.19 the vertical profiles of airflow in three positions and at different times are delineated. These three positions are selected in a way that the reader is able to study the effect of water surface on the vertical profiles of airflow. The first point is located on the upstream (upwind) land before reaching to the water surface ($x = 500\,m$), the second point is located on the water surface far from the water edge ($x = 1000\,m$) and the last one is located on the downstream (downwind) land after passing from the water surface ($x = 1300\,m$). As shown in these figures, the water surface makes some changes in the flow profiles not only over the water surface but also on the downwind land. It means that the combination of water surface's shape and the wind direction can significantly affect the distributions of airflow variables over the water and in the downwind distance outside the water body itself. These effects could help in situating land-based stations to measure meteorological parameters in lake surroundings.

The temporal distribution of airflow velocity, as well as the temperature distribution, are illustrated in Figure 6.20(a) and Figure 6.20(b) respectively. The temporal distribution are plotted for three probe locations: i) the first point is located at $x = 500$ and $z = 2.0\,m$ above the bottom surface over the upwind land, ii) the second one is at $x = 1000$ and $z = 2.0\,m$ above the water surface, and iii) the third point is located at $x = 1500$ and $z = 2.0\,m$ above the downwind land. In stable conditions ($t \approx 08:45$ till $18:00\,hr$), there is no clear trend for velocity changes in any of the selected probe locations. For unstable conditions (the remaining time), the velocity values on the water surface and on the downstream land are larger than the values on the upstream land. Figure 6.20(b) shows that the changes in temperatures values for unstable conditions are very small for all locations. However, the changes in temperature increases (from $t = 08:45\,hr$) in stable conditions, and continues until reaching unstable condition at $t = 18:00\,hr$.

506469-L-sub01-bw-Abbasi
Processed on: 9-11-2016

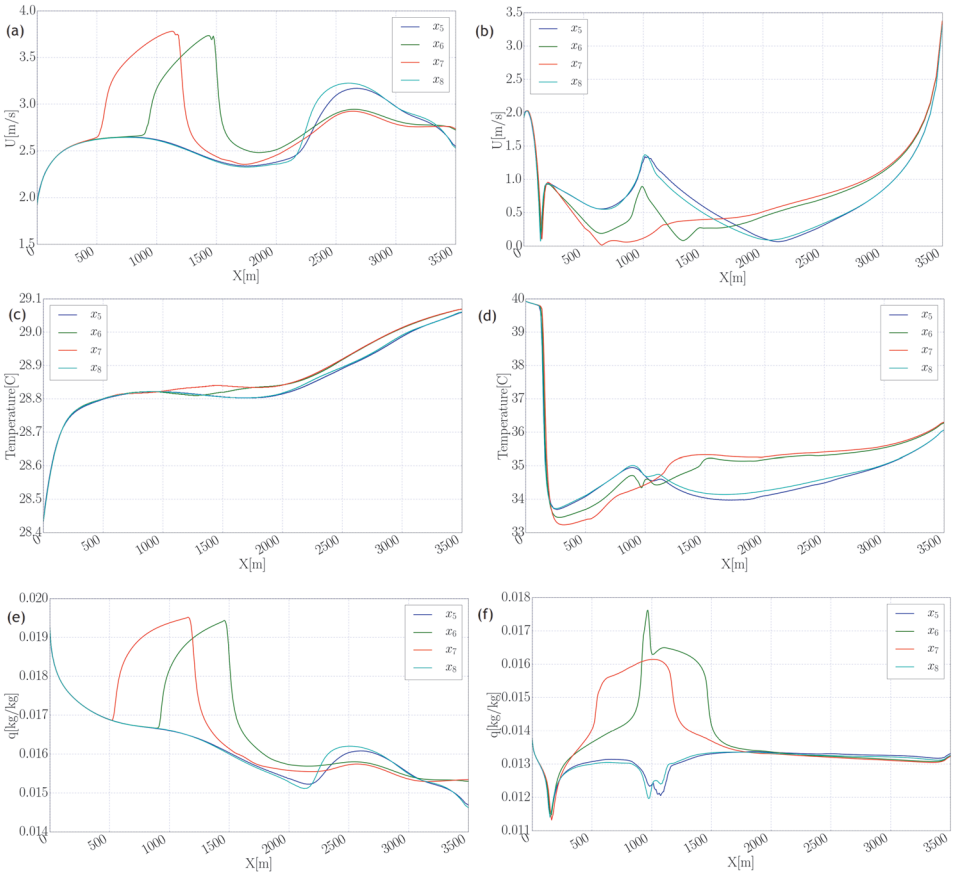


Figure 6.15: Comparison of simulated flow parameters at height 2 m above bottom surface in streamwise ($x-$)direction for different conditions: x_5: includes only land surface, x_6: includes land and water surface extending from $x \approx 900$ to $x \approx 1300\,m$, x_7: includes land and water surface extending from $x \approx 550$ to $x \approx 1200\,m$, x_8: includes only land surface: **(a)** velocity at $t = 02:00\,hr$; **(b)** velocity at $t = 15:00\,hr$; **(c)** temperature at $t = 02:00\,hr$; **(d)** temperature at $t = 15:00\,hr$; **(e)** specific humidity at $t = 02:00\,hr$; **(f)** specific humidity at $t = 15:00\,hr$.

Analysing the model results described above, shows that the water surface can affect the airflow in ABL due to its different properties in roughness, wetness and temperature. In unstable atmospheric conditions, the water surface characteristics could change the airflow pattern when compared with a homogeneous surface (the surface which includes only land) in all directions (in streamwise, vertical and perpendicular direction). However, in stable atmospheric conditions, the airflow in ABL is affected not only by the surface characteristics but also by the atmospheric stability conditions. In these situations, there is no clear direction for parameter changes in the ABL.

506469-L-sub01-bw-Abbasi
Processed on: 9-11-2016

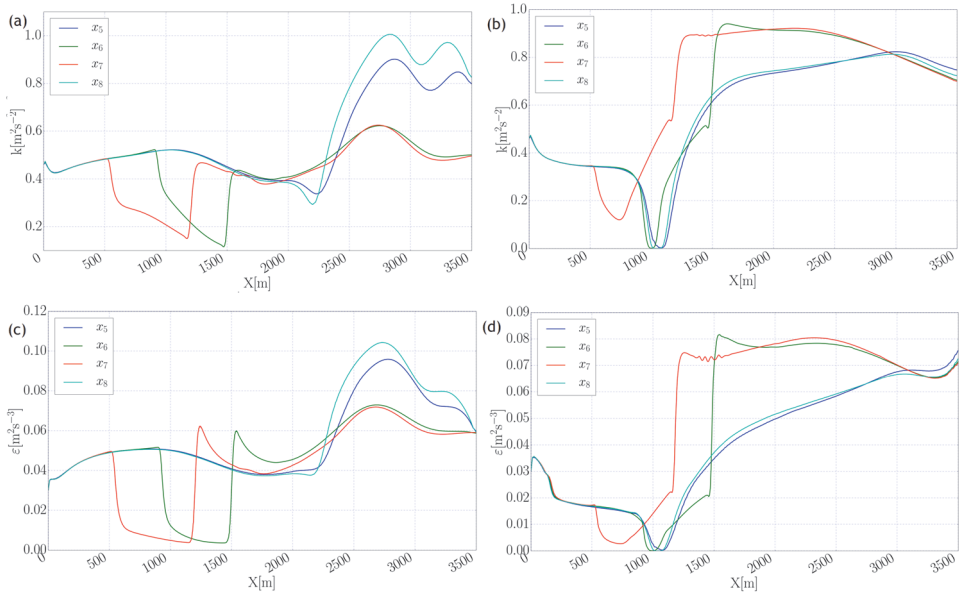


Figure 6.16: Comparison of simulated flow parameters at height 2 m above bottom surface in streamwise ($x-$)direction for different conditions: x_5: includes only land surface, x_6: includes land and water surface extending from $x \approx 900$ to $x \approx 1300\,m$, x_7: includes land and water surface extending from $x \approx 550$ to $x \approx 1200\,m$, x_8: includes only land surface: **(a)** turbulent kinetic energy at $t = 02:00\,hr$; **(b)** turbulent kinetic energy at $t = 15:00\,hr$; **(c)** dissipation rate of turbulent kinetic energy at $t = 02:00\,hr$; **(d)** dissipation rate of turbulent kinetic energy at $t = 15:00\,hr$.

6

6.9. CONCLUSION

In this study, the airflow in Atmospheric Boundary Layer (ABL) using Unsteady Reynolds Average Navier Stokes (URANS) is simulated considering the effects of sharp changes in surface characteristics from dry land to water surface and vice versa. In addition, the effect of atmospheric stability conditions on the airflow is examined. To be able to take into account the stability conditions and the buoyancy in the ABL and the non-homogeneity of the bottom surface as well, some modification were done in the flow equations and in the turbulence equations. Due to the complexity of the computational domain which includes an irregular water surface at the bottom surface, generating the geometry and the optimal computational grid is a big challenge for simulations. Adapting the boundary conditions to the available data and their transient conditions, need much effort to get reasonable and reliable results for the airflow in ABL. The results of the model were verified for three cases with different stability conditions. Validation results showed that the model has a good performance especially in unstable conditions.

The current model was used to investigate the effect of a small water surface on the airflow in ABL. The main reason for the simulation was to study the changes of the flow variables due to the available water surface and the effects of stability conditions on the parameters, especially over the water surface. The model was then used to determine

506469-L-sub01-bw-Abbasi
Processed on: 9-11-2016

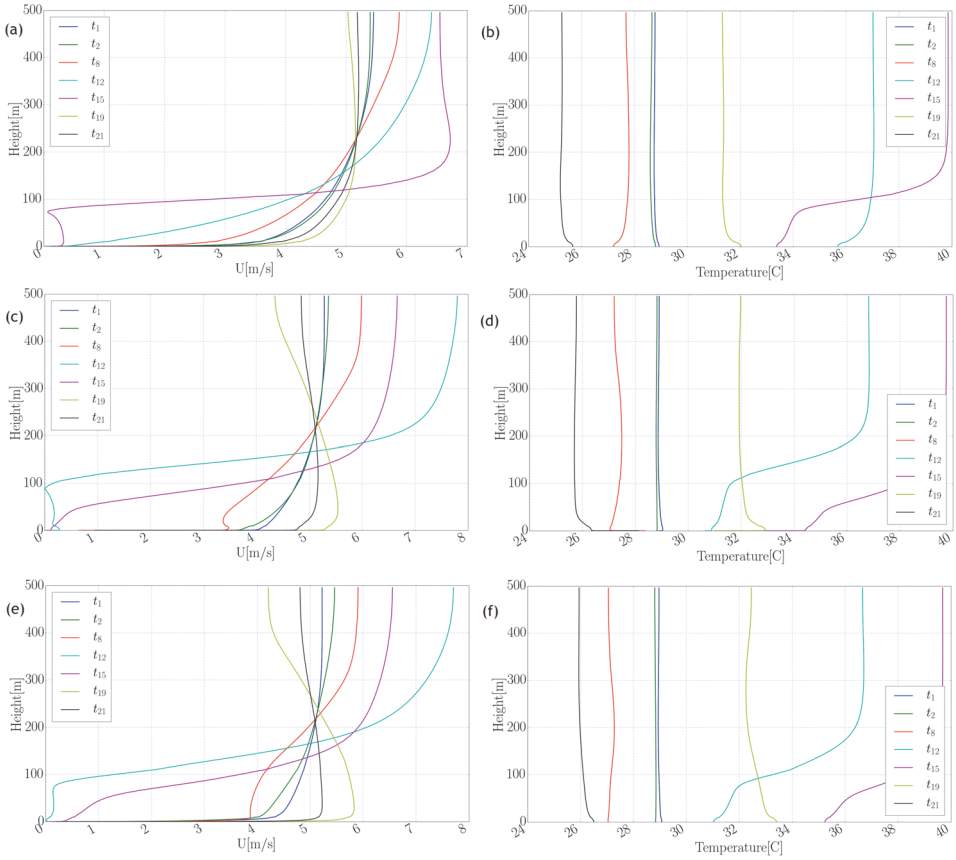


Figure 6.17: Comparison of simulated flow parameters in height ($z-$direction) for different locations in streamwise direction and for different times:$t_1 = 01:00$, $t_2 = 02:00$, $t_8 = 08:00$, $t_{12} = 12:00$, $t_{15} = 15:00$, $t_{19} = 19:00$ and $t_{21} = 24:00\,hr$: **(a)** velocity at x= 500 m on land in upstream of water surface; **(b)** temperature at x= 500 m on land in upstream of water surface; **(c)** velocity at x= 1000 m on water surface; **(d)** temperature at x= 1000 m on water surface; **(e)** velocity at x= 1300 m on land in downstream of water surface; **(f)** temperature at x= 1300 m on land in downstream of water surface.

the heat fluxes and the humidity over the water surface. The results showed that the flow pattern in the domain is affected by different parameters such as changes in roughness, wetness, temperature and the stability conditions as well. In unstable atmospheric conditions, the effect of changes in surface characteristics was dominant and a clear pattern could be detected. However, for the stable atmospheric condition no clear patterns were detected. The shape of the airflow in ABL in these conditions could be affected by the buoyancy force which is dominant compared with the changes of surface properties.

The proposed model could be used as a suitable tool to estimate parameters such as velocity, temperature, specific humidity, etc. over the water surface using the measured

506469-L-sub01-bw-Abbasi
Processed on: 9-11-2016

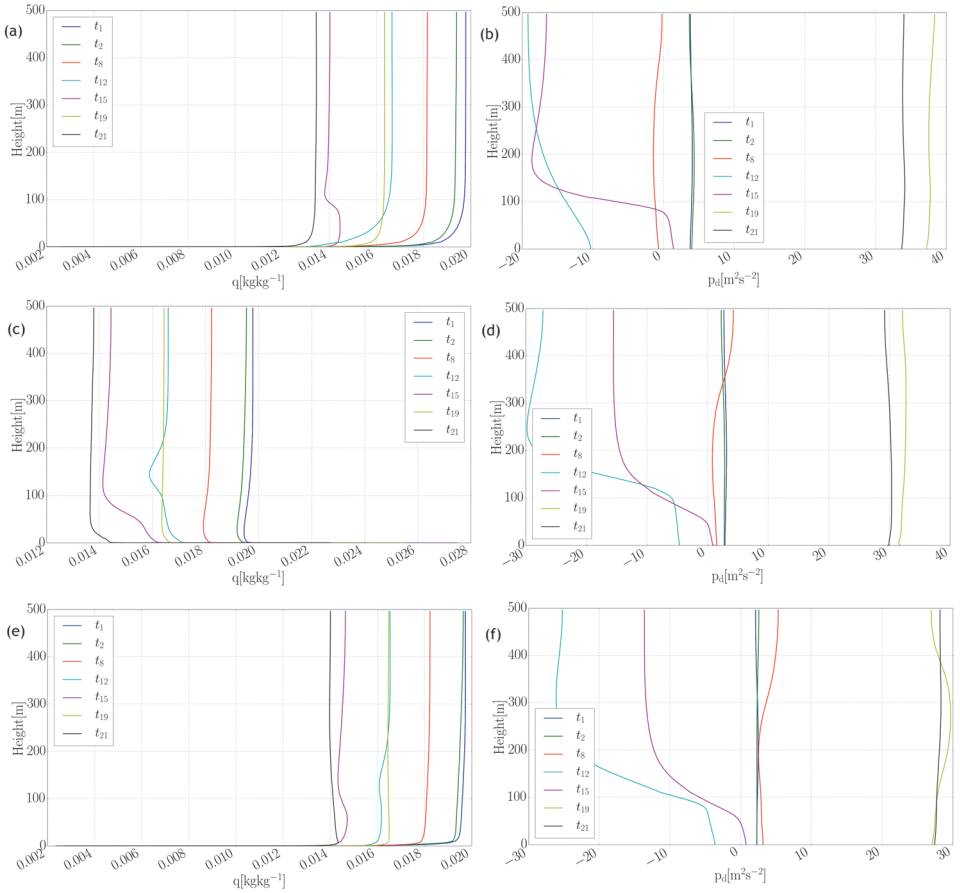


Figure 6.18: Comparison of simulated flow parameters in height ($z-$direction) for different locations in streamwise direction and for different times: $t_1 = 01:00$, $t_2 = 02:00$, $t_8 = 08:00$, $t_{12} = 12:00$, $t_{15} = 15:00$, $t_{19} = 19:00$ and $t_{21} = 24:00\,hr$: **(a)** specific humidity at x= 500 m on land in upstream of water surface; **(b)** dynamic pressure ($P_d = P_{total} - P_{static}$) at x= 500 m on land in upstream of water surface; **(c)** specific humidity at x= 1000 m on water surface; **(d)** dynamic pressure ($P_d = P_{total} - P_{static}$) at x= 1000 m on water surface; **(e)** specific humidity at x= 1300 m on land in downstream of water surface; **(f)** dynamic pressure ($P_d = P_{total} - P_{static}$) at x= 1300 m on land in downstream of water surface.

meteorological parameters in land-based stations. In addition, the results of the model will help with identifying appropriate location to install weather stations on the land in lake surroundings.

506469-L-sub01-bw-Abbasi
Processed on: 9-11-2016

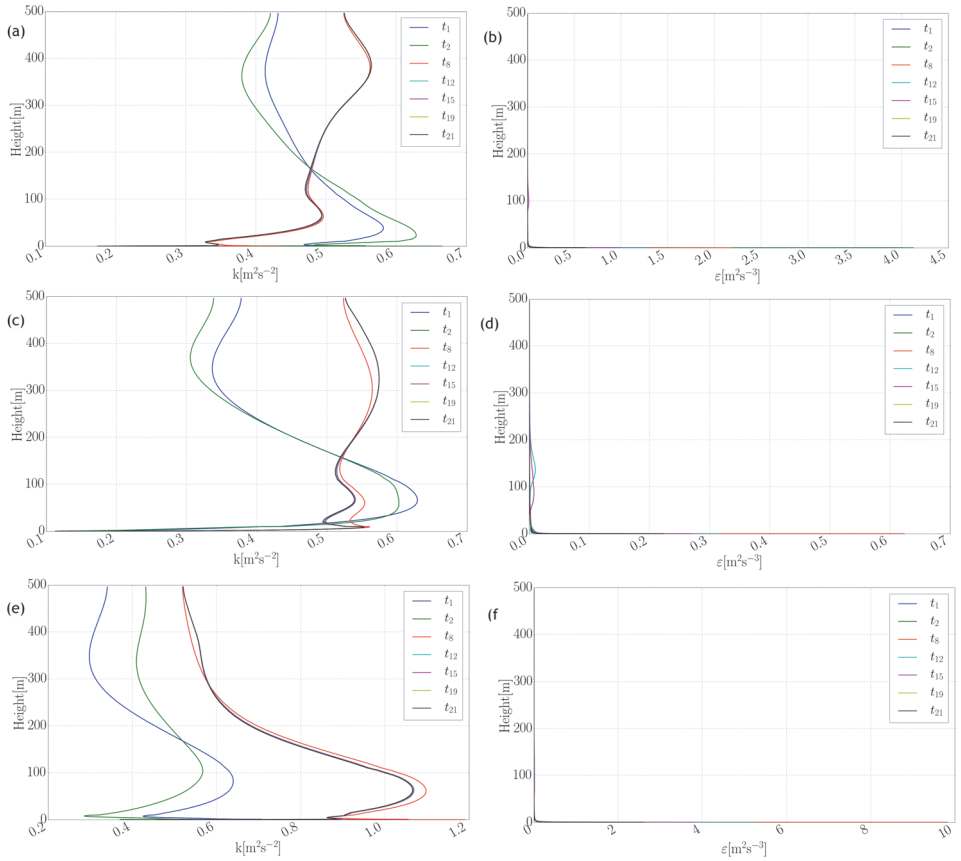


Figure 6.19: Comparison of simulated flow parameters in height ($z-$direction) for different locations in streamwise direction and for different times: $t_1 = 01:00$, $t_2 = 02:00$, $t_8 = 08:00$, $t_{12} = 12:00$, $t_{15} = 15:00$, $t_{19} = 19:00$ and $t_{21} = 24:00\,hr$: **(a)** turbulent kinetic energy at x= 500 m on land in upstream of water surface; **(b)** dissipation rate of turbulent kinetic energy at x= 500 m on land in upstream of water surface; **(c)**turbulent kinetic energy at x= 1000 m on water surface; **(d)** dissipation rate of turbulent kinetic energy at x= 1000 m on water surface; **(e)** turbulent kinetic energy at x= 1300 m on land in downstream of water surface; **(f)** dissipation rate of turbulent kinetic energy at x= 1300 m on land in downstream of water surface.

506469-L-sub01-bw-Abbasi
Processed on: 9-11-2016

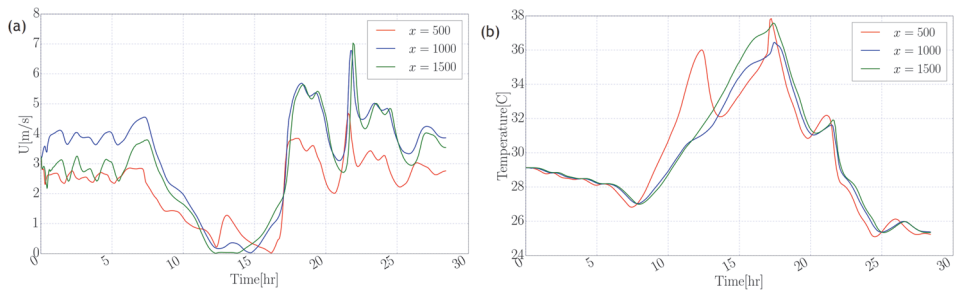


Figure 6.20: Changes of simulated flow parameters with time at height of 2 m above bottom surface in three locations: $x_1 = 500\,m$ (over upstream land), $x_2 = 1000\,m$ (over water surface) and $x_3 = 1500\,m$ (over downstream land), **(a)** velocity; and **(b)** temperature.

7

CONCLUSION AND RECOMMENDATIONS

In this research different issues related to small reservoirs were investigated. Since there is an important role for these water resources in arid and semi-arid regions, there is urgent need to studying them. According to the results of various assessments which were carried out in this study, the following conclusion could be drawn.

7.1. EVAPORATION FROM SMALL RESERVOIRS

The atmospheric stability conditions over small and shallow lakes in arid and semi-arid regions are important in estimating evaporation from open water bodies. Using the Monin-Obukhov Similarity Theory (MOST), stability conditions were used to estimate latent and sensible heat fluxes. The bulk aerodynamic transfer method was improved by using the stability parameter from MOST and the atmospheric stability adjusted transfer coefficients. From the modeling results, atmospheric instability occurred more than 65% of the time in the study period, hence it enhanced the evaporation from water surface by 44.4% on average. Using the developed method, the calculated daily average evaporation from lake Binaba during the study period was 3.6 mmd^{-1}. The effect of atmospheric instability on drag coefficient and heat (or water vapor) transfer coefficient were found to be 23.5% and 51.4%, respectively. The results correlated well with the measured values of sensible heat flux.

7.2. CFD-BASED APPROACH TO ESTIMATE EVAPORATION (CFDEVAP)

In this research, a CFD-based approach has been developed to determine the heat and mass transfer coefficients over the water surface of a semi-arid shallow and small lake. Using this method, the mass transfer coefficients that are usually used in aerodynamic mass transfer method in estimating evaporation from the water surface, could be used

506469-L-sub01-bw-Abbasi
Processed on: 9-11-2016

for measuring evaporation from the water surface. To determine the heat and mass transfer coefficients, different scenarios with different atmospheric stability conditions were considered. For each scenario the heat and mass flow (air flow) over the water surface was simulated to determine the spatial distributions of sensible and latent heat fluxes over the water surface. The evaporation values estimated by the proposed approach, were compared with the measured evaporation over the lake. The developed model predicts sensible heat fluxes accurately for unstable atmospheric conditions but it overestimates convective heat flux in stable and neutral atmospheric boundary layer. The methodology developed here represents a useful framework for estimating evaporation for water bodies, especially in regions where advection, oasis and atmospheric instability effects on evaporation are considerably high. In addition, the approach can show the spatial distribution of evaporation rate over the open water surface (fetch effects). These make it an easily applicable and cost effective approach for estimating evaporation from water surfaces. This approach was applied for lake Binaba and results showed that the minimum, average and maximum values of evaporation during the study period were 2.6, 4.2 and 6.8 $mm\,d^{-1}$, respectively. The estimated evaporation values using CFDEvap approach are a little higher than ones estimated by the mass-transfer method described in Chapter 2.

7.3. SMALL SHALLOW LAKE FRAMEWORK (SSLF)

In this study, a comprehensive framework for simulating small and shallow inland water bodies was developed to assess circulation and temperature dynamics in small reservoirs. This framework comprises many crucial steps in lake and reservoir modeling which include: creating bathymetry, generating computational grid, solving flow field and temperature dynamics, plotting desired graphs, analysing the outputs, etc. In order to produce an acceptable bathymetry applicable in CFD simulations, a new simple approach using open-source tools has been developed which could be easily implemented in different models that require the geometry of water body or similar computational domains to conduct simulations. Moreover, to consider the buoyancy effects in water body, the turbulence model was improved to take into account buoyancy effects. In commonly available measurements for small water bodies, a wide range of boundary conditions are proposed that could be adapted to suit measurements over the water surface at hand. To check performance of the framework, several test cases and a real-world lake were simulated and compared with field measurements.

The results of the proposed framework (SSLF) for different simulations have led to the following conclusions: 1) the model can estimate the temperature distribution as well as the flow field in water bodies; 2) this framework can work with a wide range of boundary conditions dependent on available measured parameters; 3) accuracy of the prepared model mainly depends on errors and uncertainties in input meteorological parameters; 4) temperature dynamics and flow pattern in the water body at a given point are strong functions of air temperature, incoming short-wave radiation, and wind velocity over the water surface. Effects of other meteorological parameters are considered implicitly in heat fluxes over the water surface as boundary conditions; 5) flow in the (small shallow) water body is fully 3-D and turbulent; 6) influence of turbidity of water on the flow field could be significant in small and shallow water bodies; 7) one of

506469-L-sub01-bw-Abbasi
Processed on: 9-11-2016

the big challenges in modeling shallow lakes is implementing heat fluxes over the water surface accurately, especially for latent heat flux (evaporative heat flux); 8) the model is very sensitive to the resolution of the computational mesh. Making a reasonable balance between the computational mesh and the needed computational resources is a very important step in simulating lake-like domains; 9) due to coupling of heat transfer processes with water flow in the lake, handling numerical issues in the model is very crucial. To solve the model in a stable and precise way, the appropriate numerical algorithms should be chosen; 10) open-source and free of charge tools could be used to develop flexible and powerful frameworks to simulate inland water bodies. A number of different approaches have been described in this study. Picking out the right turbulence model and boundary conditions are very important and can affect results significantly. It is obvious that using methods with less uncertainties, if possible, are better in computing the parameters, because they usually give better results. The approach used in this study for temperature dynamics could be applied to water quality, biological and environmental simulations of shallow water bodies as well as the model developed here.

7.4. APPLYING SSLF FOR A CASE STUDY

The lake model developed in this study (SSLF) was applied to investigate temperature profile and circulation in a shallow and small lake in the region of interest. The main aim of the simulation was to find out how the flow field and temperature distribution vary spatially and temporally in the studied shallow inland water body. As the flow in the water body is fully 3-D and turbulent, the full 3-D modified equations of the flow, considering the temperature in the water body, were solved by a CFD approach using OpenFOAM. The results for Lake Binaba show that the model overestimates the temperature distribution in the water body. This could be due to using boundary conditions with high degree of uncertainty. Accuracy of the model depends mainly on error in input meteorological parameters. Profile temperatures and flow pattern in water bodies have been found to have strong correlations with air temperature, incoming short-wave radiation, and wind velocity over water surface. Effects of other meteorological parameters were considered implicitly in heat fluxes over the water surface as boundary conditions. One of the big challenges in modeling very shallow lakes is implementing heat fluxes over the water surface accurately, especially for latent heat flux (evaporative heat flux).

According to the results obtained from the simulation, a number of improvements can be made to the lake model: 1) improving the temperature boundary condition on the bottom and sides of the lake by considering the heat fluxes through the sediments; 2) improving the methods to estimate heat fluxes over the water surface as temperature boundary condition; 3) considering the effects of reflected penetrated short-wave radiation in the water body as an extra source term in the lake; 4) an optimization methods to find the optimized number of cells and regions that should be refined in the lake.

7.5. ABL-SSL INTERACTION SIMULATION

In this part of the research, the airflow in Atmospheric Boundary Layer (ABL) using Unsteady Reynolds Average Navier Stokes (URANS) is simulated taking into account effects of sharp changes in surface characteristics from dry land to water surface and vice versa.

506469-L-sub01-bw-Abbasi
Processed on: 9-11-2016

In addition, the effect of atmospheric stability conditions on airflow is examined. To be able to take into account stability conditions and buoyancy in the ABL and the non-homogeneity of the bottom surface as well, some modifications were done in the flow equations and in the turbulence equations. Due to the complexity of the computational domain which includes an irregular water surface at the bottom surface, generating the geometry and the optimal computational grid is a big challenge for doing simulations. Adapting the boundary conditions to the available data and their transient conditions, must be carried out to get reasonable and reliable results for airflow in ABL. Results of the model were verified for three cases with different stability conditions. Validating the model showed that the model has a good performance especially in unstable conditions.

The prepared model was used to investigate the effect of a small water surface on the airflow in ABL. The main reason for the simulation was to study changes of flow variables due to the water surface and the effects of stability conditions on parameters, especially over the water surface. Results of the model then would be used to get an idea about the heat fluxes and the humidity over the water surface. Results showed that the flow pattern in the domain is affected by different parameters, such as, changes in roughness, wetness and the temperature and also the stability conditions. In unstable atmospheric conditions, the effect of changes in surface characteristics is dominant and a clear pattern could be detected. Contrary in the stable atmospheric condition no clear patterns are detected. Shape of airflow in ABL in these conditions could be affected by the buoyancy force where it is dominant in comparison with changes of surface properties.

The proposed model could be used as a suitable tool to estimate parameters such as velocity, temperature, specific humidity, etc., over the water surface using the measured meteorological parameters in the land-based stations. In addition, the results of the model will aid in finding the appropriate location to install the weather station on the land in lake surroundings.

7.6. RECOMMENDATIONS

Studying small shallow lakes in most cases could be more difficult than large or deep lakes. The biggest challenge is that the needed observations or measurements to validate the results of the model are rarely available. In addition, most of available models (open-source or commercial software) developed for inland water bodies are not applicable for the shallow small lakes due to the specific conditions. Regarding the modeling issues, figuring out the geometry of small lakes could be a big challenge. Besides this challenge, developing and solving the lake models is very sensitive to the environmental conditions and time varying boundary conditions where often there is insufficient data to implemented the model. In other words, small shallow lake modelling suffers from various issues, from computational issues, complex boundary conditions, etc., to limited insufficient on-site observations for verification. Although, there have been attempts to implement as much detail as possible in the model, due to complex conditions which exist in the ABL-SSL system, there is always room for improvements. It is obvious that having access to more observations on water surfaces would accelerate development of better simulations. A good model would be a tool to check and validate the data taken over water surfaces. A combination of in-situ observations and well-developed models would be a powerful tool in managing and evaluating small shallow water surfaces. An-

506469-L-sub01-bw-Abbasi
Processed on: 9-11-2016

other interesting direction for this work is to simulate small inland water bodies using a two-phase flow approach. This will result in the improvement of our understanding of the flow field in small lakes and reservoirs. In addition, it would be interesting to improve initial and boundary conditions in CFD models by coupling various models such as the Weather Research and Forecasting (WRF) model and OpenFOAM. Using output of the WRF model as initial and boundary conditions in OpenFOAM would be promising to improve accuracy of simulations without any significant increase in required computational resources.

506469-L-sub01-bw-Abbasi
Processed on: 9-11-2016

506469-L-sub01-bw-Abbasi
Processed on: 9-11-2016

SUMMARY

This thesis aims at developing a flexible and efficient (numerical) approach for estimating the energy balance and heat storage of small shallow lakes in arid and semi-arid regions. To reach to this aim, numerical methods and improvements in conventional methods were done.

The starting point of this thesis is understanding the role of small and shallow reservoirs in arid and semi-arid areas. In chapter 1 the importance of small lakes in improving the food security, stimulating the economy and development of the study region (Upper East Region of Ghana) is explained. As these small reservoirs have a significant impact on rural communities, they are a priority for national governments and local authorities.

Chapter 2 investigates the effect of atmospheric stability conditions over small lakes in heat fluxes from water surface. Using the Monin-Obukhov Similarity Theory (MOST), stability conditions are implemented in bulk aerodynamic transfer method to adjust transfer coefficients (for momentum, heat and water vapour). Another topic studied in this chapter is the application of values measured over-land of air temperature to estimate unknown water surface temperature values. To calculate these transfer coefficients accurately, a new computational method is developed in chapter 3. In this chapter a CFD-based approach (CFDEvap Model) is developed to determine the heat and mass transfer coefficients over the water surface. The methodology developed here represents a useful framework for estimating evaporation for water bodies, especially in regions where advection, oasis and atmospheric instability effects on evaporation are high. In addition, the approach can show the spatial distribution of evaporation over the open water surface (fetch effects). These make it an easily applicable and cost effective approach for estimating evaporation from water surfaces.

Chapter 4 is concentrates on the temperature dynamcis as well as circulation in small water bodies. In this chapter, a comprehensive framework (SSLF) comprises all crucial steps in lake and reservoir modeling which include: creating bathymetry, generating computational grid, solving flow field and temperature dynamics, plotting desired graphs, analysing the outputs, etc. is developed. As most of conventional methods fail in generating an acceptable geometry and computational grids applicable in CFD simulations, a new simple approach using open-source tools has been developed which could be easily implemented in different models that require the geometry of computational domains to conduct simulations. Moreover, to consider the buoyancy effects in water body, the turbulence model was improved. To check performance of the framework, a real-world lake (lake Binaba) as described in chapter 5 is simulated and the results are compared with field measurements.

As the energy balance of small lakes is significantly affected by the atmospheric conditions, in chapter 6 the airflow in the Atmospheric Boundary Layer (ABL) is simulated taking into account effects of sharp changes in surface characteristics from dry land to water surface and vice versa. In addition, the influence of atmospheric stability con-

506469-L-sub01-bw-Abbasi
Processed on: 9-11-2016

ditions on airflow is examined. The proposed model can be used as a suitable tool to estimate parameters such as velocity, temperature, specific humidity, etc., over the water surface using the measured meteorological parameters of land-based stations. In addition, the results of the model will aid in finding the appropriate location to install weather stations on land and also over the water surface.

Chapter 7 summarizes the findings of this research and discusses them. In addition, some additional issues on increasing the accuracy as well as the computational efficiency of the simulations, and some possible directions for further research based on the current work are briefly described.

506469-L-sub01-bw-Abbasi
Processed on: 9-11-2016

ACKNOWLEDGMENT

There are many people contributed directly or indirectly to the completion of this thesis, and I would like to express my genuine and sincere appreciation to all them.

First of all, I would like to express my sincere gratitude to my promoter, Professor Nick van de Giesen for giving me the opportunity to carry out this PhD research. Your curiosity and persistence have always been inspiring to me. Working with you is not easy, but it is extremely productive. There are so many lessons to be learned in the way you approach new challenges and never give up. Thanks a lot for never giving up on me. I am very happy that we are still working on our interest, "TAHMO". Your impeccable sense of practicality and your direct tone, have always been proven to be necessary and helpful.

I would like to specifically thank my colleague whose contribution vastly improved the content of this dissertation. Frank Ohene Annor is always full of new practical ideas and ready for collaboration. Validation of models developed in this thesis was designed and performed mostly based on his precious experiences. During our fruitful discussions, I benefited from his vast knowledge of writing business proposals. Our collaboration on TAHMO project was a life-saver for me. I'm so glad that we are working on this project.

I would also like to express my thanks to Natalie (Danezi) and her colleagues in "SURFsara" who supported me in accessing and using "SURFsara HPC-CLOUD" system to run the models. Furthermore, I would like to thank Cornelis (Slobbe) and Hassan (Hashemifarahani) with whom I could access and run the models on "HPC03" available at the department of Geoscience & Remote Sensing of Delft University of Technology.

I wish also to thank Susan (Steele-Dunne) for her advices and suggestions during the research. Her remarks on using open-source tools instead of preparing the codes from the scratch were so helpful in finding the way to do this thesis. I profoundly appreciate Professor Hrvoje Jasak (University of Zagreb) and Dr. Kazemi Kamyab for their time and valuable comments on OpenFOAM. I would like to thank my colleagues in the Valorisation Center of Delft University of Technology and TAHMO team because of their assistance and support. Thank you Theda (Olsder), Ellen (van Andel), Friso (vos de Wael), Els (Veenhoven) and Marjan (Kreijns). I would also like to express my gratitude and appreciation to the secretaries of the Water Management department of Delft University of Technology because of their great assistance in all administrative issues and beyond during the great +5 years I spent in WRM section. Thank you Betty (Rothfusz), Lydia (de Hoog), Luz (Ton-Estrada) and Petra (Jorritsma).

In addition, I appreciate all of my colleagues and friends in the Water Management department of Delft University of Technology for being always friendly, positive, and supportive. I truly enjoyed working with you. Please forgive me for never joining you for lunch. It's always been impossible for me to talk and eat, or eat and talk, simultaneously. Special thanks to Hubert Savenije, Mark Bakker, Santiago Gaitan, Camille le

506469-L-sub01-bw-Abbasi
Processed on: 9-11-2016

Coz, Rick Hagenaars, Shervan Gharai, Hongkai Gao, Wei Shao, Bas des Tombe, Jaime Polo Bermejo, Marie Charrière, Hojjat Mianabadi, Yang Lu, Nay Myo Lin, Thanda Thatoenwewin, Tim van Emmerik, Ruud van der Ent, Koen Hilgersom, Ameneh Mianabadi, Juliette Cortes Arevalo, Miriam Coenders-Gerrits, Maurits Ertsen, Wim Luxemburg, Wim Bastiaanssen, Yingrong Wen, Sandra Junier, Erik Mostert, Olivier Hoes, Gerrit Schoups, Ronald van Nooyen, Martine Rutten, Boran Ekin Aydin, Anna Solcerova, Alla Kolechkina, Frans van de Ven, Rolf Hut, Jianzhi Dong, Saket Pande, Cheema, Reza Pramana, Moshiur Rahman, Steven Weijs, Luciano Raso, Thom Bogaard, Markus Hrachowitz, Mojtaba Shafiei, Sobhan Emtehani and Mehrdad Moshtaghi, for the interesting and valuable discussions, and for their support during the research and assembling of the thesis. I am grateful to you all.

I also would like to thank all my Iranian friends in the Netherlands, particularly Enayat HosseiniAria, Hamid Ghaffarian, Dara Ghasimi, Mehdi Fasihi Harandi, Ebrahim Rahimi, Mostafa Zahmatkesh, Masoud Tohidian, Ahmadreza AhmadiMehr, Iman Madadi, Flora Anvarifar, Mohammad Chahardowli, Ebrahim Derakhshani, Hamid Saeidi, Behzad Behdani, Esmail Najafi, Mohammad Shahbazi, Mohsen Kavian, Reza Lotfi, Bashir Sedighi, Mahdi Beheshti, Mahdi Mahdipour, Javad Attarian, Zahra Rezvani, Zohreh Zahedi, Ali Sharikian, Pejman Abedifar, Mahdi Ghaemi Nia, Alireza Alemi, Mohammad Latifi, Mojtaba Hosseini Nasab and Reza Hesan for their friendship and support.

My greatest gratitude goes to my dear family; To my wife, for her moral support, for her patience and love. Maryam: I sincerely hope that I can be worthy of your unconditional trust and love. To my kids, Reyhaneh and Reza who are my “hope“ in life. Without “hope“, I could have done nothing. To my father, Mohammad Hossein and my mother, Mina for their encouragement. To my father-in-law, Hossein and my mother-in-law, Mahbubeh for their support and encouragement. To my brothers and sisters: Hossein, Hassan, Masoumeh and Maryam who have always offered me unconditional love, support and encouragement throughout my life.

Ali Abbasi
Delft, November 2016

506469-L-sub01-bw-Abbasi
Processed on: 9-11-2016

ABOUT THE AUTHOR

Ali Abbasi was born in Birjand, Iran on 11 December 1980. He studied mathematics and physics during high school. In September 2003, he got his BSc in civil engineering (hydraulics and water resources) from Iran University of Science and Technology (IUST), Tehran, Iran as the top ranked student. In February 2006, Ali got his master degree in civil engineering (hydraulic structures) from Khajeh Nasir Toosi University of Technology (KNTU), Tehran, Iran (graduated summa cum laude). Ali did his master thesis on "Water Hammer Modeling with Finite Volume Method" in which he developed a promising model to simulate the effects of length and bends of exposed penstock pipes of chained powerhouse on pressure fluctuation (water hammer) due to turbine run off. In September 2006, he joined the faculty of engineering (civil department) at the University of Birjand as a lecturer where he continued his academic career till February 2011. In April 2011, Ali moved to Delft where he joined the faculty of civil engineering and geoscience (CEG), water management department as a PhD student under supervision of Professor Nick van de Giesen. His research concerned estimating evaporation from small shallow lakes, interactions between atmospheric boundary layer and inland water surfaces, and simulating flow and circulation as well as temperature dynamics in small inland water bodies in arid and semi-arid regions (Northern Ghana and Southern Burkina Faso). Developing and applying numerical platforms based on open-source tools (OpenFOAM, MeshLab, QGIS, Python, Pandas, ADMesh, WRF, etc.), he improved the conventional methods to manage the small lakes in the study region. Since January 2016, he has joined the Trans-African HydroMeteorological Observatory (TAHMO) as a weather and climate researcher where he concentrates on improving the Numerical Weather Predictions (NWP) models such as the Weather and Research Forecasting (WRF) model in regional and continental scales to provide reliable climate data for clients and governments. He uses data assimilation techniques for locally measured parameters (from TAHMO ground-based weather stations) complemented by satellite data to generate accurate weather forecasting and consequently improving the early warning system (accurate predictions of floods and droughts); and generating valuable information for farmers and other clients.

506469-L-sub01-bw-Abbasi
Processed on: 9-11-2016

506469-L-sub01-bw-Abbasi
Processed on: 9-11-2016

LIST OF PUBLICATIONS

PEER REVIEW PUBLICATIONS

Ali Abbasi, Frank Ohene Annor, Nick van de Giesen, *Investigation of Temperature Dynamics in Small and Shallow Reservoirs. Case Stuy: Lake Binaba, Upper East Region of Ghana*, Water, **8**, 84 (2016).

Ali Abbasi, Frank Ohene Annor, Nick van de Giesen *Effects of Atmosphere Stability Conditions on Heat Fluxes from Small Water Surfaces in (Semi-) Arid Regions*, Manuscript accepted for publication in Hydrological Sciences Journal (September 2016).

Ali Abbasi, Frank Ohene Annor, Nick van de Giesen, *Developing a CFD-based Approach to Estimate Evaporation from Water Surfaces in (Semi-)Arid Regions*, Manuscript re-submitted for publication in Hydrological Processes (September 2015).

Ali Abbasi, Frank Ohene Annor, Nick van de Giesen, *A Framework to Simulate Small and Shallow Inland Water Bodies*, Manuscript re-submitted for publication in Advances in Water Resources (June 2016).

Ali Abbasi, Frank Ohene Annor, Nick van de Giesen, *The Effects of Small Water Surfaces on Turbulent Flow in the Atmospheric Boundary Layer: URANS Approch Implemented in OpenFOAM*, Manuscript submitted for publication in Environmental Modelling & Software (June 2016).

FULL TEXT CONFERENCE PAPERS

Frank Ohene Annor, **Ali Abbasi**, Nick van de Giesen, John Selker, Elizabeth Jachens, Ellen van Andel, Friso vos de Wael, Mojtaba Shafiei, *Promoting Water and Climate Education through the Trans-African Hydro-Meteorological Observatory*, the International Conference on Water and Environment in the New Millennium: Education and Capacity Building (WENM2016), December 2016, Tehran, Iran.

Ali Abbasi, Nick van de Giesen *Temperature Dynamics Investigation at Small and Shallow Lakes Using Hydrodynamic Model*, 11th International Conference on Hydroinformatics (HIC) 2014, August 2014, New York City, USA.

Ali Abbasi, Nick van de Giesen *Short-term Evaporation Estimating from Complex Small Lakes in Arid and Semi-arid Regions*, 11th International Conference on Hydroinformatics(HIC) 2014, August 2014, New York City, USA.

506469-L-sub01-bw-Abbasi
Processed on: 9-11-2016

PUBLISHED ABSTRACTS

Ali Abbasi, Frank Ohene Annor, Nick van de Giesen, Camille le Coz, *Simulating Airflow over Small Water Surfaces with WRF-OpenFOAM Coupled Model in the Upper East Region of Ghana*, 16th EMS Annual Meeting & 11th European Conference on Applied Climatology (ECAC), September 2016, Trieste, Italy.

Frank Ohene Annor, **Ali Abbasi**, Nick van de Giesen, Dirk Eilander, *Supporting Rural Sub-Saharan Africa Farmers through Satellite-based Water Level Gauging*, The 2016 European Space Agency Living Planet Symposium (LPS16), May 2016, Prague, Czech Republic.

Frank Ohene Annor, **Ali Abbasi**, Nick van de Giesen, Dirk Eilander, Gennadii Donchyts, *Operational Use of Satellites for Managing African Water Basins - A Case of Small Reservoirs in the Volta Basin*, Third Space for Hydrology Workshop (Hydrospace2015), September 2015, ESA-ESRIN, Frascati (Rome), Italy.

Frank Ohene Annor, **Ali Abbasi**, Nick van de Giesen, *Monitoring the Water Balance of Small Reservoirs in Semi-arid Regions from Space*, Mapping Water Bodies from Space(MWBS 2015), March 2015, ESA-ESRIN, Frascati (Rome), Italy.

Ali Abbasi, Frank Ohene Annor, Nick van de Giesen, *Developing a CFD-based Approach to Estimate Evaporation from Water Surfaces in (Semi-) Arid Regions*, EGU General Assembly 2015, Geophysical Research Abstracts, Vol. 17, EGU2015-10286, April 2015, Vienna, Austria.

Ali Abbasi, Nick van de Giesen,*Investigation of Temperature Dynamics in Shallow Lakes Using Three-dimensional CFD Model*, International Conference on Computational Methods in Water Resources, June 2014, Stuttgart, Germany.

Ali Abbasi, Shervan Gharari, Nick van de Giesen, *Developing a 3-Dimensional Hydrothermal Model for the Temperature Dynamics at Small and Shallow lakes*, AGU Fall Meeting, December 2013, San Francisco, USA.

Ali Abbasi, Nick van de Giesen, *Application of Three-Dimensional Hydrothermal Model for the Temperature Dynamics at Small and Shallow lakes*, Open Source CFD International Conference, October 2013, Hamburg, Germany.

Ali Abbasi, Nick van de Giesen, *Estimating of the Small Lakes Heat Budget in Energy Balance Approach*, 6th International Conference on Water Resources and Environment Research, June 2013, Koblenz, Germany.

Ali Abbasi, Nick van de Giesen, *Modeling of over Lake Wind Profile for Estimating Water Surface Evaporation Using Land-based meteorological Data*, EGU General Assembly 2013, Geophysical Research Abstracts, Vol. 15, EGU2013-12404, April 2013, Vienna, Austria.

Ali Abbasi, Nick van de Giesen, *Evaporation Modeling in Lakes in Arid and Semi-arid Regions*, EGU General Assembly 2012, Geophysical Research Abstracts, Vol. 154, EGU2012-933, April 2012, Vienna, Austria.

506469-L-sub01-bw-Abbasi
Processed on: 9-11-2016

REFERENCES

Abbasi, A., Annor, F. O., van de Giesen, N., 2015a. A Framework to Simulate Small and Shallow Inland Water Bodies in Semi-arid Regions. Advances in Water Resources (Manuscript re-submitted for publication).

Abbasi, A., Annor, F. O., van de Giesen, N., 2015b. Developing a CFD-based Approach to Estimate Evaporation from Water Surfaces in (Semi-)Arid Regions. Hydrological Processes (Manuscript re-submitted for publication).

Abbasi, A., Annor, F. O., van de Giesen, N., 2015c. The Effects of Small Water Surfaces on Turbulent Flow in the Atmospheric Boundary Layer: URANS Approch Implemented in OpenFOAM. Environmental Modelling & Software (Manuscript submitted for publication).

Abbasi, A., Annor, F. O., van de Giesen, N., 2016a. Effects of Atmosphere Stability Conditions on Heat Fluxes from Small Water Surfaces in (Semi-) Arid Regions. Hydrological Sciences Journal (Manuscript accepted for publication).

Abbasi, A., Annor, F. O., van de Giesen, N., 2016b. Investigation of Temperature Dynamics in Small and Shallow Reservoirs. Case Stuy: Lake Binaba, Upper East Region of Ghana. Water 8 (3), 1–24.

Abeysinghe, K., Nandalal, L., Piyasiri, S., 2005. Prediction of Thermal Stratification of the Kotmale Reservoir Using a Hydrodynamic Model. Journal of the National Science Foundation of Sri Lanka 33 (1), 25–36.

Abtew, W., Melesse, A., 2013. Lake Evaporation. In: Evaporation and Evapotranspiration: Measurements and Estimations. Springer Netherlands, Dordrecht, pp. 109–132.

ADMesh, 2015. ADMesh[online]. Available from: http://www.varlog.com/admesh-htm, [Accessed 20 November 2015].

Ahsan, A. K. M. Q., Blumberg, A. F., 1999. Three-dimensional Hydrothermal Model of Onondaga Lake, New York. Journal of Hydraulic Engineering 125 (9), 912–923.

Albertson, J., Parlange, M. B., 1999. Natural Integration of Scalar Fluxes from Complex Terrain. Advances in Water Resources 23 (3), 239–252.

Ali, S., Ghosh, N. C., Singh, R., 2008. Evaluating Best Evaporation Estimate Model for Water Surface Evaporation in Semi-arid Region, India. Hydrological Processes 22 (2), 1093– 1106.

Ali, S., Mishra, P. K., Islam, A., Alam, N. M., 2015. Simulation of Water Temperature in a Small Pond Using Parametric Statistical Models: Implications of Climate Warming. Journal of Environmental Engineering 142 (3), 1–13.

Alinot, C., Masson, C., 2005. $k-\varepsilon$ Model for the Atmospheric Boundary Layer Under Various Thermal Stratifications. Journal of Solar Energy Engineering 127, 438–443.

Amorocho, J., De Vries, J. J., 1980. A New Evaluation of the Wind Stress Coefficient over Water Surfaces. Journal of Geophysical Research 85 (C1), 433–442.

Anagnostopoulos, J. S., Bergeles, G., 1998. A Numerical Model for Wind Field and Pollu-

506469-L-sub01-bw-Abbasi
Processed on: 9-11-2016

tant Concentration Calculations over Complex Terrain. Application to Athens, Greece. Journal of Wind Engineering and Industrial Aerodynamics 73, 285–306.

Annor, F. O., Abbasi, A., van de Giesen, N., Bogaard, T., 2016. Flux Measurements over Small Lakes in Ghana's Upper East Region. Advances in Water Resources (Manuscript submitted for publication).

Annor, F. O., van de Giesen, N., Liebe, J., van der Zaag, P., Tilmant, A., Odai, S., 2009. Delineation of Small Reservoirs Using Radar Imagery in a Semi-arid Environment: A Case Study in the Upper East Region of Ghana. Physics and Chemistry of the Earth 34 (4-5), 309–315.

Antonopoulos, V., Gianniou, S. K., 2003. Simulation of Water Temperature and Dissolved Oxygen Distribution in Lake Vegoritis, Greece. Ecological Modelling 160, 39–53.

Appt, J., Imberger, J., Kobus, H., 2004. Basin-scale Motion in Stratified Upper Lake Constance. Limnology and Oceanography 49 (4), 919–933.

Assouline, S., Tyler, S., Tanny, J., Cohen, S., Bouzeid, E., Parlange, M., Katul, G., 2008. Evaporation from Three Water Bodies of Different Sizes and Climates: Measurements and Scaling Analysis. Advances in Water Resources 31 (1), 160–172.

Avissar, R., Pielke, R. A., 1989. A Parameterization of Heterogeneous Land Surfaces for Atmospheric Numerical Models and Its Impact on Regional Meteorology. Monthly Weather Review 117, 2113–2136.

Babajimopoulos, C., Papadopoulos, F., 1986. Mathematical Prediction of Thermal Stratification of Lake Ostrove(Vegorities), Greece. Water Resources Research 22 (11), 1590–1596.

Bagayoko, F., Yonkeu, S., Elbers, J., van de Giesen, N., feb 2007. Energy Partitioning over the West African Savanna: Multi-year Evaporation and Surface Conductance Measurements in Eastern Burkina Faso. Journal of Hydrology 334, 545–559.

Balogh, M., Parente, A., Benocci, C., 2012. RANS Simulation of ABL Flow over Complex Terrains Applying an Enhanced $k-\varepsilon$ Model and Wall Function Formulation: Implementation and Comparison for Fluent and OpenFOAM. Journal of Wind Engineering and Industrial Aerodynamics 104-106, 360–368.

Barthlott, C., Drobinski, P., Fesquet, C., Dubos, T., Pietras, C., 2007. Long-term Study of Coherent Structures in the Atmospheric Surface Layer. Boundary-Layer Meteorology 125 (1), 1–24.

Bechmann, A., 2006. Large-Eddy Simulation of Atmospheric Flow over Complex Terrain. Thesis(PhD), Risø National Laboratory, Technical University of Denmark.

Bednarz, T. P., Lei, C., Patterson, J. C., 2008. Unsteady Natural Convection Induced by Constant Surface Cooling in a Reservoir. Australian and New Zealand Industrial and Applied Mathematics Journal 48, 852–867.

Bednarz, T. P., Lei, C., Patterson, J. C., 2009. Unsteady Natural Convection Induced by Diurnal Temperature Changes in a Reservoir with Slowly Varying Bottom Topography. International Journal of Thermal Sciences 48, 1932–1942.

Beniston, M., 1986. The Influence of a Water Surface on Mesoscale Dynamics as a Function of Atmospheric Stability. Boundary-Layer Meteorology 36, 19–37.

Benjamin, C., Bogdan, T., Daniele, C., 2011. Hybrid Assessment Method for LES Models. In: Direct and Large-Eddy Simulation VIII. Vol. 15 of ERCOFTAC Series. Springer

506469-L-sub01-bw-Abbasi
Processed on: 9-11-2016

Netherlands, Dordrecht, pp. 33–38.

Benjamin Martinez, 2011. Wind Resource in Complex Terrain with OpenFOAM. Thesis(MSc), National Laboratory for Sustainable Energy, Technical University of Denmark.

Beyers, M., Jackson, D., Lynch, K., Cooper, A., Baasd, A., Delgado-Fernandezb, I., Dallairea, P.-O., 2010. Field Testing and CFD LES Simulation of Offshore Wind Flows over Coastal Dune Terrain in Northern Ireland. In: CWE2010. pp. 1–8.

Bigham Stephens, D. L., Carlson, R. E., Horsburgh, C. a., Hoyer, M. V., Bachmann, R. W., Canfield, D. E., 2015. Regional Distribution of Secchi Disk Transparency in Waters of the United States. Lake and Reservoir Management 31, 55–63.

Blanken, P. D., Rouse, W. R., Culf, A. D., Spence, C., Boudreau, L. D., Jasper, J. N., Kochtubajda, B., Schertzer, W. M., Marsh, P., Verseghy, D., 2000. Eddy Covariance Measurements of Evaporation from Great Slave Lake, Northwest Territories, Canada. Water Resources Research 36 (4), 1069–1077.

Blocken, B., Stathopoulos, T., Carmeliet, J., 2007. CFD Simulation of the Atmospheric Boundary Layer: Wall Function Problems. Atmospheric Environment 41, 238–252.

Bou-Zeid, E., Meneveau, C., Parlange, M. B., 2004. Large-Eddy Simulation of Neutral Atmospheric Boundary Layer Flow over Heterogeneous Surfaces: Blending Height and Effective Surface Roughness. Water Resources Research 40, 1–18.

Bower, S. M., Saylor, J. R., 2009. A Study of the Sherwood-Rayleigh Relation for Water Undergoing Natural Convection-Driven Evaporation. International Journal of Heat and Mass Transfer 52, 3055–3063.

Bradley, E. F., 1968. A Micrometeorological Study of Velocity Profiles and Surface Drag in the Region Modified by a Change in Surface Roughness. Quarterly Journal of the Royal Meteorological Society 94 (401), 361–379.

Branco, B. F., Torgersen, T., 2009. Predicting the Onset of Thermal Stratification in Shallow Inland Water Bodies. Aquatic Sciences 71 (1), 65–79.

Brockhaus, G. T., 2011. Hydrodynamic Design of Ship Bulbous Bows Considering Seaway and Operational Conditions. Thesis(PhD), Technischen Universit at Berlin.

Brutsaert, W., 1982. Evaporation into the Atmosphere: Theory, History, and Applications. Springer Netherlands, Dordrecht, Netherlands.

Brutsaert, W., 2005. Hydrology - An Introduction. Cambridge University Press, Cambridge, United Kingdom.

Businger, J. A., Wyngaard, J. C., Izumi, Y., Bradley, E. F., 1971. Flux-Profile Relationships in the Atmospheric Surface Layer. Journal of the Atmospheric Sciences 28, 181–189.

Cabot, W., Moin, P., 1999. Approximate Wall Boundary Conditions in the Large-Eddy Simulation of High Reynolds Number Flow. Flow, Turbulence and Combustion 63, 269–291.

Callister, E. V., 2008. A Three-Dimensional, Time-Dependent Circulation Model of Utah Lake. Thesis(MSc), Utah State University.

Cancelli, D. M., Chamecki, M., Dias, N. L., 2014. A Large-Eddy Simulation Study of Scalar Dissimilarity in the Convective Atmospheric Boundary Layer. Journal of the Atmospheric Sciences 71 (1), 3–15.

Cao, S., Tamura, T., 2006. Experimental Study on Roughness Effects on Turbulent Bound-

506469-L-sub01-bw-Abbasi
Processed on: 9-11-2016

ary Layer Flow over a Two-Dimensional Steep Hill. Journal of Wind Engineering and Industrial Aerodynamics 94, 1–19.

Carter, R., Kay, M., Weatherhead, K., 1999. Water Losses in Smallholder Irrigation Schemes. Agricultural Water Management 40, 15–24.

Casamitjana, X., Serra, T., Colomer, J., Baserba, C., Pérez-Losada, J., 2003. Effects of the Water Withdrawal in the Stratification Patterns of a Reservoir. Hydrobiologia 504, 21–28.

Casulli, V., 1997. Numerical Simulation of Three-dimensional Free Surface Flow in Isopycnal Co-ordinates. International Journal for Numerical Methods in Fluids 25, 645–658.

Casulli, V., 1999. A Semi-Implicit Finite Difference Method for Non-hydrostatic, Free-surface Flows. International Journal for Numerical Methods in Fluids 30, 425–440.

Casulli, V., Cheng, R. T., 1992. Semi-implicit Finite Difference Methods for Three-dimensional Shallow Water Flow. International Journal for Numerical Methods in Fluids 15, 629–648.

Cebeci, T., 2004. Analysis of Turbulent Flows. Elsevier Ltd, London, United Kingdom.

Chamecki, M., Meneveau, C., Parlange, M. B., 2008. A Hybrid Spectral/Finite-Volume Algorithm for Large-Eddy Simulation of Scalars in the Atmospheric Boundary Layer. Boundary-Layer Meteorology 128 (3), 473–484.

Charnock, H., 1955. Wind Stress on a Water Surface. Quarterly Journal of the Royal Meteorological Society 81 (350), 639–640.

Chen, G., Xiong, Q., Morris, P. J., Paterson, E. G., Sergeev, A., Wang, Y.-C., 2014. OpenFOAM for Computational Fluid Dynamics. Notices of the American Mathematical Society 61 (4), 354.

Chen, X., 2003a. A Free-surface Correction Method for Simulating Shallow Water Flows. Journal of Computational Physics 189, 557–578.

Chen, X., 2003b. A Fully Hydrodynamic Model for Three-dimensional, Free-surface Flows. International Journal for Numerical Methods in Fluids 42, 929–952.

Chen, Y., Wai, O. W. H., Li, Y. S., 2003. Numerical Model for Wave Refraction-diffraction Near Pearl River Estuary, China. Journal of Waterway, Port, Coastal, and Ocean Engineering 129 (6), 260–269.

Churchfield, M. J., 2013. Adding Complex Terrain and Stable Atmospheric Condition Capability to the Simulator for On/Offshore Wind Farm Applications (SOWFA). Technical report, The National Renewable Energy Laboratory, Colorado, United States.

Collaborative Organisation for ICT in Dutch Higher Education and Research, 2015. SURFsara[online]. Available from: https://www.surf.nl/en/services-and-products/hpc-cloud/technical-specifications/index.html, [Accessed 20 November 2015].

Corzo, S. F., Damián, S. M., Ramajo, D., Norberto, M. N., 2011. Numerical Simulation of Natural Convection Phenomena. Mecánica Computacional XXX, 277–296.

Craig, I., Aravinthan, V., 2007. Evaporation, Seepage and Water Quality Management in Storage Dams: A Review of Research Methods. Environmental Health 7 (3), 84–97.

Craig, I. P., 2006. Comparison of Precise Water Depth Measurements on Agricultural Storages with Open Water Evaporation Estimates. Agricultural Water Management 85, 193–200.

506469-L-sub01-bw-Abbasi
Processed on: 9-11-2016

Craig, P. D., Banner, M. L., 1994. Modeling Wave-enhanced Turbulence in the Ocean Surface Layer. Journal of Physical Oceanography 24, 2546–2559.

Crasto, G., 2007. Numerical Simulations of the Atmospheric Boundary Layer. Thesis(PhD), Facoltà di Ingegneria, Università degli Studi di Cagliari.

Croley, T. E., 1989. Verifiable Evaporation Modeling on the Laurentian Great Lakes. Water Resources Research 25 (5), 781.

Crosman, E. T., Horel, J. D., 2010. Sea and Lake Breezes: A Review of Numerical Studies. Boundary-Layer Meteorology 137, 1–29.

Dake, J. M. K., Harleman, D. R. F., 1969. Thermal Stratification in Lakes: Analytical and Laboratory Studies. Water Resources Research 5 (2), 484–495.

Davenport, D. C., Hudson, J. P., 1967. Changes in Evaporation Rates along a 17-KM Transect in the Sudan Gezira. Agricultural Meteorology 4, 339–352.

Davies, A. M., 1982a. Numerical Modelling of Stratified Flow: A Spectral Approach. Continental Shelf Research 2 (4), 275–300.

Davies, A. M., 1982b. On Computing the Three Dimensional Flow in a Stratified Sea Using the Galerkin Method. Applied Mathematical Modelling 6, 347–362.

Debolsky, V. K., Neymark, R. V., 1994. Thermally Non-uniform Flow in Water Reservoir: Numerical Investigation. Journal of Hydraulic Research 32, 25–40.

DeCosmo, J., Katsaros, K. B., Smith, S. D., Anderson, R. J., Oost, W. a., Bumke, K., Chadwick, H., 1996. Air-sea Exchange of Water Vapor and Sensible Heat: The Humidity Exchange Over the Sea (HEXOS) Results. Journal of Geophysical Research 101, 12001.

Defraeye, T., Blocken, B., Carmeliet, J., 2010. CFD Analysis of Convective Heat Transfer at the Surfaces of a Cube Immersed in a Turbulent Boundary Layer. International Journal of Heat and Mass Transfer 53, 297–308.

Defraeye, T., Blocken, B., Carmeliet, J., 2011. Convective Heat Transfer Coefficients for Exterior Building Surfaces: Existing Correlations and CFD Modelling. Energy Conversion and Management 52 (1), 512–522.

Defraeye, T., Blocken, B., Carmeliet, J., 2012. Analysis of Convective Heat and Mass Transfer Coefficients for Convective Drying of a Porous Flat Plate by Conjugate Modelling. International Journal of Heat and Mass Transfer 55, 112–124.

Delclaux, F., Coudrain, A., Condom, T., 2007. Evaporation Estimation on Lake Titicaca: A Synthesis Review and Modelling. Hydrological Processes 21, 1664–1677.

DELFT3D, 2016. Delft3D[online]. Available from https://oss.deltares.nl/web/delft3d, [Accessed 15 October 2016].

Derecki, J. A., 1981. Stability Effects on Great Lakes Evaporation. Journal of Great Lakes Research 7 (4), 357–362.

Dingman, S. L., 2015. Physical Hydrology, 3rd Edition. Waveland Press, Inc., Illinois, United States of America.

Dyer, A. J., 1967. The Turbulent Transport of Heat and Water Vapour in an Unstable Atmosphere. Quarterly Journal of the Royal Meteorological Society 93 (398), 501–508.

Dyer, A. J., Crawford, T. V., 1965. Observations of the Modification of the Microclimate at a Leading Edge. Quarterly Journal of the Royal Meteorological Society 91, 345–348.

Edson, J., Crawford, T., Crescenti, J., Farrar, T., Frew, N., Gerbi, G., Plueddemann, A., Trowbridge, J., Weller, R., Williams, A. J., Helmis, C., Hristov, T., Shen, L., Khelif, D., Jes-

506469-L-sub01-bw-Abbasi
Processed on: 9-11-2016

sup, A., Jonsson, H., Li, M., Mahrt, L., Skyllingstad, E., Vickers, D., McGillis, W., Zappa, C., Stanton, T., Wang, Q., Sullivan, P., Sun, J., Wang, S., Wilkin, J., Yue, D. K. P., 2007. The Coupled Boundary Layers and Air-Sea Transfer Experiment in Low Winds. Bulletin of the American Meteorological Society 88, 341–356.

Elbers, J., 2016. Alteddy[online]. Wageningen University, Available from: http://www.climatexchange.nl/projects/alteddy/index.htm, [Accessed 15 October 2016].

Elbers, J. A., 2002. Eddy Correlation System: User Manuel. Altera, Wageningen, Netherlnads.

Elo, A.-r., 2007. The Energy Balance and Vertical Thermal Structure of Two Small Boreal Lakes in Summer. Boreal Environment Research 12, 585–600.

Esau, I. N., Lyons, T. J., 2002. Effect of Sharp Vegetation Boundary on the Convective Atmospheric Boundary Layer. Agricultural and Forest Meteorology 114, 3–13.

Etemad-Shahidi, A., Faghihi, M., Imberger, J., 2010. Modelling Thermal Stratification and Artificial Destratification using DYRESM; Case study: 15-Khordad Reservoir. International Journal of Environmental Research 4 (3), 395–406.

Fairall, C. W., Bradley, E. F., Rogers, D. P., 1996. Bulk Parameterization of Air-Sea Fluxes for Tropical Ocean-Global Atmosphere Coupled-Ocean Atmosphere Response. Journal of Geophysical Research 101 (C2), 3747–3764.

Falconer, R. A., George, D. G., Hall, P., 1991. Three-dimensional Numerical Modelling of Wind-driven Circulation in a Shallow Homogeneous Lake. Journal of Hydrology 124, 59–79.

Fan, J., Furbo, S., 2012. Thermal Stratification in a Hot Water Tank Established by Heat Loss from the Tank. Solar Energy 86 (11), 3460–3469.

Faulkner, J. W., Steenhuis, T., van De Giesen, N., Andreini, M., Liebe, J. R., 2008. Water Use and Productivity of Two Small Reservoir Irrigation Schemes in Ghana's Upper East Region. Irrigation and Drainage 57, 151–163.

Ferrarin, C., Umgiesser, G., 2005. Hydrodynamic Modeling of a Coastal Lagoon: The Cabras Lagoon in Sardinia, Italy. Ecological Modelling 188, 340–357.

Ferziger, J. H., Perić, M., 2002. Computational Methods for Fluid Dynamics, 3rd Edition. Springer-Verlag, Berlin, Germany.

Fesquet, C., Drobinski, P., Barthlott, C., Dubos, T., 2009. Impact of Terrain Heterogeneity on Near-Surface Turbulence Structure. Atmospheric Research 94, 254–269.

Figuerola, P. I., Berliner, P. R., 2005. Evapotranspiration under Advective Conditions. International Journal of Biometeorology 49, 403–416.

Finch, J., Calver, A., 2008. Methods for the Quantification of Evaporation from Lakes. Technical report, The World Meteorological Organization's Commission for Hydrology.

Flores, F., Garreaud, R., Muñoz, R. C., 2013. CFD Simulations of Turbulent Buoyant Atmospheric Flows over Complex Geometry: Solver Development in OpenFOAM. Computers & Fluids 82, 1–13.

Fluent, 2006. Natural Convection and Buoyancy-Driven Flows[online]. Available from http://aerojet.engr.ucdavis.edu/fluenthelp/html/ug/node572.htm, [Accessed 20 November 2015].

Foudhil, H., Brunet, Y., Caltagirone, J. P., 2005. A Fine-Scale $k-\varepsilon$ Model for Atmospheric

Flow over Heterogeneous Landscapes. Environmental Fluid Mechanics 5, 247–265.

Fowe, T., Karambiri, H., Paturel, J.-E., Poussin, J.-C., Cecchi, P., 2015. Water Balance of Small Reservoirs in the Volta Basin : A Case Study of Boura Reservoir in Burkina Faso. Agricultural Water Management 152, 99–109.

Fredriksson, S., 2011. A buoyantBoussinesqSurfactantFoam Tutorial: An Introduction to FAM. Technical report, Chalmers University of Technology.

Fu, G., Charles, S. P., Yu, J., 2009. A Critical Overview of Pan Evaporation Trends over the Last 50 Years. Climatic Change 97 (1-2), 193–214.

Fu, G., Liu, C., Chen, S., Hong, J., 2004. Investigating the Conversion Coefficients for Free Water Surface Evaporation of Different Evaporation Pans. Hydrological Processes 18 (12), 2247–2262.

Gallego-Elvira, B., Baille, A., Martín-Gorriz, B., Maestre-Valero, J., Martínez-Alvarez, V., 2012. Evaluation of Evaporation Estimation Methods for a Covered Reservoir in a Semi-arid Climate (South-Eastern Spain). Journal of Hydrology 458-459, 59–67.

Gao, Y., Chen, F., Barlage, M., Liu, W., Cheng, G., Li, X., Yu, Y., Ran, Y., Li, H., Peng, H., Ma, M., 2008. Enhancement of Land Surface Information and its Impact on Atmospheric Modeling in the Heihe River Basin, Northwest China. Journal of Geophysical Research 113, 1–19.

Garratt, J., 1994. Review: the Atmospheric Boundary Layer. Earth-Science Reviews 37 (1-2), 89–134.

Gianniou, S., Antonopoulos, V., 2007. Evaporation and Energy Budget in Lake Vegoritis, Greece. Journal of Hydrology 345 (3-4), 212–223.

Giorgi, F., Avissar, R., 1997. Representation of Heterogeneity Effects in Earth System Modeling: Experience from Land Surface Modeling. Reviews of Geophysics 35 (4), 413–437.

Goff, J. A., 1957. Saturation Pressure of Water on the New Kelvin Temperature Scale. In: Transactions of the American Society of Heating and Ventilating Engineers. pp. 347–354.

Gokbulak, F., Ozhan, S., 2006. Water Loss through Evaporation from Water Surfaces of Lakes and Reservoirs in Turkey. E-WAter 2006, 1–6.

Google, 2015. Google Earth[online]. Available from https://www.google.com/earth/, [Accessed 20 November 2015].

Gooseff, M. N., Strzepek, K., Chapra, S. C., 2005. Modeling the Potential Effects of Climate Change on Water Temperature Downstream of a Shallow Reservoir, Lower Madison River, MT. Climatic Change 68, 331–353.

Goudsmit, G.-H., Burchard, H., Peeters, F., Wuest, A., 2002. Application of $k-\varepsilon$ Turbulence Models to Enclosed Basins: The Role of Internal Seiches. Journal of Geophysical Research 107 (C12), 1–13.

Gschaider, B., 2015a. groovyBC Boundary Condition[online]. Available from: https://openfoamwiki.net/index.php/Contrib/groovyBC, [Accessed 20 November 2015].

Gschaider, B., 2015b. Swak4Foam[online]. Available from: https://openfoamwiki.net/index.php/Contrib/swak4Foam, [Accessed 28 October 2016].

Han, B.-P., Armengol, J., Carlos Garcia, J., Comerma, M., Roura, M., Dolz, J., Straskraba, M., 2000. The Thermal Structure of Sau Reservoir (NE: Spain): A Simulation Approach.

506469-L-sub01-bw-Abbasi
Processed on: 9-11-2016

Ecological Modelling 125, 109–122.

Haque, M. M., Constantinescu, G., Weber, L., 2007. Validation of a 3D RANS Model to Predict Flow and Stratification Effects Related to Fish Passage at Hydropower Dams. Journal of Hydraulic Research 45 (6), 787–796.

Harbeck, G. E., 1962. A Practical Field Technique for Measuring Reservoir Evaporation Utilizing Mass-Transfer Theory. Technical report, United States Department of the Interior.

Hargreaves, D., Wright, N., 2007. On the Use of the $k-\varepsilon$ Model in Commercial CFD Software to Model the Neutral Atmospheric Boundary Layer. Journal of Wind Engineering and Industrial Aerodynamics 95, 355–369.

Heikinheimo, M., Kangas, M., Tourula, T., Vena, A., Tattari, S., 1999. Momentum and Heat Fluxes over Lakes Tamnaren and Raksjo Determined by the Bulk-aerodynamic and Eddy-Correlation Methods. Agricultural and Forest Meteorology 89-99, 521–534.

Henderson-Sellers, B., 1984. Development and Application of a Hydroclimate Lake Stratification Model. Ecological Modelling 21, 233–246.

Henderson-Sellers, B., 1986. Calculating the surface energy balance for lake and reservoir modeling: A review. Reviews of Geophysics 24 (3), 625–649.

Henderson-Sellers, B., 1988. Sensitivity of Thermal Stratification Models to Changing Boundary Conditions. Applied Mathematical Modelling 12, 31–43.

Herb, W. R., Stefan, H. G., 2005. Dynamics of Vertical Mixing in a Shallow Lake with Submersed Macrophytes. Water Resources Research 41 (W02023), 1–14.

Hertwig, D., Leitl, B., Schatzmann, M., 2011. Organized Turbulent Structures- Link between Experimental Data and LES. Journal of Wind Engineering and Industrial Aerodynamics 99, 296–307.

Hicks, B., 1975. A Procedure for the Formulation of Bulk Transfer Coefficients over Water. Boundary-Layer Meteorology 8 (3), 515–524.

HOBOTidbiT, 2015. HOBO TidbiT v2 Water Temperature Data Logger-Specifications[online]. Available from: http://www.onsetcomp.com/products/data-loggers/utbi-001, [Accessed 20 November 2015].

Hodges, B., Dallimore, C., 2014. Estuary, Lake and Coastal Ocean Model: ELCOM v3.0 User Manual. Center for Water Research, University of Western Australia, Australia.

Hodges, B. R., Imberger, J., Laval, B., Appt, J., 2000a. Modeling the Hydrodynamics of Stratified Lakes. In: Hydroinformatics 2000. pp. 1–14.

Hodges, B. R., Imberger, J., Saggio, A., Winters, K. B., 2000b. Modeling basin-scale internal waves in a stratified lake. Limnology and Oceanography 45 (7), 1603–1620.

Hondzo, M., Stefan, H., 1993. Lake Water Temperature Simulation Model. Journal of Hydraulic Engineering 119 (11), 1251–1273.

Hostetler, S. W., Bartlein, P. J., 1990. Simulation of Lake Evaporation with Application to Modeling Lake Level Variations of Harney-Malheur Lake, Oregon. Water Resources Research 26 (10), 2603–2612.

Hsieh, K.-J., Lien, F.-S., Yee, E., 2007. Numerical Modeling of Passive Scalar Dispersion in an Urban Canopy Layer. Journal of Wind Engineering and Industrial Aerodynamics 95, 1611–1636.

Huang, C., 2003. Modification of the Charnock Wind Stress Formula to Include the Ef-

506469-L-sub01-bw-Abbasi
Processed on: 9-11-2016

fects of Free Convection and Swell. In: Advanced Methods for Practical Applications in Fluid Mechanics[edited by Steven A. Jones]. pp. 47–71.

Huser, A., Nilsen, P. J., Skatun, H., 1997. Application of $k-\varepsilon$ Model to the Stable ABL: Pollution in Complex Terrain. Journal of Wind Engineering and Industrial Aerodynamics 67-68, 425–436.

Hussein, A. S., El-Shishiny, H., 2009. Influences of Wind Flow over Heritage Sites: A Case Study of the Wind Environment over the Giza Plateau in Egypt. Environmental Modelling & Software 24 (3), 389–410.

Idso, S. B., Gilbert, R. G., 1974. On the universality of the Poole and Atkins Secchi disk-light extinction equation. Journal of Applied Ecology 11 (1), 399–401.

Incropera, P. F., DeWitt, D. P., 1996. Fundamentals of Heat and Mass Transfer, forth Edition. John Wiley & Sons, New York, United States of America.

Jackson, N. A., 1976. The Propagation of Modified Flow Downstream of a Change in Surface Roughness. Quarterly Journal of the Royal Meteorological Society 102, 924–933.

Jacobs, A., Verhoef, A., 1997. Soil Evaporation from Sparse Natural Vegetation Estimated from Sherwood Numbers. Journal of Hydrology 189, 443–452.

Jacobs, A. F., Jetten, T. H., Lucassen, D., Heusinkveld, B. G., Joost P., N., 1997. Diurnal Temperature Fluctuations in a Natural Shallow Water Body. Agricultural and Forest Meteorology 88 (1-4), 269–277.

Jacovides, C., Papaioannou, G., Kerkides, P., 1988. Micro and Large-Scale Parameters Evaluation of Evaporation from a Lake. Agricultural Water Management 13, 263–272.

Jin, K.-R., Hamrick, J. H., Tisdale, T., 2000. Application of Three-dimensional Hydrodynamic Model for Lake Okeechobee. Journal of Hydraulic Engineering 126 (10), 758–771.

Jin, K.-R., Ji, Z.-G., Hamrick, J. H., 2002. Modeling Winter Circulation in Lake Okeechobee, Florida. Journal of Waterway, Port, Coastal and Ocean Engineering 128 (3), 114–125.

Joubert, E. C., Harms, T. M., Muller, A., Hipondoka, M., Henschel, J. R., 2012. A CFD Study of Wind Patterns over a Desert Dune and the Effect on Seed Dispersion. Environmental Fluid Mechanics 12, 23–44.

Józsa, J., Milici, B., Napoli, E., 2007. Numerical Simulation of Internal Boundary-Layer Development and Comparison with Atmospheric Data. Boundary-Layer Meteorology 123, 159–175.

Katul, G. G., Parlange, M. B., 1992. A Penman-Brutsaert Model for Wet Surface Evaporation. Water Resources Research 28 (1), 121–126.

Keller, A., Sakthivadivel, R., Seckler, D., 2000. Water Scarcity and the Role of Storage in Development. Technical report, International Water Management Institute, Colombo, Sri Lanka.

Kennedy, M. G., Ahlfeld, D. P., Schmidt, D. P., Tobiason, J. E., 2006. Three-dimensional Modeling for Estimation of Hydraulic Retention Time in a Reservoir. Journal of Environmental Engineering 132 (9), 976–984.

Kim, D. G., Cho, H. Y., 2006. Modeling the Buoyant Flow of Heated Water Discharged from Surface and Submerged Side Outfalls in Shallow and Deep Water with a Cross Flow. Environmental Fluid Mechanics 6 (6), 501–518.

506469-L-sub01-bw-Abbasi
Processed on: 9-11-2016

Kim, H., Patel, V., Lee, C., 2000. Numerical Simulation of Wind Flow over Hilly Terrain. Journal of Wind Engineering and Industrial Aerodynamics 87, 45–60.

Kim, H. G., Lee, C. M., Lim, H. C., Kyong, N. H., 1997. An Experimental and Numerical Study on the Flow over Two-dimensional Hills. Journal of Wind Engineering and Industrial Aerodynamics 66, 17–33.

Kim, H. G., Patel, V. C., 2000. Test of Turbulence Models for Wind Flow over Terrain with Separation and Recirculation. Boundary-Layer Meteorology 94, 5–21.

Kim, S.-E., Boysan, F., 1999. Application of CFD to Environmental Flows. Journal of Wind Engineering and Industrial Aerodynamics 81 (1-3), 145–158.

Kirillin, G., 2002. Modeling of the Vertical Heat Exchange in Shallow Lakes. Thesis(PhD), Humboldt University of Berlin.

Kirillin, G., 2010. Modeling the Impact of Global Warming on Water Temperature and Seasonal Mixing Regimes in Small Temperate Lakes. Boreal Environment Research 15, 279–293.

Kljun, N., Calanca, P., Rotach, M. W., Schmid, H. P., 2015. A Simple Two-dimensional Parameterisation for Flux Footprint Prediction (FFP). Geoscientific Model Development 8, 3695–3713.

Koblitz, T., Bechmann, A., Sogachev, A., 2013. Computational Fluid Dynamics Model of Stratified Atmospheric Boundary Layer Flow. Wind Energy 18, 75–89.

Koçyigit, M., Falconer, R., 2004a. Modelling of Wind-induced Currents in Water Basins. Proceedings of the ICE-Water, 197–210.

Koçyigit, M. B., Falconer, R. A., 2004b. Three-dimensional Numerical Modelling of Wind-driven Circulation in a Homogeneous Lake. Advances in Water Resources 27 (12), 1167–1178.

Lang, A. R. G., Evans, G. N., Ho, P. Y., 1974. The Influence of Local Advection on Evapotranspiration from Irrigated Rice in a Semi-arid Region. Agricultural Meteorology 13, 5–13.

Lang, A. R. G., McNaughton, K. G., Fazu, C., Bradely, E. F., Ohtaki, E., 1983. An Experimental Appraisal of the Terms in the Heat and Moisture Flux Equations for Local Advection. Boundary-Layer Meteorology 25, 89–102.

Lap, B. Q., Mori, K., 2007. A Two-dimensional Numerical Model of Wind-induced Flow and Water Quality in Closed Water Bodies. Paddy and Water Environment 5, 29–40.

Laval, B., Imberger, J., Hodges, B. R., Stocker, R., 2003. Modeling Circulation in Lakes: Spatial and Temporal Variations. Limnology and Oceanography 48 (3), 983–994.

Le Quéré, P., 1991. Accurate Solutions to the Square Thermally Driven Cavity at High Rayleigh Number. Computers & Fluids 20 (1), 29–41.

Lee, H. S., Yamashita, T., Haggag, M., 2009. Modelling Hydrodynamics in Yachiyo Lake Using a Non-hydrostatic General Circulation Model with Spatially and Temporally Varying Meteorological Conditions. Hydrological Processes 23, 1973–1987.

Lee, J. W., 2007. Numerical Modelling of Temperature-Induced Circulation in Shallow Water Bodies and Application to Torrens Lake, South Australia. Thesis(PhD), The University of Adelaide Applied Mathematics.

Legates, D. R., McCabe Jr., G. J., 1999. Evaluating the Use of "goodness-of-fit" Measures in Hydrologic and Hydroclimatic Model Validation. Water Resources Research 35 (1),

506469-L-sub01-bw-Abbasi
Processed on: 9-11-2016

233–241.

Lei, C., Patterson, J. C., 2001. Two- and Three-Dimensional Temperature Structures in a Shallow Wedge Subject to Solar Radiation. In: 14th Australasian Fluid Mechanics Conference. pp. 359–362.

Lei, C., Patterson, J. C., 2002. Natural Convection in a Reservoir Sidearm Subject To Solar Radiation: a Two-Dimensional Simulation. Numerical Heat Transfer, Part A 42, 13–32.

Leon, L., Lam, D., Schertzer, W., Swayne, D., Imberger, J., 2007. Towards Coupling a 3D Hydrodynamic Lake Model with the Canadian Regional Climate Model: Simulation on Great Slave Lake. Environmental Modelling & Software 22 (6), 787–796.

Lettau, H., Zabransky, J., 1968. Interrelated Changes of Wind Profile Structure and Richardson Number in Air Flow from Land to Inland Lakes. Journal of Atmospheric Sciences 25, 718–728.

Liebe, J., Andreini, M., van de Giesen, N., Steenhuis, T., 2007a. The Small Reservoirs Project: Research to Improve Water Availability and Economic Development in Rural Semi-arid Areas. Technical report, Small Reservoir Project.

Liebe, J., van de Giesen, N., Steenhuis, T., 2007b. Evaporation Losses from Small Reservoirs. Technical report, Small Reservoir Project.

Liebe, J. R., 2009. Hydrology of Small Reservoirs in Semi-arid Northern Ghana. Thesis(PhD), Cornell University.

Liebe, J. R., van de Giesen, N., Andreini, M., Walter, M. T., Steenhuis, T. S., 2009. Determining Watershed Response in Data Poor Environments with Remotely Sensed Small Reservoirs as Runoff Gauges. Water Resources Research 45 (7), 1–12.

Liu, J., Chen, J. M., Black, T. A., Novak, M. D., 1996. $E-\varepsilon$ Modelling of Turbulent Air Flow Downwind of a model forest edge. Boundary-Layer Meteorology 77, 21–44.

Liu, W.-C., Chen, W.-B., Chiu, C.-Y., 2012. Numerical Modeling of Hydrodynamic and Hydrothermal Characteristics in Subtropical Alpine Lake. Applied Mathematical Modelling 36, 2094–2109.

Livingstone, D. M., Imboden, D. M., 1989. Annual Heat Balance and Equilibrium Temperature of Lake Aegeri, Switzerland. Aquatic Sciences 51 (4), 351–369.

Losordo, T. M., Piedrahita, R. H., 1991. Modelling Temperature Variation and Thermal Stratification in Shallow Aquaculture Ponds. Ecological Modelling 54, 189–226.

Luna, Y. F., Mochidaa, A., Murakamib, S., Yoshinoa, H., Shirasawa, T., 2003. Numerical Simulation of Flow over Topographic Features by Revised $k-\varepsilon$ Models. Journal of Wind Engineering and Industrial Aerodynamics 91, 231–245.

Lyons, T. J., Halldin, S., 2004. Surface Heterogeneity and the Spatial Variation of Fluxes. Agricultural and Forest Meteorology 121, 153–165.

MacKay, M. D., Neale, P. J., Arp, C. D., Domis, L. N. S., Fang, X., Gal, G., Jöhnk, K. D., Kirillin, G., Lenters, J. D., Litchman, E., MacIntyre, S., Marsh, P., Melack, J., Mooij, W. M., Peeters, F., Quesada, A., Schladow, S. G., Schmid, M., Spence, C., Stokes, S. L., 2009. Modeling Lakes and Reservoirs in the Climate System. Limnology and Oceanography 54 (6, part 2), 2315–2329.

Mahrt, L., MacPherson, J. I., Desjardins, R., 1994. Observations of Fluxes over Heterogeneous Surfaces. Boundary-Layer Meteorology 67, 345–367.

Majdoubi, H., Boulard, T., Fatnassi, H., Bouirden, L., 2009. Airflow and Microclimate Pat-

506469-L-sub01-bw-Abbasi
Processed on: 9-11-2016

terns in a One-hectare Canary Type Greenhouse: An Experimental and CFD Assisted Study. Agricultural and Forest Meteorology 149 (6-7), 1050–1062.

Maric, T., Hopken, J., Mooney, K., 2014. The OpenFOAM Technology Primer, 1st Edition. sourceflux.

Markfort, C. D., Perez, A. L. S., Thill, J. W., Jaster, D. a., Porté-Agel, F., Stefan, H. G., 2010. Wind Sheltering of a Lake by a Tree Canopy or Bluff Topography. Water Resources Research 46, 1–13.

Maronga, B., Moene, A. F., van Dinther, D., Raasch, S., Bosveld, F. C., Gioli, B., 2013. Derivation of Structure Parameters of Temperature and Humidity in the Convective Boundary Layer from Large-Eddy Simulations and Implications for the Interpretation. Boundary-Layer Meteorology, 1–30.

Marshall, J., Adcroft, A., Hill, C., Perelman, L., Heisey, C., 1997. A Finite-Volume, Incompressible Navier Stokes Model for Studies of the Ocean on Parallel Computers. Journal of Geophysical Research 102 (C3), 5753–5766.

Martínez Alvarez, V., González-Real, M., Baille, A., Martínez, J. M., 2007. A Novel Approach for Estimating the Pan Coefficient of Irrigation Water Reservoirs. Agricultural Water Management 92 (1-2), 29–40.

Martínez-Granados, D., Maestre-Valero, J. F., Calatrava, J., Martínez-Alvarez, V., 2011. The Economic Impact of Water Evaporation Losses from Water Reservoirs in the Segura Basin, SE Spain. Water Resources Management 25, 3153–3175.

Massel, S. R., 1999. Fluid Mechanics for Marine Ecologists. Springer, Berlin, Germany.

McGloin, R., McGowan, H., McJannet, D., Cook, F., Sogachev, A., Burn, S., 2014. Quantification of Surface Energy Fluxes from a Small Water Body Using Scintillometry and Eddy Covariance. Water Resources Research 50, 494–513.

McJannet, D. L., Webster, I. T., Cook, F. J., 2012. An Area-dependent Wind Function for Estimating Open Water Evaporation Using Land-based Meteorological Data. Environmental Modelling & Software 31, 76–83.

Meissner, C., Gravdahl, A. R., Steensen, B., 2009. Including Thermal Effects in CFD Wind Flow Simulations. Journal of the Environmental Sciences 18 (8), 833–839.

MeshLab, 2015. MeshLab[online]. Available from: http://meshlab.sourceforge.net/, [Accessed 10 October 2016].

Milashuk, S., Crane, W. A., 2011. Wind Speed Prediction Accuracy and Expected Errors of RANS Equations in Low Relief Inland Terrain for Wind Resource Assessment Purposes. Environmental Modelling & Software 26 (4), 429–433.

Momii, K., Ito, Y., 2008. Heat Budget Estimates for Lake Ikeda, Japan. Journal of Hydrology 361 (3-4), 362–370.

Monin, A. S., Obukhov, A. M., 1959. A Note on General Classification of Motions in a Baroclinic Atmosphere. Tellus (11), 159–162.

Monteith, J. L., Unsworth, M. H., 2008. Principles of Environmental Physics, 3rd Edition. Elsevier Inc., Oxford, United Kingdom.

Mugabe, F., Hodnett, M. G., Senzanje, A., 2003. Opportunities for Increasing Productive Water Use from Dam Water: A Case Study from Semi-arid Zimbabwe. Agricultural Water Management 62 (2), 149–163.

Munro, D. S., Oke, T. R., 1975. Aerodynamic Boundary-Layer Adjustment over a Crop in

506469-L-sub01-bw-Abbasi
Processed on: 9-11-2016

Neutral Stability. Boundary-Layer Meteorology 9, 53–61.

Nadeau, D. F., Pardyjak, E. R., Higgins, C. W., Fernando, H. J. S., Parlange, M. B., 2011. A Simple Model for the Afternoon and Early Evening Decay of Convective Turbulence Over Different Land Surfaces. Boundary-Layer Meteorology 141 (2), 301–324.

Naithani, J., Plisnier, P.-D., Deleersnijder, E., 2007. A Simple Model of the Eco-Hydrodynamics of the Epilimnion of Lake Tanganyika. Freshwater Biology 52, 2087–2100.

OpenFOAM, 2015. CFD Direct: The Architects of OpenFOAM[online]. Available from: http://cfd.direct/, [Accessed 28 October 2016].

ÓSullivan, J. P., Archer, R. A., Flay, R. G. J., 2011. Consistent Boundary Conditions for Flows within the Atmospheric Boundary Layer. Journal of Wind Engineering and Industrial Aerodynamics 99 (1), 65–77.

Panofsky, H. A., Petersen, E. L., 1972. Wind Profiles and Change of Terrain Roughness at Riso. Quarterly Journal of the Royal Meteorological Society 98, 845–854.

Panofsky, H. A., Townsend, A. A., 1964. Change of Terrain Roughness and the Wind Profile. Quarterly Journal of the Royal Meteorological Society 90, 147–155.

Parente, A., Gorlé, C., van Beeck, J., Benocci, C., 2011. Improved $k-\varepsilon$ Model and Wall Function Formulation for the RANS Simulation of ABL Flows. Journal of Wind Engineering and Industrial Aerodynamics 99, 267–278.

Parlange, M. B., Eichinger, W. E., Albertson, J. D., 1995. Regional Scale Evaporation and the Atmospheric Boundary Layer. Reviews of Geophysics 33 (1), 99–124.

Pattanapol, W., Wakes, S. J., Hilton, M. J., Dickinson, K. J., 2008. Modeling of Surface Roughness for Flow over a Complex Vegetated Surface. International Journal of Engineering and Natural Sciences 2 (1), 18–26.

Pauken, M. T., 1999. An Experimental Investigation of Combined Turbulent Free and Forced Evaporation. Experimental Thermal and Fluid Science 18, 334–340.

Pendergrass, W., Arya, S. P. S., 1984. Dispersion in Neutral Boundary Layer over a Step Change in Surface Roughness-I. Mean Flow and Turbulence Structure. Atmospheric Environment 18 (7), 1267–1279.

Perroud, M., Goyette, S., 2010. Impact of Warmer Climate on Lake Geneva Water-temperature Profiles. Boreal Environment Research 15, 255–278.

Petersen, E. L., Taylor, P. A., 1973. Some Comparisons between Observed Wind Profiles at Riso and Theoretical Predictions for Flow over Inhomogeneous Terrain. Quarterly Journal of the Royal Meteorological Society 99, 329–336.

Pielke, R. A., Uliasz, M., 1998. Use of Meteorological Models as Input to Regional and Mesoscale Air quality Models - Limitations and Strengths. Atmospheric Environment 32 (8), 1455–1466.

Pieterse, J. E., 2013. CFD Investigation of the Atmospheric Boundary Layer under Different Thermal Stability Conditions. Thesis(MSc), Stellenbosch University.

Piomelli, U., 2008. Wall-layer Models for Large-Eddy Simulations. Progress in Aerospace Sciences 44, 437–446.

Piomelli, U., Balaras, E., 2002. Wall-layer Models for Large-Eddy Simulations. Annual Review of Fluid Mechanics 34, 349–374.

Politano, M., Haque, M. M., Weber, L. J., 2008. A Numerical Study of the Temperature

506469-L-sub01-bw-Abbasi
Processed on: 9-11-2016

Dynamics at McNary Dam. Ecological Modelling 212, 408–421.

Pontiggia, M., Derudi, M., Busini, V., Rota, R., 2009. Hazardous Gas Dispersion: A CFD Model Accounting for Atmospheric Stability Classes. Journal of Hhazardous Materials 171, 739–47.

Porté-Agel, F., Lu, H., Wu, Y.-T., 2014. Interaction between Large Wind Farms and the Atmospheric Boundary Layer. In: Procedia IUTAM. Vol. 10. Elsevier B.V., pp. 307–318.

Porté-Agel, F., Wu, Y.-T., Lu, H., Conzemius, R. J., 2011. Large-Eddy Simulation of Atmospheric Boundary Layer Flow through Wind Turbines and Wind Farms. Journal of Wind Engineering and Industrial Aerodynamics 99, 154–168.

Poussin, J. C., Renaudin, L., Adogoba, D., Sanon, A., Tazen, F., Dogbe, W., Fusillier, J. L., Barbier, B., Cecchi, P., 2015. Performance of Small Reservoir Irrigated Schemes in the Upper Volta Basin: Case Studies in Burkina Faso and Ghana. Water Resources and Rural Development 6, 50–65.

Priestley, C. H. B., Taylor, R. J., 1972. On the Assessment of Surface Heat Flux and Evaporation Using Large-Scale Parameters. Monthly Weather Review 100, 81–92.

Prospathopoulos, J., Voutsinas, S. G., 2006. Implementation Issues in 3D Wind Flow Predictions Over Complex Terrain. Journal of Solar Energy Engineering 128, 539.

Prospathopoulos, J. M., Politis, E. S., Chaviaropoulos, P. K., 2012. Application of a 3D RANS Solver on the Complex Hill of Bolund and Assessment of the Wind Flow Predictions. Journal of Wind Engineering and Industrial Aerodynamics 107-108, 149–159.

QGIS, 2015. QGIS: A Free and Open Source Geographic Information System[online]. Available from: http://www2.qgis.org/en/site/, [Accessed 28 October 2016].

Raupach, M. R., Finnigan, J. J., Brunei, Y., 1996. Coherent Eddies and Turbulence in Vegetation Canopies: The Mixing-Layer Analogy. Boundary-Layer Meteorology 78 (3-4), 351–382.

Raupach, M. R., Thom, A. S., Edwards, I., 1980. A Wind-tunnel Study of Turbulent Flow Close to Regularly Arrayed Rough Surfaces. Boundary-Layer Meteorology 18, 373–397.

Renfrew, I. A., Moore, G. W. K., Guest, P. S., Bumke, K., 2002. A Comparison of Surface Layer and Surface Turbulent Flux Observations over the Labrador Sea with ECMWF Analyses and NCEP Reanalyses. Journal of Physical Oceanography 32, 383–400.

Rhoads, J., 2014. Effects of Grid Quality on Solution Accuracy. Technical report.

Rider, N. E., Philip, J. R., Bradley, E. F., 1964. The Horizontal Transport of Heat and Moisture in a Micrometeorological Study. Quarterly Journal of the Royal Meteorological Society 84, 507–530.

Rohdin, P., Moshfegh, B., 2007. Numerical Predictions of Indoor Climate in Large Industrial Premises. A Comparison between Different $k-\varepsilon$ Models Supported by Field Measurements. Building and Environment 42, 3872–3882.

Rosenberry, D., Winter, T., Buso, D., Likens, G., 2007. Comparison of 15 Evaporation Methods Applied to a Small Mountain Lake in the Northeastern USA. Journal of Hydrology 340 (3-4), 149–166.

Rouse, W. R. W. R., Oswald, C. M. C. M., Binyamin, J., Blanken, P. D. P. D., Schertzer, W. M. W. M., Spence, C., 2003. Interannual and Seasonal Variability of the Surface Energy Balance and Temperature of Central Great Slave Lake. Journal of Hydrometeorology 4 (4), 720–730.

506469-L-sub01-bw-Abbasi
Processed on: 9-11-2016

Rueda, F. J., Schladow, S. G., 2003. Dynamics of Large Polymictic Lake. II: Numerical Simulations. Journal of Hydraulic Engineering 129 (2), 92–101.

Sartori, E., 2000. A Critical Review on Equations Employed for the Calculation of the Evaporation Rate from Free Water Surfaces. Solar Energy 68 (1), 77–89.

Schertzer, W. M., Rouse, W. R., Blanken, P. D., Walker, A. E., 2003. Over-lake Meteorology and Estimated Bulk Heat Exchange of Great Slave Lake in 1998 and 1999. Journal of Hydrometeorology 4 (4), 649–659.

Shih, T.-H., Liou, W. W., Shabbir, A., Yang, Z., Zhu, J., 1995. A new $k-\varepsilon$ Eddy Viscosity Model for High Reynolds Number Turbulent Flows. Computers & Fluids 24 (3), 227–238.

Shufen, S., Jinfeng, Y., Nan, X., Changhai, S., 2007a. Development of a Model for Water and Heat Exchange Between the Atmosphere and a Water Body. Advances in Atmospheric Sciences 24 (5), 927–938.

Shufen, S., Jinfeng, Y., Xia, N., Changhai, S., 2007b. Development of a Model for Water and Heat Exchange between the Atmosphere and a Water Body. Advances in Atmospheric Sciences 24 (5), 927–938.

Sill, B. L., 1983. Free and Forced Convection Effects on Evaporation. Journal of Hydraulic Engineering 109 (9), 1216–1231.

Silvester, S. A., Lowndes, I. S., Hargreaves, D. M., 2009. A Computational Study of Particulate Emissions from an Open Pit Quarry under Neutral Atmospheric Conditions. Atmospheric Environment 43 (40), 6415–6424.

Singh, V. P., Xu, C.-Y., 1997a. Evaluation and Generalization of 13 Mass-Transfer Equations for Determining Free Water Evaporation. Hydrological Processes 11 (3), 311–323.

Singh, V. P., Xu, C.-Y., 1997b. Sensitivity of Mass Transfer-based Evaporation Equations to Errors in Daily and Monthly Input Data. Hydrological Processes 11, 1465–1473.

Smith, R. C., Baker, K. S., 1981. Optical Properties of the Clearest Natural Waters (200-800 nm). Applied Optics 20 (2), 177–84.

Smith, S. D., 1988. Coefficients for Sea Surface Wind Stress, Heat Flux, and Wind Profiles as a Function of Wind Speed and Temperature. Journal of Geophysical Research 93 (15), 15467–15472.

SnappyHexMesh, 2015. OpenFOAM User Guide: Mesh generation with snappyHexMesh[online]. Available from: http://cfd.direct/openfoam/user-guide/snappyhexmesh/, [Accessed 28 October 2016].

Sogachev, A., Kelly, M., Leclerc, M. Y., 2012. Consistent Two-Equation Closure Modelling for Atmospheric Research: Buoyancy and Vegetation Implementations. Boundary-Layer Meteorology 145, 307–327.

Solazzo, E., Cai, X., Vardoulakis, S., 2009. Improved Parameterisation for the Numerical Modelling of Air Pollution within an Urban Street Canyon. Environmental Modelling & Software 24 (3), 381–388.

Stannard, D., Rosenberry, D., 1991. A Comparison of Short-term Measurements of Lake Evaporation Using Eddy Correlation and Energy Budget Methods. Journal of Hydrology 122 (1-4), 15–22.

Stepanenko, V., Johnk, K. D., Machulskaya, E., Perroud, M., Subin, Z., Nordbo, A., Mammarella, I., Mironov, D., 2014. Simulation of Surface Energy Fluxes and Stratification

506469-L-sub01-bw-Abbasi
Processed on: 9-11-2016

of a Small Boreal Lake by a Set of One-dimensional Models. Tellus A 66 (21389), 1–18.

Stull, R. B., 1988. An Introduction to Boundary Layer Meteorology, 1st Edition. Kluwer Academic Publishers, Dordrecht, Netherlands.

Suárez, F., Tyler, S. W., Childress, A. E., 2010. A Fully Coupled, Transient Double-diffusive Convective Model for Salt-gradient Solar Ponds. International Journal of Heat and Mass Transfer 53 (9-10), 1718–1730.

Subin, Z. M., Riley, W. J., Mironov, D., 2012. An Improved Lake Model for Climate Simulations: Model Structure, Evaluation, and Sensitivity Analyses in CESM1. Journal of Advances in Modeling Earth Systems 4, 1–27.

Sun, J., Vandemark, D., Mahrt, L., Vickers, D., Crawford, T., Vogel, C., 2001. Momentum Transfer over the Coastal Zone. Journal of Geophysical Research 106 (D12), 12437–12448.

Svensson, U., 1998. PROBE: Program for Boundary Layers in the Environment (System description and Manual). NorrkÖping : Swedish Meteorological and Hydrological Institute.

Swayne, D., Lam, D., Mackay, M., Rouse, W., Schertzer, W., 2005. Assessment of the Interaction between the Canadian Regional Climate Model and lake Thermal–hydrodynamic Models. Environmental Modelling & Software 20 (12), 1505–1513.

Sweeney, D., 2004. Integrating Biological and Hydraulic Aspects of Waste Stabilisation Pond Design. Thesis(PhD), Flinders University.

Ta, C. T., Brignal, W. J., 1998. Application of Computational Fluid Dynamics Technique to Storage Reservoir Studies. Water Science and Technology 37, 219–226.

TELEMAC, 2016. Open TELEMAC-MASCARET: the Mathematically Superior Suite of Solver[online]. Available from: http://www.opentelemac.org/, [Accessed 15 October 2016].

Tritton, D., 2007. Physical Fluid Dynamics. Clarendon Press, Oxford, United Kingdom.

Tsanis, I. K., 2006. Environmental Hydraulics: Hydrodynamic and Pollutant Transport Modelling of Lakes and Coastal Waters. Elsevier, Amsterdam, Netherlands.

van Emmerik, T. H. M., Rimmer, A., Lechinsky, Y., Wenker, K. J. R., Nussboim, S., van de Giesen, N. C., 2013. Measuring Heat Balance Residual at Lake surface Using Distributed Temperature Sensing. Limnology and Oceanography: Methods 11 (1991), 79–90.

Vendel, F., Lamaison, G., Soulhac, L., Volta, P., Donnat, L., Duclaux, O., Puel, C., 2010. Modelling Diabatic Atmospheric Boundary Layer Using A RANS CFD Code with a $k-\varepsilon$ Turbulence Closure. In: HARMO13. Vol. 0. pp. 652–656.

Verburg, P., Antenucci, J. P., 2010. Persistent Unstable Atmospheric Boundary Layer Enhances Sensible and Latent Heat Loss in a Tropical Great Lake: Lake Tanganyika. Journal of Geophysical Research 115, 1–13.

Vercauteren, N., 2011. Water Vapor and Heat Exchange over Lakes. Thesis(PhD), École Polytechnique Fédérale de Lausanne.

Vercauteren, N., Bou-Zeid, E., Parlange, M. B., Lemmin, U., Huwald, H., Selker, J., Meneveau, C., 2008. Subgrid-Scale Dynamics of Water Vapour, Heat, and Momentum over a Lake. Boundary-Layer Meteorology 128 (2), 205–228.

Vercauteren, N., Huwald, H., Bou-Zeid, E., Selker, J. S., Lemmin, U., Parlange, M. B., Lu-

506469-L-sub01-bw-Abbasi
Processed on: 9-11-2016

nati, I., 2011. Evolution of Superficial Lake Water Temperature Profile under Diurnal Radiative Forcing. Water Resources Research 47, 1–10.

Verdier-Bonnet, C., Angot, P., Fraunie, P., Coantic, M., 1999. Three-dimensional Modelling of Coastal Circulations with Different $k-\varepsilon$ Closures. Journal of Marine Systems 21, 321–339.

Vesala, T., Kljun, N., Rannik, Ü., Rinne, J., Sogachev, A., Markkanen, T., Sabelfeld, K., Foken, T., Leclerc, M. Y., 2008. Flux and Concentration Footprint Modelling: State of the Art. Environmental Pollution 152 (3), 653–666.

Vickers, D., Mahrt, L., 2010. Sea-Surface Roughness Lengths in the Midlatitude Coastal Zone. Quarterly Journal of the Royal Meteorological Society 136 (649), 1089–1093.

Vidal-López, P., Martínez-Alvarez, V., Gallego-Elvira, B., Martín-Górriz, B., 2012. Determination of Synthetic Wind Functions for Estimating Open Water Evaporation with Computational Fluid Dynamics. Hydrological Processes 26, 3945–3952.

Vinnichenko, N. A., Uvarov, A. V., Plaksina, Y. Y., Vetukov, D. A., 2011. Study of Evaporation from Water Reservoir. In: 22nd International Symposium on Transport Phenomena. Delft, Netherlands, pp. 1–11.

Vreugdenhil, C. B., 1994. Numerical Methods for Shallow-Water Flow, 1st Edition. Kluwer Academic Publishers, Dordrecht, Netherlands.

Wakes, S. J., Maegli, T., Dickinson, K. J., Hilton, M. J., 2010. Numerical Modelling of Wind Flow over a Complex Topography. Environmental Modelling & Software 25, 237–247.

Wang, J., Song, J., Huang, Y., Fan, C., 2013a. On the Parameterization of Drag Coefficient over Sea Surface. Acta Oceanologica Sinica 32 (5), 68–74.

Wang, Y., 2013. Development of a Numerical Tool to Predict Hydrodynamics, Temperature and TDG in Hydropower Flows. Thesis(PhD), University of Iowa.

Wang, Y.-S., Politano, M., Laughery, R., 2013b. Towards Full Predictions of Temperature Dynamics in McNary Dam Forebay using OpenFOAM. Water Science and Engineering 6 (3), 317–330.

Warnaka, K., Pochop, L., 1988. Analyses of Equations for Free Water Evaporation Estimates. Water Resources Research 24 (7), 979–984.

Weinberger, S., Vetter, M., 2012. Using the Hydrodynamic Model DYRESM Based on Results of a Regional Climate Model to Estimate Water Temperature Changes at Lake Ammersee. Ecological Modelling 244, 38–48.

White, F. M., 1991. Viscous Fluid Flow, 2nd Edition. McGraw-Hill, New York, USA.

Wieringa, J., 1992. Updating the Davenport Roughness Classification. Journal of Wind Engineering and Industrial Aerodynamics 44, 357–368.

Williams, D. T., Drummond, G. R., Ford, D. E., Robey, D. L., 1981. Determination of Light Extinction Coefficients in Lakes and Reservoirs. In: Proceedings of ASCE Symposium on Surface Water Impoundments. pp. 1329–133.

Wood, T. M., Cheng, R. T., Gartner, J. W., Hoilman, G. R., Lindenberg, M. K., Wellman, R. E., 2008. Modeling Hydrodynamics and Heat Transport in Upper Klamath Lake, Oregon, and Implications for Water Quality. Technical report, U.S. Geological Survey.

Wu, Y., Nair, U. S., Pielke, R. a., McNider, R. T., Christopher, S. a., Anantharaj, V. G., 2009. Impact of Land Surface Heterogeneity on Mesoscale Atmospheric Dispersion. Boundary-Layer Meteorology 133, 367–389.

506469-L-sub01-bw-Abbasi
Processed on: 9-11-2016

Wüest, A., Lorke, A., 2003. Small-Scale Hydrodynamics in Lakes. Annual Review of Fluid Mechanics 35 (1), 373–412.

Xu, C.-Y., Singh, V. P., 2000. Evaluation and Generalization of Radiation-based Methods for Calculating Evaporation. Hydrological Processes 14 (2), 339–349.

Xu, C.-Y., Singh, V. P., 2001. Evaluation and Generalization of Temperature-based Methods for Calculating Evaporation. Hydrological Processes 15 (2), 305–319.

Yamashiki, Y., Kumagai, M., Jiao, C., Nezu, I., Matsui, S., 2003. Numerical Simulation of Thermally Induced Gyres in Lake Biwa. Hydrological Processes 17, 2947–2956.

Yang, Y., Gu, M., Chen, S., Jin, X., 2009. New Inflow Boundary Conditions for Modelling the Neutral Equilibrium Atmospheric Boundary Layer in Computational Wind Engineering. Journal of Wind Engineering and Industrial Aerodynamics 97, 88–95.

Yao, H., 2009. Long-Term Study of Lake Evaporation and Evaluation of Seven Estimation Methods: Results from Dickie Lake, South-Central Ontario, Canada. Journal of Water Resource and Protection 02, 59–77.

Zeng, X., Zhao, M., Dickinson, R. E., 1998. Intercomparison of Bulk Aerodynamic Algorithms for the Computation of Sea Surface Fluxes Using TOGA COARE and TAO Data. Journal of Climate 11, 2628–2644.

Zhang, A., Gao, C., Zhang, L., 2005. Numerical Simulation of the Wind Field around Different Building Arrangements. Journal of Wind Engineering and Industrial Aerodynamics 93, 891–904.

506469-L-sub01-bw-Abbasi
Processed on: 9-11-2016